PORE-SCALE MODELLING OF TRANSPORT PHENOMENA IN HOMOGENEOUS POROUS MEDIA

by

Gerhardus P.J. Diedericks

Dissertation presented for the degree of Doctor of Philosophy
at the University of Stellenbosch.

Promoter: Professor J.P. du Plessis

20 December 1999

Declaration

I, the undersigned, hereby declare that the work contained in this dissertation is my own original work and that I have not previously in its entirety or in part submitted it at any university for a degree.

Abstract

The main purpose of this study is to develop deterministic, process-based models of incompressible Newtonian flow and electrical conduction in homogeneous, anisotropic porous media.

The foundation of the models is provided by the volume averaging theory which is used to obtain the macroscopic balance equations for momentum transport and electrical conduction. These volume averaged equations contain, amongst others, integral terms over the fluid-solid surface area where the integrands are related to the microscopic fluxes of the transport quantities. The closure modelling is conducted by employing a pore-scale model which requires explicit assumptions regarding the mean geometric properties of the porous medium microstructure and accounts for the configuration of the fluid-solid surface area. The pore-scale model also provides an estimate of the microscopic flow paths. The average geometry of different anisotropic materials, namely two types of foamlike materials, granular porous media and fibre beds, is captured in representative unit cells which form the core of the physical pore-scale model.

This particular type of closure modelling further requires a direct transformation of microscopic fluxes to the macroscopic level. It is indicated, in context of the volume averaging theory, that microscopic fluxes may be estimated by the respective macroscopic channel average fluxes. The transformation of the microscopic flux to the channel average flux is accomplished through the flux related tortuosity tensor. New definitions for the tortuosity and lineality as second-order tensors are proposed for porous media in general. Novel names, semantically in line with the respective physical meanings, are proposed for these quantities. It is shown that the definitions produce results which conform with several other published results and are applicable to anisotropic media.

Application of the modelling technique to Newtonian flow results in momentum transport equations valid for both the Darcy and Forchheimer flow regimes. The coefficients appearing in these equations are expressed in terms of fluid properties and measurable geometric features of the porous medium. The predictions of the anisotropic foamlike materials are validated against experimental pressure gradient measurements for flow through a high porosity, anisotropic knitted wire mesh rolled up to form a cylindrical plug. The predictions compare reasonably well with the experimental results.

The modelling approach is also applied to electrical conduction in anisotropic porous media saturated with an electrically conductive fluid. A macroscopic form of Ohm's law is derived as well as deterministic expressions for the formation factor. The formation factor predictions for isotropic porous media are compared to several experimental measurements as well as to semi-empirical expressions. The predictions compare favourably to the measurements.

Opsomming

Die hoofdoel van hierdie studie is om deterministiese, proses-gebaseerde modelle van onsaamdrukbare Newton-vloeiers en elektriese geleiding in homogene, anisotrope poreuse media te ontwikkel.

Die basis van die modelle is die volumetriese homogeniseringsteorie wat gebruik word om die makroskopiese balansvergelykings vir momentum transport en elektriese geleiding te verkry. Die makroskopiese vergelykings bevat, onder andere, integrasieterme oor die benatte oppervlakte waar die integrand afhanklik is van die mikroskopiese vloede van die transport groothede. Die sluitingsmodellering word uitgevoer deur gebruik te maak van 'n porie-skaal model wat spesifieke aannames in verband met die gemiddelde geometriese eienskappe van die mikrostruktuur vereis en inkorporeer die konfigurasie van die benatte oppervlakte. Die model verskaf ook 'n afskatting van die mikroskopiese vloeipatrone. Die gemiddelde geometrie van verskillende anisotrope materiale, naamlik twee tipes sponse, korrelagtige materiale en vesels, word in verteenwoordigende eenheidselle inkorporeer en vorm die kern van die fisiese porie-skaal model.

Hierdie spesifieke sluitingsmodellering vereis verder 'n direkte transformasie van mikroskopiese vloede na die makroskopiese vlak. Daar word aangetoon, in konteks van die volumetriese homogeniseringsteorie, dat die mikroskopiese vloede afgeskat kan word deur die ooreenkomstige makroskopiese kanaal-gemiddelde vloede. Die transformasie van die mikroskopiese vloed na die kanaal-gemiddelde vloed word bewerkstellig deur die vloed-gekoppelde tortuositeistensor. Nuwe definisies vir die tortuositeit en linealiteit as tweede orde tensors word voorgestel vir poreuse media in die algemeen. Nuwe name wat semanties ooreenstem met die onderskeie fisiese betekenisse word ook voorgestel vir hierdie groothede. Daar word aangetoon dat die definisies ooreenstem met gepubliseerde resultate en dat dit van toepassing is op anisotrope materiale.

Toepassing van die modelleringstegniek op Newton vloei lei tot momentum transportvergelykings wat geldig is oor beide die Darcy en Forchheimer vloeigebiede. Die koëffisiënte wat in hierdie vergelykings verskyn word uitgedruk in terme van vloeier eienskappe en meetbare geometriese eienskappe van die poreuse medium. Die voorspellings vir die anisotrope sponse word vergelyk met eksperimentele drukgradiënte vir vloei deur 'n hoë porositeit, anisotrope gevlegde metaaldraad wat opgerol is om 'n silindriese prop te vorm. Die voorspellings vergelyk goed met die eksperimentele metings.

Die modelleringsaanslag word ook toegepas op elektriese geleiding in anisotrope poreuse materiale wat versadig is met 'n elektries geleidende vloeistof. 'n Makroskopiese vorm van Ohm se wet word afgelei asook deterministiese uitdrukkings vir die formasiefaktor. Die formasiefaktor voorspellings wat van toepassing is op isotrope materiale word vergelyk met verskeie eksperimentele metings asook met semi-empiriese uitdrukkings. Die voorspellings vergelyk gunstig met die eksperimentele metings.

Acknowledgements

I wish to express my sincere gratitude to the people and organisations who inspired and assisted the development of this thesis.

Many thanks to Prof Prieur du Plessis, my promoter, for his guidance, collaborative research approach and the interest he took in my work. He was supportive in many aspects concerning my dissertation and his motivation, friendly attitude and availability to discuss sections of this study at literally any time meant a lot to me. I, therefore, greatly acknowledge Prieur's judgement and leadership in the project.

I would like to thank Prof J. LeGrand for inviting me to the Laboratoire de Génie de Procédés, IUT in Saint-Nazaire. He provided the opportunity to meet scientists in the same field and participate in laboratory experiments.

I am also grateful to Dr Agnès Montillet for the numerous fruitful discussions we had during my visit to the IUT. She was very helpful in providing data obtained from her experiments and she generously shared her knowledge.

Much of the credit for this dissertation must go to my wife, Lyndsey, who offered encouragement and support over the years. I would also like to thank Lyndsey for her perfectionistic approach in producing all of the figures in this dissertation.

Finally, I would like to thank the FRD, the University of Stellenbosch and the Harry Crossley Fund for providing financial assistance. This enabled me to do three years full time research.

Contents

Nomenclature

Roman letters

A	inertial constant, m^{-1}
$A_o, \widehat{A}_o$	total area, m^2
$A_{o(\alpha)}$	total area normal to the x_α-direction, m^2
$A_f, \widehat{A}_f$	fluid area, m^2
$A_{f(\alpha)}$	fluid area normal to the x_α-direction, m^2
A_p	effective fluid area, m^2
$A_{p(\alpha)}$	effective fluid area normal to x_α-direction, m^2
A_{vs}	geometric specific surface area, m^{-1}
A_{vd}	dynamic specific surface area, m^{-1}
$\widehat{A}_{f\mathcal{L}}$	effective streamwise part of $\widehat{A}_f$, m^2
$A_\perp$	transverse channel area for granular model, m^2
B	viscous constant, m^{-2}
B_{ij}	inertial tensor, m^{-1}
c_d	two-dimensional drag coefficient, dimensionless
c	molar concentration of a chemical species, $\mathrm{mol\ m}^{-3}$
$\overset{\circ}{c}$	deviation of molar concentration, $\left(c - \langle c \rangle^f\right)$, $\mathrm{mol\ m}^{-3}$
c_α	molar concentration of species α, $\mathrm{mol\ m}^{-3}$
d	linear dimension of isotropic RUC, m
$d_{(\alpha)}$	RUC dimension in x_α-direction, m
d_c	tube diameter, average pore diameter, m
d_n	average particle diameter, m
$d_{p(\alpha)}$	effective pore dimension in x_α-direction, m
$d_{s(\alpha)}$	dimension of solid constituent in x_α-direction, m
$d_\perp$	transverse distance for fluid flow in granular model, m
dA	infinitesimal area element, m^2
dS	infinitesimal surface element of a closed surface, m^2
dU	infinitesimal volume element, m^3
D	actual wire diameter, m
$\widetilde{e}_{\gamma i}$	cross-sectional mean flux of γ-particles in a channel, $\Gamma\ \mathrm{m}^{-2}\ \mathrm{s}^{-1}$
$\widetilde{e}_\gamma$	magnitude of $\widetilde{e}_{\gamma i}$, $\Gamma\ \mathrm{m}^{-2}\ \mathrm{s}^{-1}$
$\widehat{e}_{\gamma i}$	streamwise channel average flux of γ-particles ($\langle \widetilde{n}_{\gamma i} \rangle^c$), $\Gamma\ \mathrm{m}^{-2}\ \mathrm{s}^{-1}$
$\widehat{e}_\gamma$	magnitude of $\widehat{e}_{\gamma i}$, $\Gamma\ \mathrm{m}^{-2}\ \mathrm{s}^{-1}$
E	surface roughness as used in Appendix A, m
E	electric field strength, $\mathrm{V\ m}^{-1}$
f	Ergun type friction factor, dimensionless
f_r	friction factor related to surface roughness, dimensionless

F	formation factor, dimensionless
F_e	apparent formation factor, dimensionless
F_{ij}	shear resistance tensor, m^{-2}
F_{min}, F_{max}, F_{av}	minimum, maximum and average drag forces, N
g_i	gravity force per unit mass, m s^{-2}
$h, h_{(1)}$	characteristic length in Reynolds number, m
i	electric current, A
I	resistivity index, dimensionless
j_i	current density, A m^{-2}
j	magnitude of j_i, A m^{-2}
$\overline{j}_i$	channel average current density ($\langle j_i \rangle^c$), A m^{-2}
$j_\perp$	magnitude of current density in a transverse channel, A m^{-2}
$j_{\perp(1)}, j_{\perp(2)}$	magnitudes of transverse current densities in foam model, A m^{-2}
k'	Kozeny constant, dimensionless
k_o, k_s	shape factor, dimensionless
K	specific (Darcy) permeability, m^2 or darcy
K_p	permeability, m^3 s kg^{-1}
K_{ij}	Darcy permeability tensor, m^2
l	characteristic length of an REV, m
$L, \widehat{L}$	average streamwise displacement, m
$L_e, \widetilde{L}_e$	average tortuous channel length, m
$L_\perp$	distance over which potential difference is applied, m
$L_{\perp(\alpha)}$	distance over which potential difference is applied in x_α-direction, m
$\mathcal{L}_{ij}$	lineality tensor, dimensionless
$\mathcal{L}_{mm}$	sum of diagonal elements of $\mathcal{L}_{ij}$, dimensionless
M	inertial term coefficient, Pa m^{-3} s^2
$n_{\gamma i}, \widetilde{n}_{\gamma i}$	actual microscopic flux of γ-particle, Γ m^{-2} s^{-1}
$\widetilde{n}_\gamma$	magnitude of $\widetilde{n}_{\gamma i}$, Γ m^{-2} s^{-1}
$N_{\alpha i}$	molar flux of α-species, mol m^{-2} s^{-1}
N	viscous term coefficient, Pa m^{-2} s
p	microscopic pressure, Pa
$\overset{\circ}{p}$	pressure deviation $\left(p - \langle p \rangle^f\right)$, Pa
P	piezometric pressure (head), absolute presssure, Pa
P_f	fluid pressure, meter pressure $\left(\langle p \rangle^f\right)$, Pa
$q_i, \widehat{q}_i$	specific discharge, superficial velocity, seepage velocity, m s^{-1}
$q, \widehat{q}$	magnitude of $\widehat{q}_i$, m s^{-1}
$\widehat{Q}_i$	total discharge through an REV, m^3 s^{-1}
r_i	position vector of points on S_f, m
$\overline{r}_i$	position vector on the trace of an REV centroid, m

$\overset{o}{r}_i$	position vector of points on S_f relative to REV centroid, m
r_i^{fs}	position vector of the fluid-solid interface, m
R_h	hydraulic diameter, m
$R_{(IJ)}$	anisotropy factor, dimensionless
R_o	resistance of electrolytically saturated porous sample, Ω
$R_{(\alpha)}$	electrical resistance of tube α, Ω
R_w	resistance of a sample containing only the electrolyte, Ω
Re	Reynolds number ($\rho qh/\mu$), dimensionless
REA	Representative Elementary Area
REV	Representative Elementary Volume
RUC	Representative Unit Cell
s	arc length along designated curve, m
$s_{(\alpha)}$	cross-sectional area of tube α, m^2
S	surface, m^2
S_c	open surface area of a container, m^2
S_{ff}	fluid-fluid phase contact over S_f, m^2
S_{fs}	fluid-solid phase contact over S_f, m^2
S'_{fs}	fluid-solid surface presented to the flow, m^2
S_f	total boundary of the fluid phase ($S_{ff} + S_{fs}$), m^2
S_o	total boundary of an REV, ($S_{ff} + S_{ss}$), m^2
S_{ss}	solid-solid area in solid phase, m^2
t	time, s
T_{ij}^B	tortuosity tensor of Bear (1972), dimensionless
T_{ij}^{BB}	tortuosity tensor of Bear and Bachmat (1991), dimensionless
$u_i, \widehat{u}_i$	intrinsic phase average velocity, interstitial velocity, m s^{-1}
u	magnitude of u_i, m s^{-1}
$\widehat{u}$	magnitude of $\widehat{u}_i$, m s^{-1}
U	volume, m^3
U_o	total volume of an REV or RUC, m^3
U_f	fluid phase within REV or RUC, m^3
U_s	solid phase within REV or RUC, m^3
$\widehat{U}_{f\mathcal{L}(\alpha)}, U_{f\mathcal{L}(\alpha)}$	effective streamwise part of U_f for flow in x_α-direction, m^3
U_{ef}	effective fluid volume, m^3
$v_i, \widetilde{v}_i$	microscopic fluid velocity, m s^{-1}
$v, \widetilde{v}$	magnitude of $\widetilde{v}_i$, m s^{-1}
$v_{\gamma i}, \widetilde{v}_{\gamma i}$	microscopic velocity of γ-particle, m s^{-1}
$\widetilde{v}_\gamma$	magnitude of $\widetilde{v}_{\gamma i}$, m s^{-1}
v_i^b	boundary velocity of a material volume, m s^{-1}
$v_{\alpha i}$	velocity of α-species, m s^{-1}

V	electric potential, V
V_h, V_l	high and low electric potentials, V
$V_{h(\alpha)}, V_{l(\alpha)}$	high and low electric potentials in channel in x_α-direction, V
$\widehat{w}_i$	streamwise channel average velocity within U_f ($\langle v_i \rangle^c$), m s^{-1}
$\widehat{w}$	magnitude of $\widehat{w}_i$, m s^{-1}
$w_i, \widetilde{w}_i$	average pore velocity, m s^{-1}
$w, \widetilde{w}$	average pore speed, m s^{-1}
$x_i, x_{\gamma i}$	general position vector, x_i-coordinate, m
x_I	I principal coordinate axis, m
$\overline{x}_i$	position vector indicating centroid of REV, m
$\overline{x}_i^f$	position vector indicating centroid of fluid volume within REV, m
$\overset{o}{x}_i$	position vector relative to REV centroid, m
X	fraction of surface area offered to flow ($X = A_{vd}/A_{vs}$), dimensionless
X_e	electrical retardation factor, dimensionless

Greek letters

γ	volumetric density of Γ, Γ m^{-3}
γ_d	generalised distribution function, dimensionless
Γ	an extensive quantity
δ_{ij}	Kronecker delta, dimenionless
$\delta_a, \delta_b, \delta_c$	diameter of tubes a, b and c, m
$\boldsymbol{\delta}$	multi-dimensional Dirac distribution, unit depends on argument
Δ	difference
ϵ	volume fraction of fluid phase in U_o, porosity, dimensionless
ζ_2	x_2-component of the mean velocity in the transverse channel in the x_2-direction, m s^{-1}
η_3	x_3-component of the mean velocity in the transverse channel in the x_3-direction, m s^{-1}
ϵ_{ef}	effective porosity, dimensionless
ϵ^A	areal fraction of fluid phase in A_o, porosity, dimensionless
$\lambda, \lambda_{pqr\ldots}$	generic tensorial variable
Λ	characteristic porous medium length scale, m
Λ_{ef}	effectivity parameter, dimensionless
μ	fluid viscosity, Pa s
ν_i	unit normal vector on surfaces and directed out of the fluid volume or REV, dimensionless
ν_i^f	unit normal vector on S_{fs} directed out of the fluid, dimensionless
$\widetilde{\nu}_i, \widetilde{\nu}_{fi}$	unit vector tangent to a streamline, dimensionless
$\widetilde{\nu}_{\gamma i}$	unit vector tangent to γ-transport line, dimensionless

$\widehat{\nu}_i$	streamwise unit vector, dimensionless
$\widehat{\nu}_{\gamma i}$	unit vector in macroscopic γ-transport direction, dimensionless
$\breve{\nu}_i$	unit vector in the plane orthogonal to $\widehat{\nu}_i$, dimensionless
ξ_{ij}	areosity tensor, dimensionless
$\xi, \xi_I, \xi_{(1)}$	principal areosity value, dimensionless
ρ	fluid density, kg m^{-3}
ρ_o	resistivity of saturated porous medium, Ω m
ρ_w	resistivity of electrolyte, Ω m
ρ_p	resistivity of partially saturated porous medium, Ω m
σ	curve length along streamline, m
σ_o	electrical conductivity of saturated porous medium, Ω^{-1} m^{-1}
σ_w	electrical conductivity of electrolyte, Ω^{-1} m^{-1}
τ_{ij}	shear stress tensor, N m^{-2}
τ_w	wall shear stress, N m^{-2}
$\phi, \phi_{jkl\ldots}$	generic tensorial variable
χ	tortuosity factor, dimensionless
χ_e	electrical tortuosity factor, dimensionless
χ_{ij}	tortuosity tensor, dimensionless
χ_{mm}	sum of the diagonal terms of the tortuosity tensor, dimensionless
Ω	number of curved channels in capillary model, dimensionless

Miscellaneous

$\langle\phi\rangle$	phase average $\left(\frac{1}{U_o}\iiint_{U_f}\phi\,dU\right)$
$\langle\phi\rangle^f$	intrinsic phase average $\left(\frac{1}{U_f}\iiint_{U_f}\phi\,dU\right)$
$\langle\phi\rangle_m$	mass average operator $\left(\frac{1}{\langle\rho\rangle^f\widehat{U}_{\gamma\mathcal{L}}}\iiint_{U_f}\rho\phi\,dU\right)$
$\langle\phi\rangle^c$	streamwise channel average $\left(\frac{1}{\widehat{U}_{\gamma\mathcal{L}}}\iiint_{U_f}\phi\,dU\right)$
$\langle\phi\rangle^A$	areal average $\left(\frac{1}{\widehat{A}_o}\iint_{A_f}\phi\,dA\right)$
$\langle\phi\rangle^{fA}$	areal intrinsic phase average $\left(\frac{1}{\widehat{A}_f}\iint_{A_f}\phi\,dA\right)$
$\langle\phi\rangle^{cA}$	streamwise areal average $\left(\frac{1}{\widehat{A}_{f\mathcal{L}}}\iint_{\widehat{A}_f}\phi\,dA\right)$
∇	differential operator, nabla, del, m^{-1}

Subscripts

an	analytical predictions
exp	experimental
ijk	tensor indices
$(i), (I), (k)$	notational indices without tensorial implications
pqr	tensor indices

I	pertaining to principal direction of tensor
f	fluid phase
o	indicates fluid and solid
s	solid phase

Superscripts

$\wedge$	pertaining to streamwise direction
$\sim$	pertaining to local flow direction
$\smile$	indicates perpendicular to streamwise direction

List of Figures

List of Tables

Chapter 1

INTRODUCTION

1.1 Preface

The subject of transport in porous media includes a large number of scientific disciplines but, independent of a particular application, general developments regarding transport in porous media progress along the lines of theoretical modelling, specific applicatory models, numerical analyses and the acquirement of improved experimental results. While the theoretical contributions should be applicable to a wide range of transport processes, the specific closure models generally address a particular engineering or hydrological problem. It is intended that in this study contributions are made on both of these two fields. Although the primary focus of this work is on deterministic transport equations, the initial focus on this type of modelling stems from an approach to improve existing governing equations which are generally used in numerical solutions. This is achieved by producing closure models in terms of measurable porous medium parameters and fluid properties for the experimental and calibration coefficients generally used in numerical models. Therefore, in a broader context, the results may be used for improved numerical results even though the computational aspects of the different flow phenomena are not considered.

Besides these practical issues, the modelling of flow through porous media poses a captivating problem. Specific microscopic values are not of interest, only measurable averages, and this necessitates a clear understanding of the relation between the conceptual mathematical parameters and the physical quantities which they represent. It is, therefore, imperative to read the physical meaning in each mathematical statement. It is also inspiring to be in a position in which real life processes can be predicted and, when comparing to measurements, realise that the conceptualisation or model is

representative of the basic physical processes at work. In the engineering industry such process based models are not as frequently used as semi-empirical models and any successful predictive model will aid a better understanding of the basic physical principles. In the long term, these models might replace the semi-empirical models. This will lessen the necessity for large numbers of experimental measurements and, idealistically, lead to a single unified theory for transport in porous media.

1.2 Background to this study

With the commencement of this study a foundation has been laid in which a particular type of closure model, namely the Representative Unit Cell model, was used to obtain deterministic expressions for the flow of Newtonian fluids through isotropic porous media. This particular model, which is also referred to as the RUC-model, proved to be very successful in predicting pressure drop-velocity relations in high porosity foamlike materials and granular sandstones. Due to these successes, an additional study was undertaken using the RUC-model to quantify the transport of non-Newtonian fluids through isotropic porous media. In addition, alternative applications analysing heat transport in isotropic porous media have utilised the RUC-model.

Further extensions of the model required the inclusion of other types of materials and additional transport processes. From a structural point of view the logical next step was to extend the modelling procedure to *include anisotropic porous media.* In anisotropic porous media, the transport properties of the material are not uniform, but they differ in various directions. This lead to the introduction of additional RUC's representative of the anisotropic materials. A key concept in the RUC-model is that of the tortuosity which depends on the direction of transport in an anisotropic material. An additional feature not addressed by the isotropic modelling is the possible *tensorial nature of the tortuosity.* A quantity closely related to the tortuosity is the formation resistivity factor. An analysis of the formation factor in context of the RUC-model also presents an opportunity to investigate the success of the modelling approach when applied to *electrical conduction in isotropic and anisotropic porous media.* Since the formation factor can be directly measured, the prediction of such a parameter may serve an important validating role.

It is within this context that this study of "Pore-scale modelling of transport in homogeneous porous media" aims to model two different modes of transport in anisotropic porous media, namely Newtonian fluid transport and the transport of electrical current, by utilising a specific pore-scale model.

1.3 Main objectives and relevance

The aims of this study may be separated into two categories, namely general theoretical aspects and applicable engineering aspects. Therefore, there is a theoretical part in which the emphasis is placed on general mathematical developments which are not restricted to a particular type of pore-scale model. This category includes the following objectives:

- To find a direct relation between microscopic transport properties and macroscopic quantities that can be used in transforming transport processes on the microscopic level in any pore-scale model to the macroscopic level.
- Carman (1937) related the microscopic velocity to the macroscopic velocity via a tortuosity factor which in this context is given as a ratio of lengths. Another objective then is to aid an understanding of the tortuosity and to make a contribution towards the theoretical foundation of the Carman-type tortuosity.

However, it is also necessary to produce results which address specific needs and that can be put to practical use. Therefore, there is also an engineering aim where the main objectives are to produce deterministic expressions governing certain transport processes which will minimise empiricism and reduce the necessity for continuous measurements. The main objectives in this regard are:

- To generalise the existing RUC's for isotropic materials to be applicable to anisotropic porous media. This also includes the design of new RUC's.
- To model fluid transport at both low and intermediate Reynolds numbers and electrical conduction through the RUC's. For fluid transport it is investigated whether the same modelling procedure used for the isotropic case is still applicable for pore-scale models with variable channels.
- To obtain deterministic expressions from which the permeability and formation factor can be calculated from physical characteristics of the porous material and fluid.
- To compare the results to the predictions of other relevant models and to discuss the similarities and differences.
- Where possible, the resulting expressions should be used to validate the predictive capabilities of the model. In this regard the advantages and disadvantages of the model should be noted.

Considering the success of the isotropic RUC-model, this study addresses the need to expand the model to include other types of porous structures and transport processes. The theoretical aspects are also relevant as it strengthens the theoretical foundation of the modelling procedure. In addition, the study also aims to present practical engineering solutions for relevant problems in the chemical engineering and geohydrological industries.

1.4 Overview

The mathematical notation adopted in the majority of this study is Cartesian tensor notation implying that the transformations involved are from one set of rectangular Cartesian coordinates to another. The results are therefore applicable to any rectangular Cartesian reference frame, but not directly to curvilinear coordinates. Subscripts will be used to denote tensor indices.

In Chapter 2 most of the concepts which are used during the modelling procedures in subsequent chapters are introduced. In the initial part of Chapter 2 emphasis is put on the volume averaging theory since all further work is based upon this method to obtain balance equations for different transport phenomena. Thereafter, a number of parameters which are employed to characterise porous media are presented. These include measureable parameters relevant to different transport processes as well as conceptual parameters which are used in certain pore-scale models. In the last section of this chapter a novel generalisation of the Carman-type tortuosity factor to a flux related tortuosity tensor in the context of the volume averaging theory and applicable to general transport processes is presented. Most of the information in this section appears in

> Diedericks, G.P.J., and Du Plessis, J.P., 1995, On tortuosity and areosity tensors for porous media, *Transport in Porous media*, volume 20, pages 265-279,

except that in this paper the transport is restricted to the flow of Newtonian fluids.

In Chapter 3 consideration is given to Newtonian flow through anisotropic homogeneous porous media. Firstly, phase averaged momentum transport equations are derived whereafter the general features of the physical characteristics of the RUC-model are introduced. The flow through two types of anisotropic foamlike materials are then considered for two laminar flow regimes and this work appears in

Diedericks, G.P.J., and Du Plessis, J.P., 1997, Modelling of flow through homoge neous foams, *Mathematical Engineering in Industry*, volume 6, number 2, pages 133-154.

In the following section the general model for foamlike materials is validated against a specific data set obtained for flow through a high porosity metallic plug. This model validation appears in

Diedericks, G.P.J., Du Plessis, J.P., Montillet, A., Comiti, J. and LeGrand, J., 1998, Flow through a highly porous multifilament knit, *Chemical Engineering Communi cations*, volume 167, pages 21-49.

In the remainder of Chapter 3 the modelling methodology is applied to Newtonain flow through anisotropic granular materials and anisotropic fibre beds.

In Chapter 4 attention is focussed on electrical conduction in anisotropic homogeneous porous media. In the first part of this chapter an overview of a number of models for the formation factor are presented as well as a description of charge transport on the microscopic level. The volume averaging theory is then used to obtain a macroscopic charge balance equation and the Representative Unit Cells designed in Chapter 2 are then used in the closure modelling. In the latter part of Chapter 3 the deterministic expressions for the formation factor in the limit of isotropic materials are compared to a number of sets of measurements. The parts of this chapter applicable to isotropic porous media appears in

Diedericks, G.P.J, and Du Plessis, J.P., 1996, Electrical conduction and formation factor in isotropic porous media, *Advances in Water Resources*, volume 19, number 4, pages 225-239

while the main concepts and results of the modelling are reviewed in

Du Plessis, J.P., and Diedericks, G.P.J., 1997, *Pore-scale modelling of interstitial transport phenomena*, Chapter 2 of Fluid Transport in Porous Media, editor J.P. du Plessis, vol 13, *Advances in Fluid Mechanics, Series*, editor M. Rahman, Computa tional Mechanics Publications, Southampton, pages 61-104.

In Chapter 5 the main conclusions are summerised and possible areas for future research and applications are discussed.

There are three appendices of which the first gives an overview of two capillary models. In Appendix B different averaging theorems and rules which are utilised during the

volume averaging process are derived. In Appendix C one particular model for the derivation of the formation factor is discussed.

Chapter 2

POROUS MEDIA MODELLING PARAMETERS

2.1 Introduction

The analyses of transport phenomena in porous media provide highly complex, and intriguing, physical and mathematical problems, since it requires the accurate modelling of various transport processes within the often minute interstices of a porous medium. Integrating a function over each and every pore is virtually an impossible task and, therefore, the modeller has to represent the porous microstructure and interacting transport process by a physical or mathematical model. The increased sophistication of various engineering technologies has brought with it increased operating and material costs and therefore a greater demand for sound process designs. Mathematical and physical models of various transport phenomena in porous media have become key tools by which engineers develop and implement these designs. Using models together with different characteristics of the system being modelled, the engineer can test various operating strategies and formulate hypotheses in diagnosing the performance of ongoing projects. Improved computer technologies have also spurred the application of numerical models by creating more realistic simulations. Since transport in porous media is a study field with a broad base of practical applications in every day life, it requires analyses with a high degree of scientific rigour and precision to minimise or even eliminate prediction uncertainty.

The main objective of this chapter is to lay the foundation for the particular pore-scale modelling technique applied in this study. Firstly, a number of modelling methods which have been used to quantify transport phenomena in porous media are briefly presented. Since more extensive reviews exist for most of these models, for example

Dullien (1979) and Scheidegger (1974), this chapter only serves to emphasise certain aspects of some models which are referred to during the course of this study. However, one modelling strategy, namely the volume averaging theory, is presented in detail, since all analyses of transport processes in this study are based on this approach. Another objective of this chapter is to define most of the parameters characterising porous media which are referred to during the course of this study. This is relevant since a pore-scale porous medium model is introduced in later chapters and an understanding of geometric pore-scale parameters will prove particularly useful. Furthermore, this will also ensure clarity of meaning, especially if we consider the broad applicability and multidisciplinary nature of flow through porous media. Many of these characteristics and models are discussed in literature and are presented here only for coherence of the study and clarity, while all novel parameters are discussed in more detail.

However, a parameter which may be considered fundamental to porous media transport is the tortuous pathway available to various transport processes. Since it can be expected that all transport processes in porous media are in one way or another related to the tortuous pore-space, it is imperative that tortuosity and its relation to various transport phenomena be adequately understood. The importance of tortuosity in analyses of transport in porous media has been realised by many scientists and this has, unfortunately, led to many different parameters which are related to the geometry of the pore-space being defined as the "tortuosity". In the latter part of this chapter a novel theoretical exposition of microscopic transport fluxes is given in context of the volume averaging theory, from which a definition of the geometric tortuosity follows naturally. This analysis is applicable to a variety of transport processes and porous media in general. Many of the transport processes in porous media discussed in later chapters are built upon this general analysis of microscopic fluxes and geometric tortuosity. The newly defined tortuosity is also compared to some of the more prominent definitions of tortuosity in literature and some of the differences and similarities are discussed.

2.2 Description and classification of porous media

2.2.1 Definition of a porous medium

Porous media appear in a number of natural and industrial states and it is instructive towards an understanding of porous substances to consider a few examples. Natural porous media include geologic materials, such as soil, sand, various types of rocks and

sandstones. Additional examples are aquifers from which groundwater is extracted and natural reservoirs which yield gas or oil. Certain parts of living organisms, such as skin, bones, kidneys and even the vascular system of plants form part of porous media. Industrial or artificial porous materials include paper, textiles, untreated leather, cement, rubber foam, ceramics and towers packed with pebbles or beads. A review of physical characteristics of some natural and industrial porous materials is presented by Dullien (1979) while Kaviany (1995) discusses some applications of porous media in the fields of chemical, environmental, mechanical and petroleum engineering as well as geology. From these examples it is evident that porous media encompass a wide variety of natural and artificial substances and that it is quite inappropriate to define a porous medium as a substance with holes.

Porous media may be described as sets of solid phases and void spaces which are regularly or irregularly distributed (Bear and Bachmat, 1991). A *phase* is considered as a chemically homogeneous portion of a system which is separated from other such portions by a definite physical boundary (Bachmat 1972). A particle of a phase may be defined as a volume of phase which consists of a large number of molecules. In a fluid phase, for example, each fluid particle may exchange molecules with neighbouring particles through molecular diffusion. The kinematic properties of the group of molecules are referred to its centre of gravity which is considered as a physical point of the phase. This level at which a physical boundary of a phase interface is observed is larger than the molecular level and is referred to as the *microscopic level.* This is the usual level encountered in fluid mechanics where, for instance, the Navier-Stokes momentum equations hold and on this scale we may use the continuum description and refer to the temperature, pressure and velocity as field variables which have values at each point in space. In this study we assume that these quantities vary continuously with position, although they may have jump discontinuities at the boundaries of phases. Quantities at this level of description are denoted by the terms *local, microscopic* or *point values.*

If we define a mixture as a collection of intermingled continua called constituents, then a porous medium may formally be defined as a *multiphase mixture* (Allen *et al.*, 1988). The constituents are then the various phases and segregation among the constituents occurs at the microscopic level, where the phases behave as continua, but their small scale motions are inaccessible to direct measurement. In a porous medium the solid phase, or solid matrix, should have a more or less frequent distribution through the domain. The remaining part of the domain is referred to as the void space or pore-space. It may be occupied by any number of fluid phases. However, in this study only porous media where the void space is filled with a single fluid phase, be it liquid or gaseous, is considered.

An additional concept often referred to when considering transport in porous media is that of a pore, since flow through porous media may be visualised as taking place along certain pores. In the present analysis a pore, or equivalently a channel or capillary, is viewed as a part of the void space where the interphase boundary has a significant effect upon hydrodynamic phenomena on their interior (Scheidegger, 1974). It is implicitly implied in this idea of a pore that the flow takes place nearly parallel to the boundary between solid and void. The void space between pores is then referred to as the intrapore space. Pores have also been used to signify visible openings on the surface of a porous domain and in the present analysis such openings are referred to as pore openings.

2.2.2 Classification of porous media

Since porous media encompass such a large number of substances, it is desirable to arrange porous media into several classes. One system of classification is to group porous media according to the manner in which the solid phase is distributed and from this distribution porous media may be viewed as either periodic (ordered) or disordered (Quitard and Whitaker, 1994a). Porous media may also be classified according to the length scales of the various phases or, as is followed in this study, according to the types of void spaces or solid phases which they contain. A very useful concept according to which porous media may be classified is, therefore, the degree in which a particular phase is connected, since the transport of a particular quantity, such as momentum, mass and energy, is primarily dependent on the connectivity of the pore-space. Porous media may then be classified into two broad categories, namely connected and non-connected. According to Bear and Bachmat (1991), a domain is *connected* if any two points in the domain can be connected or linked by a curve which lies completely within that domain. They also distinguish between two types of connectivity. In a simply connected domain any closed surface placed within the domain can be shrunk to a point without leaving it. If a connected region is not simply connected, it is multiply connected, since one or more closed surfaces are contained within it. A *non-connected* spatial domain is composed of a union of disjoint domains. For example, the raisins in a hot cross bun may serve as an illustration of a non-connected solid phase, while the dough forms a multiple connected phase. On the other hand, the solid phase in a single stranded rolled-up fishing net is an example of a simply connected region.

The discussion concerning the characteristics of porous media presented in this chapter is directed towards porous media in general. However, in subsequent chapters a distinction is made between three different types of porous environments, namely foamlike materials, granular materials and prismatic bundles. The distinctive feature of *foam-*

like materials is the fact that the solid phase is simply connected for all values of the porosity and it may, therefore, be referred to as consolidated materials. However, not all consolidated materials are necessarily foamlike. *Granular materials* are considered to be the opposite of foamlike materials in that the solid material is viewed as non-connected. This implies that granular materials consist of separate granules or, in the case of sandstones, a granular structure may be identified although the granules may be cemented together to form a consolidated matrix. The *prismatic bundle* is a two-dimensional representation of the granular model and the solid material consists of bundles of unidirectional fibres or tubes.

The latter three types of materials broadly identify three types of *idealised* porous structures with distinct geometric characteristics and it can also be expected that they will have different influences on various transport processes. A first step in analysing transport in porous media in subsequent chapters is to determine whether the porous medium under investigation comply to one of these idealised types of materials, although it is acknowledged that many more different types of materials may be identified.

2.2.3 Homogeneous and heterogeneous porous media

A porous medium which is homogeneous has approximately equivalent arrangements of sets of voids spaces and solid phases. A more formal definition is given by Bear and Bachmat (1991), who stated that a porous medium domain is *homogeneous* with respect to a particular macroscopic geometric parameter characterising a specific phase of the domain, if that parameter has the same value at all points of the domain. On the other hand, if the geometric arrangement changes from point to point the medium is classified as *heterogeneous*. For example, if a porous medium has a homogeneous porosity then

$$\nabla \epsilon = \mathbf{0} \tag{2.1}$$

or in Cartesian tensor notation

$$\epsilon_{,i} = 0. \tag{2.2}$$

Therefore, a zero gradient implies a uniform value for the porosity which indicates a homogeneous material. Greenkorn and Kessler (1970) illustrated the difference between homogeneous and heterogeneous media in a similar manner by referring to the

permeability. Furthermore, as noted by Dullien (1991), a porous sample may be more homogeneous with regards to one property, for example porosity, than to another property, for example the permeability.

2.2.4 Isotropic and anisotropic porous media

Certain porous medium characteristics at a particular point in a porous domain may vary with direction. For example, the permeability of a porous material to the transport of a fluid may vary with direction depending on the geometric character of the porous medium. To incorporate this feature, a porous medium is considered to be *anisotropic* at a point with respect to a given property if that property varies with direction at that point. If the property does not differ with direction at a point, the material is considered to be *isotropic*. In isotropic materials there is no preferred direction above any other and the different phases constituting the porous domain are distributed randomly. In the course of this study attention is given to both isotropic and anisotropic porous media.

2.3 Macroscopic description of transport phenomena

In addition to understanding and classifying various characteristics of porous media, it is also important to be able to address various transport process in porous media. In principle, it would be possible to describe the transport of an extensive quantity in a porous medium by the microscopic balance laws of continuum mechanics along with appropriate interfacial and boundary conditions, for example, the Navier-Stokes equation together with the condition of no-slip at the fluid-solid interfaces in the case of momentum transport. However, the highly complex geometry of the fluid-solid interface precludes any direct solution of the microscopic boundary value problem. Furthermore, it is generally not possible to measure transport quantities at the microscopic level and any constitutive postulates will not be subject to experimental verification. In practice, only average values of the microscopic quantities are measurable and one is generally only interested in an average behaviour of the system. The microscopic transport equations must therefore be transformed to the macroscopic or laboratory level to be of practical value. At this level the porous medium may then be treated as a continuum by properly accounting for the role of each phase in the transport through the system of phases.

The concept of a change of scale is fundamental to various physical processes. According to Willis *et al.* (1991), the problem of translating a concept into a quantity that has practical utility requires an operational approach. In this approach, the concept is defined in terms of a reliable and reproducible set of experiments, or mental operations, which can then be used either to measure or recognise the quantity. For example, a quantitative description of temperature is achieved by defining the temperature in terms of a specific response of matter, rather than the intuitive physiological sensations of hot and cold. The operational approach is executed at a scale in which the phenomena defining the conceptual quantity can be observed or measured. The term scale, therefore, implies the level of measure for a physical phenomenon. The measurement then reflects the average effect of all the phenomena which occur at scales that are at or below the scale of the local measurement. We have, in effect, already applied a change of scale from the molecular to the microscopic level in the definition of a phase presented in Section 2.1.1.

The next step after such physical quantities as mass, momentum and thermal energy are operationally defined, is to determine the characteristics of the defined quantities. It has been found through observation that these quantities are conserved, which means that they satisfy balance laws or rate equations (Willis *et al.*, 1991). Therefore, the operational and rate concept allows mathematical quantification of the conservation principles at the operational scale, which, in the case of transport in porous media, is known as the macroscopic scale. At this scale measurement techniques of physical quantities, such as the mixing cup technique to determine concentrations of chemicals, or permeameters to determine the hydraulic conductivity (Sudicky, 1986), always involve a sample of pores and reflect the average behaviour in a number of microscopic channels. Another change of scale to the megascopic level may be employed when macroscopic heterogeneities appear in large field scale situations (Bear and Bachmat, 1991). A review of some change of scale methods in various transport processes is provided by Wheatcraft and Cushman (1991).

Initial attempts at attaining macroscopic transport equations relied on descriptive models of an empirical or geometric nature. The formulation of these models usually begins with a mathematical or physical description of the system where each phase is considered to be separate and occupying a different portion of space. The final set of field equations is then written in terms of material properties for each phase which are continuous and defined over the whole space. *Empirical models* are usually aided by dimensional analyses and other theoretical considerations and aim to relate the transport coefficients which appear in the macroscopic balance laws to macroscopic material properties and packing structure. According to Kemblowski and Michniewicz (1979),

Blake in 1922 was the first to introduce two dimensionless groups of parameters, namely a dimensionless friction factor and a modified Reynolds number, which allowed the correlation of experimental data of the flow of Newtonian fluids through granular beds of different heights as well as different shapes and dimensions of the granular filling. These groups are usually written as the modified friction factor

$$f_{BK} = \frac{\Delta P}{\rho q^2} \frac{d_n}{L} \frac{\epsilon^3}{(1-\epsilon)} \tag{2.3}$$

and the modified Reynolds number

$$Re_{BK} = \frac{q d_n \rho}{\mu(1-\epsilon)} \tag{2.4}$$

where ΔP means the pressure drop due to friction, ρ is the fluid density, q is the magnitude of the superficial velocity, d_n is an effective particle diameter, L is the bed height and μ is the dynamic viscosity of the fluid.

In the application of *geometric models*, one usually postulates a geometry which bears some resemblance to the porous medium, yet is sufficiently simple to allow the governing differential equations to be solved. Geometric pore structural models for fluid transport may be subdivided into two broad categories. The first category considers transport in porous media as flow around submerged objects and consists of arrays of spherical particles or flow around cylinders. These models are also known as *drag models*, since they rely in one way or another on Stokes' law. The permeability is obtained by solving the Navier-Stokes equations for flow over these objects and then the total resistance to the flow is compared with Darcy's law from which the permeability is then calculated. Often these calculations are aided by unit cells which usually contain a single sphere or cylinder, or only part of such an object. By repeating such cells the collection of objects constituting the idealised porous material is retained. Some of the models following this approach are provided by Brinkman (1947a; 1947b) and Happel and Brenner (1965), while a review of some other drag models is provided by Scheidegger (1974) and Kaviany (1995). The unit cells associated with drag models may be combined with numerical analyses to study transport in porous media as illustrated by Sangani and Acrivos (1982) and Zick and Homsy (1982).

In the second category, the pore structure is modelled by arrays of capillary tubes or conduits and these models are generally known as *capillary models* or *hydraulic radius models*. In probably one of the simplest and most well-known capillary models, the porous medium is modelled as consisting of a bundle of cylindrical capillary tubes of

possibly different diameters and equal lengths parallel to the direction of flow. This model can readily be extended to include tortuous tubes. When considering creeping flow, or low Reynolds number flow, the transport of momentum is obtained by assuming the flow to be fully developed in a capillary and by applying Hagen-Poiseuille's law to a specific tube. The macroscopic momentum balance law is then expressed in terms of macroscopic parameters of the model, such as the porosity, tortuosity and average diameter of the pores, which are then attributed to the actual porous medium (Dullien 1979; Rumpf and Gupte, 1971). Hydraulic radius models resulted in the Carman-Kozeny equation for flow at low Reynolds numbers, the Blake-Kozeny equation, the Burke-Plummer equation and the Ergun equation (Carman, 1937, 1956; Ergun and Orning, 1949; Bird *et al.,* 1960; Rumpf and Gupte, 1971). The Ergun equation accounts for flow at both low and intermediate Reynolds numbers and was constructed by Ergun and Orning (1949) by employing the hydraulic radius model. The Ergun equation, as well as a different model developed by Ahmed and Sunada (1969), have been evaluated by MacDonald *et al.* (1979) using a substantial amount of data. They concluded that the general physical model which states that the flow resistance in flow through any porous medium is the sum of a viscous contribution and an inertial contribution is adequate and the rather simple model of a porous medium as a set of parallel non-connected identical channels is reasonably satisfactorily for prediction of flow rate and pressure drop behaviour for unconsolidated media. However, MacDonald *et al.* (1979) also noted that the Ergun equation is only valid over a certain porosity range, which may be attributed to the over-simplification in the Kozeny-Carman theory in which straight parallel passages were assumed as the internal structure of the porous medium. Some other capillary models which yield adequate results are the Carman-Kozeny model (Carman, 1937; 1956) and the model of Comiti and Renaud (1989).

The main features of capillary models are summarised in Appendix A with specific reference to the Carman-Kozeny model. With these type of models it is sometimes difficult to determine certain geometric parameters of the porous medium and some of them are combined into coefficients, such as the Kozeny constant, which have to be determined experimentally (Scheidegger, 1974). Another capillary-type model, namely that of Comiti and Renaud (1989), also yields adequate results for fluid transport in porous media. In subsequent chapters some of the present results are compared to this model and, therefore, it is also presented in more detail in Appendix A. Reviews of some capillary models which are used to model fluid transport, electric transport and dispersion in porous media are presented by Dullien (1979), Scheidegger (1974), Bear (1972) and Nunge and Gill (1970).

As noted in Appendix A, special attention needs to be devoted to the expression for

the velocity which is used to transform the Hagen-Poiseuille equation in a tube to the macroscopic level. At first the average velocity in a tube was replaced by the macroscopic measurable velocity, known as the superficial or seepage velocity, q_i. It was first noted by Dupuit (Carman, 1936) that the macroscopic velocity must be less than the actual velocity within the pores and he suggested that the actual velocity be replaced by the interstitial velocity, u_i, where the magnitude of these velocities are related by

$$u = \frac{q}{\epsilon}. \tag{2.5}$$

This relationship became known as the Dupuit-Forchheimer relation (Scheidegger, 1974; Dullien 1979). However, Carman (1936) pointed out that the interstitial velocity represents only the component of the actual velocity which is parallel to the direction of flow. He noted that one must still correct for the fact that a hypothetical fluid particle, represented in the macroscopic flow equations and flowing with velocity q_i, covers a path length, L, in the same time as an actual fluid particle flowing with velocity w_i, covers an *average effective path length*, L_e. He, therefore, suggested that the average velocity in the pores be replaced by the average pore velocity w_i where

$$w = u\left(\frac{L_e}{L}\right) = \frac{q}{\epsilon}\left(\frac{L_e}{L}\right). \tag{2.6}$$

In this manner Carman extended the Dupuit-Forchheimer relation and in this process he opened a can of worms. The ratio L_e/L was termed the tortuosity, but since it appears in the pressure gradient equation of the Carman-Kozeny model as a squared quantity, many scientists refer to the squared quantity as the tortuosity (Bear, 1972). Furthermore, the exact meaning of L_e was never quantified and its actual value is seldom if ever known (Dullien, 1979). To the knowledge of the author a formal theoretical proof, without reference to a specific porous medium model, does not exist for (2.6), although expressions for tortuosity have been derived in context of other transport phenomena. Furthermore, (2.6) is only a scalar equation and it is usually applied to isotropic and anisotropic media indifferently. Carman (1937) and other investigators considered the tortuosity to be a universal constant which is independent of the porous structure, for example Haring and Greenkorn (1970) gave $L_e/L = 2.25$.

A class of geometric models which incorporates the interconnection of the pore-space is *network models*. According to these models, the flow domain, which may be one-, two- or three-dimensional, are filled with a network of capillaries which intersect at lattice points. Many different networks may be developed, such as cubic or hexagonal networks

(Dullien, 1979). It is also possible to incorporate capillary elements with different size distributions, lengths and hydraulic conductivities such as in the permeability model of Dullien (1975), or to introduce a statistical element into the configurations as proposed by Schopper (1966). Transition to the macroscopic level is similar to the capillary models, except that certain network sections may be grouped in a unit cell or a representative unit cell which may be used as building blocks of the porous domain and which can readily be used for numerical calculations. Network models are also used for analysing other transport phenomena, such as dispersion (Charlaix and Gayvallet, 1991; Charlaix *et al.*, 1988a).

Another type of porous medium model which relies extensively on computer simulations is the *lattice gas cellular automaton model* (Rothman, 1988). In this model the porous domain is covered by two-dimensional triangular lattices. The fluid is represented by a set of identical boolean particles with discrete velocities. The particles can have either a velocity of unit value along one of the six directions of the lattice or be at rest on a node of the lattice. This multiple occupancy of a lattice node is subject to an exclusion principle, which states that at a given node no two particles can have the same velocity. Therefore, a lattice node can be empty or occupied up to a maximum of seven particles. The time evolution of the system proceeds in two steps, namely propagation and collisions. During the propagation step, each particle moves one lattice unit in a direction determined by its velocity or it stays at rest. In the collision step, particles undergo instantaneous collisions at the lattice nodes during which their velocities are modified according to the conservation of mass and momentum. In the lattice gas model it is not always clear how to relate microscopic quantities to macroscopic measurable quantities and physical quantities are usually expressed in lattice units. Lattice gasses have been used to study permeability (Gutfraind and Hansen, 1994) and some structural parameters such as tortuosity (Knackstedt and Zhang, 1994).

Besides assuming some geometric pore structure and aiming to treat the system analytically, it is also possible to replace the uncertainty of knowing the pore structure and related transport phenomena with a stochastic or statistical model. As outlined by Scheidegger (1974), in a statistical model the pore structure properties and the transport variables are considered as random space functions which define specific states of the system. The actual porous medium and the transport processes are then considered as the ensemble of states of the random space functions that describe them. The expectation value of an observable physical quantity is the *statistical average* of that quantity over all states of the ensemble. For these expectation values, one tries to deduce predictions from what is known about transitions between the states in the ensemble, based on the microscopic dynamic equations. Often, in a time-stationary

process, one can make the ergodic hypothesis which states that a particularly chosen system will, in time, encounter all the states that are possible at any one given time. This hypothesis implies that the ensemble averages and time averages may be interchanged. In principle, the statistical average must be carried out over a sufficiently large number of realisations. Since, usually, only a single realisation is possible, it is customary to view the porous medium as being composed of an ensemble of blocks of geologic material in which the individual blocks are homogeneous and isotropic. The advantage of the statistical approach is that it precludes the introduction of restrictions on the geometry of the porous material, although the statistical model has been combined with geometrical models, for example in the model of Haring and Greenkorn (1970) and Guin *et al.* (1971). Stochastic methods have been applied to a variety of flow phenomena, such as fluid transport, heat conduction and dispersion (Scheidegger, 1954; 1961; Dagan, 1989).

Instead of taking the statistical average of the microscopic transport equations, one can also take a *spatial average* of these quantities over a representative elementary volume of the porous medium (Dagan, 1989). This approach of taking a spatial average is generally known as the volume averaging theory and presents a different approach for porous media modelling. Although the volume of integration is statistically selected, this approach is essentially a deterministic approach because the microscopic balance laws are averaged over the volume under consideration and it is not necessary to introduce microscopic constitutive equations. In obtaining the macroscopic equations it is also not required to invoke any particular porous medium model. In this study transport phenomena are considered by making use of the volume averaging theory and it is, therefore, discussed in more detail in the next section.

2.4 The volume averaging theory

2.4.1 The REV and averaging operations

In a porous system composed of interpenetrating continua, each phase occupies only part of the space and is separated from other phases by highly irregular surfaces. In such a multiphase mixture the variables and balance laws which describe each continuum are defined at the microscopic level. These microscopic quantities and equations may be transformed to the macroscopic level by the process of volumetric averaging which will enable one to view the porous medium as a continuum. The macroscopic balance laws then describe the average behaviour of the system in terms of variables which are

continuous functions at the macroscopic level.

This approach was given impetus and put on a sound mathematical foundation when an averaging theorem was provided for porous media which expresses the volumetric average of a spatial derivative as a spatial derivative of the volumetric average of a specific phase quantity. This theorem, also referred to as Slattery's averaging theorem, was developed by Slattery (1967) and enables one to obtain a volumetric average of a microscopic equation governing the transport of a specific phase entity of a multiphase continuum. Since these initial steps the averaging theorem has been improved and extended to also include time derivatives (Whitaker, 1969; Bachmat, 1972; Hassanizadeh and Gray, 1979; Bear and Bachmat, 1991; Gray and Lee, 1977). An additional summary of the volume averaging approach, which includes derivations of certain averaging rules, is provided by Tucker and Dessenberger (1994). The volume averaging approach has been applied to a number of transport phenomena such as fluid transport in porous media (Whitaker, 1969; Bear and Bachmat, 1991), dispersion phenomena (Gray, 1975; Tompson and Gray, 1986a; 1986b; 1986c) and electrical conduction in porous media (Suman and Ruth, 1993). Although Bear and Bachmat (1991) give a clear exposition of the volume averaging theory, more simplified derivations of some of the averaging rules are provided in Appendix B.

According to the volume averaging theory, the macroscopic equations which describe the system are derived by replacing the interpenetrating continua by a conceptual model in which each of the phases is assumed to behave as a continuum that completely fills the entire domain. These interpenetrating continua are then replaced by overlapping and coexisting continua (Drew, 1983). For each point in the macroscopic space, average values of space variables are taken over elementary volumes which are centred at each point. These specific elementary volumes over which the average is taken are known as Representative Elementary Volumes (REV's) and these volumes are defined such that their shape, size and orientation are independent of location and of time (Gray and Lee, 1977). This implies that regardless of which position is selected, the REV remains unchanged (Cushman, 1982). In the macroscopic field, an REV represents and characterises a physical point. The average is taken regardless of whether, in the real domain, this point falls within that phase or outside it. By traversing the entire porous medium with a moving elementary volume, and thus assigning average values to every point, a field of macroscopic variables is obtained which are differential functions of the space coordinates. A two dimensional representation of an REV is schematically illustrated in Figure 2.1. It contains both solid phases and void spaces and the centroid of the REV with respect to an inertial reference frame is indicated by the vector $\overline{x}_i$. The position vector of any point within the REV, also relative to an inertial reference

frame, is indicated by x_i. The vector,

$$\overset{\circ}{x}_i = x_i - \overline{x}_i \tag{2.7}$$

is the position vector of points relative to the centroid of the REV as illustrated in Figure 2.1.

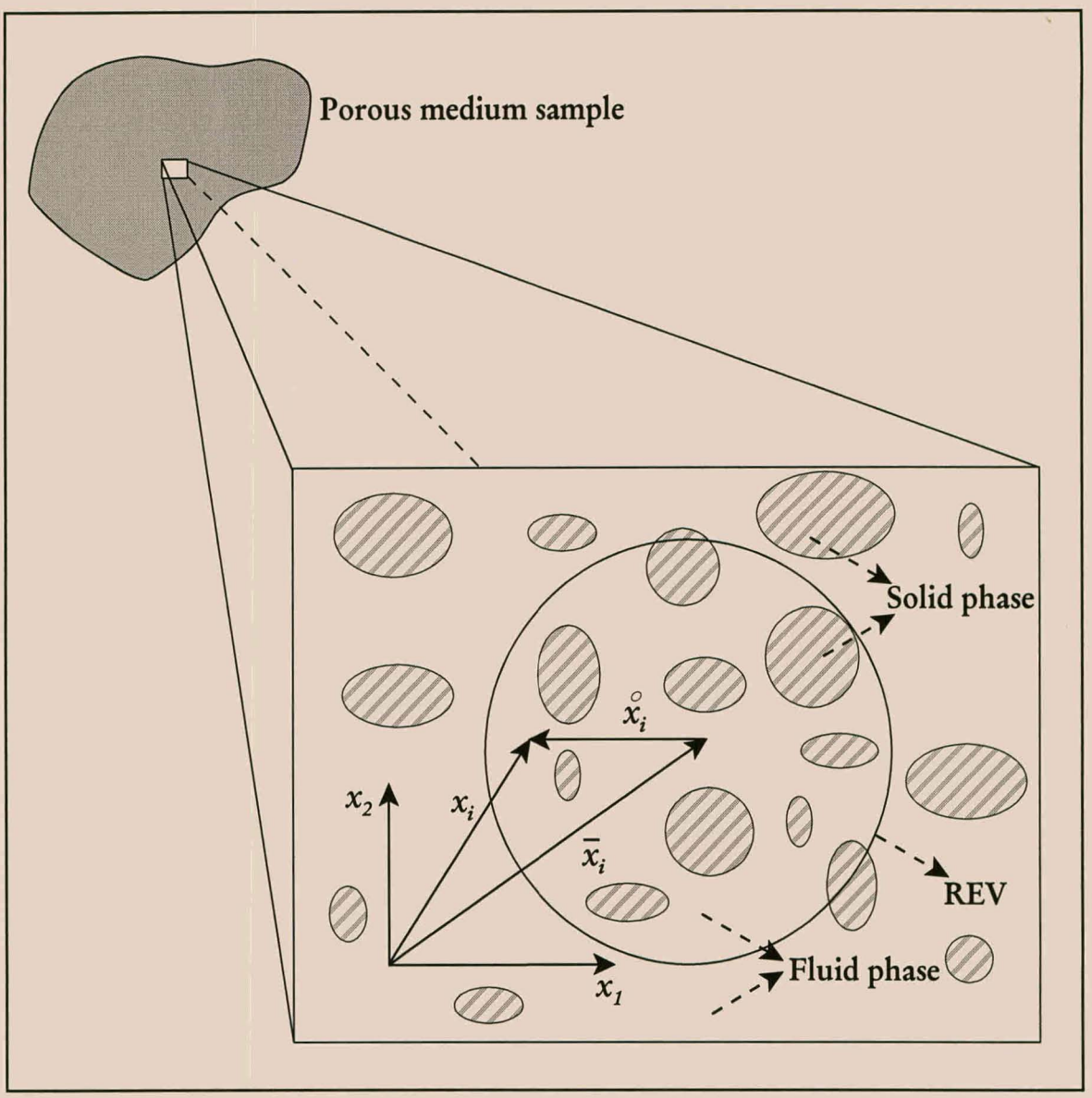

Figure 2.1. A macroscopic region and Representative Elementary Volume (REV) with the associated position vectors.

The averaged quantities are related to the microscopic quantities through averaging operators. In general three different operators are defined, namely the phase average operator, the intrinsic phase operator and the mass average operator (Hassanizadeh

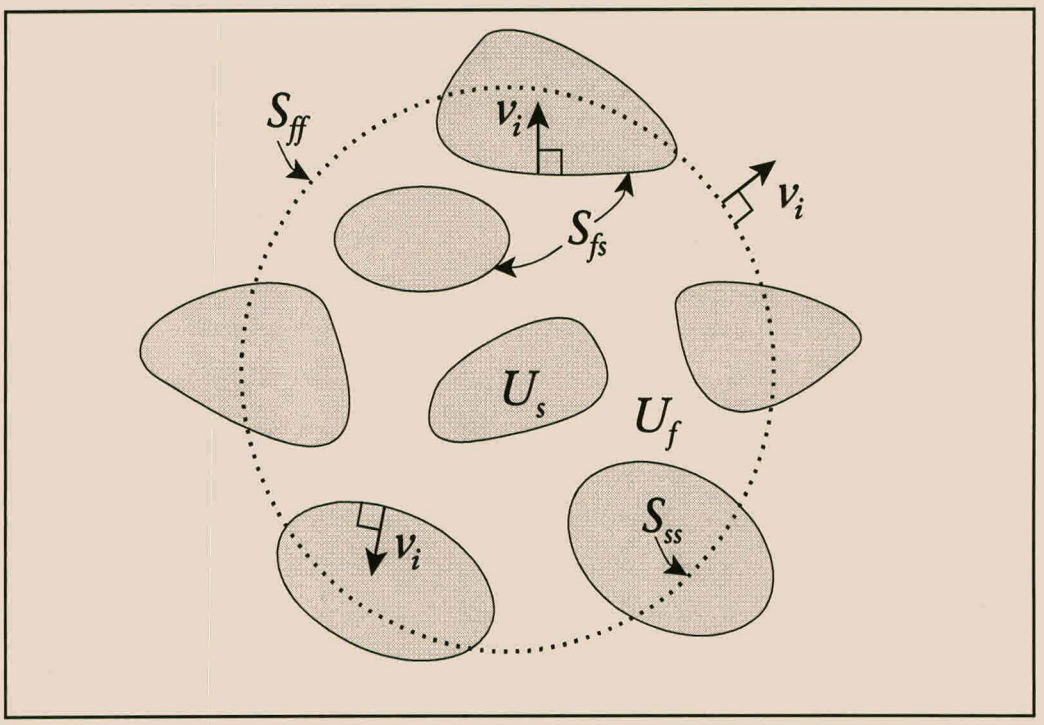

Figure 2.2. Schematic two-dimensional circular REV indicating the normal vectors on interfaces and that $S_o = S_{ff} + S_{ss}$ *and* $S_f = S_{ff} + S_{fs}$.

and Gray, 1979; Bear and Bachmat, 1991). The *phase average operator* is defined as

$$\langle \phi_{jkl\ldots} \rangle (\overline{x}_i, t) \equiv \frac{1}{U_o(\overline{x}_i)} \iiint_{U_f(\overline{x}_i)} \phi_{jkl\ldots} (\overline{x}_i + \overset{o}{x}_i, t)\, dU \tag{2.8}$$

where $\phi_{jkl\ldots}(x_i, t)$ is an extensive microscopic tensorial phase quantity of interest, $U_o(\overline{x}_i)$ is the total volume of the REV and the integral is taken over only the void or fluid volume, $U_f(\overline{x}_i)$, of the REV centred at $\overline{x}_i$. In the present study we only consider porous media which consist of two phases, namely a solid matrix and a void space which is filled with a single fluid phase. We, therefore, also refer to the void space as the fluid phase. A two-dimensional representation of a two phase REV is schematically illustrated in Figure 2.2 where the various surface areas as well as the normal vectors on interfaces are indicated. The microscopic entity $\phi_{jkl\ldots}$ as employed in (2.8), and subsequent equations, represents any function defined at the microscopic level, while the average $\langle \phi_{jkl\ldots} \rangle$ is only associated with the centroid of the averaging volume. To be more precise about the functional dependence of these variables, we express the averaged quantity as $\langle \phi_{jkl\ldots} \rangle (\overline{x}_i, t)$ indicating that it is associated with the centroid, while the integration of the microscopic quantity $\phi_{jkl\ldots} (\overline{x}_i + \overset{o}{x}_i, t)$ is performed with respect to the components of the relative local position vector, $\overset{o}{x}_i$. Therefore, the integration is performed on the microscopic local $\overset{o}{x}_i$-coordinate system attached to the centroid of the REV. The void volume over which is integrated, $U_f(\overline{x}_i)$, is also a function of the centroid,

since each different macroscopic point is associated with a different averaging volume. During this study, the functional dependence of these microscopic and macroscopic quantities are understood and will not always be explicitly indicated.

The *intrinsic phase average operator* of the fluid property $\phi_{jkl...}$ is defined as

$$\langle \phi_{jkl...} \rangle^f \equiv \frac{1}{U_f} \iiint_{U_f} \phi_{jkl...} \, dU \tag{2.9}$$

and in this case the integral is weighed to the void volume. The *mass average operator* is given as

$$\langle \phi_{jkl...} \rangle_m \equiv \frac{1}{\langle \rho \rangle^f U_f} \iiint_{U_f} \rho \, \phi_{jkl...} \, dU \tag{2.10}$$

where ρ is the bulk microscopic density function.

The values of all averaged quantities at any macroscopic point in the porous medium must be singled valued functions of the location of that point and of time, independent of the size of an REV. Therefore, certain restrictions have to be put on the size of an REV (Bear and Bachmat, 1991). As illustrated by Whitaker (1966; 1969) and Hassanizadeh and Gray (1979), if we were to compute the phase average, $\langle \phi_{jkl...} \rangle$, by using different sized averaging regions which may vary from a very small size to a very large size, the phase average will initially show large oscillations which tend to smooth out for a certain range of averaging volumes and if the size of volumes are further increased oscillations will again set in. This behaviour is explained by realising that if the centroid associated with the averaging volume, U_o, was in the solid phase, then U_f would be zero for small values of U_o. As the averaging volume, U_o, becomes larger, portions of the fluid are contained within it and the average increases from zero going through some fluctuations representative of the variations in the point values of $\phi_{jkl...}$ and because varying portions of the void volume are included in the averaging volume. As the size of this region increases these fluctuations tend to diminish and eventually within some interval of sizes for the averaging volumes, the averaged quantities will be sufficiently smooth to be independent of the size of the averaging volume. In this interval the averaging volume may be referred to as a Representative Elementary Volume. Therefore, the characteristic length of the REV, l, must be such that the average obtained is insensitive to small changes in this length. One requirement for the size independence of the REV is that

$$l_{min} \ll l \tag{2.11}$$

where the microscopic characteristic length l_{min} is representative of the distance over which significant variations in the microscopic variable $\phi_{jkl...}$ take place. In general, l_{min} is associated with a mean pore diameter or diameter of sand grains in a packed bed (Whitaker, 1969).

Equivalently, there also exists an upper bound on the size of an REV, since a further increase in the size of the averaging volume may cause large inhomogeneities of the medium to affect the stability of the average quantities. This restriction on the size of the averaging volume implies that averaged quantities should be nearly uniform or vary linearly over the averaging volume so that when averaged quantities are averaged they may be taken out of the volume integrals. The volume average of a phase quantity is allocated to the centroid of an REV which consists of many points, each of which is the centroid of a different REV. Therefore, when an average of average values is taken the size of the REV must be such that the distribution of average values across the REV is either uniform or linear so that the average value at the centroid is a representative average value and may be removed from the integration. This limit in the size of an REV may be investigated, similar to the analysis of Whitaker (1969), by taking a Taylor expansion of $\langle \phi_{jkl...} \rangle (x_i, t)$ around the centroid of an REV centred at $\overline{x}_i$, which yields

$$\langle \phi_{jkl...} \rangle = \langle \phi_{jkl...} \rangle_{\overline{x}_i} + \overset{\circ}{x}_i \left(\langle \phi_{jkl...} \rangle_{,i} \right)_{\overline{x}_i} + \frac{1}{2} \overset{\circ}{x}_i \overset{\circ}{x}_r \left(\langle \phi_{jkl...} \rangle_{,ir} \right)_{\overline{x}_i} + \cdots \tag{2.12}$$

The subscript $\overline{x}_i$ indicates that the differentials are evaluated at the centroid of the REV. If we take the phase average of this equation we obtain

$$\begin{aligned} \langle \langle \phi_{jkl...} \rangle \rangle &= \langle \phi_{jkl...} \rangle_{\overline{x}_i} \frac{1}{U_o} \iiint_{U_f} dU + \left(\langle \phi_{jkl...} \rangle_{,i} \right)_{\overline{x}_i} \frac{1}{U_o} \iiint_{U_f} \overset{\circ}{x}_i \, dU \\ &\quad + \frac{1}{2} \left(\langle \phi_{jkl...} \rangle_{,ir} \right)_{\overline{x}_i} \frac{1}{U_o} \iiint_{U_f} \overset{\circ}{x}_i \overset{\circ}{x}_r \, dU + \cdots \\ &= \epsilon \langle \phi_{jkl...} \rangle_{\overline{x}_i} + \left\langle \overset{\circ}{x}_i \right\rangle \left(\langle \phi_{jkl...} \rangle_{,i} \right)_{\overline{x}_i} + \frac{1}{2} \left\langle \overset{\circ}{x}_i \overset{\circ}{x}_r \right\rangle \left(\langle \phi_{jkl...} \rangle_{,ir} \right)_{\overline{x}_i} + \cdots \end{aligned} \tag{2.13}$$

An order of magnitude estimate for the latter derivative on the right hand side of (2.14) yields

$$\left(\langle \phi_{jkl...} \rangle_{,ir} \right)_{\overline{x}_i} = O\left(\frac{\langle \phi_{jkl...} \rangle}{l_{max}^2} \right) \tag{2.14}$$

where l_{max} is the characteristic length for volume averaged quantities and it is representative of the distance over which significant variations in the volume averaged quantities

take place (Whitaker, 1969). An order of magnitude for the latter integral term gives

$$\left\langle \overset{o}{x}_i \overset{o}{x}_j \right\rangle = \frac{1}{U_o} \iiint_{U_f} \overset{o}{x}_i \overset{o}{x}_j \, dU = \boldsymbol{O}(l^2). \tag{2.15}$$

For homogeneous porous media the phase average $\left\langle \overset{o}{x}_i \right\rangle$ is zero, since the void space is distributed evenly around the centroid of the REV and the centroid of the fluid volume coincides with that of the REV (Quintard and Whitaker, 1994b, eq(2.24); Bear and Bachmat, 1991, p123). However, in general it follows that

$$\left\langle \overset{o}{x}_i \right\rangle = \frac{1}{U_o} \iiint_{U_f} \overset{o}{x}_i \, dV = \boldsymbol{O}(l) \tag{2.16}$$

although Quintard and Whitaker (1994d, eq(1.13)) obtain a more general order of magnitude expression which reduces to (2.16) for an REV. For the spatial derivative evaluated at the centroid it follows that

$$\left(\langle \phi_{jkl\ldots} \rangle_{,i} \right)_{\overline{x}_i} = \boldsymbol{O}\left(\frac{\langle \phi_{jkl\ldots} \rangle}{l_{max}} \right). \tag{2.17}$$

Equation (2.14) may thus be written as

$$\langle \langle \phi_{jkl\ldots} \rangle \rangle = \epsilon \langle \phi_{jkl\ldots} \rangle_{\overline{x}_i} + \boldsymbol{O}\left(\frac{l \langle \phi_{jkl\ldots} \rangle}{l_{max}} \right) + \boldsymbol{O}\left(\frac{l^2 \langle \phi_{jkl\ldots} \rangle}{l_{max}^2} \right). \tag{2.18}$$

For the phase average of a phase average to be equal to the phase average it then follows that

$$l \ll l_{max} \tag{2.19}$$

which gives

$$\langle \langle \phi_{jkl\ldots} \rangle \rangle = \epsilon \langle \phi_{jkl\ldots} \rangle. \tag{2.20}$$

In view of (2.20), the average of an average is equal to the average at the centroid if the average is either uniform or vary linearly over the REV. Under these conditions Gray (1975) refers to the average as being well-behaved. From this result it is also apparent

that the volume averaging theory should be applied with caution near boundaries where there might be a sharp change in macroscopic behaviour of an average quantity.

Therefore, from (2.11) and (2.19) the size of an REV is restricted by both an upper and lower limit, which may be summarised as

$$l_{min}^3 \ll U_o \ll l_{max}^3. \tag{2.21}$$

As noted by Whitaker (1986) this inequality is a general restriction which is satisfied by many systems of practical importance and it is not an inherent restriction to the volumetric averaging approach. In analysing fluid transport in porous media, he therefore determines various other length scale constraints appearing in the averaged transport equations which have to be complied to.

Equation (2.20) is different from the expression for the phase average of an average provided by Whitaker (1969) and Gray (1975) in that the porosity, ϵ, does not appear in their expressions. In their analyses the fact that the phase average also exists in the solid phase, U_s, implies that the phase average of an average or a constant should also be taken over the solid phase and not only over fluid phase. In the present approach we do not wish to have two different types of phase averaging operators and adhere to the phase average defined in (2.8) and integrate only over the fluid phase although the quantity being integrated may also exist in the solid phase. This discrepancy regarding the definitions of the phase average when averages of averages or the average of a constant is taken is still a question open to debate and is also mentioned by Quintard and Whitaker (1994a).

In a rigorous mathematic statistical manner Bear and Bachmat (1991) also relates the size of an REV to certain geometric characteristics of the material in an REV and reach essentially the same conclusion as the restriction of inequality (2.21). Their argument is based on the statistical elements of a spatial average which is taken over an ensemble of averaging volumes to obtain a uniform estimation value for certain porous media characteristics. One of their requirements for the range of an REV is that the porosity should be nearly uniform or vary linearly with position for small changes in the size of the REV. This is essentially the same conclusion as (2.20) if $\phi = 1$. Therefore, the REV is defined specifically so that it represents the smallest volume around a macroscopic point such that adding or subtracting from it one or several channels has a negligible effect on the value of the volumetric porosity. In the macroscopic field, an REV therefore represents and characterises a physical point and may also be interpreted as an infinitesimal element of volume. However, it is not necessary to

actually select an explicit averaging volume when employing the averaging theory, but one usually assumes its existence on grounds of the particular material. Furthermore, when considering various transport processes where the state of each phase is specified by a set of relevant state variables, a range for an REV should be selected for each state variable and the volume averaging process involving them can be employed only if a common range of REV's can be found for all of them.

One advantage of the volume averaging technique is the fact that it guarantees that no microscopic terms will inadvertently be left out of the macroscopic equations (Drew, 1983). Actually, the averaging process reveals macroscopic effects which might not have been anticipated. Additionally, volume averaging provides useful physical insight into the relationships between microscopic and macroscopic behaviour. Another advantage of the volume averaging approach is the fact that it produces mathematical parameters which correlate with certain physical parameters which are directly measurable and is one of the key reasons for using this approach. However, not all averaged quantities are necessarily directly measurable. For instance, in the case of fluid discharge through a porous medium the *interstitial velocity* is given by

$$u_i = \langle v_i \rangle^f \equiv \frac{1}{U_f} \iiint_{U_f} v_i \, dU \tag{2.22}$$

where v_i is the actual microscopic velocity within the fluid phase. Although the intrinsic phase average velocity is equal to v_i when the latter is constant and therefore reasonably representative of flow conditions in the pore-space, it is not directly measurable. It is more appropriate to express the macroscopic momentum balance equation in terms of the *superficial velocity*,

$$q_i = \langle v_i \rangle \equiv \frac{1}{U_o} \iiint_{U_f} v_i \, dU \tag{2.23}$$

which is directly measurable with, for instance, a flowmeter, but less representative of the internal flow conditions than the intrinsic phase average velocity. Similar arguments also apply to other transport phenomena, for example, when considering chemical dispersion in a porous medium, the macroscopic concentration of a specific chemical species measured with the mixing cup technique is the phase average concentration

$$\langle c \rangle \equiv \frac{1}{U_o} \iiint_{U_f} c \, dU \tag{2.24}$$

since the interstitial concentration in each pore cannot be measured. When considering

flow of electric current through a porous medium saturated with an electrolyte, the current measured over such a sample would once again be the phase average current

$$\langle i \rangle \equiv \frac{1}{U_o} \iiint_{U_f} i \, dU. \tag{2.25}$$

Although the intrinsic phase average of transport quantities might be nearer in value to the actual microscopic quantity, it is preferred to use the phase averaged description, since it is physically measurable. However, when measuring the pressure gradient by placing pressure taps along a packed column during flow through such a column (Montillet *et al.*, 1992), it is the interstitial pressure

$$\langle p \rangle^f = \frac{1}{U_f} \iiint_{U_f} p \, dU \tag{2.26}$$

which is measured and in this case it would be more accurate to use the intrinsic phase average of the pressure in macroscopic balance equations (Quintard and Whitaker, 1993). Therefore, when employing the volume averaging theory it is important to have a clear understanding of which volume averaged parameters are determined through experimental measurements and to employ these parameters in the averaged balance equations.

2.4.2 Averaging identities and rules

Besides defining averaging operators, a number of averaging identities and rules have also been established. An important quantity is the *deviation* of $\phi_{jkl\ldots}$, defined as

$$\overset{o}{\phi}_{jkl\ldots}(x_i, t) \equiv \phi_{jkl\ldots}(x_i, t) - \langle \phi_{jkl\ldots} \rangle^f (\overline{x}_i, t). \tag{2.27}$$

It is important to note that the deviation of a microscopic quantity is defined with respect to the intrinsic phase average and it is not defined in the solid phase. It was originally incorrectly defined with respect to the phase average by Whitaker (1969), but later corrected due to physical considerations by Gray (1975). It is also important to note that the position vector relative to the REV centroid, $\overset{o}{x}_i$, is not the same as the deviation defined in (2.27). According to (2.27) the deviation $\overset{o}{\phi}_{jkl\ldots}$ is not unique, since it is dependent on the phase average taken with respect to the REV under consideration. For a different REV but the same point, x_i, one would then obtain a different value for the deviation. An alternate definition, which yields a unique deviation for each point,

might be to define the deviation relative to the intrinsic phase average obtained from the REV whose centroid coincides with that of the point under consideration, i.e. x_i. In this study we adhere to the definition in (2.27), but as the volume averaging theory is applied to a wider variety of applications of various transport phenomena the difference in definitions might be alleviated.

Table 2.1. Volume averaged identities.[1]

No.	Ref. eqn.	Identity
1	B.6	$\langle \phi + \lambda \rangle = \langle \phi \rangle + \langle \lambda \rangle$
2	B.7	$\langle \beta\, \phi \rangle = \beta\, \langle \phi \rangle$
3	B.8	$\langle \phi \rangle = \epsilon \langle \phi \rangle^f$
4	B.9	$\left\langle \langle \phi \rangle^f \right\rangle^f = \langle \phi \rangle^f$
5	B.10	$\langle\langle \phi \rangle\rangle^f = \langle \phi \rangle$
6	B.11	$\left\langle \langle \phi \rangle^f \right\rangle = \epsilon \langle \phi \rangle^f$
7	B.12	$\langle 1 \rangle = \epsilon$
8	B.13	$\langle 1 \rangle^f = 1$
9	B.14	$\left\langle \overset{o}{\phi} \right\rangle = 0$
10	B.15	$\langle \overset{o}{\phi} \rangle = 0$
11	B.16	$\overset{o}{\overset{o}{\phi}} = \overset{o}{\phi}$
12	B.17 - B.19	$\left\langle \overset{o}{\phi}\, \langle \lambda \rangle \right\rangle = \left\langle \langle \phi \rangle\, \overset{o}{\lambda} \right\rangle = \left\langle \overset{o}{\phi}\, \langle \lambda \rangle^f \right\rangle = 0$
13	B.22	$\left\langle \overset{o}{\phi}\, \overset{o}{\lambda} \right\rangle = \left\langle \overset{o}{\phi}\, \lambda \right\rangle = \left\langle \phi\, \overset{o}{\lambda} \right\rangle$
14	B.23	$(\overset{o}{\phi\lambda}) = \overset{o}{\phi}\overset{o}{\phi} + \overset{o}{\phi}\, \langle \lambda \rangle^f + \langle \phi \rangle^f\, \overset{o}{\lambda} - \left\langle \overset{o}{\phi}\, \overset{o}{\lambda} \right\rangle^f$
15	B.24	$\langle \phi\, \lambda \rangle = \frac{1}{\epsilon} \langle \phi \rangle \langle \lambda \rangle + \epsilon \left\langle \overset{o}{\phi}\, \overset{o}{\lambda} \right\rangle^f$

If $\phi_{jkl\ldots}$ and $\lambda_{pqr\ldots}$ are any two tensorial quantities and β is a constant, we may also formulate some other identities such as those presented in Table 2.1. These identities

[1] ϕ and λ represent general Cartesian tensorial quantities, that is $\phi \equiv \phi_{jkl\ldots}$ and $\lambda \equiv \lambda_{pqr\ldots}$.

are formally defined in Appendix B.

As previously noted the averaging theory may be used to transform balance equations to the macroscopic level and for this we require a number of averaging rules which will enable the conversion of derivatives of functions to the macroscopic level. Some of these rules are presented in Table 2.2. In these rules ν_i is a unit vector normal to the orientated area element dS. On fluid-solid surfaces, S_{fs}, it is directed out of the fluid into the solid and on fluid-fluid surfaces, S_{ff} it is directed out of the averaging volume as indicated in Figure 2.2. The velocity v_i^b is the velocity of the boundary of a material volume as employed in Appendix B, where these rules are more formally derived.

Table 2.2. Volume averaging rules.

No.	Ref. eqn.	Averaging rule
1	B.39; B.56	$\langle \phi_{jkl\ldots} \rangle_{,i} = \frac{1}{U_o} \iint_{S_{ff}} \phi_{jkl\ldots} \nu_i \, dS$
2	B.39	$\langle \phi_{jkl\ldots} \rangle_{,i}^f = \frac{1}{U_f} \iint_{S_{ff}} \phi_{jkl\ldots} \nu_i \, dS - \frac{1}{\epsilon} \langle \phi_{jkl\ldots} \rangle^f \epsilon_{,i}$
3	B.61	$\langle \phi_{jkl\ldots,i} \rangle = \langle \phi_{jkl\ldots} \rangle_{,i} + \frac{1}{U_o} \iint_{S_{fs}} \nu_i \, \phi_{jkl\ldots} \, dS$
4	B.64	$\langle \phi_{jkl\ldots,i} \rangle = \left(\epsilon \langle \phi_{jkl\ldots} \rangle^f \right)_{,i} + \frac{1}{U_o} \iint_{S_{fs}} \phi_{jkl\ldots} \nu_i \, dS$
5	B.68	$\langle \phi_{jkl\ldots,i} \rangle^f = \langle \phi_{jkl\ldots} \rangle_{,i}^f + \frac{1}{U_f} \iint_{S_{fs}} \phi_{jkl\ldots} \nu_i \, dS + \frac{1}{\epsilon} \langle \phi_{jkl\ldots} \rangle^f \epsilon_{,i}$
6	B.67	$\langle \phi_{jkl\ldots,i} \rangle = \epsilon \langle \phi_{jkl\ldots} \rangle_{,i}^f + \frac{1}{U_o} \iint_{S_{fs}} \nu_i \overset{o}{\phi}_{jkl\ldots} \, dS$
7	B.63; B.65	$\epsilon_{,i} = -\frac{1}{U_o} \iint_{S_{fs}} \nu_i \, dS = \frac{1}{U_o} \iint_{S_{ff}} \nu_i \, dS$
8	B.74	$\left\langle \frac{\partial \phi_{jkl\ldots}}{\partial t} \right\rangle = \frac{\partial \langle \phi_{jkl\ldots} \rangle}{\partial t} - \frac{1}{U_o} \iint_{S_{fs}} \phi_{jkl\ldots} \, v_i^b \, \nu_i \, dS$

To obtain the correct correspondence between the real physical situation and the theoretically averaged quantities, it is important to adhere to some simple averaging criteria as noted by Hassanizadeh and Gray (1979):

- When an averaging operation involves integration, the integral multiplied by the infinitesimal element of integration must be an additive quantity, that is an extensive quantity where an extensive quantity is any quantity dependent on the size of the system. For example, the internal energy density function, E, is not additive. Since E is defined per unit mass, $E\,dU$, is not additive either. However,

the total internal energy, $\rho E dU$, is an additive quantity and an average defined in terms of this quantity will be physically meaningful. Therefore, both volume and areal averages may be taken, and even equated, provided that both are physically meaningful (Bear and Bachmat, 1983).

- The macroscopic quantities should exactly account for the total amount of the corresponding microscopic quantities. For example, the total macroscopic fluxes through a given boundary must be equal to the total microscopic fluxes through that boundary.
- The original physical concept of a physical quantity, as first introduced into classical continuum mechanics, must be preserved by proper definition of the macroscopic quantities. However, as indicated on the next section, in deriving macroscopic equations it is in general not necessary to distinguish between macroscopic quantities that should be obtained by areal averaging and those that should be obtained by volume averaging.
- The average value of a microscopic quantity must be the same function that is most widely observed and measured in the field or in laboratory practice.

By following these rules and criteria it is possible to obtain a unified approach bridging over several scientific disciplines of obtaining a volumetric average of an equation governing the transport of a specific phase entity of a multiphase continuum.

2.4.3 Areal averaging

Besides taking an average over an REV, one may also take an average over a Representative Elementary Area (REA). An REA may be viewed as the two-dimensional equivalent of an REV and it is also defined for every macroscopic point in the porous domain. Its size is also limited by length scale constraints and, similar to inequality (2.21), it may be summarised as

$$l_{min}^2 \ll A_o \ll l_{max}^2 \tag{2.28}$$

where A_o is the total area of the REA. Two areal averaging operators may be defined, namely the *areal average*

$$\langle \phi_{jkl\ldots} \rangle^A \equiv \frac{1}{A_o} \iint_{A_f} \phi_{jkl\ldots} \, dA \tag{2.29}$$

and the *areal intrinsic phase average*

$$\langle \phi_{jkl\ldots} \rangle^{fA} \equiv \frac{1}{A_f} \iint_{A_f} \phi_{jkl\ldots}\, dA. \tag{2.30}$$

Here A_o is the total area of the REA and A_f is the fluid area. Attention has been devoted to the relation between volume and areal averages and whether areal averages should only be applied to fluxes and volume averages only to quantities which are additive over volumes. The first question was addressed by Whitaker (1969), where he indicated that volume and areal averages may be equated if the same length scale constraints apply to both the REV and the REA. Bear and Bachmat (1983) indicate in a very lucid and logical exposition that the areal intrinsic phase average and volumetric intrinsic phase average are identical provided that the constraints in inequality (2.28) are satisfied and they additionally require that both the averaged quantities should be physically meaningful.

As previously noted, an extensive property of a substance is a quantity that depends on the size of the system. Volume, mass, energy, momentum and kinetic energy are examples of extensive properties. As noted by Bear (1972, p68), the property may be a scalar property, a vectorial property or a tensorial property of any rank. With each extensive quantity may be associated an intensive property, which is the amount of that property per unit volume of the system. Therefore, according to Bear and Bachmat (1991), if γ is the volumetric density of an extensive quantity and $v_{\gamma i}$ is the microscopic velocity of such a quantity, then

$$\frac{1}{U_f} \iiint_{U_f} \gamma v_{\gamma i}\, dU = \frac{1}{A_f} \iint_{A_f} \gamma v_{\gamma i}\, dS \tag{2.31}$$

where A_f is the fluid area of an REA normal to the macroscopic flow direction. According to this analysis the volume average of the momentum density of an extensive quantity is identical to the areal average of the flux of that quantity, since the momentum density of an extensive quantity is additive over volume and the flux of the specific quantity is additive over area. Another consequence of their analysis is that the volumetric porosity is equal to the areal porosity provided both the REV and REA share a common centroid (Bear and Bachmat, 1983; 1991). This applies for all possible orientations of the REA around the centroid.

The first step when deriving balance equations for flow through porous materials by employing the volume averaging theory, is to establish the balance equation at the microscopic level. The macroscopic equations are then obtained by applying the averaging

rules to the microscopic equations. The macroscopic equations are valid at each point of the porous domain and may contain additional terms to those in the original microscopic system. A closer analysis of these additional terms are considered in the next section.

2.5 Closure of the macroscopic equations

Although the information regarding the influence of the microstructure on transport phenomena is smoothed out through the averaging process, it cannot be eliminated and it will appear in the macroscopic equations in the form of new variables which arise through the course of the averaging process. As noted by Wheatcraft and Cushman (1991), any transformation of scales implies a loss of information of the geometric configuration of the solid-void interface which manifest itself in the form of new terms in the averaged equations which have no microscopic counterpart. These additional terms, for example the surface integrals appearing in the expressions listed Table 2.2, must be replaced by constitutive parameters which allow prediction of material properties and transport behaviour at the macroscopic level. However, without the introduction of constitutive relations, the averaged equations thus contain some terms which are not macroscopically measurable and, therefore, these equations are referred to as open equations. The process whereby these additional variables are constitutively modelled is referred to as closure of the macroscopic equations.

One method to obtain closure of the macroscopic equations is to develop macroscopic constitutive relations analogous to those appearing at the microscopic level or through some theoretical development. The information about the porous medium microstructure is then lumped into coefficients which must be determined experimentally. For example, in calculating permeabilities Bear (1972) and Slattery (1972) introduce the bulk flow resistance through definition, while Whitaker (1969) employs an arbitrary linear geometric transformation to obtain the permeability as experimental coefficient. This type of closure procedure has further been applied by Bear and Bachmat (1991) and Whitaker (1967) to diffusion, dispersion and fluid transport in porous media. Empirical coefficients which have to be determined for these examples are the tortuosity, the effective diffusion coefficient, the dispersion coefficient and the permeability. A slightly different approach was followed by Tompson and Gray (1986a; 1986b; 1986c) when analysing dispersion where they propose to develop a completely separate balance law for the dispersive flux in terms of certain empirical coefficients. However, the information regarding the microstructure is still captured in empirical coefficients.

Another approach to obtain closed macroscopic equations is to determine whether it is possible to average over a minimal sample volume instead of an REV, but still retain all the geometric information about the porous medium. This smaller averaging region would then allow one to obtain the boundary values necessary to solve a transformed set of averaged equations. This approach has been investigated intensively by Quitard and Whitaker (1994a; 1994b; 1994c; 1994d; 1994e) where they have shown that in spatially periodic porous media the smaller averaging volume may be selected as a unit cell of the medium. Different unit cells may contain different distributions of fluid and void spaces, but will provide similar boundary conditions for a set of averaged equations. They suggest that the use of different weighing functions with the averaging integrals will have the effect of smoothing out the fluctuations induced by selecting a smaller averaging volume and also remove the uncertainty between the defined dependent variable and the measured quantity. Applications of their approach to Newtonian flow, diffusion and heat transfer in porous media are presented by Whitaker (1986), Quintard and Whitaker (1993) and Whitaker (1997). However, this approach is still very much theoretical and cannot, for instance, give an analytical expression for the permeability although its order of magnitude can be predicted. However, a combination of their approach with numerical simulations of flow through such unit cells may lead to practical results.

A different approach towards closure of the macroscopic equations was introduced by Du Plessis and Masliyah (1988). They introduced the concept of *an average geometry* of a porous material which may then be cast in a rectangular unit cell. Their type of unit cell is different from those previously described in context of network theory or the unit cells of Quintard and Whitaker. In their approach, the unit cell contains, on average, all the geometric information about the microstructure in a simple enough arrangement to allow quantification of the fluid-solid surface area and to solve integrals over the fluid-solid surface, such as the integrals listed in Table 2.2. The procedure for closure employed by Du Plessis and Masliyah (1988) has been used rather successfully to obtain deterministic pressure gradient expressions for flow through isotropic granular and foamlike porous media, as well as for isotropic prismatic bundles.

The approach of Du Plessis and Masliyah is in essence what this study is concerned with. Their modelling was only directed towards fluid transport in isotropic porous media. One of the objectives of this study is to model fluid transport through some anisotropic materials in a similar manner. However, a straightforward extension of their results is not possible, since certain concepts such as tortuosity and local flow velocities have to be generalised to include anisotropy. Therefore, attention is firstly devoted to obtain an alternate macroscopic representation of microscopic fluxes than the phase and intrinsic phase average fluxes. This analysis is not restricted by any geometric porous

medium model and is applicable to porous media in general. This general analysis is then applied to fluid transport in anisotropic porous media by referring to the concept of a unit cell. However, the general analysis of fluxes can be useful to other transport phenomena and this is also addressed.

However, before analysing microscopic fluxes, it is useful to first consider some definitions of geometric parameters since this study is also concerned with capturing the geometric characteristics of particular porous materials in single unit cells.

2.6 Porous medium parameters

As partially illustrated by the various porous medium models previously introduced, communication with a porous medium and interacting transport process is through macroscopic measurable parameters which reflect certain characteristics of the porous microstructure. The objective of this section is to present a number of geometric properties which are used to characterise porous media. Some of these are also discussed in literature and are presented here only for coherence of the study while some other concepts which are used to characterise porous structures may need additional clarification. In other cases, certain parameters are redefined and novel definitions presented. It is imperative that these geometric parameters are well-defined, since a fundamental part of this study is to construct geometric pore-scale models of porous structures.

2.6.1 Porosity

The porosity, ϵ, also referred to as the void fraction, is the ratio between the void volume U_f and the total volume U_o of a two-phase porous medium sample. By definition

$$\epsilon = \frac{U_f}{U_o} = \frac{1 - U_s}{U_o} \tag{2.32}$$

where U_s is the solid volume of the sample. A porosity of zero constitutes a solid material which is impermeable to fluid flow, whereas a porosity of one constitutes a void space. The porosity therefore also gives an indication of the ease with which fluid will move through the medium. Porosities of some general porous substances are provided by Scheidegger (1974), while some of the techniques for measuring the porosity are discussed by Dullien (1979) and Kaviany (1995). The effect of the packing of material on the porosity is discussed by Scheidegger (1974) and Bear (1972). In this

study only rigid porous media are considered in which a pressure gradient does not induce a change in porosity. However, Kaczmarek and Hueckel (1998) provide a closer inspection of different porosity definitions for materials where changes in porosity may occur.

In general, most porosity measurement techniques as outlined by Dullien (1979) and Kaviany (1995) yield the total porosity of the porous medium. However, in certain cases, such as percolated sandstones for instance, it is useful to calculate a porosity which is based only on the specific part of the void space which contributes to flow instead of the total void volume. This porosity is referred to as the *effective porosity* and it may depend on the particular transport process. For example, for conductivity both isolated and dead-end pores do not contribute to the effective porosity. For diffusivity dead-end pores should form part of the effective porosity since they do contribute to the transport but not the isolated pores. The effective porosity may be defined as

$$\epsilon_{ef} = \frac{U_{ef}}{U_o} \tag{2.33}$$

where U_{ef} is the fraction of the total void space contributing to the transport. A physical situation where the effective porosity is relevant is when the porous medium contains dead-end pores, which are channels with only one entrance and fluid contained within such a cavity cannot escape to contribute to the overall flow. Reference to effective porosity is also relevant in the case of consolidated sandstones where certain pores are blocked due to percolation effects. During this study the adjective effective is used to indicate a specific fraction of a specific porous medium feature which contributes to a particular transport process. It may be noted that it is actually the effective fluid volume which is used in the definition of an intrinsic phase average in the volume averaging theory.

The porosity defined above is actually the volume porosity, since it is based on volume fractions. It is also possible to define the areal porosity

$$\epsilon^A = \frac{A_f}{A_o} \tag{2.34}$$

where A_o is the total area of a two-dimensional cross-section through a porous medium. The area A_f is the total fluid area of this two-dimensional section. As discussed in Section 2.3.3 the volume porosity and areal porosity yield equal values if the sample comply to certain limits of size. Since these size limits are nearly always complied to, especially in the case of an REV and REA, the term porosity in the text refers to either of these quantities indiscriminately and differences will be indicated if necessary.

2.6.2 Specific surface areas

Another important geometric parameter is the static or geometric specific surface area which is defined as the total interstitial surface area of the pore-space to the bulk volume of the porous medium,

$$A_{vs} = \frac{total\ surface\ of\ solid\ particles}{volume\ of\ solid\ particles} = \frac{S_{fs}}{U_s}. \tag{2.35}$$

The specific area of a porous material is affected by porosity, mode of packing and by grain size and shape (Bear, 1972). This area plays an important role in cases where adsorption of materials from the fluid takes place or in chemical reactors where there might be mass transfer and electric interactions on the fluid-solid surface. The static specific surface area may be measured by mercury porosimetry and gas adsorption measurements (Dullien, 1979; Montillet *et al.*, 1992). Although the measurements are dependent on the type of measurement technique it can be measured to a high degree of accuracy. The total wetted surface per unit volume of sample is related to the specific static surface by

$$\frac{S_{fs}}{U_o} = A_{vs}(1-\epsilon). \tag{2.36}$$

Another area to consider is the dynamic specific surface area, defined as

$$A_{vd} = \frac{surface\ area\ presented\ by\ particles\ to\ flow}{volume\ of\ solid\ particles}. \tag{2.37}$$

This surface area was used by Comiti and Renaud (1989) in a model where only part of the surface area is wetted due to the overlapping of particles. According to their definition the dynamic specific surface area is generally smaller than the static specific surface area which implies that

$$A_{vd} = XA_{vs} \tag{2.38}$$

with $X \leq 1$. The limiting value of $X = 1$ corresponds to a porous medium consisting of spheres where there are only contact points, and no surface contact, between particles.

2.6.3 Particle and pore sizes

The size of particles is probably one of the most used terms in sedimentology although it is not uniquely defined except in the case of simple geometric objects such as spheres or cubes (Pettijohn *et al.,* 1972). In the case of granular materials which consist of well-defined particles the size of a particle is unique and reasonably well-defined. However, for granular materials which do not exhibit definite granules it is possible to define an equivalent particle diameter, d_n, such as

$$d_n = \frac{6}{A_{vs}} \tag{2.39}$$

where A_{vs} is given by (2.35). Problematic to this approach is that for irregular particles, such as sand grains, the size commonly depends on the method of measurement. As discussed by Bear (1972), a particle-size distribution is usually associated with unconsolidated or granular materials and the relative sizes of particles in a porous system may be measured by sieve analysis where the granular material is shaken on a sieve with square openings of a specified size so that the size of a particle is based on the side dimension of a square hole. In hydrometer analyses the size of a particle is the diameter of a sphere which settles in water at the same velocity as the particle. Table 2.3 summarises some other definitions of particle sizes as obtained from Pettijohn *et al.* (1972).

In the case of consolidated or foamlike materials it is not possible to identify individual grains and it is more appropriate to consider the sizes of pores or channels. However, as outlined by Scheidegger (1974) it is intuitively appealing to also refer to the size or diameter of pores in the case of granular materials. However, a general problem is that the channels along which flow occurs are generally not cylindrical and not of uniform shape along their entire length. A parameter which is used as indicator of the average size of pores, mostly in context of the hydraulic radius models, is the average pore diameter, d_c which is expressed as four times the hydraulic radius, R_h where

$$\begin{aligned} R_h &= \frac{\textit{cross-section available for flow}}{\textit{wetted perimeter}} \\ &= \frac{\textit{volume available for flow}}{\textit{total wetted surface}} \\ &= \frac{\textit{volume of voids / volume of bed}}{\textit{wetted surface / volume of bed}} \\ &= \frac{\epsilon U_o}{S_{fs}}. \end{aligned} \tag{2.40}$$

Table 2.3. Various definitions for particle sizes according to Pettijohn *et al.* (1972).

Name	Definition
Surface diameter	The diameter of a sphere having the same surface area as the particle.
Volume diameter	The diameter of a sphere having the same volume as the particle.
Drag diameter	The diameter of a sphere having the same resistance to motion as the particle in a fluid of the same viscosity and at the same velocity.
Projected area diameter	The diameter of a sphere having the same projected area as the particle when viewed in a direction perpendicular to a plane of stability.
Free-falling diameter	The diameter of a sphere having the same density and the same free-falling speed as the particle in a fluid of the same density and viscosity.
Stokes' diameter	The free-falling diameter in the low Reynolds number flow regime.
Sieve diameter	The width of the minimum square aperture through which the particle will pass.
Specific surface diameter	The diameter of a sphere having the same ratio of surface area to volume as the particle.

With (2.36) the average pore diameter is

$$\begin{aligned} d_c &= 4R_h \\ &= \frac{4\epsilon U_o}{S_{fs}} \\ &= \frac{4\epsilon}{A_{vs}(1-\epsilon)}. \end{aligned} \tag{2.41}$$

Some methods which may be applied to define a pore-size distribution are discussed by Dullien (1979; 1991), Bear (1972) and Corey (1977).

2.6.4 Staggering

In addition to the connectivity of the void space, the amount of pore-space actively or effectively traversed by the fluid is also determined by the amount of staggeredness of the solid material. With staggeredness we indicate the degree to which the solid phase is distributed randomly or disorderly. In the case of maximum staggering all available void sections are traversed by fluid at all times. In the case of minimum staggering the medium becomes stratified at the microscopic level and certain channels contain all the moving fluid. The sections connecting the stratified channels may contain stagnant fluid which do not contribute to the flow through the porous medium. A two-dimensional example of maximal and minimal staggered porous media for flow in a particular direction is illustrated in Figure 2.3. In Figure 2.3a some of the fluid between consecutive cylinders will not contribute to flow in the overall flow direction and these zones contain stagnant fluid. In Figure 2.3b all the fluid which moves in the macroscopic flow direction is also forced to move locally normal to it and all the available void volume is used for fluid transport.

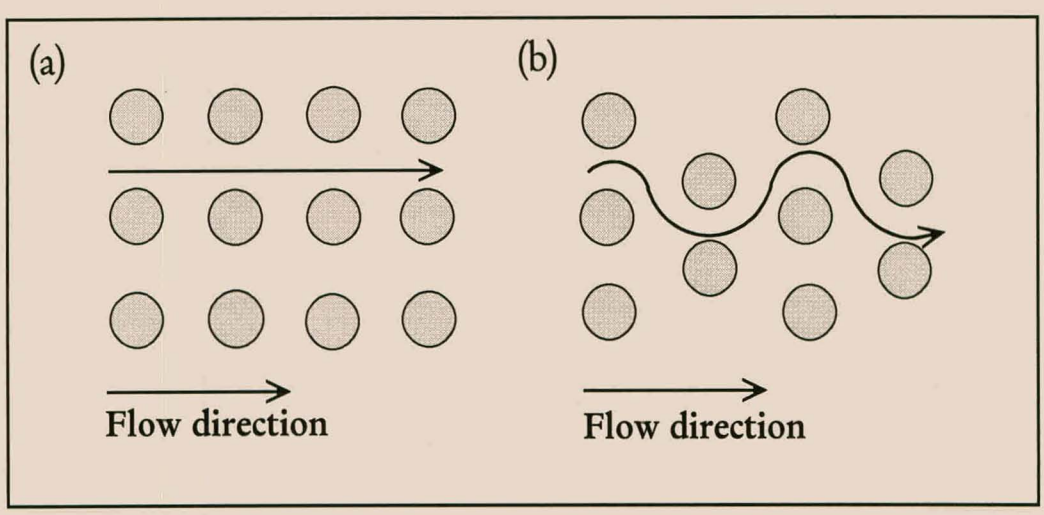

Figure 2.3. A two-dimensional schematisation of a porous medium with (a) minimum staggering and (b) maximum staggering.

While discussing the porosity it was mentioned that it is possible for only a portion of the void volume to be accessible for transport and to take part in a particular transport process. This necessitated the introduction of the effective porosity. It would appear as if the effectiveness of the void volume to be accessible to transport depends on the staggering and connectivity of the pore-space. In view of (2.33) it is possible to

introduce an effectiveness parameter

$$\Lambda_{ef} = \frac{\epsilon_{ef}}{\epsilon} = \frac{U_{ef}}{U_f}. \tag{2.42}$$

For the situation where $\Lambda_{ef} = 1$ the effective porosity is equal to the actual porosity which implies that the pore-space is connected at all points, there are no dead-end channels and staggering of the material is such that there are no stagnant zones. The existence of dead-end channels which is only accessible to flow from one direction is a typical example of a structural feature which will decrease the value of the effectiveness parameter as well as the effective porosity. It is acknowledged that the effectiveness is only an extension of the effective porosity, but its incorporation in certain idealised porous medium models may aid understanding of certain pore-scale transport processes.

2.6.5 Formation factor and resistivity index

The formation factor, F, is an electrical property of a fluid-saturated porous medium used in studies of electric discharge through porous media and the interpretation of electric logs. The known values of the resistivity of certain rock formations obtained through the formation factor are used to determine the added resistivity of oil or gas in the formation. It was originally introduced by Archie (1942) in connection with electrical logging of gas and oil wells as the ratio between the resistivity of a porous sample saturated with brine to the bulk resistivity of brine. Therefore, for any electrolyte the formation factor is given by

$$F = \frac{\rho_o}{\rho_w} \tag{2.43}$$

where ρ_o is the electrical resistivity of the porous medium saturated with an electrolyte and ρ_w is the resistivity of the electrolyte. It follows from this definition that F is always greater than unity. A change in this expression may be made by replacing each resistivity by its reciprocal, the conductivity, to give

$$F = \frac{\sigma_w}{\sigma_o} \tag{2.44}$$

where σ_o is the conductivity of the electrolytically saturated porous medium and σ_w is the conductivity of the electrolyte. Since the resistivity of a conductor is proportional to the resistance of the same conductor (Kip, 1969, p168), the formation factor is also

expressed in terms of the ratio of the resistance of the saturated porous medium (R_o) to the resistance of the electrolyte (R_w), that is

$$F = \frac{R_o}{R_w}. \tag{2.45}$$

This expression relies on the condition that the volume of electrolyte has the same external dimensions as the saturated porous medium and both the resistances are measured using the same relative orientation of the electrodes.

An important feature of the formation factor is that it is directly measurable without recourse to any porous medium model. It gives an indication of the influence of the pore structure on the resistance of the sample to the flow of electric current. According to Cornell and Katz (1953), the value of the formation factor depends on the available cross-sectional void area of the sample and on the increased distance which the electric current must flow due to the tortuous pore structure. Some techniques for measuring the formation factor are reported by Carman (1956), Bear (1972) and Jacquet (1991).

Wyllie and Rose (1950) found that the electrical conductivity of a sediment was inversely proportional to the porosity and introduced an equation of the form

$$F = \frac{X_e}{\epsilon} \tag{2.46}$$

where X_e is termed the electrical retardation factor. Since the formation factor and the porosity are measurable quantities, the electrical retardation is as it appears in (2.46) may be determined through experiment. This has prompted many workers, for instance Wyllie and Spangler (1952), Cornell and Katz (1953) and Schopper (1966), to propose a model of the porous medium such that the flow paths of fluid particles described by the model are identical to that of an electric current, implying that the electrical tortuosity is identical to the hydraulic tortuosity. Through these models the electrical retardation is thus related to the electrical tortuosity. In Appendix A two different expressions are derived for X_e in context of the capillary model where the equivalence of electrical flow and fluid flow is assumed. However, Clennell (1997) demonstrated the non-equivalence of electrical and hydraulic pathways for porous media in general and concluded that electrical and hydraulic tortuosities are not identical. Johnson and co-workers (Johnson, *et al.*, 1982; 1987) as well as Cummins and Chang (1987) have considered acoustic wave propagation through porous media and related X_e to the tortuosity that appears in their acoustic wave equations. The formation factor is therefore a useful quantity since it is measurable and applicable to other non-electric transport phenomena in porous media.

In cases where the porous medium is only partially saturated with an electrolyte, the electrical properties of the medium are expressed through the resistivity index

$$I = \frac{\rho_p}{\rho_o} = \frac{F_e}{F} \tag{2.47}$$

where ρ_p is the in situ resistivity of the partially saturated porous medium and F_e is an apparent formation factor (Wyllie and Spangler, 1952). The resistivity index depends on the level of saturation as well as the method of saturation (Wyllie and Rose, 1950).

2.6.6 Areosity scalar

The areosity is only a recent addition to the set of pseudo geometric parameters characterising porous media. It was defined without a formal theoretical proof by Ruth and Suman (1992) and Suman and Ruth (1993) when considering transport through cubic arrays of connecting tubes. In their analyses they discuss fluid and electric transport by referring to rectangular parallelepiped-shaped REV's. Such an REV has linear dimensions $L_{(k)}$ and total face areas $A_{o(k)}$. The sides of the REV normal to the $k = 2, 3$ directions are insulated and the macroscopic direction of flow is in the $k = 1$ direction. An additional feature of the REV is that any cross-sectional cut normal to the x_1-direction yields an effective fluid-fluid area $A_{p(1)}$, which may mathematically be expressed as

$$A_{p(1)} = \iint_{A_{f(1)}} \tilde{\nu}_1 \nu_1 \, dA \tag{2.48}$$

where $A_{f(1)}$ is the total fluid area normal to the x_1-direction, $\tilde{\nu}_1$ is the component in the x_1-direction of the unit vector $\tilde{\nu}_i$ representing the direction of the microscopic flow on the fluid-fluid area and ν_1 is the magnitude of a unit outwardly directed normal vector to the area element dA. Since the REV's were always selected normal to the macroscopic flow direction, $\nu_i = \hat{\nu}_1$ in (2.48) where $\hat{\nu}_i$ is a unit vector indicating the macroscopic flow direction. The area $A_{p(1)}$ is not a tensorial quantity, hence the index in brackets. The areosity for the x_1-direction is then defined as

$$\xi = \xi_{(1)} = \frac{A_{p(1)}}{A_{o(1)}} \tag{2.49}$$

where $A_{o(1)}$ is the total area of the REV normal to the x_1-direction. The areosity is therefore a dimensionless quantity similar to the porosity.

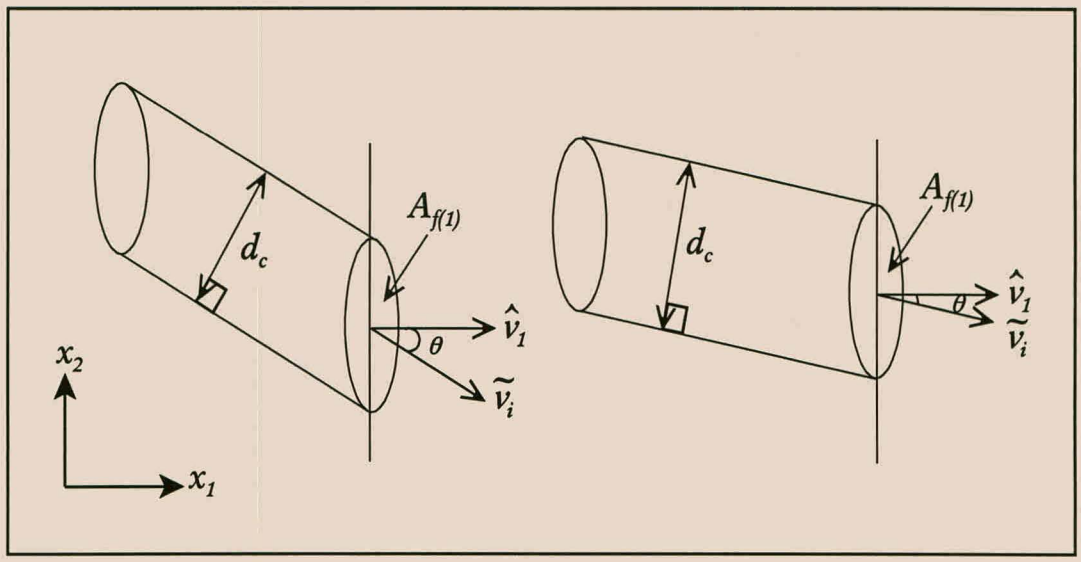

Figure 2.4. Pore channels with equal diameters at different inclined angles which intersect a plane have different fluid-fluid areas, but equal areosities.

However, as noted by Suman and Ruth (1993), the areosity is not equal to the areal porosity, since the areal porosity $\epsilon = A_{f(1)}/A_{o(1)}$ is associated with all open fluid area, whereas the areosity also incorporates the microscopic direction of flow. This point may be further clarified by considering the tubes with equal diameters in Figure 2.4 which intersect a plane at different angles. These may be viewed as pore channels intersecting an REA at different angles to the streamwise direction. When the plane is not normal to the tube, the fluid-fluid area $A_{f(1)}$ in the plane is an ellipse and this area is given by

$$A_{f(1)} = \frac{\pi d_c^2}{4\cos\theta} \tag{2.50}$$

where d_c is the diameter of the tube and θ is the angle between the tube and the streamwise direction. When calculating the areal porosity of the plane the area of the ellipse is the relevant area to consider yielding a porosity of

$$\epsilon = \frac{A_{f(1)}}{A_{o(1)}} = \frac{\pi d_c^2}{4A_{o(1)}\cos\theta}. \tag{2.51}$$

Since the fluid-fluid area is a function of the angle between the tube and the plane, the porosity in all these cases are different. However, when calculating the areosity the appropriate area to consider is the area of the fluid which moves normally across the plane, and in this case, it is given according to (2.48) by

$$A_{p(1)} = A_{f(1)}\cos\theta = \frac{\pi d_c^2}{4}. \tag{2.52}$$

Therefore, the areosity,

$$\xi_{(1)} = \frac{\pi d_c^2}{4A_{o(1)}} \tag{2.53}$$

is in fact equal for both the inclined tubes in Figure 2.4. However, only for the case where the intersecting plane is normal to the tube axis, is the areal porosity and areosity equal. Therefore, any two-dimensional cross-section through a porous medium contains some pore areas through which transport takes place only in the direction of macroscopic flow, while over other areas transport takes place diagonally and in others even parallel to the cutting plane. The effective area contributing to the areosity is defined specifically to take into account only those areas which contribute effectively to flow perpendicular to the cross-section. The distinction between the effective and total fluid areas have also been indicated by Walsh and Brace (1984) and used by them to calculate the permeability and formation factor of isotropic porous media.

Ruth and Suman (1992) and Suman and Ruth (1993) do not devote much attention to the directional dependence and probable tensorial nature of the areosity and effective area and only consider it in specific examples in one particular direction. However, the incorporation of the direction of microscopic flow when calculating certain geometric parameters will prove to be of substantial importance and this is investigated in Section 2.6.7 where a more general theoretical exposition of microscopic transport processes is presented. The definition of the areosity tensor is then given for any arbitrary flow direction.

2.6.7 Permeability

The permeability indicates the degree of conductivity of a porous medium with respect to the permeation by a Newtonian fluid. The permeability, K_p, was originally defined as the coefficient of proportionality in Darcy's law (Bear, 1972, p120; Hassanizadeh and Gray, 1980) which relates the pressure gradient, or more specifically the piezometric head, linearly to the discharge velocity, q_i at low Reynolds number flow and is given by

$$q_i = -K_p \left(P_{f,i} - \rho g_i\right) \tag{2.54}$$

where K_p is the permeability, P_f is the fluid pressure, the density of the fluid is given by ρ and g_i is the vector of gravitational acceleration directed downward. By incorporating

the gravity term with the fluid pressure, the total pressure gradient is given by

$$P_{,i} = P_{f,i} - \rho g_i \tag{2.55}$$

and (2.54) may be written as

$$q_i = -K_p P_{,i}. \tag{2.56}$$

Equation (2.56) is known as Darcy's law in honour of Henry Darcy (1803-1858), a French engineer (Tokaty, 1971). He was the first to propose such a relationship and published it in 1856, based on his experiments with vertical flow through sand used for water filtration. As a result, he is recognised as the father of groundwater hydraulics (Franzini and Finnemore, 1997). Darcy's law today remains an empirical law, based only on experimental evidence. Subsequently, it has been observed that the proportionality does not hold if the flow is not in a certain seepage velocity domain (Scheidegger, 1974). For flow through granular porous media, the flow is considered to be in this domain if the Reynolds number (Re) is less than one, where the Reynolds number is defined as

$$Re = \frac{d_{10} q \rho}{\mu} \tag{2.57}$$

where d_{10} is the effective particle size (the 10 % finer than volume) and μ is the dynamic viscosity of the fluid. Darcy's law is also used in a number of other important areas besides the analysis of groundwater flow which include the approximate analysis of unsaturated soil moisture movement, the flow of oil in petroleum reservoirs and for the design of chemical and ceramic filters and related processes.

As noted by Dullien (1979), permeability used in this general sense is dependent on the pore structure, properties of the permeating fluid and the mechanisms of flow. If the permeability is written only in terms of the contribution of the pore-space to the conductivity, then it is referred to as the specific permeability or Darcy permeability, K, and Darcy's law takes the form

$$q_i = -\frac{K}{\mu} P_{,i} \tag{2.58}$$

where $K_p = K/\mu$ and P is the piezometric pressure. The Darcy permeability has the units of length squared and is also expressed in the unit darcy, while the permeability

has the units of m^3 s kg^{-1} (Bear, 1972; Allen *et al.*, 1988). If the traversing fluid is water, the specific permeability is then also referred to as the hydraulic conductivity. Some permeability and hydraulic conductivity values for a number of different porous substances are presented by Carman (1937), Scheidegger (1974) and Bear (1972).

In anisotropic materials the permeability may differ with direction of flow and reference is then made to a permeability tensor. Darcy's law may then be written as

$$q_i = -\frac{1}{\mu} K_{ij}(P_{f,j} - \rho g_j) \tag{2.59}$$

where K_{ij} is the Darcy permeability tensor. Many investigators have shown theoretically that the permeability tensor is symmetric. For example, Scheidegger (1974), Bear and Bachmat (1991) and Neumann (1977) referred to the volume averaging theory and some statistical considerations to indicate the symmetry. In addition, Guin *et al.* (1971) made use of a capillary-type model and a statistical distribution of pore sizes. Scheidegger (1974) discusses the permeability measurements in anisotropic porous media of various authors which also substantiates the symmetric tensor properties of permeability. Therefore, there is general consensus that the permeability tensor is symmetric regardless of the preferential orientation of the pores in the microstructure. The coordinate axes with respect to which the permeability tensor may be diagonalised are referred to as the principal axes of the medium or the material coordinates. The permeabilities in each of the principle directions depend on the shape, orientation and the concentration of the solid phase within a porous medium (Rice, *et al.*, 1970; Scheidegger, 1974).

Usually the measurements of permeability are assumed to be made along the principle axes of the specimen although they could be measured in any direction. However, Scheidegger (1959; 1974) has pointed out that measurements not along the principle axes can be made in two different ways with two different results due to the fact that the pressure gradient vector and flow vector are not collinear. Various techniques for measuring and calulating the permeability in saturated consolidated and unconsolidated porous media are discussed by Liakopoulos (1965), Rice *et al.* (1970) and Corey (1977) while Mallants *et al.* (1997) compared the performance of three different measurement techniques of the hydraulic properties of unsaturated heterogeneous soils. The measurement of the coefficients in the permeability tensor for two-phase flow is discussed by Dullien and Dong (1996).

2.6.8 Ordered and disordered porous media

Sometimes a parameter which describes a certain porous medium characteristic may include information also reflected by a number of other parameters. This is the case for the concept of order and disorder in porous media, since it is closely related to homogeneity, isotropy and staggering. The concept of order and disorder has been considered form a theoretical point of view by Quintard and Whitaker (1994a; 1994b; 1994c; 1994d; 1994e). In their analyses ordered media exhibit a definite ordered pattern of the solid material and these materials therefore have a spatially periodic structure similar to the material illustrated in Figure 2.3a. From a mathematical point of view a porous medium is disordered with respect to an averaging volume, which in the present case we select as an REV, when

$$\left\langle \overset{o}{x}_i \right\rangle_{,j}^{f} \ll \delta_{ij} \tag{2.60}$$

where δ_{ij} is the Kronecker delta. They also indicate that ordered porous media are associated with homogeneous materials.

2.7 Pore-scale transport and tortuosity

2.7.1 Introduction

The substantial curvature of flow lines within the void space is fundamental to multi-phase flow and flow through porous media. In essence flow through porous media is concerned with the effect of the void space on transport processes and this inevitably brings up the concept of tortuosity, where tortuosity is used as term to describe the sinuosity and interconnectedness of the pore-space as it affects transport processes. Clennell (1997) has indicated that even in cases where a discrete tortuosity factor does not appear in the final transport equations tortuosity or related concepts are actually used in the construction of the various models, which may vary from capillary network models (Dullien, 1979) to continuum models.

As discussed in context of capillary models in Section 2.2, the concept of tortuosity was initially introduced by Carman (1937) as a corrective factor needed to model the influence of the tortuousness of the domain available for displacement of a fluid phase. The need for an additional geometric parameter arose from a recognition that the porosity plus some average pore diameter and a shape factor represent insufficient

information for determination of transport properties in porous media. The concept of tortuosity was introduced because different porous media with the same porosity, hydraulic radius and shape factor were found to have different transport properties. The tortuosity was intended to correct for these discrepancies.

Tortuosity was firstly introduced via the capillary model of the pore-space and, therefore, quantification of the tortuosity for a specific macroscopic flow direction implies referral to two lengths, namely the effective average path length, $\widetilde{L}_e$ and the length, $\widehat{L}$, of the corresponding displacement through the bed, which is normally the bed thickness. The tortuosity as introduced in (2.6) may then be viewed as the ratio between the displacement of a fluid particle between two points and the length of the actual tortuous flow path traversed through the void space between these two points. In this form the definition is at the microscopic level as it relates to a single particle and the resulting pathway within the void space. Another possibility is to relate the tortuosity to the ratio between the macroscopic displacement and the average of the total length of the microscopic pathways travelled by fluid particles to achieve the averaged macroscopic displacement.

Therefore, there is a fair amount of ambiguity associated with the phrase "effective average path length". Bear (1972) also provides two different interpretations of this average length. Firstly, it may be calculated by averaging the actual length of the flow channels which implies that the average path length is equal to the total length of the interconnected pore-space. Such a definition of tortuosity would render it independent of fluid or fluid mechanical properties. This tortuosity is referred to by Bear (1972, p117) as the geometric tortuosity. In the second instance, the average path length may be calculated by averaging the actual distance travelled by all particles passing through a particular cross-section of a porous medium at a particular instant. In this case, the tortuosity is dependent on a large number of structural as well as fluid mechanical properties and is referred to as kinematic tortuosity (Scheidegger, 1974, p23, p132). Some of the parameters influencing the kinematic tortuosity, as illustrated by Spearing and Matthews (1991), are pore size distributions, variable flow speeds in different channels and percolation effects.

At present the name tortuosity is a source of frequent misunderstanding due to different definitions and interpretations. This is especially evident in the review article of Clennell (1997) with the appropriate title: "Tortuosity: a guide through the maze". As a result of the inconsistencies in the definition of tortuosity it is sometimes, for example Dagan (1989), regarded as a "fudge factor" and its incorporation into analyses of flow through porous media is avoided. In addition, it is also questioned whether the tortuosity really exists as a fundamental attribute of the pore-space in the same manner as porosity is

a definite property.

However, it may also be viewed that tortuosity as a concept forms the basis of flow through porous media. It bridges across a number of disciplines and influences various transport phenomena such as heat transport, acoustics, chemical diffusion and electrical conduction. Interrelated to all these phenomena is the effect of the tortuous microscopic pore-space on the particular transport phenomenon and, it can therefore be expected, that an advancement in the understanding of this effect in one domain of porous media transport will also lead to a better understanding of other phenomena.

In addition, the tortuosity as a porous medium parameter has shown to be useful and important as it facilitates calculation of the average flow speed in channel sections, a fact which was discussed briefly by Carman (1937). The approximation of intrapore flow speeds has also become of importance in closure schemes for the volume averaged momentum transport equation. Analytical quantification of the integral expression in this equation, which contains the actual velocity gradients on the fluid-solid surfaces (Bear and Bachmat, 1986; Du Plessis and Masliyah, 1988), requires an accurate analysis of the actual intrapore velocities. Accounting for non-Darcy inertial phenomena at high Reynolds number flow also requires calculation of the average flow speed in channel sections, since modelling of the Forchheimer effects requires an accurate representation of the microscopic flow field (Ruth and Ma, 1992). Similar arguments apply to other fields of transport, since in modelling the constitutive terms which arise through the course of the volume averaging process, the microscopic transport fluxes within the channels or their gradients on fluid-solid interfaces are required to be known. However, these quantities are generally not amenable to rigorous mathematical quantification and in certain instances the phase averages thereof may not be sufficiently representative. Interest in the concept of tortuosity is especially vivid among experimentalists in the field of porous media and theoretical analyses may aid the understanding and therefore correct application of the corrective measures. Tortuosity is related to a direct interest in being able to predict or model various transport processes, for instance fluid flow, diffusion and electrical conduction in porous media. A more general and mathematically based definition of tortuosity which is not dependent on a particular model, as is attempted in this section, may enhance the capability of accurate prediction of experimental results as well as further future research in this field considerably.

One of the main objectives of this section is to generalise the tortuosity as introduced by Carman (1937) and possibly to remove some the ambiguities with regard to the effective path length. This is achieved by considering the problem of obtaining a more appropriate representation of microscopic fluxes than the intrinsic phase average and phase average fluxes. The tortuosity is then fairly general as it is derived in context of

the volume averaging theory and it is not restricted to a particular type of flow, but it is applicable to any flux through the porous medium. The estimation of a channel flux stems from Carman's (1937) original problem of obtaining a channel velocity more appropriate than the interstitial velocity. It is also indicated that the newly defined tortuosity, termed the flux field tortuosity, is relevant in calculating average fluxes in channels. Initially it was not the intention to analyse tortuosity per se, but to obtain macroscopic approximations to the microscopic velocity and other microscopic flux fields and to consider the influence of variable pathways on transport phenomena. Within this formalism and theoretical framework a well-defined flux field related retardation tensor evolved naturally. Since the effect of this tensor is to describe the retardation of the transport each component has a value less than one. This tensor gives an estimate of the straightness of the flowpaths and has been termed the lineality tensor while the tortuosity tensor is described by its inverse. It is also an additional objective of this section to introduce the lineality and to qualify its physical meaning. Furthermore, the newly defined lineality are related to other prominent definitions of the tortuosity and the similarities and differences are discussed.

2.7.2 Overview of tortuosity concepts

2.7.2.1 Types of tortuosities

The mathematical modelling of tortuosity is a subject of active research and novel ways of describing its influence on transport processes are presented fairly often in literature. Dullien (1979) reviewed some tortuosity concepts rather critically, but an extensive and a detailed overview of tortuosity is presented by Clennell (1997).

According to the analysis of Clennell (1997) four classes of tortuosities may be distinguished. Firstly, there is the geometric tortuosity which is related to the shortest length between inflow and outflow points that avoids the solid obstacles. The geometric tortuosity is an objective characteristic of the pore structure and its value is the same for all transport processes through the porous medium. This geometric tortuosity is different from the geometric tortuosity of Bear (1972) which depends on an interpretation of the total length of the pore-space. The second class of tortuosity measures consists of "retardation factors" extracted from the transport properties of the porous medium. The tortuosities in this class are closely related to an effective transport length and hydraulic tortuosity, electrical tortuosity and diffusional tortuosity may serve as examples. The tortuosity introduced by Carman (1937) also falls in this class and so also does the flux field tortuosity. Thirdly, there are tortuosity parameters which enter into some

simplified construct of the real pore-space, such as a network model. Finally, there are tortuosity measures which are nothing more than adjustable correction factors in an empirical model. As noted by Clennell (1997), none of the four classes of tortuosity is exclusively correct or incorrect, rather each is distinct and they cannot and must not be used interchangeably. The classification of Clennell (1997) eliminates reference to the kinematic tortuosity as used by Bear (1972), which would be more appropriate in unsteady transport since it depends on the actual distance travelled by particles.

Also of importance in the analyses of tortuosity is the direction of the average flow or discharge which renders the tortuosity a tensor. The tensorial nature of tortuosity has been pursued by Bear (1972) and Bear and Bachmat (1991). In the former case Bear (1972, p107-111) expressed the tortuosity tensor in terms of the volume average of the product of the cosines and sines of the angles between the microscopic pathways and the externally applied driving force. This also gives the tensorial nature, since in an anisotropic porous medium tortuosity must vary with direction. Bear and Bachmat (1991) give a different tensorial definition of tortuosity which they derive when obtaining an average of a spatial derivative of a scalar which satisfies the condition that the second derivative thereof is zero, that is $\phi_{,jj} = 0$. It is defined (Bear and Bachmat, 1991, p129) as the total static moment of the oriented elementary surfaces comprising the S_{fs}-surface, with respect to planes passing through the centroid of an REV, per unit volume of the fluid phase within the total volume of the REV. These workers have found it convenient to define the tortuosity tensor so that each component has a value less than one, which is the inverse of the Carman tortuosity factor, and as previously noted in this study these tenors are referred to as lineality tensors.

Ruth and Suman (1992) and Suman and Ruth (1993) have considered various types of tortuosities in context of network models, but an important parameter which emerged from their analyses is the areosity presented in Section 2.5.6. The importance of the areosity has also been noted by Clennell (1997), but the disadvantage of the analyses of Suman and Ruth is that although the areosity incorporates the macroscopic flow direction it is not a tensorial quantity and it is only derived in context of networks of connected tubes. During this study the areosity is derived as a second order tensor in context of the volume averaging theory and it is applicable to porous media flow in general.

Dullien (1979) noted that the tortuosity of a porous medium is a fundamental property of the streamlines, that is the lines of flux, in the conducting capillaries. It measures the deviation from the macroscopic flow direction in the fluid at every point. A key feature in the tortuosity definitions is, therefore, the nature of the flow lines of the particular transport quantity through the porous medium. The flow lines or transport lines are

influenced by a variety of factors such as a pore-size distribution in the medium, serial pore non-uniformities such as constrictions and bulges in the flow channels, cross-flow between different channels which is related to the staggering of the solid phase, the availability of the pore space to transport which includes the effect of dead-end pores and percolation effects. When introducing a definition for the tortuosity it is important to determine which of these factors are to be included by the tortuosity and which are to be related on their own to transport in porous media. It may therefore be necessary to impose certain restrictions on the porous medium and to systematically raise the complexity of the model to obtain an unobstructed view of each factor.

2.7.2.2 Equivalence of the different tortuosities

The different classes of tortuosities discussed in the previous section lack a common denominator and as noted by Clennell (1997) they are distinct. However, within the second class there are a number of different tortuosities which are related to different flow phenomena. In this section it is investigated whether the different tortuosities may be related to each other.

Experiments concerned with tortuosity in the second class may be divided into two distinct categories, namely fluid flow or pressure drop determinations, which include measuring the permeability, and electrical conductivity and molecular diffusion measurements, which include measuring the formation factor and effective diffusion coefficient, respectively. In the electrical measurements the electrical retardation factor (X_e) is related to the formation factor and the porosity as shown in (2.46), while analogous expressions apply to steady state diffusion measurements with the effective diffusion coefficient taking the place of the formation factor. Since the formation factor and porosity can be measured the electrical retardation may be obtained uniquely by experiment. The electrical retardation is very useful because its value is deduced from direct measurements of the formation factor and porosity. However, the electrical retardation is not necessarily equal to the electrical tortuosity which implies that the relation between the formation factor, porosity and electrical tortuosity still depends on a porous medium model. Suman and Ruth (1993) used a network model to obtain a relation between the formation factor and porosity while the use of a capillary model is illustrated in Appendix A. The correctness of such a model can be tested by predicting the formation factor and comparing it with measurements. A similar argument applies to diffusional tortuosity with the bulk and effective diffusivities taking the place of the bulk and effective conductivities in the definition of the formation factor. In addition, the frequency dependent acoustic tortuosity has been related to the electrical

retardation by Johnson *et al.* (1982).

In contrast to the electrical retardation factor, the value of the hydraulic tortuosity cannot be deduced from direct measurements of permeability and porosity. Invariably the concept of hydraulic tortuosity appears in some mathematical models of permeability and so introduces an additional unknown parameter. These models, such as the Carman-Kozeny model, are nearly always one-dimensional and consist of some conduits, representing the pore structure. The hydraulic tortuosity is a measure of the tortuousness of these conduits used in the model. These studies were primarily aimed at packed beds with uniform average discharge resulting in a scalar tortuosity factor with respect to that specific direction. The effect of constrictions in the conduits, if at all considered, is assigned to the value of the average conduit diameter. Therefore, a problem associated with the use of the hydraulic tortuosity is that in practice it is only a measure of the discrepancy between the permeability predicted by a model and the measured permeability, unless the model is predictive and the hydraulic tortuosity is calculated from the physical attributes of the porous material.

Within the second class of definitions Clennell (1997) showed that it is possible to link some of the retardation factors in a rigorous way. The guidelines for a comparison depends on being able to convert the the transport to an overall flux and, amongst others, to identify the equations that underlie the physics of the transport process under consideration. The main conclusion is that if the physics underlying the transport is different, the tortuosity is different. In this framework Clennell (1997) shows, with reference to the work of Koplik *et al.* (1988), that the diffusional tortuosity obtained from steady diffusion is equivalent to the electrical tortuosity. It is also indicated that there are no rigorous results relating hydrodynamic tortuosity to other retardation factors except in the asymptotic limit of high frequency where inviscid flow and high frequency oscillatory flow both experience a limiting no-slip tortuosity (Johnson *et al.*, 1987). The difference between hydraulic and electrical flow paths are also illustrated through numerical models, for instance Zhang and Knackstedt (1995), where the microscopic balance laws are solved within a tractable numerical porous medium.

2.7.3 Local and streamwise directions

To render the results as general as possible, consider Γ to be any extensive quantity of the fluid phase, that is, any quantity which is proportional to the size of the system. The volumetric density of Γ, that is, the amount of Γ per unit volume of fluid, is defined

(Bear and Bachmat, 1991, p31) as

$$\gamma(x_i, t) = \frac{d\Gamma}{dU_f}. \tag{2.61}$$

Examples are mass density or solute concentration, that is, mass of solute per unit volume of liquid. It is also assumed that γ is finite, continuous and differentiable everywhere within U_f. With $x_{\gamma i}$ the position vector of a moving particle of the Γ-continuum, the velocity of a Γ-particle is given by the rate of change of its position in time, that is

$$v_{\gamma i} = \frac{\partial x_{\gamma i}}{\partial t}. \tag{2.62}$$

A streamline is defined as a curve along which a sequence of particles move at a given instant (Whitaker, 1968). By this definition, the tangent to a streamline at each point on it is collinear with the velocity vector at that point. It also follows that for any scalar Γ-continuum a streamline, which is a vector line of the velocity field $v_{\gamma i}$, is also a vector line of the total flux, $n_{\gamma i} = \gamma v_{\gamma i}$, of that continuum. According to Bear and Bachmat (1991) this line is named a γ-transport line of the Γ-continuum.

With the above definitions it is now possible to define transport directions for any Γ-continuum. Let s be a curve length measured along a γ-transport line and let $\tilde{\nu}_{\gamma i}$ be the unit tangent vector along a γ-transport line at each point in U_f, that is

$$\tilde{\nu}_{\gamma i} \equiv \frac{dx_{\gamma i}}{ds}. \tag{2.63}$$

The actual velocity of a particle in the Γ-continuum is then

$$v_{\gamma i} = \tilde{v}_{\gamma i} = \tilde{v}_\gamma \tilde{\nu}_{\gamma i} \tag{2.64}$$

where $\tilde{v}_\gamma$ is the magnitude of the velocity. Consequently, all quantities pertaining to the local or microscopic transport direction are accentuated with a tilde. The total flux of γ-transport may then be expressed as

$$\tilde{n}_{\gamma i} = \gamma \tilde{v}_{\gamma i} = \gamma \tilde{v}_\gamma \tilde{\nu}_{\gamma i} \tag{2.65}$$

where both the magnitude and direction of $\tilde{n}_{\gamma i}$ are dependent on position.

According to the definition of the intrinsic phase average operator, the average flux of γ-transport through the porous medium is

$$\langle \tilde{n}_{\gamma i} \rangle^f = \frac{1}{U_f} \iiint_{U_f} \tilde{n}_{\gamma i} \, dU = \frac{1}{U_f} \iiint_{U_f} \tilde{n}_\gamma \, \tilde{\nu}_{\gamma i} \, dU. \tag{2.66}$$

It is important to note that the intrinsic phase average flux may be considered as the volume integral of the actual flux of γ-particles, weighed over the void volume of the REV, that is, over U_f. The *average transport direction*, also referred to as the *streamwise direction*, for γ-transport is defined as the direction of the intrinsic phase average flux, and a corresponding average transport direction unit vector is denoted by $\hat{\nu}_{\gamma i}$. Correspondingly, all quantities pertaining to the streamwise direction are presented as hatted quantities. The unit vectors introduced for an REV are schematically illustrated in Figure 2.5.

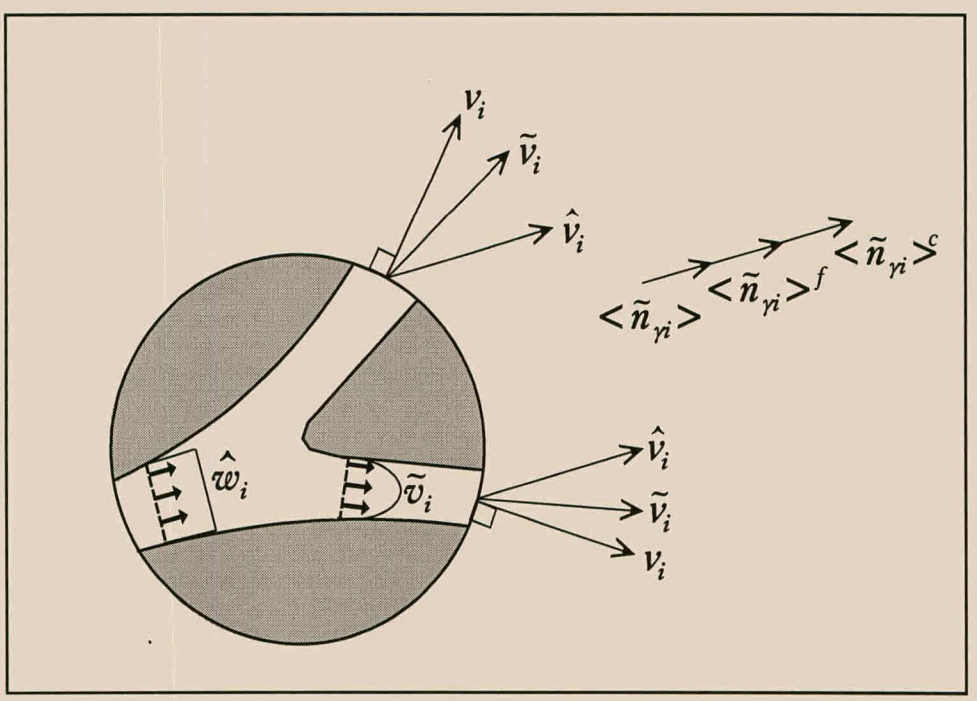

Figure 2.5. Planar cross-section through an REV with relevant unit vectors and velocity directions.

The phase average flux is given by

$$\langle \tilde{n}_{\gamma i} \rangle = \frac{1}{U_o} \iiint_{U_f} \tilde{n}_{\gamma i} \, dU = \frac{1}{U_o} \iiint_{U_f} \tilde{n}_\gamma \, \tilde{\nu}_{\gamma i} \, dU \tag{2.67}$$

and it is also directed in the streamwise direction. In this case the volumetric integral of the actual γ-flux is weighed over the total volume of an REV, that is, over U_o. The

phase average and intrinsic phase average transport flux of γ-particles are related by

$$\langle \tilde{n}_{\gamma i} \rangle = \epsilon \langle \tilde{n}_{\gamma i} \rangle^f \tag{2.68}$$

and in general the magnitudes of these two fluxes are smaller than the actual microscopic flux at a point. In the next section the possibility is explored of extracting another macroscopic flux which is more representative of the actual microscopic flux than these two existing average fluxes.

2.7.4 The average streamwise channel flux

The average flux $\frac{1}{U_f} \iiint_{U_f} \tilde{n}_\gamma \tilde{\nu}_{\gamma i} \, dU$ yields a resultant vector in the average transport direction, that is a vector collinear with $\hat{\nu}_{\gamma i}$. It is the objective of this section to determine a representative average magnitude of $\tilde{n}_\gamma$ which will give the same flux as $\langle \tilde{n}_{\gamma i} \rangle^f$ through the REV at each instant. Therefore, the interstitial average flux is defined as that flux $\tilde{e}_{\gamma i} = \tilde{e}_\gamma \tilde{\nu}_{\gamma i}$, collinear with $\tilde{n}_{\gamma i}$ at each point of U_f, but of constant magnitude $\tilde{e}_\gamma$, which yields the same average flux through U_f as the actual flow. However, we cannot simply replace $\tilde{n}_\gamma$ by $\tilde{e}_\gamma$, since the resulting flux is in the macroscopic transport direction and $\iiint_{U_f} \tilde{\nu}_i dU$ may in general not be directed streamwise. Since its projection $\hat{\nu}_i \hat{\nu}_m \iiint_{U_f} \tilde{\nu}_m dU$ is always streamwise, we may require that

$$\tilde{e}_\gamma \hat{\nu}_{\gamma i} \hat{\nu}_{\gamma m} \iiint_{U_f} \tilde{\nu}_{\gamma m} \, dU \equiv \iiint_{U_f} \tilde{n}_{\gamma i} \, dU. \tag{2.69}$$

This defining equation of the magnitude of the interstitial average flux provides one of the main contributions of this study and from it other transport parameters may be derived.

Since the streamwise unit vector $\hat{\nu}_{\gamma i}$ is constant over an REV, and hence also over U_f, and from (2.66) and (2.69), it follows that

$$U_f \langle \tilde{n}_{\gamma i} \rangle^f = \tilde{e}_\gamma \hat{\nu}_{\gamma i} \iiint_{U_f} \tilde{\nu}_{\gamma m} \hat{\nu}_{\gamma m} \, dU. \tag{2.70}$$

It is apparent that $\tilde{e}_\gamma \hat{\nu}_{\gamma i}$ yields a vector in the average transport direction and $\tilde{e}_\gamma$ may thus be hatted, yielding a notational simplification, namely that $\tilde{e}_\gamma = \hat{e}_\gamma$. This equivalence is a consequence of the fact that only flow components in the average transport direction need to be considered. Therefore, if the streamwise direction is

known, then microscopic fluxes in channels perpendicular to this direction need not be equal to the streamwise fluxes as long as they sum to zero within an REV.

The *effective transport volume* appearing on the right hand side of (2.70), and denoted by $\widehat{U}_{f\mathcal{L}}$, is defined as

$$\widehat{U}_{f\mathcal{L}} \equiv \iiint_{U_f} \widetilde{\nu}_{\gamma m} \widehat{\nu}_{\gamma m} \, dU. \tag{2.71}$$

The effective transport volume constitutes that part of the fluid volume contributing to the flux of the Γ-continuum in the direction of the macroscopic flow. Even for porous systems where $\Lambda_{ef} = 1$ the effective transport volume may be less than U_f, since in the channel sections which are not collinear with $\widehat{\nu}_{\gamma i}$ only a fraction of a channel contributes to flow in the $\widehat{\nu}_{\gamma i}$-direction whereas the remainder carries fluid normal to $\widehat{\nu}_{\gamma i}$. This effective transport volume depends on the configuration of the intrapore flux field which in turn depends on the transport process under consideration its interaction with the geometry of the pore-space.

In consideration of (2.66), (2.70) and (2.71) the *streamwise channel average flux* of any extensive property, is given by

$$\langle \widetilde{n}_{\gamma i} \rangle^c = \widehat{e}_\gamma \widehat{\nu}_{\gamma i} = \frac{1}{\widehat{U}_{\gamma\mathcal{L}}} \iiint_{U_f} \widetilde{n}_{\gamma i} \, dU. \tag{2.72}$$

This flux is proposed as an estimate of the actual interstitial flux. The *streamwise channel average flux* of the Γ-continuum, $\langle \widetilde{n}_{\gamma i} \rangle^c$, may be viewed as the volume integral of the actual microscopic flux weighed over the effective transport volume, $\widehat{U}_{f\mathcal{L}}$. It is important to note the respective differences between (2.66), (2.67) and (2.72). The channel average flux is larger than the intrinsic phase average or phase average fluxes due to the reduced space available for transport in the macroscopic transport direction. It is therefore expected that the channel average flux is more representative of the actual flux in the channels than the intrinsic phase average or phase average fluxes. If the microscopic flux, $\widetilde{n}_{\gamma i}$ is constant in direction and magnitude, then the channel average flux is equal to the microscopic flux.

2.7.5 Streamwise lineality tensor

From (2.70), and utilising the fact that $\widehat{\nu}_{\gamma i}$ is spatially uniform in U_f, it furthermore follows that

$$\langle \widetilde{n}_{\gamma i} \rangle^f = \langle \widetilde{n}_{\gamma m} \rangle^c \frac{1}{U_f} \iiint_{U_f} \widetilde{\nu}_{\gamma m} \widehat{\nu}_{\gamma i} \, dU. \tag{2.73}$$

On the right hand side of (2.73) is the inner product of the streamwise channel average flux with the *lineality tensor* which is defined as

$$\mathcal{L}_{ij} \equiv \frac{1}{U_f} \iiint_{U_f} \widetilde{\nu}_{\gamma i} \widehat{\nu}_{\gamma j} dU. \tag{2.74}$$

The microscopic vector $\widetilde{\nu}_i$ indicates the direction of microscopic flow while $\widehat{\nu}_i$ is a unit vector in the macroscopic flow direction and it is uniform in each REV. The lineality tensor represents an average over a sample volume and depends on the macroscopic flow direction and given boundary conditions.

It can be shown that $\mathcal{L}_{ij}$ is a second order Cartesian tensor by considering two sets of rectangular Cartesian coordinates in which x_i is the position vector of a general point in system S while x_i' is the position vector of the same point in system S'. As presented by Hay (1953), the components of any vector field b_i transform between these two systems according to the relation

$$b_i' = \frac{\partial x_i'}{\partial x_m} b_m. \tag{2.75}$$

In the S' system the unit vector tangent to a transport line is given, analogous to (2.63), by

$$\begin{aligned} \widetilde{\nu}_{\gamma i}' &= \frac{dx_{\gamma i}'}{ds} \\ &= \frac{\partial x_{\gamma i}'}{\partial x_{\gamma m}} \frac{dx_{\gamma m}}{ds} \\ &= \frac{\partial x_{\gamma i}'}{\partial x_{\gamma m}} \widetilde{\nu}_m. \end{aligned} \tag{2.76}$$

The unit vector indicating the streamwise direction transforms according to (2.75),

$$\widehat{\nu}_i' = \frac{\partial x_{\gamma i}'}{\partial x_{\gamma m}} \widehat{\nu}_{\gamma m}. \tag{2.77}$$

By making use of (2.76) and (2.77), the lineality in the S' system may be written as

$$\begin{aligned} \mathcal{L}'_{ij} &= \frac{1}{U_f}\iiint_{U_f} \tilde{\nu}'_{\gamma i}\hat{\nu}'_{\gamma j}dU \\ &= \frac{1}{U_f}\iiint_{U_f} \frac{\partial x'_{\gamma i}}{\partial x_{\gamma m}}\tilde{\nu}_{\gamma m}\frac{\partial x'_{\gamma j}}{\partial x_{\gamma n}}\hat{\nu}_{\gamma n}dU \end{aligned} \tag{2.78}$$

The coefficients of transformation, for example $\frac{\partial x'_{\gamma i}}{\partial x_{\gamma m}}$, can only be moved outside of the integral if they are constant over an REV. This is only true for rectangular Cartesian coordinates in which case

$$\mathcal{L}'_{ij} = \frac{\partial x'_{\gamma i}}{\partial x_{\gamma m}}\frac{\partial x'_{\gamma j}}{\partial x_{\gamma n}}\mathcal{L}_{mn} \tag{2.79}$$

which follows the law of transformation of second order tensors. Therefore, $\mathcal{L}_{ij}$ is a second order Cartesian tensor and when the lineality is referred to as a tensor, a Cartesian tensor is understood where the law of transformation only applies to rectangular Cartesian coordinates.

It also follows from (2.73) and (2.74) that

$$\langle\tilde{n}_{\gamma i}\rangle^f = \langle\tilde{n}_{\gamma m}\rangle^c \frac{1}{U_f}\iiint_{U_f} \tilde{\nu}_{\gamma m}\hat{\nu}_{\gamma i}\,dU \equiv \langle\tilde{n}_{\gamma m}\rangle^c \mathcal{L}_{mi}. \tag{2.80}$$

Therefore, (2.68) may be extended so that the various macroscopic fluxes are related by

$$\langle\tilde{n}_{\gamma i}\rangle = \epsilon\langle\tilde{n}_{\gamma i}\rangle^f = \epsilon\langle\tilde{n}_{\gamma m}\rangle^c \mathcal{L}_{mi}. \tag{2.81}$$

An additional result which follows from equations (2.67) and (2.74) is that

$$\hat{U}_{f\mathcal{L}} = U_f\mathcal{L}_{mm} \tag{2.82}$$

for any specific direction of the macroscopic transport. It is acknowledged that an averaging process of microscopic balance equations, for instance the momentum equation, does not lead directly to the channel average flux. The surface integrals of the fluid-solid interface, however, which arise due to averaging and appearing in macroscopic balance

equations, contain actual flux gradients which thus need to be approximated quantitatively. The channel average flux may then be used to approximate these quantities. For example, as shown in the next chapter in the averaged momentum transport equation the average streamwise velocity is crucial to obtain a proper quantification of the Darcy permeability. Furthermore, this velocity is also needed for theoretical prediction of the coefficient of the Forchheimer term for higher Reynolds number flow as is shown in the next chapter.

2.7.6 Lineality for a Representative Elementary Area (REA)

In the development of the lineality presented in the previous section the average of fluxes were taken over an REV, thereby implying that these quantities have physical meaning as volume averages and are thus additive over volumes. Only in cases where these fluxes are also additive over areas, and thus physically meaningful as areal averages, may the lineality be developed in context of an REA. Therefore, in quite a similar manner as was done for an REV, the lineality concept may be developed for an REA with its centroid collocated with that of the REV. The REA is orientated normal to the macroscopic transport direction and therefore $\widehat{\nu}_{\gamma i}$ is a unit normal to the REA as illustrated in Figure 2.6. From the equivalence of areal and volumetric averages evaluated for an REA and REV sharing a common centroid presented in Section 2.3.3, it follows that the complementary definition of (2.65) in terms of an REA is

$$\langle \tilde{n}_{\gamma i} \rangle^{fA} = \frac{1}{\widehat{A}_f} \iint_{\widehat{A}_f} \tilde{n}_{\gamma i} \, dA. \tag{2.83}$$

Here $\widehat{A}_f$ is the fluid area of the REA. Similar to equation (2.64) it follows that

$$\langle \tilde{n}_{\gamma i} \rangle^{A} = \frac{1}{\widehat{A}_o} \iint_{\widehat{A}_f} \tilde{n}_{\gamma i} \, dA \tag{2.84}$$

where $\widehat{A}_o$ is the total area of the REA. It is important to note that both the REV and REA relevant to the previous two equations share a common centroid and pertain to exactly the same macroscopic point. In addition, there are no restrictions on the orientation of the REA, except that it is normal to the macroscopic transport direction.

In total conformity with the defining equation, (2.65), of the interstitial average flux $\tilde{e}_{\gamma i}$, it follows that we require for the REA

$$\tilde{e}_{\gamma} \widehat{\nu}_{\gamma i} \widehat{\nu}_{\gamma m} \iint_{\widehat{A}_f} \tilde{\nu}_{\gamma m} \, dA \equiv \iint_{\widehat{A}_f} \tilde{n}_{\gamma i} \, dA. \tag{2.85}$$

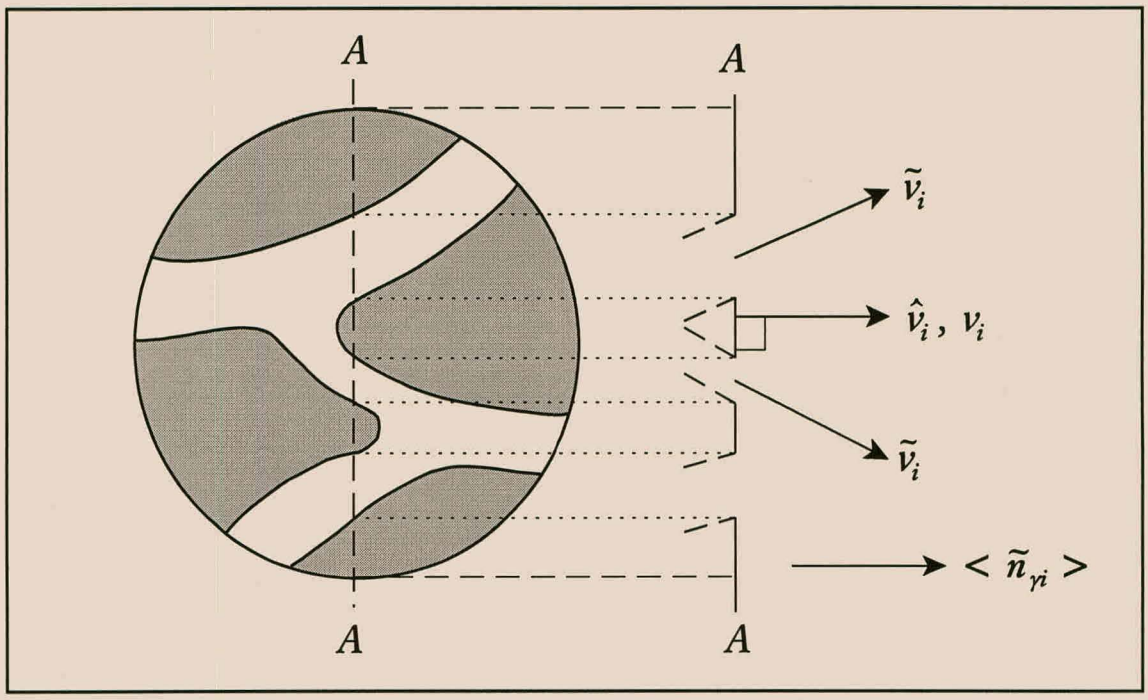

Figure 2.6. Side view of an REA along section A-A on the right hand side with its centroid collocated with that of the REV on the left.

Following along the same lines as for the REV, the *average streamwise channel flux* may be written as

$$\langle \tilde{n}_{\gamma i} \rangle^{cA} \equiv \hat{e}_\gamma \hat{\nu}_{\gamma i} = \frac{1}{\hat{A}_{f\mathcal{L}}} \iint_{\hat{A}_f} \tilde{n}_{\gamma i} \, dA \tag{2.86}$$

where for an REA the equivalent *effective streamwise area* may be defined as

$$\hat{A}_{f\mathcal{L}} \equiv \iint_{\hat{A}_f} \tilde{\nu}_{\gamma m} \hat{\nu}_{\gamma m} \, dA \tag{2.87}$$

and it once again follows that $\tilde{e}_\gamma = \hat{e}_\gamma$. Equations (2.84) and (2.85) may subsequently be used to obtain the flux relation

$$\hat{e}_\gamma \hat{\nu}_{\gamma m} \mathcal{L}_{mi} = \langle \tilde{n}_{\gamma i} \rangle^{fA} \tag{2.88}$$

which yields the lineality tensor in context of an REA,

$$\mathcal{L}_{ij} \equiv \frac{1}{\hat{A}_f} \iint_{\hat{A}_f} \tilde{\nu}_{\gamma i} \hat{\nu}_{\gamma j} \, dA. \tag{2.89}$$

Equations (2.88), (2.83) and (2.84) then yield one of the most important general results of this section, namely

$$\langle \tilde{n}_{\gamma i} \rangle \;=\; \epsilon \langle \tilde{n}_{\gamma i} \rangle^{f} \;=\; \epsilon \langle \tilde{n}_{\gamma m} \rangle^{cA} \mathcal{L}_{mi}. \tag{2.90}$$

In view of (2.81), it is apparent that this identity holds for both an REV and an REA.

Some characteristics of the lineality tensor are subsequently investigated, but in the case of an REA it may be added that the effective streamwise area may be related to the lineality tensor by

$$\widehat{A}_{f\mathcal{L}} \;=\; \widehat{A}_f \mathcal{L}_{mm}. \tag{2.91}$$

For isotropic porous media this expression implies that

$$\mathcal{L}_{ij} \;=\; \mathcal{L}_{mm} \widehat{\nu}_{\gamma i} \widehat{\nu}_{\gamma j} \;=\; \frac{\widehat{A}_{f\mathcal{L}}}{\widehat{A}_f} \widehat{\nu}_{\gamma i} \widehat{\nu}_{\gamma j} \tag{2.92}$$

which concludes the lineality tensor for an REA.

2.7.7 Areosity of a porous medium

As discussed in Section 2.6.6 the concept of areosity was introduced by Ruth and Suman (1992) and Suman and Ruth (1993) to quantify the effective fraction of the total cross-sectional surface area available for fluid discharge through a plane cutting the porous medium at right angles to the direction of average discharge. An expression for this effective area has been obtained for an REA as given by (2.87). In the present notation the areosity, as introduced in (2.49), closely corresponds with the lineality as defined for an REA and may be defined, according to the definition of Suman and Ruth (1993), as

$$\xi_{ij} \;\equiv\; \frac{1}{\widehat{A}_o} \iint_{\widehat{A}_f} \tilde{\nu}_i \widehat{\nu}_j \, dA \;=\; \epsilon \mathcal{L}_{ij}. \tag{2.93}$$

On comparison of (2.93) with (2.48) and (2.49) it is evident that the definitions for areosity and lineality are identical except for the porosity as multiplicative factor. This is due to the areosity being defined by Suman and Ruth (1993) as a phase average,

whereas the lineality is defined here as an intrinsic phase average. However, (2.93) is a Cartesian tensorial quantity applicable to any transport direction and may be viewed as a generalisation of the areosity introduced by Suman and Ruth (1993).

In the case of homogeneous media the areosity scalar $\xi_{(I)}$, given by (2.49) for discharge collinear to a material coordinate x_I, corresponds as follows to the present notation

$$\xi_{(I)} = \xi_{II} = \epsilon \mathcal{L}_{II} \tag{2.94}$$

where I may be 1, 2, or 3. Before the lineality tensor is further investigated it is instructive to first apply this general analysis to fluid transport and to give some indication of the physical meaning of the parameters introduced thus far.

2.7.8 Interpretation of the lineality

2.7.8.1 Conceptual interpretation

The lineality, as defined in (2.74), may be interpreted in two different ways depending under which conditions the $\widetilde{\nu}_{\gamma i}$-field is assumed to be determined. In one instance the $\widetilde{\nu}_{\gamma i}$-field may be considered as the actual flux field for a specific type of transport. This implies that the $\widetilde{\nu}_{\gamma i}$-field for fluid transport and electrical conduction through the same porous medium and with the same orientation with regard to the macroscopic flow may be different. Under these conditions the lineality falls into the second class of tortuosities according to the classification of Clennell (1997) presented in Section 2.6.1.

However, another interpretation is also possible which focuses on the assumption of uniform average pore speed which implies that each particle travels the same distance in a specific unit of time. This is equivalent to interpreting the average path length which the particles travel as the total channel length and yields the lineality a geometric property of the void space. The uniform pore speed may be achieved by discharging an inviscid fluid in the absence of inertial effects through the porous medium. The only reason for considering the flow of such a fluid is to obtain a flow line at every available position of the pore-space. Therefore, the lineality according to (2.97) may be a geometric feature of the pore-space if the $\widetilde{\nu}_{\gamma i}$-field is determined by neglecting inertial effects and allocating the same maximum streamwise volume to all transport processes through the porous medium. This geometric lineality is different from the geometric tortuosity of Clennell (1997) and more akin to the geometric tortuosity of Bear (1972, p117).

Different transport processes move differently through the pore-space and since the derivation of the lineality is fairly general without any restrictions on the $\tilde{\nu}_{\gamma i}$-field it seems more appropriate to view the lineality in terms of the former type of interpretation.

2.7.8.2 Physical interpretation

If $\Gamma = U_f$ is the volume of the fluid phase, then $\gamma = 1$ and $\tilde{n}_{\gamma i} = v_i$ is then the actual microscopic velocity of the fluid moving through a unit area of a channel in the porous medium. From the definitions of the various averaged quantities and (2.90), the superficial velocity and intrinsic phase average velocity are related to the channel average velocity,

$$w_i \equiv \widehat{w}_i = \langle v_i \rangle^{cA} \tag{2.95}$$

through the relation

$$\widehat{q}_i = \epsilon \widehat{u}_i = \epsilon \widehat{w}_m \mathcal{L}_{mi} \tag{2.96}$$

where each variable is hatted only to indicate that all these velocities pertain to the streamwise direction. Here

$$\mathcal{L}_{ij} = \frac{1}{\widehat{A}_f} \iiint_{\widehat{A}_f} \tilde{\nu}_{fi} \widehat{\nu}_{fj} \, dA \tag{2.97}$$

is the hydraulic lineality tensor and in this case $\tilde{\nu}_{fi}$ is a unit tangent vector to a streamline and $\widehat{\nu}_{fi}$ is a unit vector indicating the direction of macroscopic discharge, that is, the streamwise direction. A conceptualisation of the respective magnitudes of the velocities in (2.96) are schematically illustrated in Figure 2.7. These macroscopic velocities are proportional to the integral of the microscopic velocities over an REV and inversely proportional to the volumes to which the integrals are weighted. The effective streamwise volume is the smallest and therefore the streamwise channel velocity is the largest and also the nearest to the areal average of the actual velocity in each channel.

The particular definition of the lineality according to (2.97) may be visualised by referring to the well-known capillary representation of porous media. Accordingly, consider the discharge of a fluid at an intrapore speed of uniform magnitude $\tilde{w}$, through a porous

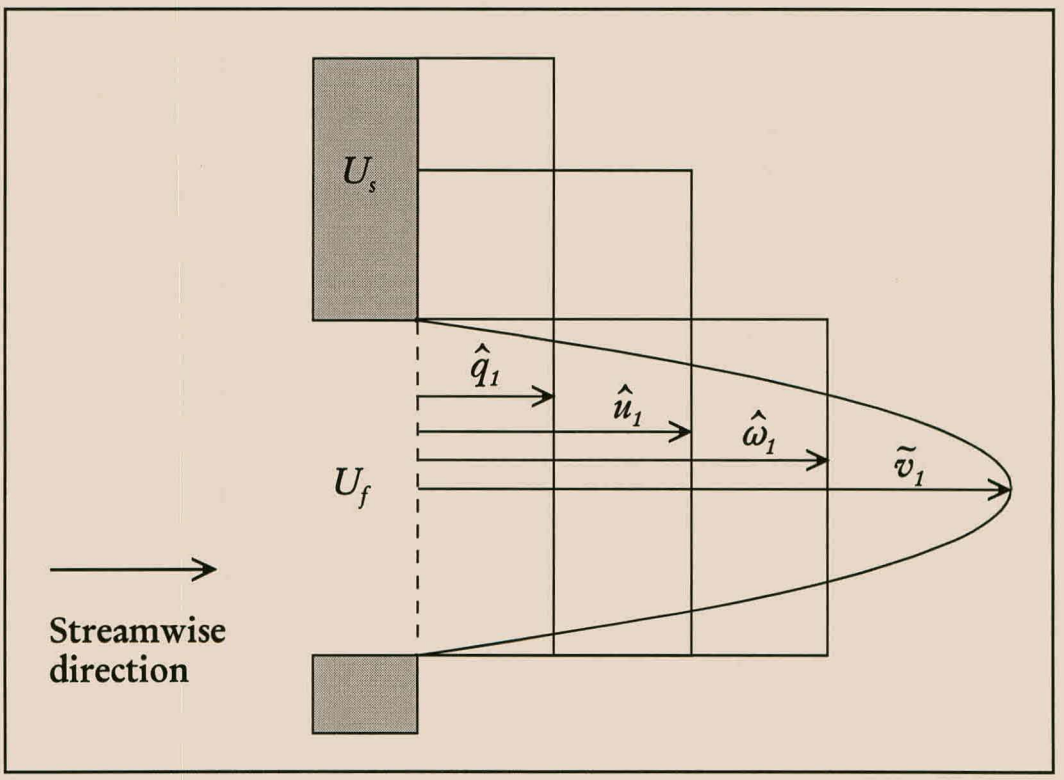

Figure 2.7. Schematic display of the velocity relationships according to (2.96).

material represented by a bundle of slanted capillaries of uniform cross-section contained within two hypothetical parallel planes. The planes are both perpendicular to the streamwise direction at a streamwise distance $\widehat{L}$ apart, one forming the upstream boundary and the other the downstream boundary of the REV as shown in Figure 2.8. The discharge progresses through the bundle of stream tubes of uniform cross-section and equal length $\widetilde{L}_e$. These stream tubes are stacked in such a manner as to completely fill U_f. This implicitly implies that the fluid is forced through all void sections of the interconnected pore-space, inertial effects will not cause recirculation and stagnant zones are also considered absent. All tubes emanate from the upstream plane and culminate in the downstream one with no interchange on the side flanks of the REV.

The areal cross-section of the bundle, $\widehat{A}_{f\mathcal{L}}$, is obtained from the REA with its centroid collocated with that of the REV. Overall volume conservation of the fluid phase yields

$$\widetilde{L}_e \widehat{A}_{f\mathcal{L}} = U_f = \widehat{L}\widehat{A}_f. \tag{2.98}$$

It then follows immediately from (2.91) that

$$\mathcal{L}_{mm} = \frac{\widehat{L}}{\widetilde{L}_e}. \tag{2.99}$$

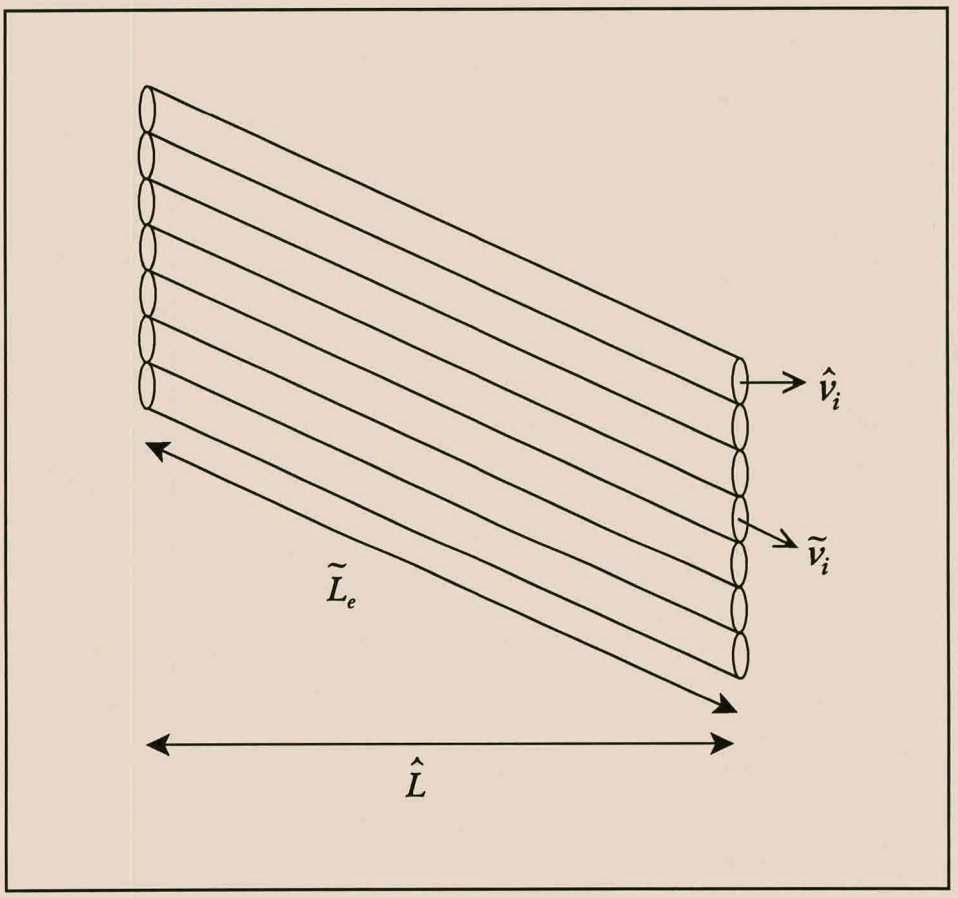

Figure 2.8. Two-dimensional representation of a skewed capillary model.

For this simple example it follows that the lineality reduces to a ratio of lengths. Also, in this example the total channel length and the length of streamlines are equal since the fluid flows through all void sections, and therefore, either interpretations of the lineality are applicable.

Following a similar argument as presented by Scheidegger (1974, p137) the time taken for a fluid particle to traverse the intrapore length $\tilde{L}_e$ with average speed, $\tilde{w}$, is given by $t = \tilde{L}_e/\tilde{w}$. Similarly, the distance $\hat{L}$ is traversed in time, $t = \hat{L}/\hat{u}$, from which it follows that

$$\hat{u} = \frac{\hat{L}}{\tilde{L}_e}\,\tilde{w}. \tag{2.100}$$

On comparison of (2.100) with (2.96) and (2.99), it follows that $\tilde{w}$, which is the average pore speed, is equal to $\hat{w}$, the magnitude of the channel average velocity. The simplification of the present general theory to one-dimensional flow in capillaries, or more

specifically (2.100), is in agreement with (2.6) previously obtained by Carman (1937) for such a capillary model. According to Knackstedt and Zhang (1994), the tortuosity correcting factor L_e/L introduced by Carman (1937) and generalised in (2.96) is an overestimate of the correction for the tortuous flow paths due to the assumption that the channel average velocity is identical in all channels.

Therefore, (2.96) is a generalisation of the extension of the Dupuit-Forchheimer relation by Carman (1937). This analysis provides a theoretical exposition of a more representative microscopic velocity and indicates that the coefficient appearing within this formalism compares to the tortuosity as a ratio of lengths. We refer to this quantity as the lineality, since larger values of the lineality indicate how straight the flow is in comparison with tortuosity which increases with the tortuousness of the porous medium. The lineality tensor $\mathcal{L}_{ij}$ is subsequently shown to be equal to the inverse of the tortuosity tensor.

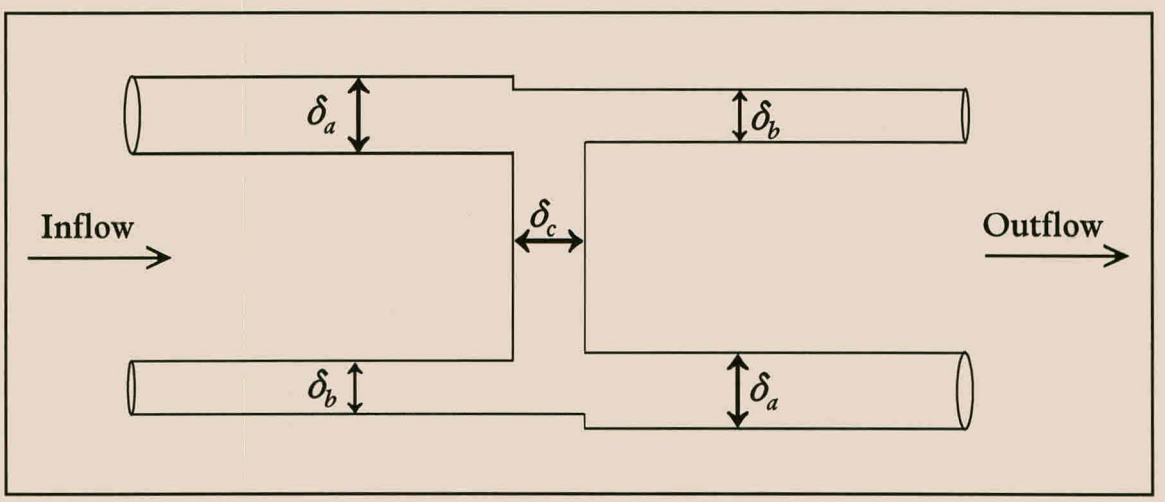

Figure 2.9. The tube system of Suman and Ruth (1992) which is used to illustrate that the channel average velocity is independent of the cross-flow in channel c.

Some more physical insight may be given into (2.95) and the influence of velocities in channel sections perpendicular to the streamwise direction by considering fluid transport through the arrangement of tubes provided by Ruth and Suman (1992) and illustrated in Figure 2.9. If the total area of channels a and b, that is $\frac{\pi}{4}(\delta_a^2 + \delta_b^2)$, is kept constant then the discharge and thus $\widehat{q}_1$ remains constant. If, furthermore, the cross-section of channel c is kept constant, then it implies that U_f is constant and the lineality and porosity are therefore also constant.

If the cross-sections of channels a and b are now altered, but keeping the total area and thus the lineality constant, corresponding changes will be induced in the flow through

channel c. This, however, will not influence $\widehat{w}_1$, which is in the same direction as $\widehat{q}_1$, since the tilde and hatted direction vectors are mutually perpendicular in channel c. Neither the streamwise component of the lineality nor the average streamwise velocity is a function of the velocity in channel c.

As an additional note we may add that from analyses of fluid transport through various types of conduits (Bird *et al.*, 1960) it is apparent that the actual fluid velocity is not uniform, but it is a function of the radius of the conduit. However, it is proposed that the estimated channel average velocity is more representative of the actual velocity than the intrinsic phase average velocity and it should be more appropriate for analyses which addresses fluid transport on the microscopic level. This does not imply that viscosity should be neglected when considering fluid transport.

2.7.9 Tortuosity of a porous medium

As noted in the previous section, tortuosity is related to the amount of sinuosity of the pore-space and, therefore, the *tortuosity*, χ_{ij}, of the porous medium is defined as the inverse of the lineality and it may be obtained from the following defining equation,

$$\mathcal{L}_{im}\chi_{mj} \equiv \delta_{ij}. \tag{2.101}$$

In the case of fluid transport it then follows from (2.96) that

$$\widehat{q}_j\chi_{jm} = \epsilon\widehat{w}_i\mathcal{L}_{ij}\chi_{jm} = \epsilon\widehat{w}_i\delta_{im} = \epsilon\widehat{w}_m. \tag{2.102}$$

Since tortuosity is the inverse of the lineality we may also write

$$\chi_{mm} = \frac{\widetilde{L}_e}{\widehat{L}}. \tag{2.103}$$

The present theory is thus consistent with the definition of tortuosity as given by Carman (1937; 1956, p12) in his extension of the Dupuit-Forchheimer equation (Dullien, 1979).

2.7.10 Symmetry of the lineality tensor

The lineality tensor as introduced here is applicable to a number of transport phenomena, since it is derived for a general Γ-continuum. For the remainder of the discussion

the subscript γ is neglected keeping in mind the general nature of the arguments presented. From the definition of the streamwise lineality tensor it immediately follows that

$$\mathcal{L}_{ij} \equiv \widehat{\nu}_j \frac{1}{U_f} \iiint_{U_f} \widetilde{\nu}_i \, dU. \tag{2.104}$$

The local vector $\widetilde{\nu}_i$, indicating the microscopic transport direction at each point within U_f, may now be split into a streamwise component and a component normal to the streamwise direction, that is

$$\mathcal{L}_{ij} = \widehat{\nu}_j \frac{1}{U_f} \iiint_{U_f} (\widetilde{\nu}_m \widehat{\nu}_m \widehat{\nu}_i + \widetilde{\nu}_m \breve{\nu}_m \breve{\nu}_i) \, dU \tag{2.105}$$

where $\breve{\nu}_i$ is a unit vector normal to $\widehat{\nu}_i$. In the case of isotropic porous media any axis directed streamwise is also an axis of symmetry and therefore, the latter component in (2.105) adds to zero, yielding

$$\mathcal{L}_{ij} = \widehat{\nu}_i \widehat{\nu}_j \mathcal{L}_{mm}. \tag{2.106}$$

The streamwise lineality tensor is thus symmetric for *isotropic* porous media and may be diagonalised, yielding orthogonal principal axes with real eigenvalues of equal lineality. For materials which are *homogeneous* with respect to porosity and structure the latter component in (2.105) is thus also zero and for these materials the streamwise lineality tensor has orthogonal principal axes with real eigenvalues which are not necessarily equal.

It often occurs that information regarding a particular transport process within the void volume of an REV is unknown, but information regarding the direction of transport is available on the fluid-fluid interface, S_{ff}, of the particular REV. In such cases it would be useful to have the lineality tensor written as a surface integral. This can be achieved by considering the identity

$$(\overset{\circ}{x}_i \widehat{\nu}_j \widetilde{\nu}_m)_{,m} = \widetilde{\nu}_i \widehat{\nu}_j + \overset{\circ}{x}_i \widehat{\nu}_j \widetilde{\nu}_{m,m} \tag{2.107}$$

in which $\overset{\circ}{x}_i$ is a position vector relative to the REV centroid, $\widehat{\nu}_i$ is a streamwise unit vector uniform over an REV, and $\widetilde{\nu}_i$ is a unit vector field in U_f everywhere tangent to

the local transport lines. From the intrinsic phase average of the first term on the right hand side of this equation, it then follows that

$$\frac{1}{U_f}\iiint_{U_f}\tilde{\nu}_i\hat{\nu}_j\,dU = \frac{1}{U_f}\iiint_{U_f}(\overset{\circ}{x}_i\hat{\nu}_j\tilde{\nu}_m)_{,m}\,dU - \frac{1}{U_f}\iiint_{U_f}\overset{\circ}{x}_i\hat{\nu}_j\tilde{\nu}_{m,m}\,dU. \tag{2.108}$$

Application of the divergence theorem, as given in (B.57), to the first term on the right hand side of (2.108), then yields

$$\frac{1}{U_f}\iiint_{U_f}\tilde{\nu}_i\hat{\nu}_j\,dU = \frac{1}{U_f}\iint_{S_{ff}}\overset{\circ}{x}_i\hat{\nu}_j\tilde{\nu}_m\nu_m\,dS + \frac{1}{U_f}\iint_{S_{fs}}\overset{\circ}{x}_i\hat{\nu}_j\tilde{\nu}_m\nu_m\,dS - \frac{1}{U_f}\iiint_{U_f}\overset{\circ}{x}_i\hat{\nu}_j\tilde{\nu}_{m,m}\,dU. \tag{2.109}$$

The second term on the right hand side of this equation is zero, since $\tilde{\nu}_i$ is perpendicular to ν_i on S_{fs} under the condition that the transport is confined to the fluid phase. Furthermore, the latter term expresses the divergence of $\tilde{\nu}_i$, which in effect takes account the possibility that the number of flow lines which enter a microscopic volume may be different to the number of lines exiting the volume. Therefore, the factor $\tilde{\nu}_{m,m}$ is zero, except at stagnation points where streamlines divide or converge. The latter term in (2.109) may only be neglected if stagnation points are ignored in which case the streamwise lineality is then given by

$$\mathcal{L}_{ij} = \frac{1}{U_f}\iint_{S_{ff}}\overset{\circ}{x}_i\hat{\nu}_j\tilde{\nu}_m\nu_m dS. \tag{2.110}$$

This expression for the streamwise lineality tensor is therefore a special case of the more general defining equation (2.74). When applied to the model of a bundle of tubes introduced in Section 2.6.8, it yields the same answer as (2.99).

2.7.11 Comparison with other tortuosity definitions

It seems instructive towards further clarification to relate and compare the current definition of tortuosity and lineality to some other definitions presented in the literature.

2.7.11.1 Zero order tensorial expressions

Both ratios, $\frac{\widetilde{L}_e}{\widehat{L}}$ and $\frac{\widehat{L}}{\widetilde{L}_e}$, of the average path length to the streamwise displacement, have been used as definitions for tortuosity (Carman, 1956; Dullien, 1979). It would appear that whichever one is selected is just a matter of definition. In this study the tortuosity is related to

$$\chi \equiv \frac{\widetilde{L}_e}{\widehat{L}} \tag{2.111}$$

since the term tortuosity refers semantically to a measure of the tortuousness of the pore structure and should, accordingly, be equal or larger than unity. On the other hand, the lineality expresses the straightness of the interconnected pore-space and is therefore expressed as the inverse of the tortuosity.

In the proposal by Carman (1937) the tortuosity was meant to correct for the extra path length and the directional change of the dynamic driving force, since the local gradient of the driving force along a stream tube is different from the gradient of the average driving force (Bear, 1972, p110). This interpretation then leads to tortuosity being defined as

$$\chi' \equiv \left(\frac{\widehat{L}}{\widetilde{L}_e}\right)^2. \tag{2.112}$$

However, in a statistical analysis of fluid flow through porous media Scheidegger (1954) also calculates the average of local fluid angles relative to the macroscopic driving force and prefers to refer to the unsquared ratio as the tortuosity.

Kemblowski and Michniewicz (1979) as well as Epstein (1989) concluded that a squared definition is actually a combination of two correcting factors of which one factor is ascribed to the velocity correction introduced by Carman and the other is a correction for the additional path length which a fluid particle follows through the pore-space. Kemblowski and Michniewicz (1979) also note that in the case of power law fluids the velocity and interstitial distance which the particles travel are raised to different powers, and therefore, one should use the proper correction for the velocity and not combine various factors in one correction term. However, Bear (1972, p115) advocates a squared definition of tortuosity in context of electric transport in porous media. The tortuosity then accounts for the reduced area available for charge transport as well as for the difference between the directions of the average flow and local flow. In the

present analysis the lineality is only a proportionality tensor between fluxes and no other physical phenomena is ascribed to it and this is reflected in the fact that the lineality reduces to a ratio of lengths.

Furthermore, in chemical engineering practice frequent reference is made to tortuosity as merely the ratio of the two lengths, implying a correction only for the extra path length (Comiti and Renaud, 1989). In the extension of the Dupuit-Forchheimer equation by Carman (1937; 1956, p12) only the unsquared ratio appears and, since the effect of an external driving force on the streamlines is not considered, the unsquared ratio is taken as the definition of tortuosity.

Another interesting tortuosity function is provided by Foscolo *et al.* (1983). They define the tortuosity as

$$\chi^F = \frac{\textit{average path length of fluid elements}}{\textit{bed height}} \tag{2.113}$$

and present a rationale to obtain the tortuosity as a function of the porosity. They argue that at any distance along the bed the fraction of fluid that proceeds axially by a distance δl is ϵ. The remaining fraction of fluid $(1-\epsilon)$ moves a distance δl laterally, and of this a further fraction ϵ will move forward an amount δl in its next transition. The fraction of fluid that travels a total distance of $2\delta l$ is the initial axial fraction and the lateral fraction, giving a total fraction of $\epsilon(1-\epsilon)^{2-1}$. By not moving any fluid in the axial direction again, it follows that the total fraction of fluid that progresses a distance $i\delta l, i = 1, 2, \ldots,$ in progressing an axial distance δl is $\epsilon(1-\epsilon)^{i-1}$. The tortuosity according to (2.113) then becomes

$$\begin{aligned} \chi^F(\epsilon) &= \sum_{i=1}^{\infty} \frac{i\delta l\epsilon(1-\epsilon)^{i-1}}{\delta l} \\ &= \sum_{i=1}^{\infty} i\epsilon(1-\epsilon)^{i-1} \\ &= \frac{1}{\epsilon} \end{aligned} \tag{2.114}$$

where the infinite sum has a limit equal to the reciprocal of the porosity (Swokowski, 1992). The advantages of this expression for the tortuosity is that it only depends on the porosity and it satisfies the requirement that

$$\chi^F(1) = 1. \tag{2.115}$$

According to Foscolo *et al.* (1983), such a model for tortuosity strikes a balance between simplicity and reality. An extension of this model to allow particles to move at inclined angles is provided by Punčochář and Drahoš (1991).

However, as summarised by Du Plessis and Diedericks (1997), the tortuosity depends on the type of material and a general expression such as (2.114) may not be appropriate for porous media in general. In addition, the relevant volume of fluid that moves axially is $U_{f\mathcal{L}}$ as presented in (2.71). Secondly, by using ϵ as the fraction of fluid that moves axially the fluid volume is weighted to the total volume although only the movement of fluid particles are considered. It is, therefore, suggested that

- the volume of fluid that moves axially be changed to $U_{f\mathcal{L}}$ and
- the axial fluid volume must be weighted only to the fluid volume, since only the movement of fluid volumes are considered.

If the axial direction is denoted by x_I, then the fraction of fluid that moves axially is given by $\mathcal{L}_{II}$ which, according to (2.74), is the axial component of the lineality tensor. By continuing the argument of Foscolo *et al.* (1983) with the abovementioned changes it follows from (2.114) that the tortuosity is given by

$$\chi^F = \sum_{i=1}^{\infty} I\mathcal{L}_{II}(1-\mathcal{L}_{II})^{i-1} = \frac{1}{\mathcal{L}_{II}}. \tag{2.116}$$

This indicates that the incorporation of the local direction of flow in the streamwise direction is important in calculation of the tortuosity and, as previously indicated, the lineality relates to the unsquared definition of tortuosity. However, for calculation of the tortuosity value one still has to revert to a particular porous medium model. In conclusion, it may be mentioned that Epstein (1989) noted that Foscolo *et al.* (1983) fail to distinguish between the average velocity in a tortuous capillary and the interstitial axial velocity and make reference only to the additional path length effect of tortuosity. The abovementioned changes to the tortuosity of Foscolo *et al.* (1983) are consistent with the analysis of Epstein (1989) and allows the tortuosity to correct for the increase in the capillary velocity over the interstitial velocity.

Another important issue is the relation between hydraulic and electrical tortuosity. As noted by Wyllie and Spangler (1952), the identification of electric and fluid tortuosities does not involve any closer analogy between the mechanisms of electrical and fluid flow in porous media than the assumption that, since both fluid and electrical conduction

involve, ipso facto, the presence of fluid, the average path length pertaining to the one case must be very similar to, if not identical with, that pertaining to the other. From the definition of the lineality, the electrical and hydraulic tortuosities are equivalent if the streamlines and electrical flow lines are equivalent. This, in turn, depends on the particular model which is used to obtain the $\tilde{\nu}_i$-field for the different transport phenomena. The application of the present analysis to the flow of electrical charge in porous media is pursued in more detail in chapter four.

2.7.11.2 First order tensorial expressions

In analysing mass transfer during flow through porous media, Gray (1975) proposed a tortuosity vector given in the present notation by

$$\chi_i^G = \frac{1}{U_f} \iint_{S_{fs}} \overset{o}{c} \nu_i \, dS \tag{2.117}$$

with $\overset{o}{c}$ being defined as the deviation of the local molar concentration of a chemical species from the intrinsic phase average concentration. A similar tortuosity vector has been introduced by Whitaker (1967) and Slattery (1972) except that they use the actual species concentration, c, in the definition. The tortuosity vector in (2.117) is dependent on the geometric configuration of the solid phase through the integral over the fluid-solid surface and indeed accounts for a decrease in diffusion rate due to the geometry of the porous medium (Lehner, 1979). Although Whitaker (1967) applies the tortuosity vector to various geometric models, its relation with the tortuosity as discussed by Carman (1956) has not been indicated. This tortuosity vector serves as an example of a quantity being defined as the tortuosity merely because it is related to geometry of the pore-space. Furthermore, this definition only appears in the context of diffusive transport and, if the concentration of chemical species is either zero or uniform, the tortuosity vector is also zero which limits its general usage as a parameter characterising porous media structures.

2.7.11.3 Second order tensorial expressions

The tortuosity is frequently defined as a scalar tortuosity factor with respect to the macroscopic transport direction. However, in general the tortuosity varies with direction in anisotropic media and thus requires a second order tensorial definition. When considering mass conservation of a species in a porous medium, Bear (1972, p107)

introduced the macroscopic tortuosity as a second order tensor by defining

$$T_{ij}^{B} = \frac{1}{U_f} \iiint_{U_f} \left(\frac{ds}{dl}\right)^2 \tilde{\nu}_i \tilde{\nu}_j dU \tag{2.118}$$

with l the length measured along the axis of a channel and s the curve length measured along a streamline. The tensor $\tilde{\nu}_i\tilde{\nu}_j$ represents a matrix whose nine elements are products of sines and cosines of the angles between the direction of a streamline at a point and the coordinate axis. This tensor has as diagonal components the fraction of the void volume presented to the flow in a certain direction relative to the total fluid volume. Although this definition and the lineality both relate to the average of the microscopic pathways of the fluid particles, they differ with respect to the incorporation of the streamwise direction. According to the present analysis, the volume of interest in defining the tortuosity is the effective streamwise volume, expressed by (2.71). The proposed definition of tortuosity differs from (2.118) as a definition of tortuosity, since it does not differentiate between the total void volume and the effective volume of fluid contributing to flow in a specific direction.

Another expression for the tortuosity has been proposed for porous media in general, by Bear and Bachmat (1991, p129) when analysing the average of a gradient in terms of the gradient of the average. According to the present notation they define the tortuosity as

$$T_{ij}^{BB} = \frac{1}{U_f} \iint_{S_{ff}} \nu_i \overset{\circ}{x}_j \, dS \tag{2.119}$$

and also indicate that it is symmetric. Here ν_i is the i-th component of the unit normal on the surface S_{ff} and $\overset{\circ}{x}_j$ is the position vector of the surface element dS relative to the centroid of the REV. Here integration is performed over the total fluid-fluid surface of the REV whilst the lineality in (2.110) is obtained if the integration is performed over the effective fluid-fluid area defined by the areosity. Once again, the main difference between these definitions arises due to the differences regarding the incorporation of the streamwise direction at local level.

It may be noted that the latter definition, (2.119), may also be cast in the form (Bear and Bachmat, 1991):

$$\iint_{S_{ff}} \overset{\circ}{x}_j \nu_i \, dS = \overline{x}^f_{j,i} + \frac{1}{\epsilon}\left(\overline{x}^f_j - \overline{x}_j\right)\epsilon_{,i} \tag{2.120}$$

with $\overline{x}_i$ the centroid of the REV and $\overline{x}_i^f$ the centroid of the fluid-filled part of the REV. In the case of isotropic porous media the fluid space is uniformly distributed about $\overline{x}_i$, which renders $\overline{x}_i^f = \overline{x}_i$ and thus (2.120) yields

$$T_{ij}^{BB} = \delta_{ij} \quad \Rightarrow \quad T_{II}^{BB} = 1 \tag{2.121}$$

since $\overline{x}_{j,i}^f = \delta_{ji}$ for isotropic porous media. A tortuosity value of unity is therefore predicted for isotropic media, casting some doubt on its validity as a measure of tortuosity.

Bear and Bachmat (1991) also indicate that

$$\left\langle \overset{o}{x}_j \right\rangle_{,i} = -\epsilon\delta_{ij} + \frac{1}{U_o}\iint_{S_{ff}} \nu_i \overset{o}{x}_j \, dS. \tag{2.122}$$

This result is confirmed by the analysis of Quintard and Whitaker (1994b; 1994d; 1995e) in which they use $\left\langle \overset{o}{x}_i \right\rangle_{,j}$ as a parameter to measure the order or disorder of a particular porous system. For a disordered system they require that $\left\langle \overset{o}{x}_i \right\rangle_{,j} \ll \delta_{ij}$ which indirectly confirms (2.121) for an isotropic material.

2.7.12 Discussion and conclusions

During the overview of tortuosity it emerged that there are numerous definitions and interpretations of tortuosity which where classified according to Clennell (1997) into four different classes. The lineality introduced in this section corresponds to the various retardation factors belonging to the second class. It was also noted that the direction of macroscopic transport is important in the definition of the tortuosity as well as the ability to relate the transport of different phenomena to their respective fluxes.

Due to the historical relation of the tortuosity with the work of Carman (1937), this section focused on generalising the initial definition of tortuosity by considering the problem of obtaining an average flux within a flow channel which may be used to represent the actual unknown flux. A defining equation for this average flux, termed the streamwise channel average flux, has been introduced. From this defining equation a number of features, namely the effective streamwise volume, the lineality tensor and tortuosity tensor have been derived. These derivations were conducted for both an REV and an REA, while the tensorial nature of the definitions ensure that the proposed definitions apply equally to anisotropic media. The parameter which describes the

straightness of flow is termed the lineality while its inverse which is a measure of the crookedness is termed the tortuosity.

The streamwise channel average flux is proposed as a better general estimate of the actual intrapore fluxes than the intrinsic phase average flux. A formal relationship has been derived between the channel average flux and the phase and intrinsic phase average fluxes, applicable to porous media in general. It was also shown that a factor of paramount importance in determining the tortuosity is the streamline direction and orientation, as well as the effective area of streamwise transport as defined by the areosity.

The general expression for the lineality was applied to a capillary model where it was shown that both the lineality and tortuosity reduce to a ratio of lengths. It was also indicated through a simple tubular model that the streamwise channel average velocity is independent of cross-flow between different streamwise channels.

The only factor that may be considered arbitrary in the definition of the lineality is the volume appearing in the denominator of the (2.74). In the definition (2.74) it is the fluid volume, but without loss of generality it may also have been the total volume (U_o) of the REV under consideration. The inclusion of the total volume would still allow the lineality to reduce to a ratio of lengths when applied to the capillary model and the symmetry conditions for the lineality would also be unaltered. A possible advantage of scaling the effective volume to the total volume may be the removal of the porosity as a dependent variable from the definition of the lineality. This may be illustrated by considering the tube system of Suman and Ruth (1993) introduced in Section 2.6.7 and illustrated in Figure 2.9. If the total area of the streamwise channels ($\frac{\pi}{4}(\delta_a^2+\delta_b^2)$) is kept constant, but the diameter of the cross-flow channel δ_c is varied, then the lineality would also vary through the changes invoked in the fluid volume. However, if the total volume is used in the ratio of the lineality, then it will be independent of the cross-flow between different streamwise channels. The lineality can also be compared to the areosity for the inclined tubes intersecting an REA as shown in Figure 2.4. The lineality for this system is

$$\mathcal{L}_{(1)} = \frac{A_{p(1)}}{A_{f(1)}} = \cos\theta \tag{2.123}$$

and depends on the angle between the axes of the tubes and the REA. However, the angular dependence stems from the variable fluid area in the denominator and not from the effective streamwise area which is the essential feature which the lineality represents. A weighting to the total area would render the areal lineality equal to the areosity which

is the same for all the cases in Figure 2.4. However, the initial definition of the lineality is left unaltered and the effective streamwise volume is weighted to the fluid volume.

An alternate expression for the lineality was derived in terms of an integral over the fluid-fluid volume of an RUC while it was also shown that the lineality is symmetric for isotropic porous media as well as for porous media homogeneous with respect to porosity and structure. The lineality and tortuosity were also related to some of the classical definitions of tortuosity and some differences and similarities were discussed. The most noteworthy difference is the inclusion of the effective streamwise volume or area in contrast to the total volume or total fluid-fluid area which appear in the different definitions.

It is envisaged that the lineality and streamwise channel average flux will be used in different pore-scale models and for different transport phenomena. Through such a process, the contributions and differences of various transport phenomena and porous medium characteristics may be illustrated.

2.8 Summary

During this chapter some fundamental concepts regarding the analysis of transport in porous media have been presented. These included descriptive geometric parameters as well as parameters by which to classify porous structures. An introduction was given regarding some modelling techniques to obtain macroscopic descriptions of flow through porous medium. Some porous medium modelling techniques were noted which may aid comparison with the modelling approach applied in the dissertation. In was also shown in which manner Carman (1936) introduced the initial definition of the tortuosity.

The volume averaging theory, on which this study is based, was presented in some detail. The statistical properties of the REV were presented and some averaging rules and identities were derived. Additional porous medium and transport parameters were presented in context of the volume averaging theory.

In the latter section the general problem of obtaining a channel average flux more representative of the actual microscopic flux than the interstitial phase averaged flux was addressed. The solution of this problem led to the definition of the streamwise channel average flux which is proposed as pore-scale estimate of the actual interstitial flux. The tortuosity and lineality tensors evolved naturally within this formalism and it was indicated that the tortuosity tensor is dependent, among other things, on the

configuration of the microscopic flux lines and the direction of macroscopic transport. The derivation of the lineality and tortuosity is general and applicable to any flux field within homogeneous porous media. Two different interpretations of the tortuosity were presented. One of these interpretations conforms to a general class of tortuosities where the tortuosity depends on the type of transport process. The other interpretation enables the calculation of a geometric tortuosity where the microscopic flux lines are equivalent for various transport processes if the complete pore-space is equally accessible to transport and if the streamline configuration is not influenced by fluid mechanical effects, such as inertial effects.

The present discussion takes the tortuosity beyond its usage in capillary and hydraulic radius models and the visualisation that flow takes place through tortuous conduits. However, it was also indicated that the lineality and tortuosity reduce to a ratio of lengths under certain simplifying conditions. The lineality and tortuosity were also related to some of the classical definitions of tortuosity presented in literature. The derivation of the lineality for an REA provides a more general proof of the areosity than was previously presented by Suman and Ruth (1993).

This chapter leans more towards the theoretical side, but in subsequent chapters it is indicated how a combination of the channel average flux with pore-scale porous medium models and the volume averaging process provide a powerful combination to model various physical transport phenomena in porous media. Therefore, in subsequent chapters the results of this section are applied to various different transport phenomena to indicate its usefulness and to aid modelling of various physical phenomena. In the analysis of transport in porous media reference is also made to the geometric parameters introduced during this chapter. This chapter therefore provides the theoretical platform from which transport processes can be analysed with the aim of producing practical results which may be used in industry or to aid numerical simulations of transport processes.

Chapter 3

FLOW THROUGH ANISOTROPIC POROUS MEDIA

3.1 Introduction

This chapter is devoted to the analysis of the flow of Newtonian fluids through essentially anisotropic homogeneous porous materials. Considering the large amount of different types of porous materials which exist, a general theory accurately describing the flow through all types of materials is at best an arduous task and inevitably some selection is required. In this chapter emphasis is, therefore, put on a particular general modelling strategy which is applied to a selected number of materials rather than on a more general approach partially applicable to an abundance of materials. However, to obtain some diversity of porous structures three materials with distinct geometric characteristics have been selected, namely foamlike materials, granular porous media and fibre beds. The geometry of these types of materials are idealised in context of a so-called Representative Unit Cell (RUC). For materials which differ substantially from these idealised media a different RUC will have to be constructed, but the modelling strategy introduced may be retained. Flow through these types of materials have already been analysed with the RUC model, but the analyses were restricted to isotropic materials (Du Plessis and Masliyah, 1988; Du Plessis and Masliyah, 1991; Du Plessis, 1994; Du Plessis and Diedericks, 1997). However, as subsequently indicated a generalisation to include anisotropy is rather tedious and impossible without the development of Section 2.6.4 concerning the channel average fluxes. This chapter then also serves the purpose of implementing the general theory previously developed to obtain results useful for practical applications.

At first fluid transport is considered through anisotropic foamlike materials. These re-

sults are then compared to experimental pressure drop measurements taken during flow through high porosity anisotropic metallic plugs. The results are important as these types of materials are presently being used as mist eliminators in the chemical engineering industry. During this discussion the RUC model is applied in different ways and its limitations and benefits are discussed. Thereafter, flow through anisotropic granular materials and prismatic bundles are considered although these analytical analyses are not validated against any experimental data and is included for completeness.

It is the overall objective of this chapter to apply the general theory developed in Chapter 2 to particular flow problems and to indicate its practical utility. Furthermore, some restraints are put on the materials under investigation to produce more specific results which are of practical and industrial use and which may be used to eliminate prediction uncertainty of calibration coefficients and to minimise empiricism.

3.2 Darcy's law

The flow of fluids, be it in rivers, in aqueducts or in the design of boats and sails, may be considered as one of the oldest investigated phenomena. Writings indicate that fluid motion was investigated in a scientific manner as early as 600 B.C. by Thales of Miletus (Tokaty, 1971). However, in the modern era of information technology and micro processors, fluid mechanics, including flow through porous media, is a physical phenomenon of frequent and active research which finds application in a wide variety of engineering and scientific fields. Due to the large amount of fields where flow through porous media is of essence, many models are continuously produced for analyses of a wide variety of transport phenomena. As noted in Chapter 2, some of these models are purely theoretical, while others are semi-empirical and most often used in engineering fields and other models are more of a numerical nature. There are not many purely deterministic models which can predict transport processes from only certain geometric information about the porous medium. The main objective of this chapter is to obtain a deterministic, or at least very near deterministic, model for fluid transport in anisotropic homogeneous porous media.

One of the most profound relations applicable to flow through porous media is the relationship between the pressure gradient and superficial velocity developed by Henry Darcy about 140 years ago (Darcy, 1856). The empirical Darcy law relates the flow of water through a porous medium with a unit cross-sectional area to the product of the hydraulic gradient and a constant named the hydraulic conductivity. However, Darcy's law has been applied to problems as diverse as groundwater hydraulics, petro-

leum reservoir exploration, soil physics, geophysics, food drying processes and chemical engineering. As shown in (2.58) for one-dimensional flow it reads

$$q_i = -\frac{K}{\mu}(P_{f,i} - \rho g_i) = -\frac{K}{\mu}P_{,i} \tag{3.1}$$

where μ is the dynamic viscosity of the fluid, K is the Darcy permeability coefficient of the porous medium, P is the piezometric pressure and q_i is the superficial or seepage velocity (Bear, 1972; Dullien, 1979). The coefficient of proportionality is referred to as the hydraulic permeability only if (3.1) is applied to the flow of water. The permeability coefficient appearing in Darcy's law has to be determined experimentally and current efforts seem to indicate that determination of the permeability coefficient, or other coefficients it is related to, by means other than empirical measurement would be rather difficult (Rice, *et al.*, 1970). Much effort has been expended on attempting to obtain analytical expressions for the permeability coefficient (Kaviany, 1995). Some of the models developed for this purpose have been introduced in Chapter 2 and various expressions relating K to the porosity and other structural parameters are presented by Dullien (1979). However, these models still contain parameters which have to be inferred from experiment and a purely deterministic equivalent of Darcy's law is still a quest for many porous media modellers.

There are also additional limitations to Darcy's law which modellers attempted to remedy through the introduction of empirical terms and factors. For example, to account for the influence of macroscopic interfaces in a porous medium, Brinkman (1947a; 1947b) added a macroscopic diffusion term to Darcy's law leading to

$$P_{f,i} = \rho g_i - \frac{\mu}{K}q_i + \mu^* q_{i,jj} \tag{3.2}$$

where μ^* is an effective viscosity. To accommodate available experimental data Brinkman (1947a; 1947b) found that the effective viscosity should be the same as the fluid viscosity. However, volume averaging of the Navier-Stokes equations for flow in porous media indicate that the two viscosities are in general different (Gray and O'Neill, 1976). According to Qin and Kaloni (1994), for flow through a porous medium with high permeability and rigid boundaries Brinkman's equation give preferable results. However, Brinkmans's equation is inertia-free and hence valid only for creeping flow.

As noted in Chapter 2, although a porous medium may be homogeneous with respect to porosity, structure and microstructural characteristic lengths, certain macroscopic porous medium properties may vary with direction at a particular point, yielding the

material anisotropic with respect to that property (Bear and Bachmat, 1991). As a consequence, the permeability of anisotropic porous media varies with the direction of fluid flow or pressure gradient (Bear, 1972; Rice, *et al.,* 1970; Scheidegger, 1974). Extensions of (3.1) to incorporate the directional dependence of the permeability subsequently led to the introduction of a tensorial Darcy equation for an anisotropic porous medium which also relates the superficial velocity linearly to the pressure gradient through the permeability tensor, K_{ij} of the porous medium,

$$q_i = -\frac{1}{\mu} K_{ij} P_{,j}. \tag{3.3}$$

According to this equation if the porous medium has an arbitrary orientation with respect to a coordinate system and if the pressure gradient is directed along a specific coordinate, then in general there are three different flow rates in each of the coordinate directions whereas in an isotropic medium the flow will be along the direction of the pressure gradient. As noted in Section 2.5.7, it is generally accepted that the permeability tensor for homogeneous materials is symmetric and proofs in this regard are presented by Neuman (1977), Whitaker (1969) and Whitaker (1996) although their arguments do not show that the permeability must be symmetric for all porous media. Szabo (1968) assumed that the permeability is dependent upon the structural characteristics of the porous medium and that the medium is structurally symmetric with respect to three mutually perpendicular planes and from these assumptions he showed that Darcy's law is valid in each of the directions normal to these planes of symmetry and the permeability follows the transformation laws of second-order Cartesian tensors. By accepting the symmetry of the permeability tensor, it was indicated that it may be diagonalised by Bear and Bachmat (1991) and Szabo (1968) and the coordinate axes in which the permeability tensor is diagonal is often referred to as the principal material axes of the medium (Whitaker, 1969; Neuman, 1977; Bear and Bachmat, 1991).

According to Rice *et al.* (1970), the differences in the directional permeabilities depend on the shape, orientation and concentration of the particles which form the bed or, for a consolidated medium, were consolidated into a porous bed. Measurements of anisotropic permeability are made by simultaneously measuring the flow rate and pressure drop. Usually the measurements are assumed to be made along the principal axes of the specimen, that is the directions which characterise the thee principal components of the permeability tensor. In practice this generally corresponds to making the measurements perpendicular to the bedding plane and at various angles parallel to the bedding plane. The maximum and minimum permeabilities in this plane, if perpendicular, are assumed to be the principal permeability components in that plane. Dullien (1979) has indicated that two types of directional permeability measurements are possible: In the one case,

the flow is confined to the direction of interest and the component of the pressure gradient in that direction is measured while in the second case the pressure gradient is fixed and the component of the flow in the direction of the pressure gradient is measured. These measured permeabilities are not the same but, as further noted by Dullien (1979), the differences between these two types of permeabilities are small enough in practice to be neglected. However, when the measurements are made in the principal directions of the medium then the pressure gradient vector and the flow vector are collinear and the measurement of permeability is unambiguous.

Therefore, the diagonal components of the permeability tensor must still be determined empirically. It would be desirable to predict the permeabilities from fundamental knowledge about the characteristics of the porous medium, such as the pore size distribution, the porosity and the structure of the material, of course, only possible for idealised porous media with well-defined geometric properties. The current effort is just such an approach and aims to minimise direct permeability measurements. Following the analysis of Du Plessis (1992a), and as summarised in Du Plessis and Diedericks (1997), the average flow through various isotropic porous media are described by the phase average Navier-Stokes equation obtained by making use of volume averaging concepts. A closed form of the equation is obtained by a rectangular modelling representation of the average geometry as well as quantification of the microscopic fluid-solid interaction in terms of the superficial velocity and measurable macroscopic characteristics of the porous medium. This includes accurate quantification of viscous shear stresses as well as the introduction of local flow recirculation in channel sections to account for the inertial effects predominant at high Reynolds number flow. For application to anisotropic materials it is necessary to include a streamwise channel velocity as a more accurate estimate of the actual velocity than the interstitial velocity. This in turn warrants quantification of tortuosity as a ratio of fluid volumes. In this manner a rigorous mathematical description of the fluid-solid interaction allows derivation of a relationship between the pressure gradient and superficial velocity in terms of structural parameters of the porous medium.

3.3 The Forchheimer equation

Another limitation of Darcy's law is the fact that it is only valid over a limited range of Reynolds numbers (Bear, 1972). The Reynolds number (Re) had its origin in flow through conduits and it is a dimensionless number expressing the ratio between the inertial and viscous forces and is used as a criterion to distinguish between various flow

regimes. For flow in porous media it is generally defined as

$$Re \equiv \frac{q\rho h}{\mu} \tag{3.4}$$

where q is usually selected as the magnitude of the superficial velocity, h is some selected length dimension of the porous medium, ρ is the density of the fluid and μ is the dynamic viscosity of the fluid. It has been found experimentally that the linear relation between pressure gradient and superficial velocity breaks down for flow above a certain Reynolds number limit (Bird *et al.*, 1960; MacDonald *et al.*, 1979). Summaries of data indicating this deviation are also presented, amongst others, by Bear (1972) and Kaviany (1995). In general four flow domains have been identified, namely a Darcy or creeping flow regime, an inertial flow regime, an unsteady laminar flow regime and a turbulent flow regime (Bear, 1972; Bennethum and Giorgi, 1997). In this study the aim is to predict pressure gradients in only the first two domains.

Consequently, quite a number of efforts have been made to furnish a universal expression relating the pressure gradient to the specific discharge by adding additional empirical terms to Darcy's law. For example, Dupuit (1863) and Forchheimer (1901) added an additional empirical term, which is proportional to the square of the velocity, to Darcy's law and proposed

$$P_{,i} = -\frac{\mu}{K}q_i - \beta\rho q q_i \tag{3.5}$$

where β is an inertial parameter and ρ is the density of the fluid. A multitude of works exist which present experimental evidence for the use of the Forchheimer equation, for instance Tek (1957), Ward (1964), Beavers and Sparrow (1969) and Dullien and Azzam (1973). From the analysis of MacDonald *et al.* (1979) it also appears as if the correlative form of the relationship between the pressure gradient and velocity best representative for high Reynolds number flows seems to be a Forchheimer-type equation of the form

$$-P_{,i} = Mqq_i + Nq_i \tag{3.6}$$

where N and M are empirical coefficients which depend on structural parameters of the porous medium and the fluid viscosity (Ahmed and Sunada, 1969; Hassanizadeh and Gray, 1987). At low values of the superficial velocity, the first term on the right hand side of (3.6) becomes much smaller than the second. Neglecting the first term, reduces the pressure gradient to Darcy's law. As indicated by models applicable to this flow

regime, such as the Carman-Blake-Kozeny equation, momentum dissipation takes place through molecular transfer, that is, by virtue of the velocity gradients as a result of the viscosity. Conversely, for higher superficial velocities the second term on the right hand side is negligibly small in comparison with the first one, and discarding it, a square law is obtained for the pressure gradient.

Theoretical derivations of the Forchheimer equation have been attempted using several different methods, for example dimensional analysis Ward (1964), volume averaging (Ahmed and Sunada, 1969; Cvetković, 1986; Ruth and Ma, 1992), homogenization (Mei and Auriault, 1991) and hybrid mixture theory coupled with order-of-magnitude arguments (Hassanizadeh and Gray, 1987). In general, these theoretical methods recover generalised non-linear equations of which the classical Forchheimer equation is a quadratic approximation. However, Mei and Auriault (1991) recover a classical quadratic Forchheimer-type equation only for anisotropic materials and for the isotropic case they find a cubic correction to Darcy's law. Additional information on the developments of the Forchheimer equation is provided by Hannoura and Barends (1981).

For this flow regime there are differences of opinion as to the exact reasons for momentum dissipation and the three most commonly suggested causes of the non-linearity are turbulence, microscopic inertial forces and increased microscopic drag forces (Bennethum and Giorgi, 1997). One case where the non-linear relationship, or so-called Forchheimer effect, is attributed to the onset of turbulence within the flow channels is the development of the Burke-Plummer equation (Bird *et al.*, 1960). However, experimental evidence indicates that the non-linear dependence appears before the onset of turbulence and it is generally agreed that it is not initiated by turbulence (Beavers and Sparrow, 1969; Scheidegger, 1974). This is also indicated by, amongst others, Ahmed and Sunada (1969) where they show that energy losses caused by turbulence of flow through porous media may be neglected and, therefore, the causes for the Forchheimer effect are also sought in other inertial effects such as flow separation and curvature of stream tubes (Carman, 1937; Dullien, 1979). Hassanizadeh and Gray (1987) derived the Forchheimer equation by attributing the origin of the non-linearity to increased macroscopic drag on the pore walls. A simplified form of their equation is

$$\epsilon P_{,i} = (a_1 + a_2 v^s)\, v_i^s \tag{3.7}$$

where v_i^s is the velocity of the fluid relative to the solid phase and a_1 and a_2 are coefficients which may depend on the fluid density, the porosity and the temperature. In addition, they also note that these coefficients cannot be determined theoretically and must be measured (Hassanizadeh and Gray, 1988). However, Barak (1987) con-

tested their argument and supported the view that, as the Reynolds number changes, microscopic inertial forces contribute to the change of the microscopic steamline shape and flow pattern in the pore-space. Ruth and Ma (1992) and Ma and Ruth (1993) investigated the physics behind the Forchheimer relation by using the volume averaging approach and indicated that it is related to microscopic inertial effects which are manifested through terms involving integrals over the fluid-solid surface. By applying the averaged momentum transport equation to some simplified conditions they concluded that it is due to microscopic inertial forces which indirectly distort the area integral term by affecting the local pressure and velocity fields. Their conclusion is similar to that of Chetković (1986) who indicated that inertial effects for flow in porous media should not be treated in the same manner as, for example, the maroscopic resistivity force or macroscopic stress, with regard to defining their macroscopic constitutive equations. Both the resitivity force and the macroscopic stress have their origin in the in microscopic forces, either over S_{fs} or in U_f, while the macroscopic inertial forces are of a different nature and are of kinematical origin and are direct functions of the microscopic flow. The author supports this point of view that the microscopic pressure differences at high Reynolds number flow are caused by microscopic flow separation due to the changing streamline configuration.

The Forchheimer effect has also been modelled with moderate success by Du Plessis and Masliyah (1988; 1991) as being the result of flow velocity development within channel sections. However, these results were improved by Du Plessis (1994) where the inertial effects were attributed to local flow separation within the channels. Regardless of the reasons behind the nonlinearity, it would appear as if a Forchheimer-type equation yields an adequate semi-empirical relation between the pressure gradient and superficial velocity during flow through porous media. Additional experimental data also indicates that at high Reynolds number flow the pressure difference conforms to a square drag law (MacDonald *et al.,* 1979; Bird *et al.,* 1960; Aravin and Numerov, 1965; Montillet *et al.,* 1992).

3.4 Transport equations

3.4.1 Fluid velocities

The present analysis of flow through anisotropic porous media is based upon a volumetric averaging approach as outlined in Chapter 2. Accordingly, intrapore transport entities and equations may be averaged volumetrically over a Representative Elementary

Volume (REV) to derive macroscopic balance equations for various transport phenomena. As previously noted, an REV is regarded as a volumetric element of the porous medium bounded in size by both an upper and lower limit to be representative of local flow conditions within the porous medium. Conceptually an REV is defined for each point of the porous domain and it is assumed to have a constant size, shape and orientation at all times.

The phase average of the actual fluid velocity field over an REV yields the *superficial velocity*, q_i, which is defined as

$$q_i = \langle v_i \rangle \equiv \frac{1}{U_o} \iiint_{U_f} v_i \, dU. \tag{3.8}$$

The superficial velocity is also referred to as the Darcy velocity (Fried and Combarnous, 1971; Allen *et al.*, 1988) or the filter velocity (Flügge, 1972; Dullien, 1979). It quantifies the average discharge velocity through the porous medium and is thus obtainable by overall experiment. The intrinsic phase average velocity, also named the *interstitial velocity*, is defined as

$$u_i = \langle v_i \rangle^f \equiv \frac{1}{U_f} \iiint_{U_f} v_i \, dU. \tag{3.9}$$

This is the average velocity at which fluid particles are displaced in the general flow direction as they traverse the porous medium and has, therefore, been used to approximate the actual fluid velocity (Irmay, 1961). These two velocities are related according to the relationship

$$q_i = \epsilon \, u_i. \tag{3.10}$$

It is evident that at each point the directions of u_i and q_i are identical signifying the macroscopic *streamwise* direction at that point. The streamwise direction may be indicated by the streamwise unit vector $\hat{\nu}_i$.

According to the analysis in Section 2.6, it is possible to introduce another macroscopic velocity, namely the channel average velocity. The analysis of Section 2.6 was derived for a general Γ-continuum and to make the results specific to the transport of Newtonian fluids it is necessary to set $\Gamma = U_f$. It thus follows that $\gamma = 1$, $\tilde{n}_{\gamma i} = v_i$ and the flux field of Section 2.6 relates directly to the fluid velocity field. The channel average velocity

then follows from (2.72) and it may be expressed as

$$\widehat{w}_{\gamma i} \equiv \widehat{w}_i = \frac{1}{U_{f\mathcal{L}}} \iiint_{U_f} v_i \, dU. \tag{3.11}$$

The volume to which the integral in (3.11) is weighted is the effective streamwise volume and according to (2.71) it is defined as

$$U_{f\mathcal{L}} \equiv \widehat{U}_{f\mathcal{L}} = \iiint_{U_f} \widetilde{\nu}_m \widehat{\nu}_m \, dU \tag{3.12}$$

where $\widehat{\nu}_i$ is the streamwise unit vector and $\widetilde{\nu}_i$ is a unit vector tangent to the streamlines at each point in the fluid phase. Unlike the superficial velocity the average streamwise channel velocity is not a measurable velocity and it is only of a conceptual nature which may aid quantification of the actual interstitial velocity.

From (2.81), and as also shown in (2.96), it follows that these velocities are related according to

$$q_i = \epsilon u_i = \epsilon \widehat{w}_m \mathcal{L}_{mi} \tag{3.13}$$

and the different velocities are schematised in Figure 2.7.

3.4.2 Microscopic transport equations

The fluid traversing the porous medium is assumed to

- consist of a single incompressible Newtonian fluid with
- constant density, ρ and
- constant viscosity, μ.

The *continuity equation* for mass conservation for

- incompressible flow

in the interstitial fluid volume may be expressed as

$$v_{i,i} = 0 \tag{3.14}$$

where v_i is the actual fluid velocity field within the channels of the porous domain.

The shear stress tensor for incompressible Newtonian fluids may be expressed (Bird *et al.*, 1960; Whitaker, 1968) as

$$\tau_{ij} = \mu(v_{i,j} + v_{j,i}) \tag{3.15}$$

and with (3.14) it follows that

$$\tau_{ij,j} = \mu v_{i,jj}. \tag{3.16}$$

With these fluid properties the *microscopic Navier-Stokes equation* governing the interstitial flow is given, in Cartesian tensor notation, by

$$\rho\frac{\partial v_i}{\partial t} + \rho\left(v_j v_i\right)_{,j} + p_{,i} - \rho g_i - \mu v_{i,jj} = 0 \tag{3.17}$$

where g_i is the gravitational force per unit mass acting on the fluid, p is the mean microscopic pressure at each point and v_i is the actual fluid velocity within the channels of the porous domain (Bird *et al.*, 1960; Whitaker, 1968; Slattery, 1972). The temporal term accounts for the rate of increase of momentum per unit volume while the second term on the left hand side represents the rate of momentum gain by convection per unit volume. The third term represents the pressure force on the fluid per unit volume with the fourth term being the gravitational force on the fluid. The last term on the left hand side of (3.17) accounts for the rate of momentum gain by viscous transfer per unit volume (Bird, 1960, p78). Together (3.14) and (3.17) govern the actual interstitial fluid motion at any point within the fluid volume.

At the microscopic level it is mostly impossible to describe the geometry of the interfacial boundaries and to observe or measure interstitial variables. Should the complex interfacial boundaries of the fluid volume be known an attempt could be made to arrive at a numerical solution for the fluid velocity field which is mostly an ardeous task. To overcome these difficulties, interstitial variables are volumetrically averaged yielding transport equations which govern the average transport behaviour at the macroscopic level.

3.4.3 Macroscopic transport equations

The macroscopic continuity and Navier-Stokes equations which govern the average behaviour of the flow are derived by volumetrically averaging (3.14) and (3.17) over an REV. The resulting governing equations are general in the sense that they apply to fluid transport in any porous medium which satisfy the averaging constraints discussed in Chapter 2. It is further assumed that

- the flow is laminar without the influence of body forces except for gravity,
- local flow separation within the microscopic channels is allowed and
- a no-slip condition applies to all fluid-solid surfaces.

The volumetric averaging rules and identities presented in Tables 2.1 and 2.2 are used to derive the macroscopic transport equations. Therefore, by employing averaging Rule 2 in Table 2.2 together with (3.8) and the condition of no-slip, the phase average of the left hand side of the continuity equation, (3.14), may be written as

$$\begin{aligned} \langle v_{i,i} \rangle &= \langle v_i \rangle_{,i} + \frac{1}{U_o} \iint_{S_{fs}} v_i \, \nu_i \, dS \\ &= q_{i,i} + \frac{1}{U_o} \iint_{S_{fs}} v_i \, \nu_i \, dS \\ &= q_{i,i}. \end{aligned} \tag{3.18}$$

The *macroscopic continuity equation* is thus given by

$$q_{i,i} = 0. \tag{3.19}$$

According to Identity 1 in Table 2.1, the momentum transport equation (3.17) may be averaged term by term. The phase average of the temporal term yields

$$\begin{aligned} \left\langle \rho \frac{\partial v_i}{\partial t} \right\rangle &= \rho \frac{\partial \langle v_i \rangle}{\partial t} - \frac{\rho}{U_o} \iint_{S_{fs}} v_i v_m^b \nu_m \, dS \\ &= \rho \frac{\partial q_i}{\partial t} \end{aligned} \tag{3.20}$$

since the volume of the fluid phase contained within the averaging volume is independent of time thus implying that the boundary velocity of the fluid-solid surface is zero.

By employing Rule 2 twice and using Identity 15, the phase average of the convective term yields

$$\begin{aligned}
\langle \rho(v_j v_i)_{,j} \rangle &= \rho \langle (v_j v_i)_{,j} \rangle \\
&= \rho \langle v_i v_j \rangle_{,j} + \frac{\rho}{U_o} \iint_{S_{fs}} \nu_j v_i v_j \, dS \\
&= \rho \langle v_i v_j \rangle_{,j} \\
&= \rho \left(\frac{1}{\epsilon} \langle v_i \rangle \langle v_j \rangle + \epsilon \left\langle \overset{o}{v}_i \overset{o}{v}_j \right\rangle^f \right)_{,j} \\
&= \rho \left(\frac{1}{\epsilon} q_i q_j \right)_{,j} + \rho \left(\epsilon \left\langle \overset{o}{v}_i \overset{o}{v}_j \right\rangle^f \right)_{,j}.
\end{aligned} \tag{3.21}$$

The phase average of the pressure term may be written via Rule 5 as

$$\langle p_{,i} \rangle = \epsilon \langle p \rangle^f_{,i} + \frac{1}{U_o} \iint_{S_{fs}} \overset{o}{p} \nu_i \, dS. \tag{3.22}$$

The phase average of the body forces yields

$$\begin{aligned}
\langle \rho g_i \rangle &= \rho \langle g_i \rangle \\
&= \rho g_i \langle 1 \rangle \\
&= \epsilon \rho g_i.
\end{aligned} \tag{3.23}$$

The phase average of the last term in (3.15) may be written by means of Rule 2 in the following form

$$\begin{aligned}
\langle \mu v_{i,jj} \rangle &= \mu \langle v_{i,jj} \rangle \\
&= \mu \langle v_{i,j} \rangle_{,j} + \frac{\mu}{U_o} \iint_{S_{fs}} v_{i,j} \nu_j dS.
\end{aligned} \tag{3.24}$$

The first term on the right hand side of (3.24) may be further analysed according to the same rule such that (3.24) becomes

$$\begin{aligned}
\langle \mu v_{i,jj} \rangle &= \mu \langle v_i \rangle_{,jj} + \frac{\mu}{U_o} \left(\iint_{S_{fs}} v_i \nu_j \, dS \right)_{,j} + \frac{\mu}{U_o} \iint_{S_{fs}} v_{i,j} \nu_j dS \\
&= \mu \langle v_i \rangle_{,jj} + \frac{1}{U_o} \iint_{S_{fs}} \mu v_{i,j} \nu_j \, dS \\
&= \mu q_{i,jj} + \frac{1}{U_o} \iint_{S_{fs}} \mu v_{i,j} \nu_j \, dS
\end{aligned} \tag{3.25}$$

where the condition of no-slip once again forces the surface integral which explicitly contains the velocity as a factor to be zero.

Collecting the various terms leads to the following *phase average of the momentum transport equation*

$$\rho\frac{\partial q_i}{\partial t} + \rho\left(\frac{1}{\epsilon}q_j q_i\right)_{,j} + \epsilon\langle p\rangle^f_{,i} - \epsilon\rho g_i - \mu q_{i,jj} + \rho\left(\epsilon\left\langle \mathring{v}_j\mathring{v}_i\right\rangle^f\right)_{,j} - \frac{1}{U_o}\iint_{S_{fs}}\left(\mu v_{i,j}\nu_j - \mathring{p}\nu_i\right)dS = 0. \tag{3.26}$$

Derivations of the momentum transport equation are also presented, amongst others, by Whitaker (1969), Du Plessis and Masliyah (1988), Bear and Bachmat (1991), Tucker and Dessenberger (1994) and Whitaker (1997). The first five terms on the left hand side of (3.26) closely resemble the left hand side of the microscopic Navier-Stokes equation in (3.17) in that these terms describe similar features of the flow as their microscopic counterparts except for the level of application. For example, the first term on the left hand side of (3.26) represents the time rate of change of the superficial velocity while the second and fifth terms account for the macroscopic convection and diffusion of momentum, respectively. The fifth term on the left hand side is also known as the Brinkman correction (Whitaker, 1986; 1996; Brinkman, 1947a; 1947b) and conditions under which it may be neglected are discussed by Whitaker (1986) and Quintard and Whitaker (1994a). The latter three terms arise through the course of the averaging process and contain all the information regarding the influence of the porous medium lost during the averaging process on the traversing fluid. Whitaker (1996; 1997) refers to the momentum dispersion term, $\rho\left(\epsilon\left\langle \mathring{v}_j\mathring{v}_i\right\rangle^f\right)_{,j}$ as a volume filter and to the latter two terms as surface filters, since the microscopic information that can be extracted from these terms in the closure problem will be filtered by them. Their evaluation is dependent on the local flow conditions within the porous microstructure and for closure explicit assumptions regarding the pore-space must be introduced.

In the case of a

- uniform, time-independent superficial velocity field,

the temporal, inertial and macro-viscous terms disappear leaving the following pressure gradient equation

$$\epsilon U_o P_{,i} = \iint_{S_{fs}}(\mu v_{i,j}\nu_j - \mathring{p}\nu_i)\,dS - \rho\left(\epsilon\left\langle \mathring{v}_j\mathring{v}_i\right\rangle^f\right)_{,j}. \tag{3.27}$$

Here the pressure head, $P_{,i} = \langle p \rangle^f_{,i} - \rho g_i$, also includes the gravity term. The fluid-solid integral must be solved on each and every point of the fluid-solid interface and, therefore, requires an adequate description of the fluid-solid surface and corresponding surface interactions.

3.5 The Representative Unit Cell (RUC)

In general, analyses of the interactions on the fluid-solid surfaces require two sets of information. In the first instance it is necessary that the configuration of the interstitial fluid-solid surface be adequately modelled. In addition, it is also necessary to address the flow pattern within the porous medium configuration. In this section a pore-scale model is introduced which addresses both these points through a conceptual representation of the pore-space from which information on the internal flow configuration can be retrieved. With this model it is then possible to determine approximate values of the surface integral in (3.27) in terms of measurable parameters. However, as indicated in Chapter 4 this model extends beyond fluid flow and may also be used for other transport quantities, but for this chapter, focus is only placed on the flow of Newtonian fluids.

The actual interstitial pore-space is seldom amenable to rigorous analysis due to the vast amount of structural data required. Du Plessis and Masliyah (1988), therefore, proposed a pore-scale modelling procedure which aims to approximate the porous material by imbedding the average geometric characteristics of the porous material as found in an REV within the smallest hypothetical unit cell of rectangular geometry, positioned with its volumetric centroid collocated with that of the corresponding REV. Such a Representative Unit Cell (RUC) provides the facility to consider flow conditions within the most elementary control volume of the particular porous medium and still have all the geometric properties of the REV at hand for modelling of physical phenomena. The RUC differs from the REV in that the latter is large enough to give reasonable representative averages whereas the RUC is of minimal size into which the average geometry is built. The average geometric characteristics of a porous medium are represented within a rectangular RUC by suitable arrangement of blocks of solid material. The initial modelling of Du Plessis and Masliyah (1988) and additional applications of their approach (Du Plessis and Roos, 1994; Van der Westhuizen and Du Plessis, 1994; Smit *et al.*, 1998) focussed essentially on isotropic porous media. However, the concept of an RUC is presently extended to also incorporate certain types of anisotropic porous media.

The first question to be raised in conjunction with an RUC is what is the average geometry of a porous material. It is not a quantity that is exactly quantifiable, but it may be understood to imply the most important observable features of a porous medium. For instance, one of the primary features to consider when constructing an RUC is the geometric character and connectivity of the material matrix. In this regard a distinction has been made between foamlike materials, granular materials, and prismatic bundles as summarised by Du Plessis and Diedericks (1997). One of the primary differences amongst these RUC's is the nature of the solid phase which has distinct structures. In the case of foamlike materials the solid material forms a simply connected phase, while in granular materials the solid phase is non-connected. For the prismatic bundles the solid bars are also non-connected and this model may be interpreted as the two-dimensional equivalent of the granular model. On the other hand, variations in the sizes of the solid constituents are neglected in favour of an average grain diameter or pore diameter which has been incorporated in each RUC. Other porous medium features which are also considered when constructing an RUC are the porosity of the medium and the configuration of the fluid-solid surface area. Therefore, without directly defining the average geometry we can obtain an intuitive feeling of how to construct an RUC.

The volume of solid material present in an RUC is chosen such that the correct porosity, of the porous medium it resembles, is reflected in the RUC. The solid material is then arranged in rectangular fashion within the RUC to conform with the basic geometric features of the original porous matrix it is meant to represent. Another important feature included in an RUC is the correct relative fluid-solid surface areas for flow in the various directions. Adequate modelling of the fluid-solid surfaces is closely related to adequate modelling of the characteristic lengths or linear dimensions of an RUC. Due to the adopted rectangular arrangement within the RUC, the fluid-solid surface will provide pair-wise sets of parallel surfaces, possibly with some lateral displacement. Any particular arrangement of the solid is required to provide mutually perpendicular duct sections for fluid discharge and the directions of such sections will for the sake of convenience be called the *principal directions* of an RUC. Therefore, with each RUC we may associate three mutually orthogonal axes and this coordinate system related to the RUC is referred to as material coordinates of an RUC or RUC-coordinates. An additional assumption which is implicitly assumed is that the RUC-coordinates are collinear with the principal axes of the permeability. These principal directions must be determined prior to the construction of an RUC through experiment. The analyses of Mast and Potter (1963) and Potter and Mast (1963) indicate that it is possible to infer the principal axes of the permeability from grain characteristics and orientation. In a fibrous material it is natural that one of these axes should be parallel with the

fibres. In addition, the principal directions of the permeability should remain invariant throughout the porous medium as is the case for homogeneous materials.

It is also important to note that an RUC is developed to complement the volume averaging theory and therefore an RUC is selected as the smallest possible REV. This implies that the characteristic lengths or dimensions of an RUC cannot be selected at random, but they are related to the actual smallest volume around a point into which all the general features of the material may be embedded. Therefore, the average geometry incorporated in an RUC is not actually the overall geometry of the material, but only the average geometry within an REV at a macroscopic point. RUC's which represent homogeneous materials are representative of each point in the macroscopic domain. The dimensions or characteristic lengths of an RUC are based on the solid-to-solid or pore-to-pore distance. In the case of well-defined granular porous media this distance may be uniquely measured as the distance from the centre of one particle to the centre of an adjacent particle from scanning electron micrographs. For more complicated materials one will have to try and establish individual grains and determine the centre-to-centre distance for any number of particles and take an average thereof. For foamlike materials a particle size is not relevant and the mere conceptualisation of a pore or channel is also problematic. However, a pore-to-pore distance may be obtained from scanning electron micrographs as the distance from the boundary on the inside of a channel to the boundary of the adjacent channel. More often than not, such a distance will not be obtainable and it is then more appropriate to consider such a distance only of conceptual importance. For such cases the characteristic lengths will then have to be inferred indirectly from its relation to other measurable quantities.

In Figure 3.1 a rectangular RUC is shown for two-dimensional flow through an anisotropic porous medium. For isotropic porous media the two-dimensional RUC's are square and the surfaces of all the parallel pairs which form the duct sections are equal distances apart. However, as illustrated in Figure 3.1, for anisotropic RUC's the different channels may have different sizes. For macroscopic flow in the x_1-direction the RUC and solid block B are rectangular rather then square as in isotropic media. According to the notation adopted for the anisotropic RUC's all numbers in subscripts appear in brackets to indicate that they form part of a subscript and not a tensorial index. An assumption in the construction of isotropic RUC's is that one channel section may always be aligned collinear with direction of the macroscopic flow. In anisotropic materials the directions of the discharge and applied pressure gradient may differ and then it is more appropriate not to relate the orientation of the RUC with the flow, but with the geometric properties of the porous medium. However, for simplicity the x_1-coordinate is selected as the macroscopic flow direction, but this restriction is relaxed at a later stage.

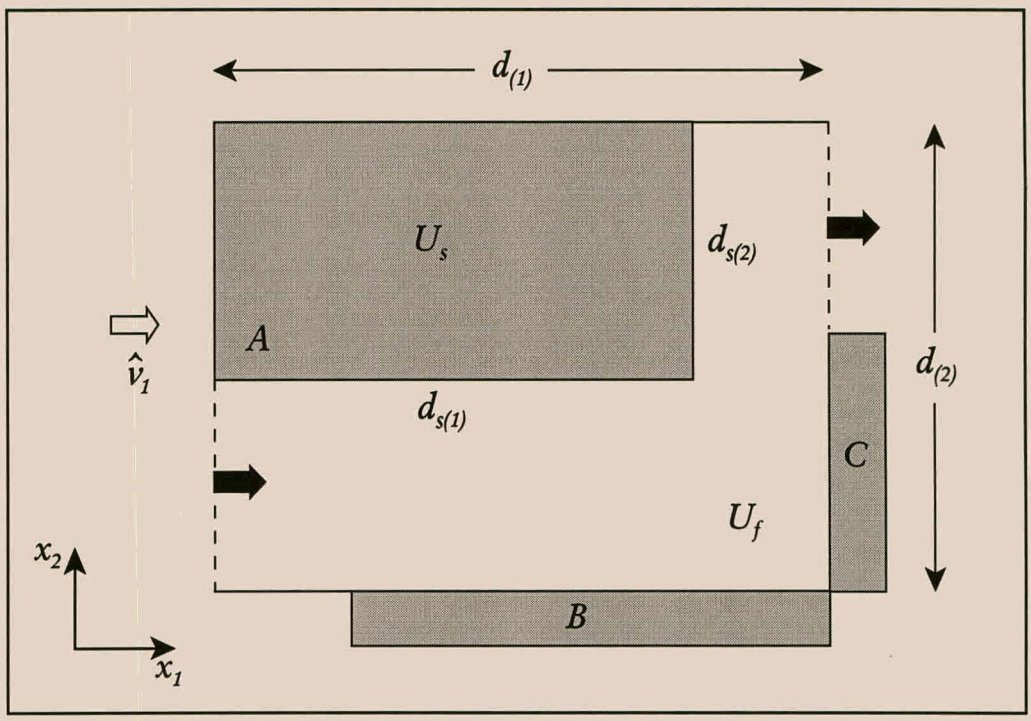

Figure 3.1. An RUC for a two-dimensional anisotropic porous medium.

Since the average geometry of a particular porous medium is obtained before being embedded in an RUC certain directional priorities may be induced due to the fact that each RUC contains channel sections which allow flow in only one particular orthogonal direction per RUC. It may thus be necessary to consider the average transport through different RUC's, each of which is exhibiting a different permutation of directional changes. Therefore, a number of different RUC's, all with the same basic geometric characteristics, can be constructed for each material. Since certain flow phenomena, such as velocity and pressure gradient, add vectorially, it is necessary to consider flow through all the possible RUC's to obtain an ensemble average of the flow. For calculation of geometric characteristics consideration of one RUC for a particular type of material is sufficient, but for modelling transport processes the flow through all RUC's must be incorporated, at least hypothetically. As an example, the streamwise channel section in Figure 3.1 is followed by a channel section to the left. This effect should be eliminated by also considering a complementary RUC for which the streamwise channel is followed by channel to the right. Conceptually this implies that it may be necessary to consider results from as many as four complementary RUC's in a three-dimensional isotropic case and sixteen in a three-dimensional anisotropic case. However, for practical calculations less RUC's may be considered due to symmetry considerations.

A further novel feature of the model is the fact that it combines modelling of the porous medium microstructure with consideration of the flow through the channels, since it is not sufficient to only know the physical structure of the porous medium, but also the flow

patterns in various flow regimes (Ruth and Ma, 1992). Therefore, another important feature to consider during the construction of an RUC is the average tortuous pathway which fluid particles follow. In this regard two assumptions regarding the RUC have to be made. Firstly, there exits no dead-end pores and secondly, the arrangement of solid material in an RUC complies to a principle of maximum staggering and maximum interconnectivity of channel sections and thus forcing the fluid to traverse all channels. This implies that flow which enters the RUC is displaced laterally to the maximum before it exits the cell. These conditions are applied for the determination of the flow in Figure 3.2. It may be noted that the position of block C in Figures 3.1 and 3.2 is determined by the assumption of maximum staggering while block B may be anywhere along the outside of the RUC.

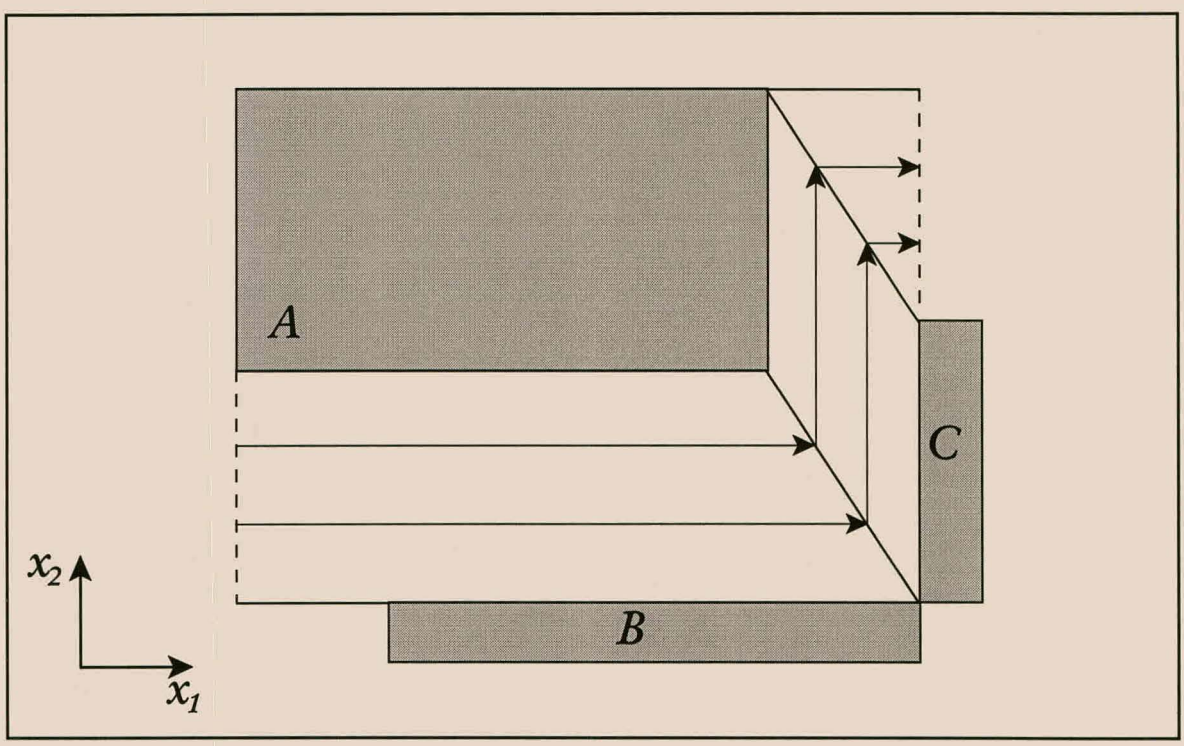

Figure 3.2. Flow lines through an RUC.

The fluid-fluid area on each face of an RUC is defined as the effective cross-sectional area or effective streamwise area for transport in a particular principal direction and, therefore, the open area on each face follows from (2.87) and is given by

$$A_{p(I)} \equiv \widehat{A}_{f\mathcal{L}} = \iint_{A_{f(I)}} \tilde{\nu}_m \hat{\nu}_m dA \tag{3.28}$$

where the subscript I indicates that the area is perpendicular to the x_I-direction. Since the effective streamwise area also appears in the definition of the areosity as expressed in

(2.93), it implies that an RUC has a constant areosity in each of the directions parallel to its sides. It is, however, important to note that the fluid-fluid interface $A_{f(I)}$ for any cross-section through an RUC may vary according to the particular manner in which it is constructed, that is

$$A_{p(I)} \leq A_{f(I)} \leq A_{o(I)} \qquad I = 1,2,3 \tag{3.29}$$

where the subscript I has been added to these scalar quantities to indicate any of the three principal directions of an RUC. Therefore, the fluid-fluid areas perpendicular to each of the six sides of an RUC are selected as the smallest area which contributes to flow in that particular direction. When determining averages over the RUC care must thus be exerted to obtain results corresponding to that of the original REV or REA. This means, for example, that an areal average over the fluid phase of an REA implies sectioning an RUC and taking an average over all the two-dimensional sections.

As mentioned during the discussion of the physical interpretation of the lineality, the streamlines may be determined under various conditions. Since the RUC contains the average geometry and small scale variations in the pore sizes have been ignored in favour of uniform channels, it is preferable to assume that the total void volume in an RUC contributes to the flow. Therefore, in the calculation of the quantities introduced in Chapter 2, such as the lineality, areosity and streamwise channel velocity, the streamlines through an RUC are assumed to be of equal length and piece-wise straight along the transverse duct sections as shown in Figure 3.2. However, different flow patterns are introduced when the fluid-solid interactions are modelled depending on the contribution of viscosity and inertial effects. For all types of flow the lateral exchange of fluid with neighbouring RUC's is not allowed, despite the fluid-fluid area on the flanks not being zero. This is equivalent to modelling the RUC as a stream tube containing blocks of solid material. As previously noted, the macroscopic flow direction in Figure 3.2 is assumed for the sake of simplicity to be collinear with the x_1-direction. The particular structure embedded in the RUC then determines the effective streamwise area $A_{p(1)}$ which, for the two-dimensional RUC in Figure 3.1, is proportional to $(d_{(2)} - d_{s(2)})$. Hence the effective streamwise volume is given by

$$U_{f\mathcal{L}(1)} = A_{p(1)} d_{(1)}. \tag{3.30}$$

Should the streamwise direction be along the x_2-coordinate then the effective streamwise volume is

$$U_{f\mathcal{L}(2)} = A_{p(2)} d_{(2)}. \tag{3.31}$$

Therefore, in general it may be stated that the streamwise volume in any material direction of an RUC is given by

$$U_{f\mathcal{L}(I)} = A_{p(I)}d_{(I)} \tag{3.32}$$

where $I = 1, 2$ for the two-dimensional case and depending on the direction of macroscopic flow.

The lineality can now be obtained from (2.74) and (2.89) to give for an RUC

$$\mathcal{L}_{11} = \frac{A_{p(1)}d_{(1)}}{U_f} = \frac{A_{p(1)}}{A_{f(1)}}. \tag{3.33}$$

Since the tortuosity is by definition the inverse of the lineality it follows that

$$\chi_{11} = \frac{U_f}{A_{p(1)}d_{(1)}}. \tag{3.34}$$

The other components of the tortuosity tensor are zero, since $\widehat{\nu}_2 = 0$ and an average over the RUC in Figure 3.2 and an additional RUC where the streamwise channel is followed by a channel to the right will indicate that $\mathcal{L}_{21} = 0$. However, should the streamwise direction be along the x_2-direction then all the lineality components will be zero except

$$\mathcal{L}_{22} = \frac{A_{p(2)}d_{(2)}}{U_f}. \tag{3.35}$$

When considering the lineality it is important to remember that the second tensorial index indicates the direction of macroscopic discharge.

By considering once again the streamwise direction along the x_1-coordinate, the *average streamwise channel velocity* from (3.11) is given by

$$\widehat{w}_1 = \frac{1}{U_{f\mathcal{L}(1)}} \iiint_{U_f} v_1 \, dU. \tag{3.36}$$

For flow through an RUC, this velocity is equal to the area average channel velocity in a streamwise channel. It furthermore follows, by making use of (3.33) and (3.34), for streamwise discharge along the x_1-coordinate axis that (3.13) may be written as

$$q_1 = \epsilon u_1 = \frac{A_{p(1)}d_{(1)}}{\epsilon U_f}\widehat{w}_1 = \frac{\epsilon \widehat{w}_1}{\chi_{11}}. \tag{3.37}$$

If the discharge is considered to be collinear with the x_2-direction a similar equation may be derived. The tortuosity component obtained in each of the RUC-directions describes the fractional fluid volume available for flow in that particular direction.

In considering flow through an RUC it is also possible to estimate fluid speeds in the transverse channels which are perpendicular to the streamwise direction. According to the definition of the superficial velocity, the total volume of fluid flowing through an RUC is $Q_1 = q_1 A_{o(1)}$. Since an RUC has only one streamwise channel, all fluid moves through this channel which implies that $Q_1 = \widehat{w}_1 A_{p(1)}$. However, all the fluid that moves through the streamwise channel also moves through the transverse channel as shown in the RUC's in Figures 3.1 and 3.2. It therefore follows that a mass balance over the RUC for discharge in the x_1-direction yields

$$\widehat{w}_1 A_{p(1)} = \zeta_2 A_{p(2)} = q_1 A_{o(1)} \tag{3.38}$$

with ζ_2 being the average velocity in the transverse channel in the x_2-direction and $A_{o(1)}$ is the total area of the RUC facing the x_1-direction. By making use of (3.38), the various intrapore speeds are related to the magnitude of the superficial velocity as follows:

$$\widehat{w}_1 = \frac{\chi_{11} q_1}{\epsilon} \tag{3.39}$$

$$\zeta_2 = \frac{A_{p(1)}}{A_{p(2)}} \cdot \frac{\chi_{11} q_1}{\epsilon}. \tag{3.40}$$

It should be noted that each of the vector components $\widehat{w}_1$ and ζ_2 pertains to average discharge along the x_1-coordinate axis, but each is a component, along the direction suggested by the index, of a different velocity vector.

The anisotropy in the shape of materials may be characterised in many materials by an empirical factor known as the shape anisotropy factor. Various porous media characteristics have been used in literature as a measure of the degree or extent of anisotropy which exists within a particular material. Huber and Gibson (1988), for example, have used the ratio of intercept lengths of repetitive cells in polymer foams while Rice *et al.* (1970) and Barak and Bear (1981) have used measured permeabilities as indication of the anisotropy present in a particular material. In this study it is proposed that the degree of anisotropy be reflected by the ratios between the various tortuosity components. The proposed *anisotropy factors*, $R_{(IJ)}$, are therefore given by

$$R_{(IJ)} \equiv \frac{\chi_{II}}{\chi_{JJ}} \tag{3.41}$$

which indicates that the degree of anisotropy is determined by the volume of fluid available for flow in each of the material directions. A ratio of tortuosities, which was derived through application of a capillary model during various flow configurations, has also been used as anisotropy factor by Montillet *et al.* (1992).

In conclusion it follows that an RUC is thus a single cell into which the most important geometric features of a porous medium is summarised and it is different from the repetitive unit cells employed in network theory. Neither is an RUC a unit cell which contains only a small portion of the material as introduced by Quintard and Whitaker (1994a-e). An interesting consequence of averaging the geometry is that a combination of any number of RUC's will not produce the original material. The selection of a rectangular arrangement is purely for the sake of simplifying calculations. It may appear crude, but it does take into account the correct dimensionality of the structure and the basic features of the porous material. These general features of RUC's represent what may be referred to as the basic model which includes the most relevant features. If necessary, any other particulars will have to be modelled additionally, as shown by Du Plessis and Roos (1994) and in Section 3.8 where a particular test case is considered.

In a practical case the first step in constructing an RUC is usually a determination of the linear dimensions of the RUC and thus the pore-to-pore or solid-to-solid length scale and from this U_o and A_o are known. The volume U_s of solid material which goes into the RUC is subsequently determined by the porosity and from this U_f and A_f can be calculated. Once the dimensions and structure of the RUC are known, the particular transport coefficients can be determined since, during the closure modelling, these coefficients are expressed in terms of structural parameters of the RUC as well as measurable fluid properties.

3.6 Analysis of the momentum dispersion term

For a closure model of the last term in (3.27), referred to as the momentum dispersion term or the macroscopic form resistance term, it is necessary to obtain a macroscopic representation of the velocity deviations. This term poses certain modelling difficulties and has often been assumed to be zero, or small compared to the other terms in the momentum equation (Du Plessis, 1991).

In this section the momentum dispersion term is analysed in context of the RUC-model. For a uniform porosity field, application of Slattery's averaging theorem, (B.39; B.56;

Bear and Bachmat, 1991 eq2.3.31), to the macroscopic form resistance term leads to

$$\begin{aligned} \rho\left(\epsilon\left\langle \overset{\circ}{v}_j \overset{\circ}{v}_i\right\rangle^f\right)_{,j} &= \frac{\rho\epsilon}{U_f}\iint_{S_{ff}} \overset{\circ}{v}_j\overset{\circ}{v}_i\nu_j\,dS + \rho\left\langle \overset{\circ}{v}_j \overset{\circ}{v}_i\right\rangle^f \epsilon_{,j} \\ &= \frac{\rho}{U_o}\iint_{S_{ff}} \overset{\circ}{v}_j\overset{\circ}{v}_i\nu_j\,dS \end{aligned} \tag{3.42}$$

where ν_i is a unit normal vector to the fluid-fluid surface S_{ff} and the porosity gradient may be neglected for homogeneous porous media. Since the superficial velocity and porosity fields are uniform, the surface integral only depends on the actual velocity field at the entrances and exits of an REV, or in the present model, an RUC. Since the flow of fluid out of one RUC is the same as that flowing into the next RUC, the velocity deviations at the entrance of an RUC are equal to those at the exit, thus implying that the surface integral in (3.42) is zero. This view of the flow applies to intermediate as well as low Reynolds number flow and justifies neglecting the form resistance term from (3.27), which yields a pressure gradient equation of

$$\epsilon U_o P_{,i} = \iint_{S_{fs}} (\mu v_{i,j}\nu_j - \overset{\circ}{p}\nu_i)\,dS. \tag{3.43}$$

According to the analysis by Ruth and Ma (1992), the macroscopic form resistance term represents a macroscopic gradient and it is not related to the Forchheimer term. The fact that it is zero does not preclude microscopic inertial effects from causing microscopic recirculation which, according to Ruth and Ma (1992), will not appear in the macroscopic form resistance term, but in the remaining surface integral term.

3.7 Modelling of flow through homogeneous foams

The first type of material for which a closure model is developed with aid of the RUC concepts previously introduced is anisotropic foamlike materials. Most porous medium models of fluid flow are directed towards granular materials for their importance in geohydrology and usage as media in packed beds. However, recently, the utilization of metallic foams as bed material has become important in applications in electrochemical engineering where detailed knowledge about the specific surface is necessary to quantify mass transfer balances and to determine the efficiency of metallic electrodes. Accurate predictive measures of structural parameters can therefore be of aid to chemical and mechanical engineering design. It is, therefore, the main objective of this section to provide deterministic expressions for the pressure gradient through homogeneous foams

which are valid over both the Darcy and non-Darcy flow regimes. One of the key features in this approach is the introduction of a pore-scale model representative of the material under investigation.

Many natural materials may be foamed and techniques also exist for the fabrication of foamed solids from metals, polymers and glasses. Many foamlike materials have a reticulated or cellular structure and are classified as either open celled or closed celled. As summarised by Maiti *et al.* (1984a; 1984b), in open cell foams the solid material is distributed as beams or columns which form the cell edges such as in sponges, while in closed cell foams the solid is distributed as plates which form the cell faces with soap foam being an example. Although porous foams exhibit a wide variety of complex microstructures (Gibson and Ashby, 1988; Maiti *et al.,* 1984a), in this section a distinction has only been made between two different open cell foam structures. In the first distinctive foam structure to be modelled, the solid material consists of strands of approximate uniform cross-section, but may have different lengths. The channel sections available for flow may then have different sizes, that is, possibly differing areas and lengths. In the present work this type of foam is considered at high porosities and is referred to as foams of Type A. The second type of foam considered has as characteristic feature channel sections which have an approximate uniform cross-section, but possibly varying lengths. No restrictions are placed on the configuration of the solid material. This type of foam is considered at relative low porosities and will be referred to as Type B foams.

The secondary modelling necessary for closure of the macroscopic pressure gradient equation, (3.43), is provided by consideration of a Representative Unit Cell (RUC). In the former part of this section the various RUC's for the two types of foams are constructed and the internal velocities are related to the superficial velocity. Thereafter, the shear stresses and microscopic pressure differences are modelled to produce a closed form of (3.43). The resulting momentum transport equation is valid over both the Darcy and Forchheimer flow regimes and is expressed in terms of the fluid properties and measurable geometric features of the porous medium.

3.7.1 Modelling of the porous medium microstructure

It is the objective of this section to recapture the information regarding the porous microstructure lost during the averaging process. The average geometry is obtained by considering the geometric character of the material matrix and modelling the average tortuous pathway and the total fluid-solid surface area. These characteristics are then

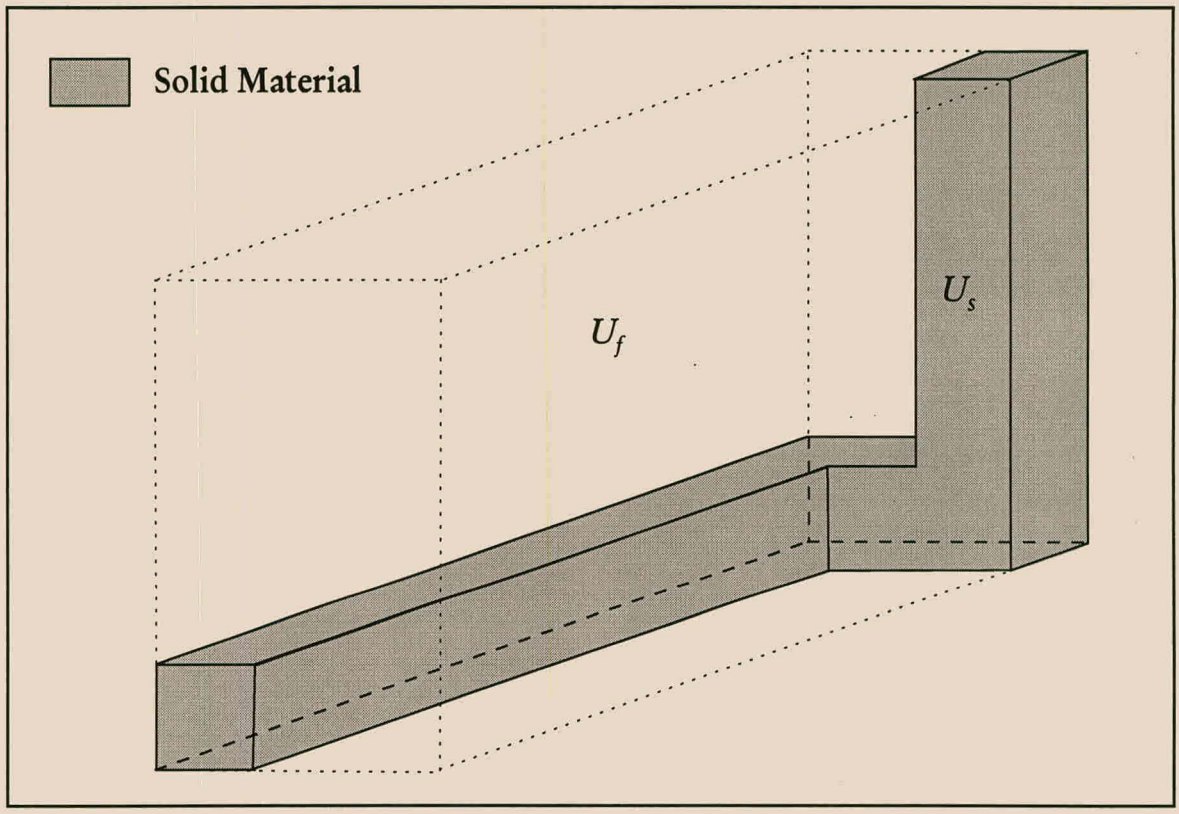

Figure 3.3. A typical RUC for a foam of Type A.

represented within a rectangular RUC by suitable arrangement of blocks of solid material.

Since the average geometry is obtained before being embedded in the RUC a total number of sixteen different RUC's, all with the same geometric characteristics, can be constructed for each of the particular foam structures under consideration. An example of a typical RUC for a foam of Type A is given in Figure 3.3. The RUC is considered to be constructed of three solid bars, indicated by the shaded areas in Figure 3.3, while the remaining volume is occupied by fluid. Incorporation of neighbouring RUC's will render an arrangement in which each channel section is formed by two sets of parallel flat plates, as illustrated in Figure 3.4. The hypothetical arrangement of solid material in neighbouring RUC's provides maximum possible staggering and maximum interconnection of resulting duct sections within the RUC. As previously noted, a key assumption of the RUC concept is that there is no lateral exchange of fluid with neighbouring RUC's, but the fluid which is forced through an RUC is maximally displaced laterally within the cell before it exits. The hypothetical positioning of surrounding RUC's, as illustrated in Figure 3.4, therefore also facilitates calculation of the fluid-solid interaction on the 'outside' surfaces of an RUC, since the shear stresses on the outside surfaces of a particular RUC are identical to the shear stresses on the neighbouring RUC's on the inside of the RUC under consideration.

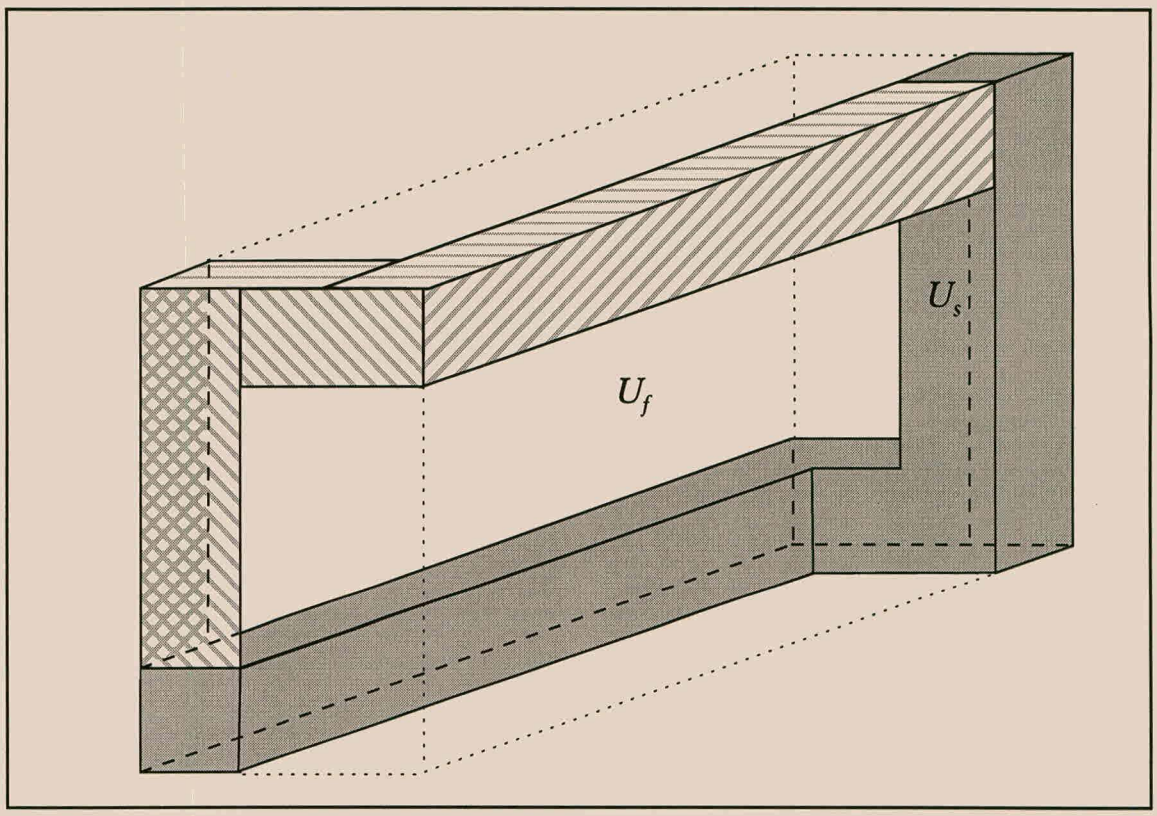

Figure 3.4. A typical RUC for a foam of Type A indicating the positioning of fluid-solid surfaces from neighbouring RUC's.

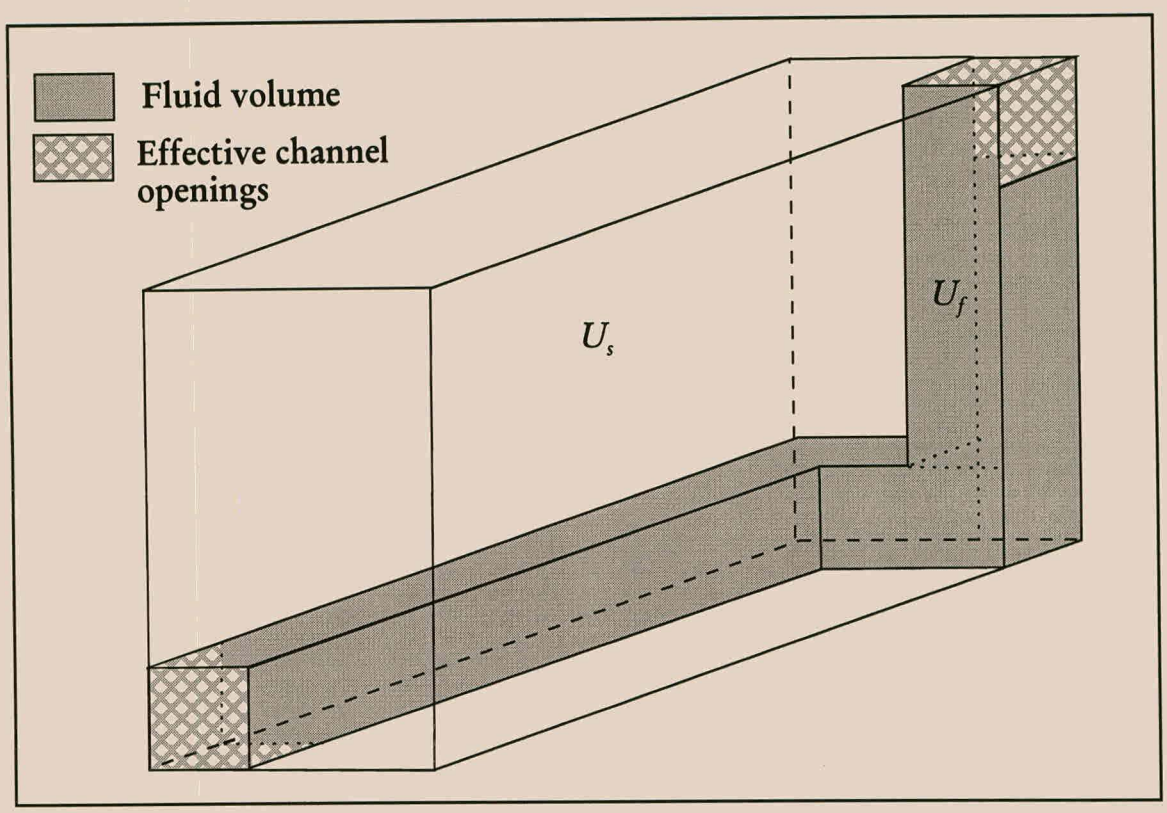

Figure 3.5. A typical RUC for a foam of Type B.

The average geometry for a foam of Type B may be represented by an RUC containing three mutually orthogonal channel sections of square cross-section but having different lengths as illustrated in Figure 3.5. It has to be noted that in this case the fluid volume in Figure 3.5 is shaded while the remaining volume is occupied by solid. For coherence of the model the particular arrangement of channel sections within the RUC is required to exhibit similar flow conditions in all three orthogonal directions. All effective channel openings $A_{p(I)}$, from which fluid can enter or exit the RUC, are also illustrated in Figure 3.5.

A further feature of the model is the fact that it combines modelling of the porous medium microstructure with consideration of the flow through the channels. Low Reynolds number flow through an RUC may be considered to follow piece-wise linear streamlines as shown in Figure 3.2. For foams of Type B as well as isotropic foams it is a fairly realistic flow model as it also allows the diagonal stresses in junctions to be calculated. However, in the case of foams of Type A the fair amount of staggering between the two opposite surface sections of a particular channel requires consideration of an alternative flow model as subsequently indicated. For flow at high Reynolds numbers inertial effects may cause flow separation within channels and, as shown in Section 3.7.2.3, the flow model for this regime reflects these effects.

The various RUC dimensions and channel areas for a foam of Type A and for a Type B foam are illustrated in Figures 3.6 and 3.7, respectively. All the fluid-solid surfaces in these figures are labelled with capital letters. Solid letters are used for visible surfaces and outlined letters for hidden surfaces. Also included in these figures are the RUC-coordinates. For the sake of algebraic simplicity all further tensorial expressions in this work will refer to these RUC-coordinates. In addition, all further vector indexes represent components along these axes and are therefore indicated by capital letters.

A number of geometric relationships may be determined by consideration of only one RUC for each type of foam. For both types of foam the fluid volume of an RUC, U_f, may be written in terms of the porosity, ϵ, as

$$U_f = \epsilon U_o = \epsilon d_{(1)} d_{(2)} d_{(3)} \tag{3.44}$$

with U_o the total volume of an RUC. The characteristic lengths $d_{(1)}$, $d_{(2)}$ and $d_{(3)}$ define the dimensions of an RUC and are approximately equal to the real pore-to-pore or solid-to-solid distance. Another important structural parameter is the total wetted surface, S_{fs}, which is expressed in terms of other porous medium characteristics in Table 3.1. From these expressions it is possible to infer that, should the two types of foams with

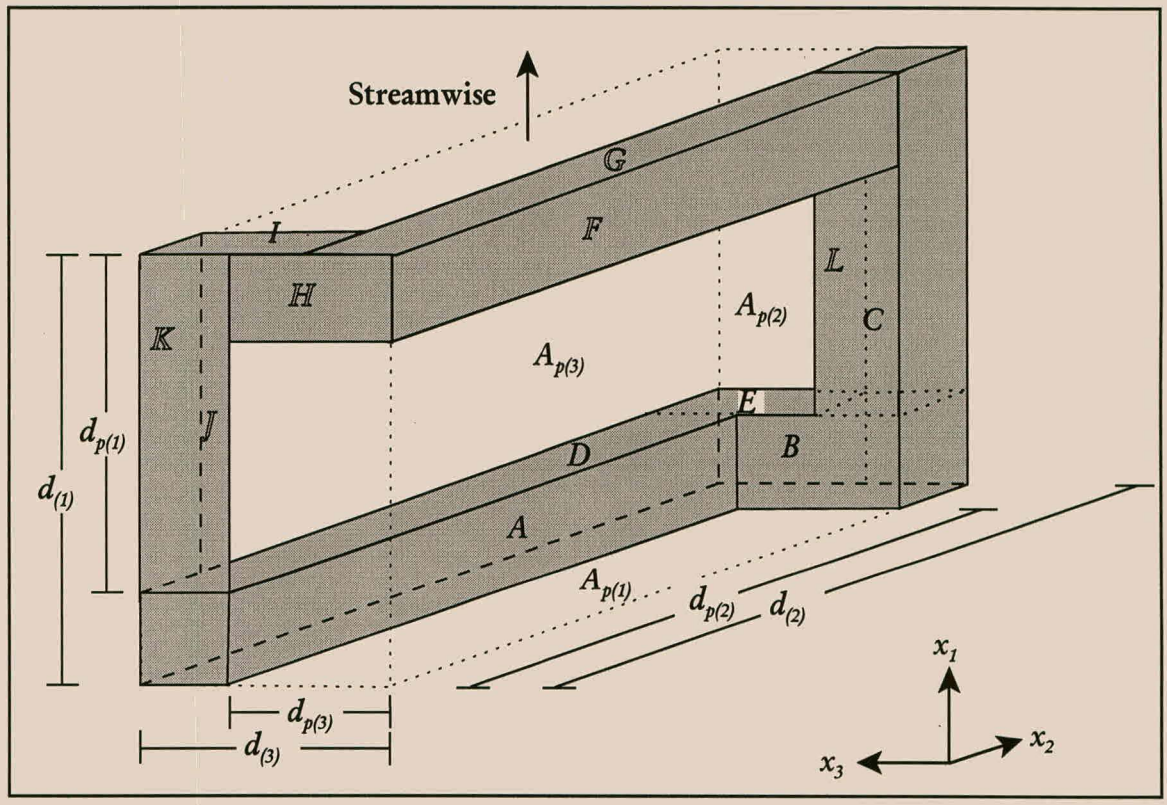

Figure 3.6. An RUC for a foam of Type A with an $x_1 \rightarrow x_3 \rightarrow x_2$ flow sequence indicating the various dimensions of the fluid-solid surfaces.

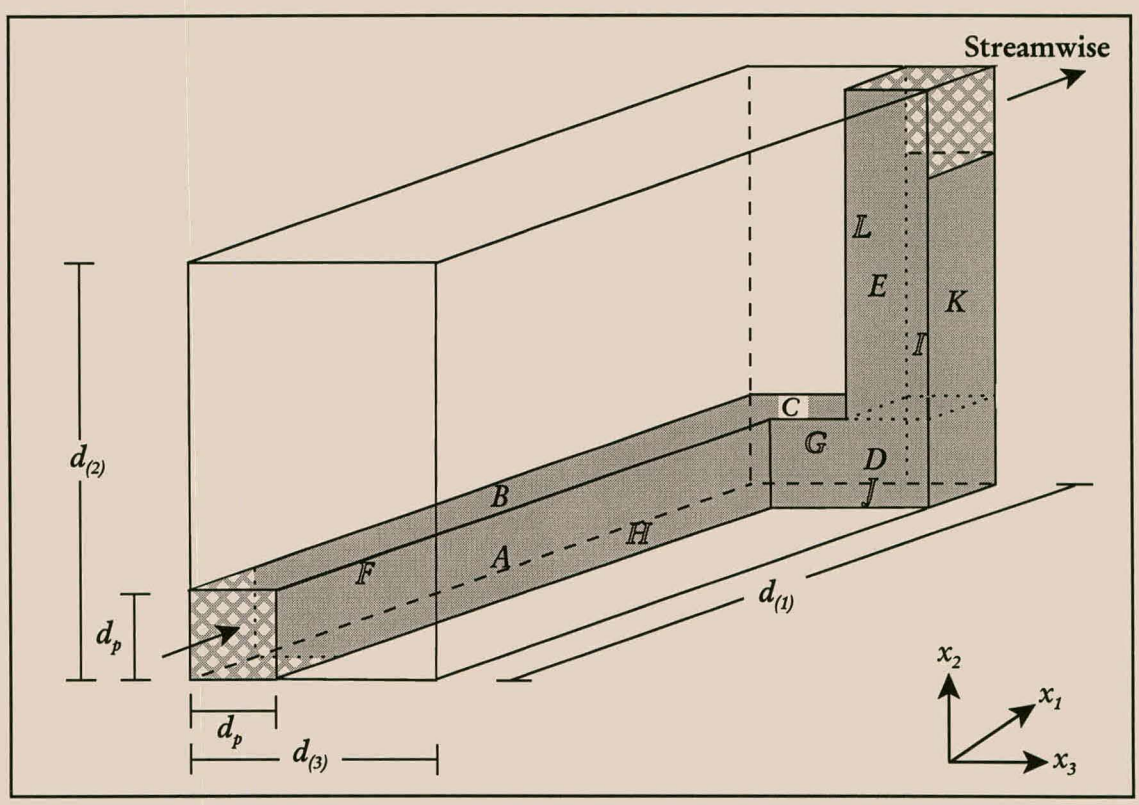

Figure 3.7. An RUC for a foam of Type B with an $x_1 \rightarrow x_3 \rightarrow x_2$ flow sequence indicating the various dimensions of the fluid-solid surfaces.

porosities of ϵ_A and ϵ_B, respectively have equal fluid-solid surfaces, then $\epsilon_A = (1 - \epsilon_B)$. However, for equal porosities the fluid-solid surfaces in the foams will differ. Although a unique relationship between the fluid-solid surface and porosity is not obtainable for the anisotropic case, it can be inferred from the change of S_{fs} with porosity for isotropic foams, as given by Du Plessis *et al.* (1994; eq21), that the fluid-solid surface of both types of foam will also increase with porosity to reach a maximum value before it decreases.

Table 3.1. Summary of geometric characteristics.

Foams of Type A	Foams of Type B
$A_{p(1)} = d_{p(2)}d_{p(3)} = (d_{(2)} - d_s)(d_{(3)} - d_s)$	
$A_{p(2)} = d_{p(1)}d_{p(3)} = (d_{(1)} - d_s)(d_{(3)} - d_s)$	$A_{p(1)} = A_{p(2)} = A_{p(3)} = A_p$
$A_{p(3)} = d_{p(1)}d_{p(2)} = (d_{(1)} - d_s)(d_{(2)} - d_s)$	
$S_{fs} = 4d_s\left(d_{p(1)} + d_{p(2)} + d_{p(3)}\right)$	$S_{fs} = 4d_p\left(d_{(1)} + d_{(2)} + d_{(3)} - 3d_p\right)$
$\chi_{11} = \dfrac{U_f}{A_{p(1)}d_{(1)}} = \dfrac{\epsilon d_{(2)}d_{(3)}}{d_{(2)}d_{(3)} - d_{(2)}d_s - d_{(3)}d_s + d_s^2}$	$\chi_{11} = \dfrac{U_f}{A_{p(1)}d_{(1)}}$
$\chi_{22} = \dfrac{U_f}{A_{p(2)}d_{(2)}} = \dfrac{\epsilon d_{(1)}d_{(3)}}{d_{(1)}d_{(3)} - d_{(1)}d_s - d_{(3)}d_s + d_s^2}$	$\chi_{22} = \dfrac{U_f}{A_{p(2)}d_{(2)}}$
$\chi_{33} = \dfrac{U_f}{A_{p(3)}d_{(3)}} = \dfrac{\epsilon d_{(1)}d_{(2)}}{d_{(1)}d_{(2)} - d_{(1)}d_s - d_{(2)}d_s + d_s^2}$	$\chi_{33} = \dfrac{U_f}{A_{p(3)}d_{(3)}}$

The effective cross-sectional flow area in each of the flow directions are indicated by $A_{p(1)}$, $A_{p(2)}$ and $A_{p(3)}$, respectively and these are expressed in terms of other porous medium characteristics in Table 3.1. In an RUC, any cross-sectional area normal to an RUC-coordinate yields the same effective cross-sectional flow area for discharge in that particular direction. For foams of Type B the mean channel cross-sectional areas are the same in every direction.

Within an anisotropic RUC and for streamwise flow in the x_I-direction, application of (3.32) leads to an effective volume of

$$U_{f\mathcal{L}(I)} = A_{p(I)}d_{(I)} \tag{3.45}$$

with no summation intended over the index $I(= 1, 2, 3)$. The generalisation of the streamwise volume may be used to determine the tortuosity for flow in each material

direction according to (3.34) and the resulting scalar tortuosity components in each of the RUC-directions are also listed in Table 3.1. An extension of (3.38) to a three-dimensional RUC yields

$$\widehat{w}_1 A_{p(1)} = \zeta_2 A_{p(2)} = \eta_3 A_{p(3)} = q_1 d_{(2)} d_{(3)} \tag{3.46}$$

with ζ_I and η_I the average velocities in the transverse channels in the x_2-direction and x_3-direction in an RUC, respectively. For an average discharge along the x_1-coordinate axis, the various intrapore speeds are then related to the magnitude of the superficial velocity as follows:

$$\widehat{w}_1 = \frac{\chi_{11} q_1}{\epsilon} \tag{3.47}$$

$$\zeta_2 = \frac{A_{p(1)}}{A_{p(2)}} \cdot \frac{\chi_{11} q_1}{\epsilon} \tag{3.48}$$

$$\eta_3 = \frac{A_{p(1)}}{A_{p(3)}} \cdot \frac{\chi_{11} q_1}{\epsilon}. \tag{3.49}$$

From these relationships it is apparent that the magnitudes of the various channel velocities in the case of foams of Type A differ according to the ratio of the respective channel areas. According to the model for foams of Type B, all intrapore channel velocities have equal magnitudes. These velocity expressions are subsequently used in deriving a relationship between the pressure gradient and superficial velocity.

3.7.2 Modelling of the interstitial fluid-solid interaction

As previously noted, the quantitative evaluation of the surface integral in (3.43) is subject to knowledge of the actual intrapore velocity gradients at the channel surfaces of the RUC. The aim of the following analytical model is then to express the surface integral in (3.43) in terms of macroscopic variables such as the superficial velocity and the porosity. For convenience (3.43) is now solved for the x_1-direction only, but the following analysis is equally applicable to the other RUC-directions. For this discharge direction the intrapore Reynolds number, on which a distinction between various flow regimes is based, is defined as

$$Re_{(1)} \equiv \frac{\rho q_1 h_{(1)}}{\mu} \tag{3.50}$$

with the characteristic length, $h_{(1)}$, appearing in the Reynolds number given by

$$h_{(1)} = \frac{2d_{(2)}d_{(3)}}{d_{(2)} + d_{(3)}}. \tag{3.51}$$

This definition of the characteristic length is based upon the definition of the hydraulic diameter for flow between parallel plates, since the present analysis draws on analogies with flow between parallel plates.

3.7.2.1 Low Reynolds number flow limit for foams of Type A

At low Reynolds numbers of the interstitial flow ($Re_{(1)} \ll 10$) it is assumed that the viscous shear stresses along S_{fs} predominate the fluid-solid interaction and, as asymptote in the case of very low Reynolds number flow, fully developed Poiseuille flow is assumed within each channel section. Due to directional preferences in an RUC, a complete view of the flow requires the analyses of the flow through at least four RUC's. For example, the flow through the RUC in Figure 3.6 moves firstly in the x_1-direction, then in the x_3-direction and then in the x_2-direction before exiting the RUC. This RUC has a so-called $x_1 \rightarrow x_3 \rightarrow x_2$ flow sequence. However, complimentary to this RUC it is also required to consider the flow in an RUC with an $x_1 \rightarrow -x_3 \rightarrow -x_2$ flow sequence as shown in Figure 3.8. Due to symmetry considerations the only other two RUC's which need to be considered should have an $x_1 \rightarrow x_2 \rightarrow x_3$ and an $x_1 \rightarrow -x_2 \rightarrow -x_3$ flow sequence, respectively. Since the velocity distribution forms a vector field, an average over these four RUC's will ensure that the streamwise direction is along the x_1-coordinate.

By strictly adhering to the piece-wise linear flow pattern as illustrated in Figure 3.2, it follows, in the notation of the given RUC in Figure 3.6, that an average over the four RUC's listed above yields

$$\begin{aligned}\iint_{S_{fs}} \mu v_{1,j}\nu_j dS \;=\; & \frac{7}{8}\mu v_{1,2}\nu_2 B + \frac{7}{8}\mu v_{1,2}\nu_2 H + \frac{7}{8}\mu v_{1,3}\nu_3 A + \frac{7}{8}\mu v_{1,3}\nu_3 F \\ & + \frac{1}{2}\mu v_{1,2}\nu_2 C + \frac{1}{2}\mu v_{1,3}\nu_3 L\end{aligned} \tag{3.52}$$

where B, H, A, F, C and L are surface sections within the RUC. The shear stresses in channel sections not aligned streamwise, thus cancelling out in (3.52), are included in the pressure deviation, since the surface integral of the pressure difference is equal to the driving force for flow through the transverse channels. The fractions in the first four terms of (3.52) appear because the corresponding surfaces do not only have streamwise

shear stresses, but they are also available to transverse flow similar to the corner section in Figure 3.2. For example, surface B in Figure 3.6 has one shear stress component in the x_1-direction, but the equivalent surface in the RUC presented in Figure 3.8 (also denoted by B) contains two shear stress components. The corresponding surfaces in the RUC's with an $x_1 \to x_2 \to x_3$ and an $x_1 \to -x_2 \to -x_3$ flow sequence have only one shear component. An average over the RUC's then results in the factor $\frac{7}{8}$ in (3.52). A similar argument applies to the last two terms in (3.52), although surfaces C and L strictly do not form part of streamwise channels.

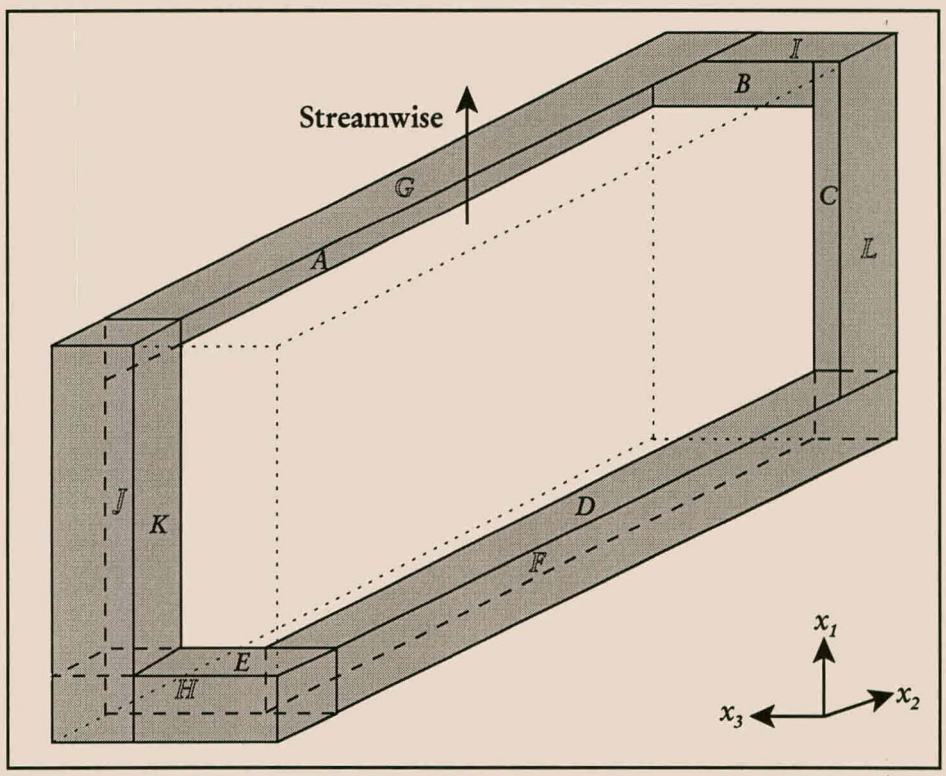

Figure 3.8. An additional RUC for a foam of Type A with an $x_1 \to -x_3 \to -x_2$ flow sequence.

Although a macroscopic transverse pressure gradient does not exist, there are local pressure gradients which forces the fluid transversely through the channel sections. Since the flow in a channel is assumed to be fully developed, the flow is not accelerating and, consequently, the local pressure force is equal to the resultant shear resistance force along a channel. Therefore,

$$\begin{aligned} -\iint_{S_{fs}} \overset{\circ}{p}\nu_1 dS \;=\; \mu\Big\{&\Big(\frac{6}{8}v_{3,2}\nu_2 C + \frac{6}{8}v_{3,2}\nu_2 J\Big) + \Big(\frac{6}{8}v_{3,1}\nu_1 G + \frac{6}{8}v_{3,1}\nu_1 D\Big) \\ &+ \Big(\frac{6}{8}v_{2,1}\nu_1 I + \frac{6}{8}v_{2,1}\nu_1 E\Big) + \Big(\frac{6}{8}v_{2,3}\nu_3 L + \frac{6}{8}v_{2,3}\nu_3 K\Big) \\ &+ \frac{1}{4}v_{3,2}\nu_2 H + \frac{1}{4}v_{2,3}\nu_3 A + \frac{1}{2}v_{2,1}\nu_1 D + \frac{1}{2}v_{3,1}\nu_1 E\Big\} \end{aligned} \tag{3.53}$$

where C, J, G, D, I, E, K and L are the fluid-solid surface sections forming transverse channel sections. Once again, each surface area is shared between two perpendicular channels due to the staggering of the parallel plate sections. According to (3.43) the complete pressure gradient is obtained by adding (3.52) and (3.53).

However, to conform to a uniform modelling approach for all types of RUC's it is preferred to model the flow as if it takes place in three distinct channels sections, one in each direction without having surface sections shared between them. Therefore, each channel is viewed to consists of two pairs of parallel plates and flow only takes place in one direction per channel. In addition, only one shear stress component appears on each fluid-solid surface axially along each channel section. For foams of Type B, which is subsequently addressed, as well as isotropic foams this is a fairly realistic model and it conforms to the piece-wise linear approach. However, due to the fair amount of staggering between two opposite surface sections of a particular channel in the case of foams of Type A, this flow model neglects some streamwise shear stress components (the last two terms in (3.52)) in favour of transverse stresses with a reallocation of transverse stresses (the last four terms in (3.53)). Therefore, if the channel in the x_1-direction is formed by the two pairs, (A, F) and (B, H) and the channel in the x_2-direction is formed by the (C, J) and (D, G) pairs, then a reallocation of some stresses in (3.52) and (3.53) leads to a surface integral of

$$\begin{aligned}\iint_{S_{fs}} (\mu v_{1,j}\nu_j - \overset{o}{p}\nu_1)\, dS &= \mu v_{1,2}\nu_2 B + \mu v_{1,2}\nu_2 H + \mu v_{1,3}\nu_3 A + v_{1,3}\nu_3 F \\ &+ \mu(v_{3,2}\nu_2 C + v_{3,2}\nu_2 J) + \mu(v_{3,1}\nu_1 G + v_{3,1}\nu_1 D) \\ &+ \mu(v_{2,1}\nu_1 I + v_{2,1}\nu_1 E) + \mu(v_{2,3}\nu_3 K + v_{2,3}\nu_3 L). \end{aligned} \tag{3.54}$$

According to this model the flow within a rectangular channel is, therefore, considered as the superposition of flow between two sets of parallel plates. This analysis is more appropriate for isotropic materials and low porosity anisotropic materials and somewhat less accurate at very high porosities where there is a fair amount of staggering between the plates.

According to the parallel plate configuration, the magnitudes of the velocity gradients normal to the fluid-solid surfaces in a given channel are given by

$$\mu v_{i,j}\nu_j = -\frac{6\mu\overline{v}_i}{d_{p(\nu_k)}} \tag{3.55}$$

where $d_{p(\nu_k)}$ is the distance between the set of parallel plates on which ν_k is a normal vector and $\overline{v}_i$ is the relevant average velocity in the channel (Whitaker, 1968). In view

of this result, the overall expression for the surface integral in (3.54) for a discharge in the x_1-direction becomes

$$\iint_{S_{fs}} (\mu v_{1,j}\nu_j - \overset{o}{p}\nu_1)\, dS = -6\mu \left(\frac{\widehat{w}_1}{d_{p(3)}} 2A + \frac{\widehat{w}_1}{d_{p(2)}} 2B + \frac{\eta_3}{d_{p(2)}} 2C + \frac{\eta_3}{d_{p(1)}} 2D + \frac{\zeta_2}{d_{p(1)}} 2E + \frac{\zeta_2}{d_{p(3)}} 2L \right). \tag{3.56}$$

The next step is to write this equation in terms of the superficial velocity. With reference to (3.47), (3.48) and (3.49) as well as the expressions for the various surface areas, the pressure gradient along the x_1-coordinate axis from (3.43) may be expressed as

$$\epsilon P_{,1} = -\frac{6\mu\chi_{11}q_1}{\epsilon U_o} \left(\frac{2A}{d_{p(3)}} + \frac{2B}{d_{p(2)}} + \frac{2CA_{p(1)}}{d_{p(2)}A_{p(3)}} + \frac{2DA_{p(1)}}{d_{p(1)}A_{p(3)}} + \frac{2EA_{p(1)}}{d_{p(1)}A_{p(2)}} + \frac{2LA_{p(1)}}{d_{p(3)}A_{p(2)}} \right) \tag{3.57}$$

or, equivalently,

$$\epsilon P_{,1} = -\frac{6\mu\chi_{11}q_1 d_s}{\epsilon U_o} \left(\frac{2d_{p(2)}}{d_{p(3)}} + \frac{2d_{p(3)}}{d_{p(2)}} + \frac{2d_{p(1)}A_{p(1)}}{d_{p(2)}A_{p(3)}} + \frac{2d_{p(2)}A_{p(1)}}{d_{p(1)}A_{p(3)}} + \frac{2d_{p(3)}A_{p(1)}}{d_{p(1)}A_{p(2)}} + \frac{2d_{p(1)}A_{p(1)}}{d_{p(3)}A_{p(2)}} \right). \tag{3.58}$$

From the rectangular geometry of an RUC it is possible to relate most geometrical parameters with one another, as is partially illustrated in Table 3.1. Therefore, it does not matter which particular parameters are selected to express (3.58), since the final parameters selected in applications will depend on the particular material under consideration and the available experimental information.

3.7.2.2 Low Reynolds number flow limit for foams of Type B

The surface integral expression, (3.43), for discharge along the x_1-coordinate axis, is obtained in a similar manner as was done for foams of Type A. Therefore, since the channel sections are orientated orthogonally with respect to the streamwise direction, only the shear stresses which occur in transverse channels contribute to the pressure deviation term. Therefore, with reference to the RUC for a foam of Type B, schematically illustrated in Figure 3.7, and equivalent to (3.52) and (3.53), the overall pressure

gradient is

$$\begin{aligned}\epsilon P_{,1} &= \frac{1}{U_o}\iint_{S_{fs}}(\mu v_{1,j}\nu_j - \overset{o}{p}\nu_1)dS \\ &= \frac{\mu}{U_o}\Big((v_{1,3}\nu_3 A + v_{1,3}\nu_3 F) + (v_{1,2}\nu_2 B + v_{1,2}\nu_2 H) \\ &\qquad + (v_{3,2}\nu_2 C - v_{3,2}\nu_2 J) + (v_{3,1}\nu_1 G - v_{3,1}\nu_1 D) \\ &\qquad + (v_{2,1}\nu_1 I + v_{2,1}\nu_1 E) + (v_{2,3}\nu_3 K + v_{2,3}\nu_3 L)\Big) \end{aligned} \tag{3.59}$$

since according to (3.43) the momentum dispersion is zero for flow through an RUC. In accordance with (3.55), the microscopic velocity gradient in each channel is given by

$$\mu v_{i,j}\nu_j = -\frac{6\mu\overline{v}_i}{d_p} \tag{3.60}$$

since all channels have equal cross-sections. By making use of this result, the pressure gradient becomes

$$\epsilon P_{,1} = -\frac{6\mu}{U_o d_p}(2\widehat{w}_1 A + 2\widehat{w}_1 B + 2\eta_3 C + 2\eta_3 G + 2\zeta_2 E + 2\zeta_2 K)\,. \tag{3.61}$$

According to (3.47) through (3.49) the average channel speeds in the transverse channels are equal to the intrapore speed in the streamwise channel. Together with the expressions for the various surface areas, the surface integral expression from (3.61) may then be written as

$$\begin{aligned}\epsilon P_{,1} &= -\frac{6\mu\chi_{11}q_1}{\epsilon U_o}\Big(4(d_{(1)} - d_p) + 4(d_{(2)} - d_p) + 4(d_{(3)} - d_p)\Big) \\ &= -\frac{6\mu\chi_{11}q_1 S_{fs}}{\epsilon U_o d_p}. \end{aligned} \tag{3.62}$$

Introduction of either (3.58) or (3.62) into (3.43) yields a macroscopic pressure gradient equation in terms of macroscopic measurable parameters valid over the Darcy regime for foams of Type A and foams of Type B, respectively.

3.7.2.3 Non-Darcy flow asymptote for foams of Type A

In the non-Darcy limit the flow is considered to be laminar with developed interstitial recirculation, but no turbulence is yet present. The inertial phenomenon is accounted

for by modelling the gradual increase with Reynolds number of flow recirculation on the streamwise lee-side surface of solid material (Du Plessis, 1992b), as is schematically shown in Figure 3.9. In the limit of reasonable high pore Reynolds numbers ($Re_{(1)} \gg 100$), it then amounts to form drag locally within the pore channels.

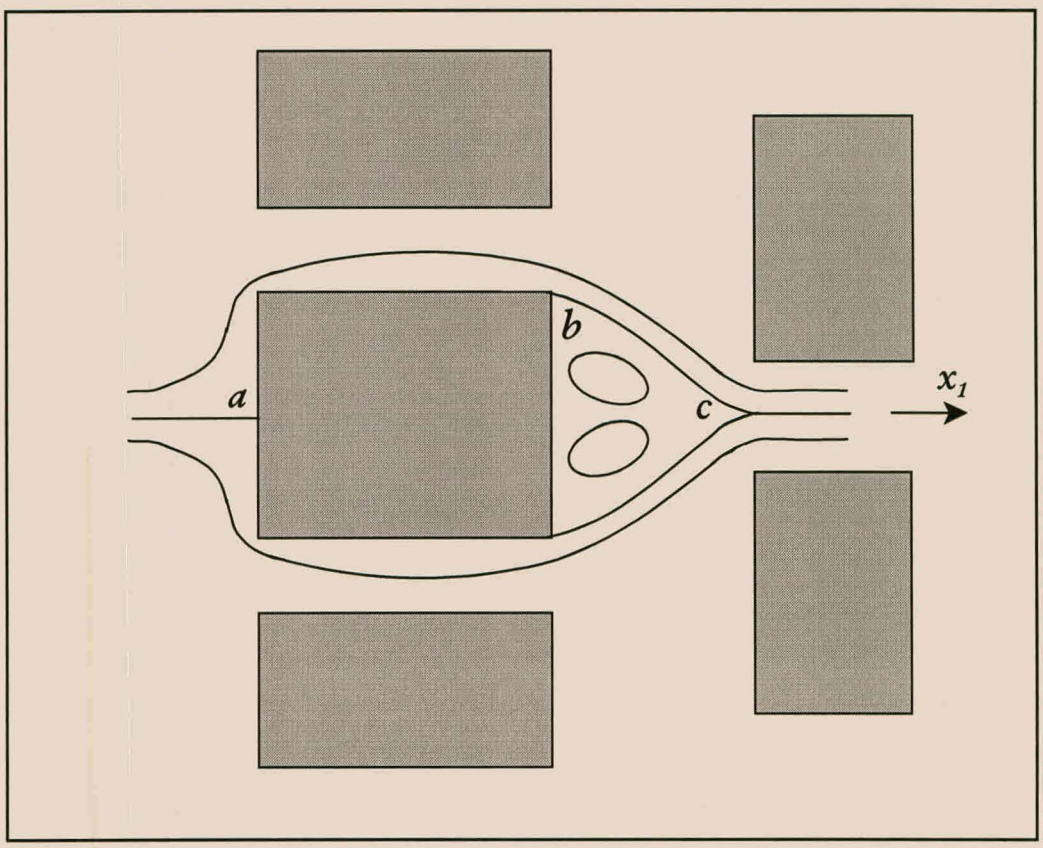

Figure 3.9. A two-dimensional schematic representation of interstitial flow recirculation.

Since the momentum dispersion, (3.42), is zero and acknowledging that viscous shear stresses become insignificant in comparison with form drag at moderate to high Reynolds number flow, on average the only non-zero contribution to (3.43) is due to the pressure difference, pairwise over surface sections normal to the streamwise direction and because of intrapore recirculation. By making use of the definition of the drag coefficient, c_d, (Whitaker, 1968) the surface integral expression along the selected x_1-coordinate axis for the RUC illustrated in Figure 3.6 is given by

$$\begin{aligned} \epsilon P_{,1} &= -\frac{1}{U_o}\int\int_{S_{fs}} \overset{o}{p}\nu_1 \, dS \\ &= -\left(\frac{\widehat{w}_1^2 c_d \rho}{2U_o} D + \frac{\widehat{w}_1^2 c_d \rho}{2U_o} E\right). \end{aligned} \tag{3.63}$$

The drag coefficient to be used here for flow over a square bar is equal to 2.05, but may be

suitably adjusted should the structure of the material under study deviate substantially from that of a square bar. This is only one method to model the recirculating flow, since it may also be possible to present an argument in favour of using the interstitial velocity as the recirculating velocity or to deduce the pressure difference across the solid material from the Bernoulli equation. A more detailed discussion of the high Reynolds number limit is presented in Section 3.9.5.3.

By making use of the expression for the average streamwise channel velocity, (3.39), as well as the expressions for the fluid-solid surfaces, it follows from (3.63) that

$$\epsilon P_{,1} = -\frac{c_d \rho \chi_{11}^2 q_1^2}{2\epsilon^2 U_o} \left(d_s d_{p(2)} + d_s d_{p(3)} \right) \tag{3.64}$$

valid for relative high Reynolds number flow.

3.7.2.4 Non-Darcy flow asymptote for foams of Type B

In a similar manner as in the previous case, the inertial phenomenon for foams of Type B is accounted for by modelling the recirculation of the fluid on the downstream side of the solid material. The equivalent of (3.63) is therefore obtained by considering the pressure difference, pairwise over surface sections normal to the streamwise direction. With reference to the RUC in Figure 3.7 and for flow in the x_1-direction it then follows that

$$\begin{aligned} \epsilon P_{,1} &= -\frac{1}{U_o} \iint_{S_{fs}} \overset{o}{p} \nu_1 \, dS \\ &= -\left(\frac{\widehat{w}_1^2 c_d \rho}{2U_o} G + \frac{\widehat{w}_1^2 c_d \rho}{2U_o} E \right) \end{aligned} \tag{3.65}$$

with c_d the drag coefficient for flow over a square bar. By making use of the expression for the average streamwise channel velocity, (3.39), and the expressions for the fluid-solid surfaces, (3.65) may be written as

$$\epsilon P_{,1} = -\frac{c_d \rho \left(\chi_{11}\right)^2 q_1^2}{2\epsilon^2 U_o} \left(d_p (d_{(2)} - d_p) + d_p (d_{(3)} - d_p) \right). \tag{3.66}$$

Expressions for the transport of momentum have been developed for both the Darcy and Forchheimer regimes and conclude the modelling of the interstitial fluid-solid interaction.

3.7.3 Generalisation to multi-directional flow

The expressions for the pressure gradient determined in (3.58) and (3.62) are only applicable when the directions of the superficial velocity and macroscopic pressure gradient coincide with one of the RUC-coordinates. However, in anisotropic materials such conditions can generally be obtained in laboratory experiments but not very often in field experiments. The objective of this section then, is to obtain a shear resistance tensor F_{ij} and to discuss the possibility of an inertial tensor, B_{ij}, such that

$$\epsilon P_{,i} = -\mu F_{ij} q_j - \rho q B_{ij} q_j \tag{3.67}$$

valid over both the Darcy and Forchheimer regimes. It is expected that the shear resistance tensor as well as the inertial tensor will only be functions of the geometry of the porous medium.

3.7.3.1 Shear resistance tensor

As indicated in Section 3.2, the permeability tensor is generally accepted as being diagonal relative to the principal axes of the porous medium. According to the RUC-approach the diagonal components of the permeability follows form the assumption that the RUC is aligned with the principal axes of the material. However, this may be substantiated by realising that for low Reynolds number flow each component of the surface integral expression (3.43) may be solved independently from each other, since the shear stresses within channel sections are linearly related to the intrapore velocity which in turn is linearly related to the macroscopic velocity (Nikolaevskii, 1959; Neuman, 1977; Whitaker, 1986). Therefore, for a low Reynolds number discharge not collinear with one of the RUC-directions, the pressure gradient in (3.43) may be written as

$$\begin{aligned} \epsilon P_{,i} &= -\mu F_{ij} q_j \\ &\quad -\mu(F_{i1} q_1 + F_{i2} q_2 + F_{i3} q_3) \quad i = 1,2,3 \end{aligned} \tag{3.68}$$

with F_{ij} *a diagonal shear friction tensor.* In the RUC approach, the symmetry is evident since each component of the pressure gradient is related to only the component of the superficial velocity which is in the same direction.

For foams of Type A, the diagonal components of F_{ij} may be obtained from (3.58) and

are given by

$$
\begin{aligned}
F_{11} &= \frac{6\chi_{11}d_s}{\epsilon U_o}\left(\frac{2d_{p(3)}}{d_{p(2)}}+\frac{2d_{p(2)}}{d_{p(3)}}+\frac{2d_{p(1)}A_{p(1)}}{d_{p(3)}A_{p(2)}}+\frac{2d_{p(3)}A_{p(1)}}{d_{p(1)}A_{p(2)}}\right.\\
&\qquad\left.+\frac{2d_{p(2)}A_{p(1)}}{d_{p(1)}A_{p(3)}}+\frac{2d_{p(1)}A_{p(1)}}{d_{p(2)}A_{p(3)}}\right)\\
F_{22} &= \frac{6\chi_{22}d_s}{\epsilon U_o}\left(\frac{2d_{p(1)}}{d_{p(3)}}+\frac{2d_{p(3)}}{d_{p(1)}}+\frac{2d_{p(2)}A_{p(2)}}{d_{p(1)}A_{p(3)}}+\frac{2d_{p(1)}A_{p(2)}}{d_{p(2)}A_{p(3)}}\right.\\
&\qquad\left.+\frac{2d_{p(3)}A_{p(2)}}{d_{p(2)}A_{p(1)}}+\frac{2d_{p(2)}A_{p(2)}}{d_{p(3)}A_{p(1)}}\right)\\
F_{33} &= \frac{6\chi_{33}d_s}{\epsilon U_o}\left(\frac{2d_{p(2)}}{d_{p(1)}}+\frac{2d_{p(1)}}{d_{p(2)}}+\frac{2d_{p(3)}A_{p(3)}}{d_{p(2)}A_{p(1)}}+\frac{2d_{p(2)}A_{p(3)}}{d_{p(3)}A_{p(1)}}\right.\\
&\qquad\left.+\frac{2d_{p(1)}A_{p(3)}}{d_{p(3)}A_{p(2)}}+\frac{2d_{p(3)}A_{p(3)}}{d_{p(1)}A_{p(2)}}\right).
\end{aligned}
$$

In the case of foams of Type B the diagonal components of the shear friction tensor follows from (3.62) and are given by

$$
\begin{aligned}
F_{11} &= \frac{6\chi_{11}S_{fs}}{\epsilon d_{(1)}d_{(2)}d_{(3)}d_p}\\
F_{22} &= \frac{6\chi_{22}S_{fs}}{\epsilon d_{(1)}d_{(2)}d_{(3)}d_p}\\
F_{33} &= \frac{6\chi_{33}S_{fs}}{\epsilon d_{(1)}d_{(2)}d_{(3)}d_p}.
\end{aligned}
$$

The shear friction tensor as defined here is an intrinsic local property of the porous medium and thus independent of external boundary conditions or streamline configuration. A comparison of (3.3) with (3.69) indicates that the shear friction tensor is related to the Darcy permeability by

$$K_{II} = \frac{\epsilon}{F_{II}} \tag{3.69}$$

with no summation implicated over the tensor index I.

3.7.3.2 Inertial tensor

In Section 3.3 possible causes of the non-linear relation between the pressure gradient and superficial velocity for intermediate to high Reynolds number flow have been discussed. The Forchheimer-type equation as presented in (3.6) is a scalar equation applicable to the situation where the pressure gradient and superficial velocity are collinear.

For anisotropic materials the pressure gradient and superfical velocity are not neccessarily collinear and the coefficient of proportionality between these two quantities may be a tensor. In this section the possible existence and tensorial nature of the coefficient relating the presssure gradient to the superfial velocity is investigated.

In contrast to flow at low Reynolds numbers, conclusive evidence cannot be produced to indicate that the contribution of the inertial effect to the pressure gradient can be expressed through a *symmetrical* second order tensor in context of the RUC-approach. An argument in favour of the existence of an inertial tensor may be formulated by realising that although the material coordinates, the superficial velocity and pressure gradient are not collinear, the fluid still traverses the RUC in fixed channels. Each component of the superficial velocity directed along a material coordinate will therefore enter an RUC along a material direction and then recirculate around the solid material blocking the channel. But if it is assumed that each component recirculates around the solid symmetrically, its effect on the pressure gradient perpendicular to its original direction will add vectorially to zero. Therefore, each component of the fluid only contributes to the pressure gradient in its own direction. The magnitude of this pressure gradient is then calculated by considering the form drag of that specific component around the solid strand. In view of this argument, it may then be possible to consider each component of the pressure gradient along each of the material coordinates individually and the diagonal components of the symmetrical inertial tensor may be deduced from (3.64) and (3.66).

On the other hand, the main concern regarding the derivation of a symmetric inertial tensor resides with the non-linear relationship between the pressure gradient and the velocity. Due to the flow pattern through the RUC's the channel velocities which are related to the different components of the superficial velocity will in some channels flow in the same direction and in other channels in opposite directions. Although the velocities in opposite directions will, on average, add to zero, the pressure forces related to the velocities due to form drag will not add to zero since the forces are related to the square of the velocities. Therefore, the various components of the superficial velocity are coupled and each component of the pressure gradient may not be solved independently. In addition, the resultant recirculating streamline configuration may not be symmetric and be to complex to determine uniquely due to the recirculation of three velocity components around each solid strand.

The view that a pressure gradient-velocity relationship in the form of (3.67) for intermediate Reynolds number flow does not exist has also been put forward by Barak and Bear (1981), although their arguments concentrate more on the mathematical aspects of finding such a relationship and not so much on the physics of the phenomenon. How-

ever, they do provide some experimental evidence in favour of their viewpoint. Their result is partly in agreement with the analysis of Cvetković (1986, eqn(82)) who related the pressure gradient to the superficial velocity according to

$$-\epsilon P_{,i} = R_{ij}q_j + qC_{ij}q_j + R_{ijk}q_jq_k + R_{ijkl}q_jq_kq_l. \tag{3.70}$$

Cvetković (1986) also mentioned that the inertial tensor C_{ij} has a different relation with the anisotropy than the friction tensor R_{ij} and although R_{ij} may be isotropic for certain porous media, C_{ij} will maintain a tensorial character. Whitaker (1996) derived a Forchheimer correction tensor similar to the second term in (3.67) for spatially periodic porous media. He also indicated that the Forchheimer tensor is not symmertic and the exact functional dependence of this tensor still needs to be determined. Therefore, the nature of the inertial tensor B_{ij} in (3.67) is not further pursued in context of the RUC-model and the results obtained for the intermediate Reynolds number flow domain are only valid for anisotropic materials where the pressure gradient is collinear with the superfical velocity. However, the variable flow conditions in the different directions are taken into consideration in the modelling approach.

3.7.4 General momentum transport equation

Two expressions, relating the pressure gradient and velocity, have been developed for anisotropic foams, applicable to flow at low as well as intermediate Reynolds numbers. An expression for the whole range can be obtained by addition of these two expressions, valid in their respective regions. The two limiting conditions were also combined by Comiti and Renaud (1989) as well as by Du Plessis (1994). The latter justified the addition through reference to the asymptote matching technique (Churchill and Usagi, 1972) which has been used successfully with a shifting parameter of one as summarised by Du Plessis and Diedericks (1997).

The pressure gradient may thus be expressed in the form of (3.6), which in the case of one-dimensional flow along the x_1-coordinate axis, yields

$$-\frac{1}{q_1}P_{,1} = Mq_1 + N. \tag{3.71}$$

Except for the porosity as multiplicative factor, the coefficient M is given by either (3.64) or (3.66) and N is given by either (3.58) or (3.62) for foams of Type A and Type B, respectively. These coefficients are now completely determined by measurable

structural parameters of the porous medium and direct permeability measurements are not necessary.

It is important to note further that the expressions derived for the surface integral in (3.43) are restricted by certain porosity limits. For foams of Type A a trivial porosity limit is obtained when $d_{min} = d_s$ and for foams of Type B when $d_{min} = d_p$. Therefore, foams of Type A has a lower bound and foams of Type B an upper limit on porosity. These limits are rather trivial, since it is expected that no porous material outside of these limits can exist for the types of foam under consideration and are generally only of theoretical value.

In conclusion, it may also be noted that the flow of fluid through isotropic foamlike porous media was formerly modelled by Du Plessis *et al.* (1994), and also summarised in Du Plessis and Diedericks (1997), employing a similar modelling technique as was done here for anisotropic foams. If the porous medium is an isotropic foamlike medium, the RUC's presented in Figures 3.6 and 3.7 take on a cubic form and the channels in all RUC's then have equal cross-sections and equal lengths. It is interesting to note that both types of foam then describe exactly the same isotropic material. Inspection of the RUC's indicates that the geometric structure of the RUC in Figure 3.7, for the isotopic case, represents isotropic foams within a porosity range of $0 \leq \epsilon \leq \frac{1}{2}$. The RUC for foams of Type A, for example Figure 3.6, simplify to isotropic foamlike materials with a porosity between $\frac{1}{2} \leq \epsilon \leq 1$. In the limit of isotropy, the present model yields equal expressions for the pressure gradient predictions for the two types of foams which are also the same as the expressions formerly obtained by Du Plessis *et al.* (1994) for flow through isotropic foams.

3.8 Flow through a highly porous anisotropic multifilament knit

3.8.1 Introduction

In general, the presence of anisotropy in various porous materials increases the difficulty in assessing transport phenomena, since certain distinctive qualities of the material are functions of the transport direction. The accuracy of the analytical modelling of such complex systems is very difficult to determine and, for the quantitative validation of models, one has to revert to the comparison of model predictions to results of controlled experiments over a wide spectrum of simple benchmark cases. In this section one such

set of data, obtained for pressure drop tests over a cylindrical plug of very high porosity and with some anisotropy with respect to the geometry of the microstructure, is used to validate the model for homogeneous anisotropic foams.

The porous medium is formed by a knitted stainless steel wire mesh rolled up to form a cylindrical plug. The theoretical pore-scale model developed in the previous section is applied predictively over both the Darcy and non-Darcy regimes, requiring only that the porosity, dimensions of the wire and characteristic lengths of the plug be known. In addition, it is also indicated in which manner the basic model may be extended to incorporate salient features of the porous material not included in the RUC's developed in the previous section.

3.8.2 The porous medium

The porous medium under investigation is generally used in the chemical and petroleum industries as mist eliminators as well as for separators in the naval, atomic engineering and air conditioning industries. The material constituting the porous medium consists of two wires, each with a diameter of $D = 0.16$ mm, intertwined to form a double strand, which is then knitted to produce a wire mesh as indicated in Figure 3.10. The knitted wire is then tightly rolled to form a cylindrical anisotropic plug with an overall diameter of approximately 60 mm. The length of an individual plug varies between 14.35 and 15.35 cm.

The knitted plug exhibits large pore openings when viewed from the side, but when viewed axially, the material is pressed closely together with only small openings, thus revealing some anisotropy in the geometry of the plug. The porosity, or void fraction, of the plug has been determined as $\epsilon = 0.941$.

3.8.3 Experimental pressure gradient measurements

The pressure gradient occurring during fluid flow through the porous medium was measured by Dr. A. Montillet at the Laboratoire de Génie de Procédés, Institut de Université, Saint-Nazaire in France. The experimental equipment and layout are presented by Diedericks *et al.* (1998). A cylindrical cell with diameter 0.06 metres was packed with seven cylindrical porous plugs corresponding to a porous medium with a total length of approximately 1.03 metres. Several pressure taps allowed pressure gradient measurements to be taken in an axial length at intervals from 0.05 to 0.86

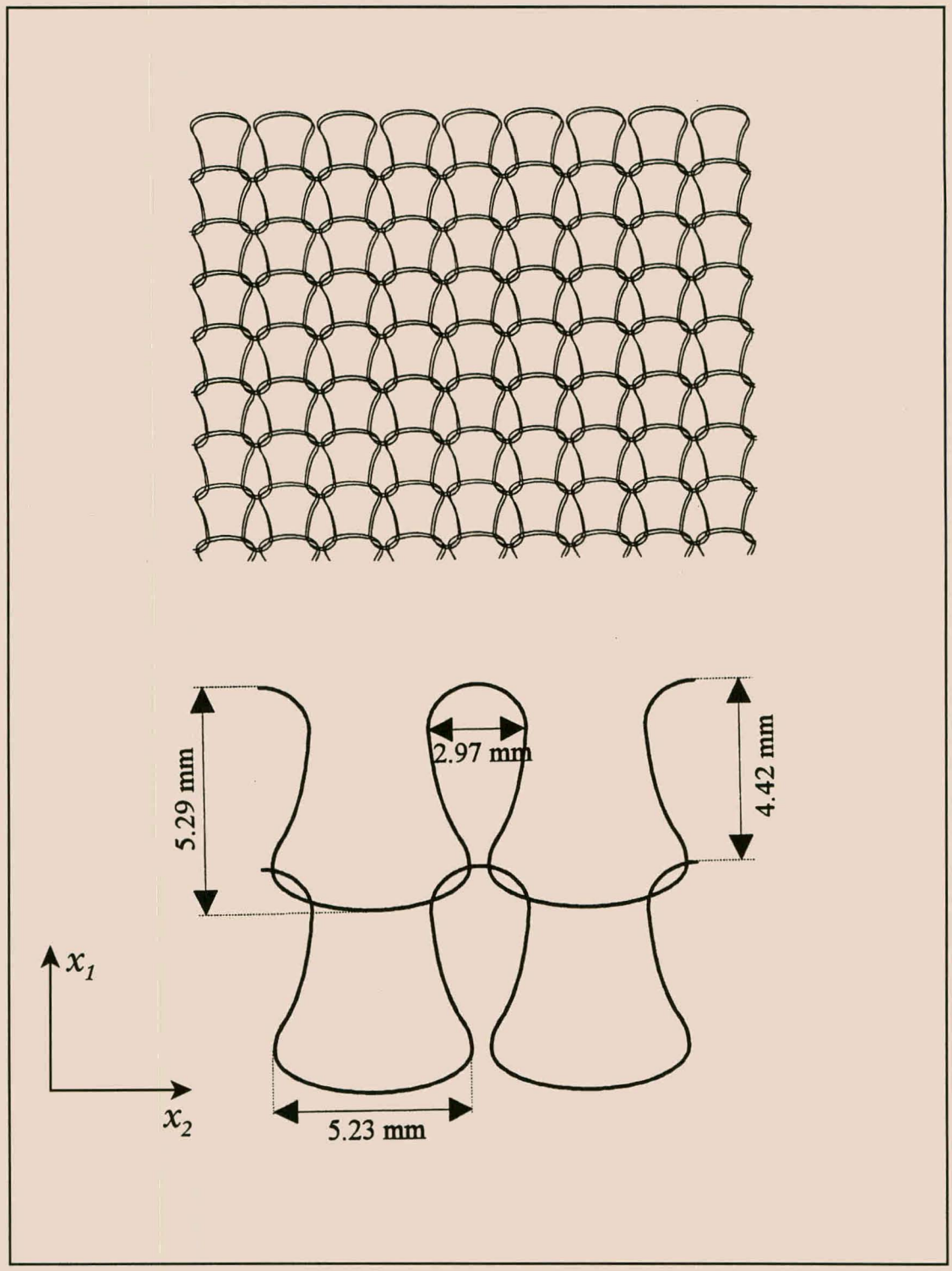

Figure 3.10. A schematisation of the wire mesh indicating the dimensions of the knit.

metres along the porous medium. Additional lengths above and below the plugs acted as calming sections. Experiments were performed with water and air, respectively, to verify the reproducibility of the results. With the water flow, the temperature was regulated at $25°C$. With the air flow, special care was taken to regulate the temperature

and the absolute pressure which was measured at the medium level of the test section. These were measured for each imposed flow rate and a variable area flowmeter was used for both fluids. The estimated uncertainty ranged between 1 and 5%. Depending on its value, the pressure drop was measured with straight or inclined manometers and in these cases the estimated uncertainty lied between 0.5 and 5%. The highest uncertainties (5%) were reached with only the lower flow rates.

Table 3.2. Fluid characteristics and experimental results.

$\mu\ (Pa.s)$	0.899×10^{-3}
$\rho\ (kg.m^{-3})$	997
$M_{exp}\ (Pa.m^{-3}.s^2)$	242 860
$N_{exp}\ (Pa.m^{-2}.s)$	15 024

As indicated in Appendix A, the experimental pressure drop data may be presented in terms of f/d_c versus d_c/Re where f is a friction factor defined as

$$f = |P_{,1}| \frac{\epsilon^3 d_c}{(1-\epsilon)\rho q_1^2} \tag{3.72}$$

while Re is a Reynolds number defined as

$$Re = \frac{\rho q_1 d_c}{\mu} \tag{3.73}$$

and q_1 is the magnitude of the superficial velocity, $P_{,1}$ is the pressure head across the plugs and d_c is a characteristic length of the porous medium. The direction of discharge, which is axial along the plugs, is taken as the x_1-coordinate axis. A correlating equation was calculated from a least squares fit through the experimental data, which comprised 81 points, and is given by

$$\frac{f}{d_c} = 2.36 \times 10^8 \frac{d_c}{Re} + 3440. \tag{3.74}$$

The mean relative scatter between the experimental and calculated data is 2.3% (Diedericks *et al.*, 1998). This representation is convenient to gather data obtained from fluids

with different characteristics as it does not require an estimation of d_c and the representation furthermore allows a simple linear averaging of the data. To ease comparison with the theoretical model, (3.74) may also be expressed as a Darcy-Forchheimer type equation in the form of (3.6) where the coefficients M and N, as well as the physical characteristics of the working fluid, which in this case is water at $25°C$, are given in Table 3.2.

3.8.4 Modelling of the porous medium microstructure

3.8.4.1 The RUC representation

A closure scheme for the macroscopic momentum balance equations applicable to anisotropic porous media has been presented in Section 3.7, in which the average geometry of the material in an REV is imbedded within a Representative Unit Cell (RUC). The first step in adequately modelling fluid flow through the knitted wire is to obtain an RUC of the material.

The porous medium to be modelled is a cylindrical plug and would in effect necessitate a cylindrical RUC to embed the average geometry. However, compensation for a rectangular RUC is made by selecting the x_1-direction as the axial direction and the x_2-direction of the RUC as the circumferential direction of the plug. The x_3-direction in the RUC then corresponds to the radial direction of the plug. If the two intertwined wires are assumed to form a single unit, the material then conforms to a foam of Type A and may be represented by the RUC given in Figure 3.6. Characteristics of the material that have been modelled in the RUC are the feature that the solid strands form a continuum and the possible tortuous pathway available for flow. Accurate modelling of the dimensions of the RUC and the solid strands will ensure that the total fluid-solid surface is also well represented.

3.8.4.2 Equivalent solid strands

In the RUC representation the two intertwined wires of diameter, D, have to be substituted by an 'equivalent' set of perpendicular straight prismatic bars of square cross-section. Requiring mass equivalence per unit length for the wires of diameter D and the model of side length d_s, gives

$$d_s = \sqrt{\frac{\pi}{2}} D = 0.2005 \text{ mm}. \tag{3.75}$$

The estimate of this effective diameter leads to the possible loss of shear stress due to the fact that the model was taken to conserve mass in accordance with the double wire and in the process the actual wetted surface was diminished by a 20% fraction. The extent to which this effect is cancelled partially by the touching of the wires is not readily determinable and will be ignored.

3.8.4.3 Geometric characteristics

For ease of reference a number of geometric characteristics introduced in Sections 3.5 and 3.7 are recapped. For instance, the fluid filled part of an RUC, U_f, may be written in terms of the porosity, ϵ, as

$$U_f = \epsilon U_o = \epsilon d_{(1)} d_{(2)} d_{(3)} \tag{3.76}$$

with U_o the total volume of an RUC. The effective cross-sectional area open to discharge in the x_1-direction is

$$A_{p(1)} = d_{p(2)} d_{p(3)} = \left(d_{(2)} - d_s\right)\left(d_{(3)} - d_s\right). \tag{3.77}$$

The effective channel areas in the other directions may be determined similarly. The effective volume available for discharge in the x_1-direction is then

$$U_{f\mathcal{L}(1)} = A_{p(1)} d_{(1)}. \tag{3.78}$$

In the remainder of the fluid volume of the RUC, $(U_f - U_{f\mathcal{L}(1)})$, the fluid thus flows in directions normal to the x_1-direction.

The tortuosity component for discharge in the x_1-direction is defined as the ratio between the total fluid volume and the effective volume available for discharge in the x-direction, which mathematically yields

$$\chi_{11} \equiv \frac{U_f}{U_{f\mathcal{L}(1)}}. \tag{3.79}$$

This expression complies to the analyses of Suman and Ruth (1993) and that of Chapter 2 in which it is indicated that in materials with variable channel dimensions and multiple flowpaths the tortuosity as a ratio of volumes is more appropriate than a ratio of lengths.

However, it has been shown in Chapter 2 that for an isotropic material the tortuosity, as given in (3.79), reduces to a ratio of lengths since the channels have equal areas. By making use of (3.76), (3.77) and (3.78) this tortuosity component may be expressed as

$$\chi_{11} = \frac{\epsilon d_{(2)} d_{(3)}}{d_{(2)} d_{(3)} - d_{(2)} d_s - d_{(3)} d_s + d_s^2}. \tag{3.80}$$

The tortuosities for discharge in the other material directions may be determined in a similar manner and, as indicated in Table 3.1, are given by

$$\chi_{22} = \frac{\epsilon d_{(1)} d_{(3)}}{d_{(1)} d_{(3)} - d_{(1)} d_s - d_{(3)} d_s + d_s^2} \tag{3.81}$$

$$\chi_{33} = \frac{\epsilon d_{(1)} d_{(2)}}{d_{(1)} d_{(2)} - d_{(1)} d_s - d_{(2)} d_s + d_s^2}. \tag{3.82}$$

The total fluid-solid surface area within the RUC may be written as

$$S_{fs} = 4 d_s \left(d_{p(1)} + d_{p(2)} + d_{p(3)} \right) = 4 d_s \left(d_{(1)} + d_{(2)} + d_{(3)} - 3 d_s \right). \tag{3.83}$$

In an RUC the dynamic specific surface area is equal to the static specific surface area and it is therefore defined as the magnitude of the fluid-solid interface S_{fs} per solid volume U_s, yielding

$$A_{vd} \equiv \frac{S_{fs}}{U_s}. \tag{3.84}$$

The void volume, U_f, within the RUC under consideration may also be expressed as

$$\begin{aligned} \epsilon d_{(1)} d_{(2)} d_{(3)} &= A_{p(1)} d_{(1)} + A_{p(2)} d_s + A_{p(3)} d_s \\ &= d_{(1)} d_{(2)} d_{(3)} - d_{(3)} d_s^2 - d_{(1)} d_s^2 - d_{(2)} d_s^2 + 2 d_s^3 \end{aligned}$$

from which it may be deduced that

$$d_{(3)} = \frac{2 d_s^3 - d_{(1)} d_s^2 - d_{(2)} d_s^2}{\epsilon d_{(1)} d_{(2)} - d_{(1)} d_{(2)} + d_s^2}. \tag{3.85}$$

This equation may be used to infer $d_{(3)}$ indirectly, since the wires of the plug are closely pressed together and folded over each other in the radial direction, complicating direct measurement.

3.8.4.4 Form drag coefficient

Calculation of the pressure gradient at intermediate Reynolds number flow, requires the form drag coefficient, c_d, for flow over the equivalent solid strands. The value predicted by the model geometry for a square bar is $c_d = 2.05$. However, the solid material modelled deviates substantially from that of a square bar and it would seem appropriate to acknowledge this in the pore-scale modelling and a physically more representative value for the form drag coefficient may be selected.

As partially illustrated in Figure 3.10, the two adjacent cylindrical wires are intertwined to some extent, offering, at different locations, different cylindrical surfaces for form drag initiation in the streamwise direction. The average between the maximum and minimum drag forces instigated during flow over the two intertwined wires is proposed as a more representative drag force. The minimum amount of drag is initiated when the one wire is completely screened behind the other and the surface area presented to the streamwise direction is that of a single wire. In this case the minimum drag force initiated is given by

$$F_{min} = 1.1Dl\left(\frac{1}{2}\rho v^2\right) \tag{3.86}$$

where Dl is the projected area of a cylinder with diameter D and length l. The factor in brackets is a kinetic energy factor. The drag coefficient for form drag initiation for flow over a cylinder is a function of Reynolds number. For flow at relative high Reynolds numbers the drag coefficient may be taken as $c_d = 1.1$, which is the asymptotic value for two-dimensional flow over a cylinder (Whitaker, 1968).

The maximum drag will be initiated when the wires do not screen each other and both lie next to each other normal to the flow. The surface area of both wires are then equally exposed to the flow. The drag initiated by these two wires may be considered to be equal to that of a single cylinder of diameter $2\,D$. Therefore, the maximum drag force over the cylinders is given by

$$F_{max} = 2.2Dl\left(\frac{1}{2}\rho v^2\right). \tag{3.87}$$

The average drag force to be used in the model is considered to be an average of these two extreme cases. Therefore,

$$F_{av} = 1.65Dl\left(\frac{1}{2}\rho v^2\right) = 0.264l\left(\frac{1}{2}\rho v^2\right) \tag{3.88}$$

where use was made of the measured dimension of the wire, D.

However, compensation has to be made for the fact that the cylindrical wires are modelled as a square bar. To obtain the value of the form drag coefficient for the model, the drag force corresponding to the square bar is set equal to F_{av} obtained by (3.88), which yields

$$c_d d_s l \left(\frac{1}{2}\rho v^2\right) = 0.264 l \left(\frac{1}{2}\rho v^2\right) \tag{3.89}$$

where d_s is the diameter of the square bar determined in (3.75). It therefore follows that

$$c_d = 1.32. \tag{3.90}$$

To obtain an equivalent drag force for flow over the square bar, therefore requires that the form drag coefficient be appropriately reduced to about 65% of the model value of 2.05 for a perfectly square cross-section.

3.8.4.5 Pressure gradient equations

The porous plug conforms to a foam of Type A and, therefore, the pressure drop relations derived in Section 3.7 are applicable to predict the pressure gradient across the plug from the structural parameters of the material. The pressure gradient in the Darcy regime, (3.58), is given by

$$\begin{aligned} -\frac{1}{q_1}P_{,1} &= N \\ &= \frac{6\mu\chi_{11}d_s}{\epsilon^2 U_o}\left(\frac{2d_{p(2)}}{d_{p(3)}} + \frac{2d_{p(3)}}{d_{p(2)}} + \frac{2d_{p(1)}A_{p(1)}}{d_{p(2)}A_{p(3)}} + \frac{2d_{p(2)}A_{p(1)}}{d_{p(1)}A_{p(3)}}\right. \\ &\qquad \left. + \frac{2d_{p(3)}A_{p(1)}}{d_{p(1)}A_{p(2)}} + \frac{2d_{p(1)}A_{p(1)}}{d_{p(3)}A_{p(2)}}\right). \end{aligned} \tag{3.91}$$

while the expression in the Forchheimer regime, (3.64), is

$$\begin{aligned} -\frac{1}{q_1}P_{,1} &= Mq_1 \\ &= \frac{c_d\rho\chi_{11}^2}{2\epsilon^3 U_o}\left(d_{p(2)}d_s + d_{p(3)}d_s\right). \end{aligned} \tag{3.92}$$

The different parameters in these equations which are known are the porosity, the friction factor, the fluid density and the diameter of the solid material. It is shown in the remainder of this chapter in which manner the other structural parameters of the porous medium may be obtained.

3.8.5 Comparison with experimental results

The expressions for the pressure drop through foams of Type A obtained in Section 3.7, and presented for convenience in (3.91) and (3.92), are now compared to the experimental data in two ways. In the first case, the porous plug is considered as a perfectly isotropic material. The pressure gradient expressions (3.91) and (3.92), then simplify greatly and from these results it can be determined to which extent the anisotropy influences the flow.

Secondly, the values of the two characteristic lengths $d_{(1)}$ and $d_{(2)}$ are inferred from microscopic measurements. These are then used to predict the pressure gradient for both low and intermediate Reynolds number flow. In both these cases the model is applied deterministically.

3.8.5.1 Isotropic model

For an isotropic material the RUC has a cubic form and a number of geometric simplifications may be introduced which are summarised in Table 3.3. A further advantage of the cubic RUC for isotropic materials compared to the rectangular RUC in anisotropic materials, is the fact that spatial distribution of the solid material within the RUC uniquely defines the tortuosity of the pore structure as a function of porosity. For the particular foam structure considered, it was formerly derived (Smit and Du Plessis, 1999) that

$$\chi = 2 + 2\cos\left[\frac{4\pi}{3} + \frac{1}{3}\arccos(2\epsilon - 1)\right]. \tag{3.93}$$

According to this equation, the experimentally measured porosity of 0.941 corresponds to a tortuosity value of

$$\chi = 1.30. \tag{3.94}$$

In the isotropic case the volume of solid material within the RUC may be used to calculate the dimensions of the RUC, d, as follows

$$U_s = (1-\epsilon)d^3 = 3dd_s^2 - 2d_s^3 \tag{3.95}$$

yielding a value for the RUC dimension of

$$d = 1.35 \text{ mm}. \tag{3.96}$$

Here use was made of the diameter of the solid material in (3.75). According to (3.96), the dimensions of the RUC are smaller than any of the solid-to-solid distances presented in Figure 3.10. This indicates that the RUC is only a conceptual model and the basic features of the porous medium can be incorporated into unit cells which are smaller than any repetitive building block of the material.

Table 3.3. Geometric characteristics for an RUC for isotropic foamlike materials.

$d_{(1)} = d_{(2)} = d_{(3)} = d$
$d_{p(1)} = d_{p(2)} = d_{p(3)} = d_p$
$A_{p(1)} = A_{p(2)} = A_{p(3)} = A_p = d_p^2$
$\chi_{11} = \chi_{22} = \chi_{33} = \chi$

By making further use of some geometric features of an isotropic RUC, it also follows (Du Plessis and Masliyah, 1988; Du Plessis 1992a; Du Plessis *et al.*, 1994) that

$$d_p d_s = \frac{S_{fs}}{12} \tag{3.97}$$

$$S_{fs} = \frac{6\epsilon(\chi-1)d^3}{\chi d_p} \tag{3.98}$$

$$d_p = \frac{S_{fs}}{6d(\chi-1)} \tag{3.99}$$

and the pore width may also be expressed as

$$d_p = \frac{(3-\chi)d}{2}. \tag{3.100}$$

The pressure gradient for isotropic materials valid over both the Darcy and non-Darcy flow regimes may be determined from (3.91) and (3.92). By utilising the geometric reductions in Table 3.2, by applying (3.97), (3.98) and (3.100) to the Forchheimer limit and (3.97) and (3.99) to the Darcy limit, the pressure gradient becomes

$$\begin{aligned} -\frac{1}{q_1}P_{,1} &= Mq_1 + N \\ &= \frac{c_d\rho\chi^2}{2\epsilon^3 d^3}\frac{2S_{fs}}{12} + \frac{72\mu\chi d_s}{\epsilon^2 d^3} \\ &= \frac{c_d\rho\chi^2}{2\epsilon^2}\frac{(\chi-1)}{\chi}\frac{2}{(3-\chi)d} + \frac{6\mu\chi S_{fs}}{\epsilon^2 d^3 d_p} \\ &= \frac{c_d\rho}{d}\frac{\chi(\chi-1)}{\epsilon^2(3-\chi)} + \frac{36\mu\chi(\chi-1)}{\epsilon^2 d^2}. \end{aligned} \tag{3.101}$$

This pressure drop expression is the same as the pressure gradient prediction formerly obtained for isotropic foams by Du Plessis *et al.* (1994) and also summarised by Du Plessis and Diedericks (1997). If the structural parameters determined for an isotropic medium are inserted into (3.101) the numerical values for the two coefficients M and N may be obtained and are given in Table 3.4.

Table 3.4. Parameters required and model predictions for isotropic modelling.

Parameters		Predictions		Comparisons	
ϵ	0.941	χ	1.30		
$d_s\ (m)$	2.005×10^{-4}	$A_{vd}\ (m^{-1})$	19 051		
$d\ (m)$	0.00135	$M\ (Pa.m^{-3}.s^2)$	252 835	M/M_{exp}	1.04
c_d	1.32	$N\ (Pa.m^{-2}.s)$	7 819	N/N_{exp}	0.52
$\mu\ (Pa.s)$	0.899×10^{-3}				
$\rho\ (kg.m^{-3})$	997				

On comparison with the experimentally measured pressure gradient, as given in Table 3.2, it becomes apparent that the pressure gradient in the Darcy regime is under predicted while it is predicted nearly correctly in the Forchheimer regime. This comparison is schematically illustrated in Figure 3.11.

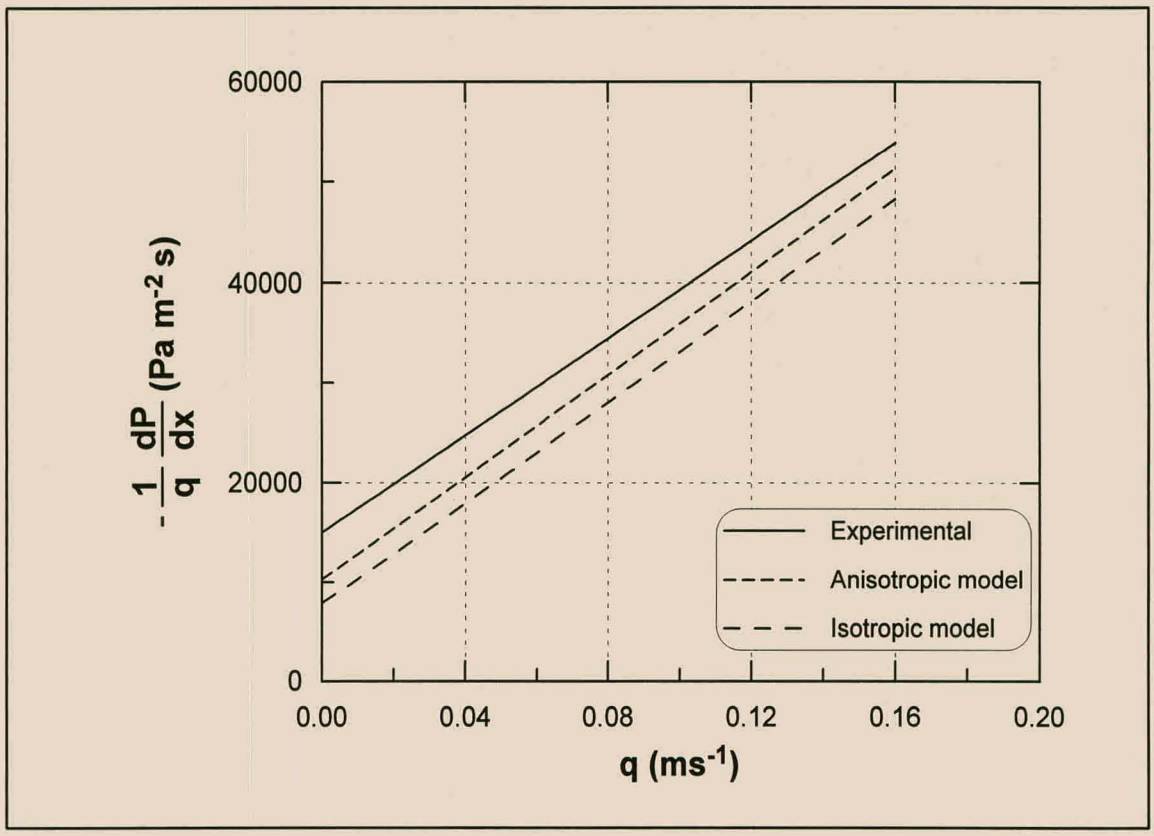

Figure 3.11. Comparison between experimental and predicted pressure gradients.

3.8.5.2 Deterministic anisotropic model

In this case the model is also used in a deterministic manner to predict the pressure gradient over both the Darcy and Forchheimer regimes. The structural parameters necessary for obtaining the pressure drop are the porosity, the solid diameter of the foam strands and two characteristic lengths.

The porosity of the plug and wire diameter may be fairly accurately determined. However, there is an amount of uncertainty involved in determining the characteristic lengths. If the dimensions of the wire mesh on the outer surface of the plug is measured by microscope, as schematically illustrated in Figure 3.10, the following two average dimensions in the x_1-direction (axial) and the x_2-direction (circumferential) are determined as $d'_{(1)} = 4.86$ mm and $d'_{(2)} = 4.10$ mm, respectively. These lengths are representative of the characteristic lengths. The measured distance $d'_{(1)}$ extends from the top point of one of the interlocking loops of the wire mesh to the base of the loop where the distance between the two legs of the loop is narrowest and, in this case, where it meets the next loop. However, this distance appears to vary greatly, as the position of the bottom loop is not fixed with regards to the top one. It is therefore suggested that the average solid-to-solid distance in the axial direction be half the maximum measured

distance and therefore as axial characteristic length it is proposed that

$$d_{(1)} = 2.43 \text{ mm}. \tag{3.102}$$

The projection of the circumferential widths of the loops on a plane through the centre of the plug varies from zero to a maximum and then decreases again. In a rectangular reference frame such a projection should yield equal spacings and it is therefore suggested that the characteristic length in the x_2-direction be an average between the maximum and minimum projected widths and therefore it is proposed that

$$d_{(2)} = 2.05 \text{ mm}. \tag{3.103}$$

It must be understood, however, that these measurements are extremely difficult to quantify and the results mostly represent reasonable guesses. In the present case, the values given are fairly accurate as it is taken as slightly less than the length of periodicity of the mesh in the two principal directions. According to the definition of an RUC the dimensions thereof must correlate with the dimensions of the smallest possible REV. The characteristic length in each material direction is therefore the smallest dimension representative of the material and in this case not necessarily the outer dimensions of the plug.

Table 3.5. Parameters required and model predictions for deterministic anisotropic modelling.

Parameters		Predictions		Comparisons	
ϵ	0.941	χ_{11}	1.51		
$d_s\ (m)$	2.005×10^{-4}	χ_{22}	1.48		
$d_{(1)}\ (m)$	0.00243	χ_{33}	1.14		
$d_{(2)}\ (m)$	0.00205	$A_{vd}\ (m^{-1})$	19 003		
$d_{(3)}\ (m)$	0.00065	$M\ (Pa.m^{-3}.s^2)$	256 238	M/M_{exp}	1.06
c_d	1.32	$N\ (Pa.m^{-2}.s)$	10 302	N/N_{exp}	0.68
$\mu\ (Pa.s)$	0.899×10^{-3}				
$\rho\ (kg.m^{-3})$	997				

The third dimension is not easily determined as it varies considerably radially across the thickness of the plug due to the fact that a rectilinear representation is used to present the axially symmetric geometry. In favour of the rectangular modelling, however, is the fact that the inner portion of the plug, near to the would-be axis of symmetry, appears to be folded instead of rolled and this presents a geometry more akin to the present model than to a purely axially symmetric one. Nevertheless, an effective third dimension may be derived from the model geometry, the known porosity and the calculated values of $d_{(1)}$ and $d_{(2)}$. Using (3.85), the third dimension is

$$d_{(3)} = 0.65 \text{ mm}. \tag{3.104}$$

It is questionable whether $d_{(3)}$ can be measured experimentally because of its variability across the plug. Visual observations indicated that the layers of the mesh are pressed tightly together in the radial direction implying that the radial dimension of the RUC should be on the same order of magnitude as the wire diameter as is reflected in (3.104).

With the dimensions of the RUC known and by making use of the geometric characteristics previously presented, it is possible to determine the tortuosity and specific dynamic surface area as presented in Table 3.5. The coefficients for the pressure gradient equation may now be calculated from (3.91) and (3.92), and are also given in Table 3.5. This result is also compared to the experimentally obtained pressure drop in Figure 11.

3.8.6 Discussion

3.8.6.1 Factors influencing the pressure gradient

When the plug is considered as being isotropic, the model under predicts the pressure drop in the Darcy regime by 48% and over predicts in the Forchheimer regime by only 4%. The isotropic model only yields a single tortuosity value, which is slightly less than the average of the tortuosities obtained in the anisotropic case. However, in favour of the isotropic model is the fact that it is fairly easy to apply since only the porosity and diameter of the solid strands are required for the prediction, which renders this application purely deterministic as no use is made of the measured pressure drops.

When applying the anisotropic model to obtain pressure drop predictions, the results are reasonably good. The pressure gradient in the Darcy regime is under predicted by about 32%. This may be attributed to the reduction of the frictional fluid-solid surface

by approximately 20% when modelling the double wire as a single solid bar. The pressure gradient in the Forchheimer regime is over predicted by only 6% and reflects the difficulty in modelling the inertial effect induced by the intertwined and twisting double wire. On the whole, the anisotropic model therefore yields a more accurate analysis than in the isotropic case, although it was necessary to obtain two additional structural parameters.

It would appear from the plug that the tortuosity in the radial direction should be close to unity, since straight channels can be observed visually if the plug is viewed from the side. This observation seems to be confirmed by the tortuosities determined in the anisotropic case, since the tortuosity in the streamwise direction is calculated to be approximately 70% higher than in the radial direction. This is an additional advantage of the anisotropic model, since it is possible to determine the differences in tortuosities in the various principal directions. Both applications of the model yields nearly the same value for the specific dynamic surface area which indicates that it is not dependent on the anisotropy of the material.

The parameters which are required for application of the model are the porosity, the diameter of the solid strands (D), which are related to d_s, and the characteristic lengths $d_{(1)}$ and $d_{(2)}$. In contrast to the porosity and diameter of the solid stands which are determined to a high degree of accuracy, there is a measure of uncertainty with regard to d_s and the characteristic lengths of the RUC. It is, therefore, important to investigate the sensitivity of these parameters on the predicted pressure gradients as expressed in terms of the coefficients $N = N(\mu, \epsilon, d_{(1)}, d_{(2)}, d_{(3)}, d_s)$ and $M = M(c_d, \rho, \epsilon, d_{(1)}, d_{(2)}, d_{(3)}, d_s)$ as given in (3.91) and (3.92), respectively. Only the influence of the structural parameters are investigated which implies that the porosity, fluid viscosity and density remain constant. The sensitivity is conducted by considering the changes in N and M by varying one of the structural parameters while the remaining measurements remain fixed. For example, the dependencies of N and M on $d_{(1)}$ are determined by keeping $d_{(2)}$ and d_s equal to the measured values and calculating $d_{(3)}$ from (3.85). The sensitivity is then expressed by the percentage difference of the predicted values of N and M from the measured values. For the viscous coefficient the percentage difference is calculated as

$$\%Difference = \frac{N - N_{exp}}{N_{exp}} \times 100.$$

Similar expressions apply to M and the structural parameters. According to this expression for the percentage difference negative values indicate that the measured value is under estimated while positive values indicate over predictions.

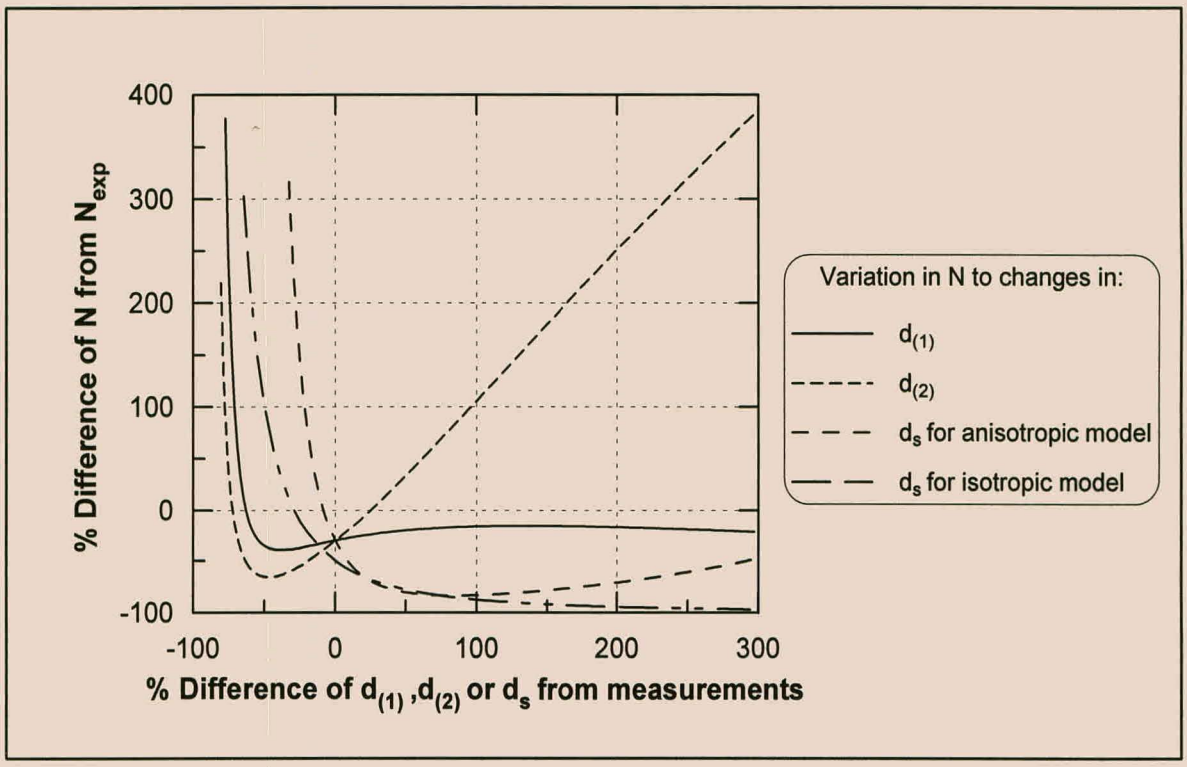

Figure 3.12. The sensitivity of the viscous shear coefficient to changes in the characteristic lengths and dimensions of the solid.

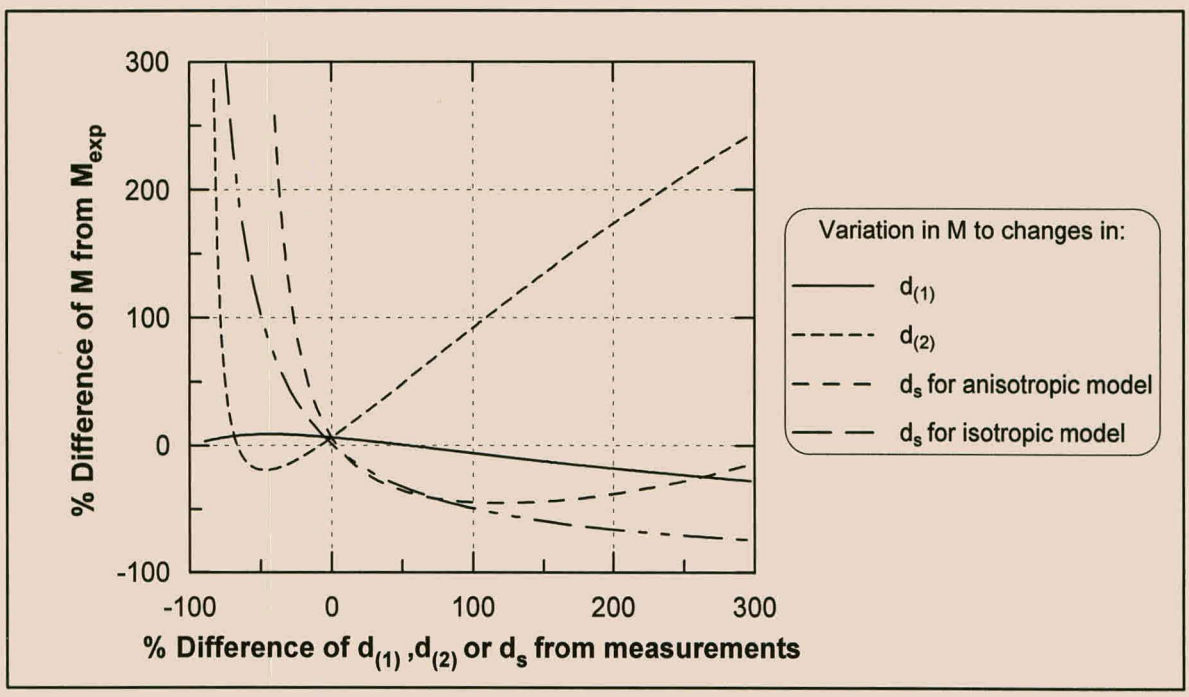

Figure 3.13. The sensitivity of the inertial coefficient to changes in the characteristic lengths and dimensions of the solid.

From Figures 3.12 and 3.13, it may be deduced that an over estimation of up to 300% in the evaluation of $d_{(1)}$ would lead to a maximum error of 50% in the predictions of N and M. By under estimating $d_{(1)}$ the maximum error on M is only 15%, but the predictions of N will differ with 300% from N_{exp}. Also indicated in these figures are the dependencies of the pressure gradient on $d_{(2)}$ obtained by using the measured values of $d_{(1)}$ and $d_{(3)}$ together with the value of $d_{(3)}$ from (3.85). From the figures it is evident that N and M are critically dependent on a correct evaluation of $d_{(2)}$, since the errors in predicting N and M increases approximately linearly with an over estimate of $d_{(2)}$. However, under predicting $d_{(2)}$ by more than 50% leads to differences of up to 300% in the calculations of N and M. By considering the graphs for the anisotropic model where d_s was varied, it is evident that larger values of d_s will lead to lower predictions of N and M. However, under predicting d_s will lead to large differences in the pressure gradient coefficients since a 20% lower value already has an error on the order of 100%. For the isotropic model similar trends apply to the predictions of N and M.

3.8.6.2 Inclusion of wall-effects

An additional source of viscous dissipation which may be included is the effect of the macroscopic boundary of the container in which the porous plugs are imbedded during the pressure gradient measurements. Since the plug is consolidated no changes in the structure of the material is expected near the bounding wall and it is viewed that the container only introduces an additional wetted surface and changes in the porosity next to the wall are neglected. The simplifications of the macroscopic Navier-Stokes equations introduced in Sections 3.4.3 and 3.6 are therefore still valid. Following Carman (1937), who made an initial attempt at addressing the wall effect, the wall effect on the inertial term is negligible and only the viscous term needs to be corrected.

In the Darcy regime the wall effect may be included by assuming that the pressure force over the plugs consists of two contributions, namely a pressure force balanced by the resistance in the porous medium and a force balanced by the wall shear stress, that is

$$\left.\frac{dP}{dx_1}\right|_{tot} = \left.\frac{dP}{dx_1}\right|_{eqn(3.91)} + \left.\frac{dP}{dx_1}\right|_{w}. \tag{3.105}$$

The effects of the porous medium on the pressure gradient is given by the macroscopic Navier-Stokes equations and has been modelled to yield (3.91). The contribution from the wall shear stress is obtained by considering a balance of forces over the container

which yields an overall pressure gradient of

$$\left.\frac{dP}{dx_1}\right|_{tot} = -Nq_1 + \frac{\tau_w 2\pi R_c L_c}{\pi R_c^2 L_c} \tag{3.106}$$

where R_c is the radius of the container and L_c is the total length of the array of plugs. The additional pressure gradient due to the wall shear stress,

$$\left.\frac{dP}{dx_1}\right|_{w} = \frac{2\tau_w}{R_c} \tag{3.107}$$

is viewed to only influence local flow conditions next to the wall. It may, therefore, be modelled by considering a thin sheet with a radial distance $d_{(3)}$ parallel to the wall to form an annular space, which may be approximated as two parallel plates at each point on the wall. With such an approximation the magnitude of the wall shear stress is obtained from an expression similar to (3.55) and over one RUC width from the wall the axial velocity is given by (3.47), yielding an additional pressure loss of

$$\left.\frac{dP}{dx_1}\right|_{w} = -\frac{12\mu\chi_{11}q_1}{\epsilon R_c d_{(3)}}. \tag{3.108}$$

A combination of this expression with (3.105) leads to an overall pressure gradient prediction where the wall effects are included.

For the isotropic case the low Reynolds number pressure gradient expression contains an additional friction term, $\frac{12\mu\chi}{\epsilon d R_c} = 368$ Pa m^{-2}s, which yields a total viscous factor of $N = 8187$ Pa m^{-2}s. It follows in a similar manner from (3.108) and (3.106) for the anisotropic case that $N = 10302 + 888 = 11190$ Pa m^{-2}s which under predicts the measured pressure gradient by approximately 26%. This implies that the inclusion of the wall effects improved the predictions by only 4%. The wall effect from the container has a marginal effect on the shear stresses and the lower prediction may be attributed to the reduction of the total surface area of the wires when approximating it as a single solid bar.

3.8.6.3 Predictions with a capillary model

Modelling the flow through the knitted wire is not restricted to the RUC-approach, but being a general engineering problem, other models may also be applied. An appreciation

for the present model may be obtained by considering one other model, namely a capillary model, and noting that the porous material is a particularly complex material due to the high porosity, double wire and the fact that it is rolled to form a plug.

According to Dullien (1979), the capillary approach is not reputed to be suitable for modelling fluid transport in porous media where the porous material is characterised by a porosity larger than 0.6. In the reviews of Carman (1956) and Happel and Brenner (1965), both reported a limitation of the validity of the famous Kozeny equation for porosities larger than 0.8 in the case of flow in the Darcy regime. Nevertheless, a careful observation of experimental data indicates that the limit of validity remains uncertain. The physical reason for the discrepancy resides with the idea that the capillary model applies only when the flow resembles flow in conduits and that this idea breaks down if the particles are too far from each other. It then becomes necessary to take into account the special character of the flow which is more similar to flow around objects and which may be modelled as Stokes' flow.

However, recent experimental works (Montillet *et al.*, 1992; Montillet, 1995) have shown that a capillary-type model can give a good estimate of pressure gradients, both in the viscous and inertial flow regimes, for Newtonian fluid flow through porous media with a reticulated structure and with porosities in the range of 0.97. Moreover, the same capillary model, as introduced by Comiti and Renaud (1989), has been successfully tested in fluidized beds of spheres with porosities in the range of 0.41 to 0.65 (Sabiri *et al.*, 1996). This model has also been tested to predict the pressure drops for flow through the knitted wire presently under investigation.

This model is discussed in Appendix A and as indicated in (A.22) the pressure drop may be expressed as

$$\frac{f}{d_c} = A + \frac{B}{Re/d_c} \tag{3.109}$$

where f is a friction factor, d_c is the diameter of a capillary while A and B are the inertial and viscous terms, respectively. According to (A.23) and (A.24) these are expressed as

$$A = 0.0968 A_{vd} \chi^3 \tag{3.110}$$

and

$$B = 2A_{vd}^2 \chi^2 (1 - \epsilon) \tag{3.111}$$

where A_{vd} is the dynamic specific surface area and χ is the tortuosity. A comparison of the regression curve through the measurements as given in (3.74) with the general expression for the pressure gradient presented in either (A.22) or (3.109) implies that

$$A = 0.0968 A_{vd} \chi^3 = 3440\,\mathrm{m}^{-1} \tag{3.112}$$

and

$$B = 2A_{vd}^2 \chi^2 (1 - \epsilon) = 2.36 \times 10^8\,\mathrm{m}^{-2}. \tag{3.113}$$

Use of these measured values of A and B to solve for the tortuosity and dynamic specific surface area leads to $A_{vd} = 50172\ \mathrm{m}^{-1}$ and $\chi = 0.891$ which is an unphysical results for the tortuosity.

However, estimates of the coefficients A and B can be made with this model by assuming that the dynamic specific surface area, A_{vd}, is equal to the static specific surface area, A_{vs}, from which it then follows that

$$A_{vd} \approx A_{vs} = \frac{4}{D} = 25000\,\mathrm{m}^{-1}. \tag{3.114}$$

The static specific surface area represents the ratio of the total surface area of the porous medium to the volume of solid material. For chemical engineering purposes, the use of A_{vd} is more appropriate since the overlapping of particles may prevent a certain part of the total surface area from being available for heat or mass transfer. When considering the experimental values for the tortuosity as presented by Carman (1956), in particular those for steel wool, an estimate for the tortuosity may be taken as

$$\chi = 1.14. \tag{3.115}$$

Incorporation of these estimates in equations (3.112) and (3.113) leads to values of $A = 3585\ \mathrm{m}^{-1}$ and $B = 9.85 \times 10^7\ \mathrm{m}^{-2}$. The comparison of these values with the experimental measurements in (3.112) and (3.113) indicates that the capillary model gives a good estimate of A, the constant of the inertial term. On the other hand, the calculated value of B, the constant of the viscous term in (3.112) is under predicted by approximately 60%. Such a discrepancy may be explained by noting that the viscous term of the capillary model is calculated from the Poiseuille flow in a pore, but the viscous flow through the knitted wire may be dominated by Stokes' drag forces.

From the experimental value of B, it is also possible to calculate the Kozeny constant for further comparison with literature data obtained for high porosity porous media. The expression for the Kozeny constant, k', follows from (A.7) and the viscous contribution to (3.109), which is given by (3.111), and it may be written as

$$k' = \frac{\epsilon^3}{\mu q(1-\epsilon)^2 A_{vd}^2}\left(\frac{dP}{dx_1}\right). \tag{3.116}$$

From the experimental viscous constant in (3.74), it follows that $k' = 6.4$. In Carman (1956), a value of $k' = 4.7$ is given for a pleated steel wire ($A_{vs} = 12600$ m^{-1} and $\epsilon = 0.7$) and for a packed bed of glass fibres with an 0.4 mm diameter, the Kozeny constant is given as $k' = 6.5$ ($A_{vs} = 10100$ m^{-1} and $\epsilon = 0.685$). Happel and Brenner (1965) present a review of theoretical and experimental values for k' for different configurations of flow through stacked cylinders, namely flow parallel to the cylinders, flow perpendicular to the cylinders and flow through randomly stacked cylinders. In general, for a porosity in excess of 0.8, the value of k' is larger than 5 and increases considerably with an increase in porosity. As previously noted, this phenomenon is attributed to a variation of the nature of the flow in the range of porosities larger than 0.8. For porosities less than 0.8, it is well admitted that the flow can be described as flow in capillary ducts. For materials with higher porosities and fibrous materials, a correct prediction of the viscous term of the pressure drop requires the flow to be considered as flow around objects, and thus to consider the frictional resistance of quasi-isolated particles. The value of the Kozeny constant obtained in this work is consistent with those reported in the literature, and further indicates that a capillary-type approach is not suitable for modelling the flow in the knitted wire.

3.8.7 Summary and conclusions

In the previous two sections a general predictive model for flow through anisotropic foams has been developed and also applied to predict the pressure gradient through an anisotropic multifilament knit. The basic model required the introduction of RUC's for two different types of foams which were referred to as foams of Type A and foams of Type B, respectively. The introduction of rectangular RUC's allowed quantification of interstitial fluid velocities through the description of tortuosity as a ratio of fluid volumes. Accurate quantification of the microscopic fluid-solid interaction resulted in a macroscopic momentum balance equation valid over both the Darcy and Forchheimer flow regimes. Since the pressure gradient equations are expressed in terms of macroscopic characteristics of the porous material, experimental pressure gradient

measurements are minimised and the model may be used predictively.

Pressure gradient measurements through a highly porous, anisotropic, multifilament knit were presented. These results are independent of a specific model and may thus be used to quantitatively test theoretical models describing flow through these types of porous media.

The design of a rectangular RUC configuration for the knit posed certain modelling difficulties in that the porous medium is cylindrical, anisotropic and consists of a twisted double wire. However, it was shown in which manner the basic model may be adjusted to account for these difficulties which also required the introduction of a physically more realistic drag coefficient for flow over the wires. As a first approximation the multifilament knit was modelled as being isotropic. It has been shown that this isotropic model gives a fairly accurate prediction for the inertial term, but under predicts the pressure drop in the Darcy regime by about 48%. The anisotropic model for laminar flow through the multifilament knit has been applied in a deterministic way and it required that the porosity, diameter of the solid strands and characteristic lengths of the porous plug be known. In this case, the pressure drop in the Darcy regime is under predicted by about 32%, while in the non-Darcy regime, the pressure gradient is over predicted by 6%. From the results obtained it would appear that the model may be applied successfully to a variety of flow configurations to obtain pressure gradients as well as additional structural information such as the total interstitial fluid-solid surface area.

It was also indicated that the model is sensitive to a correct evaluation of the circumferential characteristic length as well as to the diameter of solid bars in an RUC, but the predictions are fairly insensitive to the streamwise characteristic length. The results were also interpreted in terms of a capillary model and its limitations at high porosities were illustrated.

A complete analysis of flow through anisotropic foams has been developed for useful practical applications in terms of geometric characteristics of the material. Deterministic pressure gradient predictions may thus be obtained for various industrial applications of foamlike porous materials.

3.9 Flow through anisotropic granular porous media

3.9.1 Introduction

Granular materials are many-particle-systems of macroscopic constituents characterised by a large variety of shapes and sizes. They are important in many technological applications such as transport and stockage of powders for chemical engineering and food processing, in mining, pharmaceutical industries and soil mechanics. They also appear in geophysics in the form of geological formations, deserts and tectonic plates as well as in astrophysics, for example in asteroids and interstellar dust. Probably the most natural anisotropic granular materials appear in many types of sandstones which may have a layered structure in which the material matrix tends to be anisotropic towards a preferred direction (Pettijohn *et al.*, 1972). Important contributions have been made to the understanding of phenomena related to granular media such as avalanche statistics, force networks in packings, segregation and stratification, convection and heaping under vibration, sound propagation and dune formation. In these analyses modern tools are used from statistical mechanics similar to those applied to disordered systems, phase transitions, instabilities or intermitted behaviour and the performance of discrete particle simulations. Various experimental results and theoretical or semi-empirical models which are directed towards fluid transport, dispersion, electrical conduction and heat transfer through granular materials are presented by Carman (1956), Bear (1972), Scheidegger (1974), Dullien (1979) and Kaviany (1995), to name but a few. Studies on the behaviour of granular media and processes related to granular media are an active field of research with many practical applications.

The main objective of this section is to derive a deterministic expression relating the pressure gradient to the flow rate of Newtonian fluids through essentially anisotropic granular porous media. From the previous examples it is evident that the most distinctive feature of granular materials is an unconsolidated solid matrix where the solid material is non-connected and individual granules may be identified. However, in certain types of sandstones the granules may be cemented together to form a consolidated structure (Rice *et al.*, 1970) and in the present classification system these materials are also considered as granular, since grains may be identified, although it is acknowledged that they may fall in a grey area.

The fluid transport process is assessed by referring to the volume averaged Navier-Stokes equations. The fluid-solid surface integral terms appearing as a result of the volumetric

averaging in the momentum transport equations may be treated analytically through the introduction of a particular pore-scale model, namely the RUC model discussed in Section 3.5. Therefore, in this section an RUC for idealised anisotropic granular porous media is introduced and a closure scheme is presented to obtain macroscopic momentum transport equations for flow through these types of materials. In the previous section RUC's for idealised anisotropic foamlike materials have been presented and used to close the open averaged momentum transport equations. However, an important distinction between foamlike materials and granular media is that in granular materials individual granules may be identified and the strandlike structure of the foams is absent. It is considered that the flow characteristics may differ between these two types of materials and that the RUC's introduced in the previous section are not applicable to granular materials and RUC's characteristic to anisotropic granular materials should be introduced.

The format of this section is similar to that of Section 3.7 where a closure scheme for flow through anisotropic foamline materials is presented. Firstly, the governing momentum transport equations are presented whereafter an RUC for a particular type of anisotropic granular material is introduced. Various geometric relations and velocity approximations within the RUC are presented whereafter the RUC is used to produce a closure scheme for the governing fluid transport equations. The problem of flow of Newtonian fluids through isotropic granular materials has been addressed by Du Plessis (1991; 1994) and applied to various types of isotropic flow problems (Du Plessis and Roos, 1994; Du Plessis and Roos, 1995). The present analysis extends the previous modelling to include anisotropic materials and also illustrate in a applicatory manner the importance of a pore-scale model combined with the channel average velocity and tortuosity introduced in Chapter 2.

3.9.2 Macroscopic fluid transport equations

The macroscopic continuity equation (3.19) and momentum equations (3.26) derived in Section 3.4.3 apply to any homogeneous porous medium. These equations, therefore, also govern the flow of Newtonian fluids through anisotropic homogeneous granular materials. Furthermore, the closure problem is also considered in the context of the RUC model and, therefore, the transport of a time-independent incompressible Newtonian fluid flowing in the x_1-direction is governed by (3.43), given here again for ease of reference

$$\epsilon U_o P_{,1} = \iint_{S_{fs}} (\mu v_{1,j} \nu_j - \mathring{p} \nu_1) dS. \tag{3.117}$$

This is the equation on which attention is focussed. However, the configuration of the fluid-solid surface and flow pattern through foamlike and granular media are considered to be different and necessitates the introduction of RUC's particular to each type of material.

3.9.3 Modelling of the porous medium microstructure

Since the characteristic feature of granular media is an unconsolidated solid phase, the original Representative Unit Cell (RUC) of Du Plessis (1991) for isotropic granular porous media consisted of a single cube of solid material centrally within a cubic RUC. The flow characteristics in an ensemble of RUC's were considered to be equal in all three macroscopic directions which allowed the RUC to be aligned with the macroscopic flow direction. These ideas are presently extended to idealised anisotropic granular materials which consist of granular grains or particles which may have different physical dimensions in different directions and consequently giving rise to directional preferences for fluid transport. The corresponding RUC's are, therefore, not cubic but rectangular. Initially, the assumption that an RUC may be aligned with the macroscopic flow direction is retained.

An RUC for anisotropic granular porous media is illustrated in Figure 3.14 and consists of a right-angled parallellepipedum. Although other types of RUC's are also possible, such as skewed parallellepipedums, attention is restricted to right angles only. Centrally within the RUC there is a block of solid material aligned with the sides of the RUC and which is also considered to be a right-angled parallellepipedum. A coordinate system attached to the RUC is also presented and the RUC is aligned with the macroscopic flow which in the present case is selected as the x_1-direction. The fluid volume in the RUC is given by

$$U_f = \epsilon U_o = \epsilon d_{(1)} d_{(2)} d_{(3)} \tag{3.118}$$

where $d_{(1)}$, $d_{(2)}$ and $d_{(3)}$ are the respective linear dimensions of the RUC and ϵ is the porosity of the material. The solid phase is

$$U_s = d_{s(1)} d_{s(2)} d_{s(3)} = (1-\epsilon) U_o, \tag{3.119}$$

where $d_{s(1)}$, $d_{s(2)}$ and $d_{s(3)}$ are the respective linear dimensions of the solid material within the RUC.

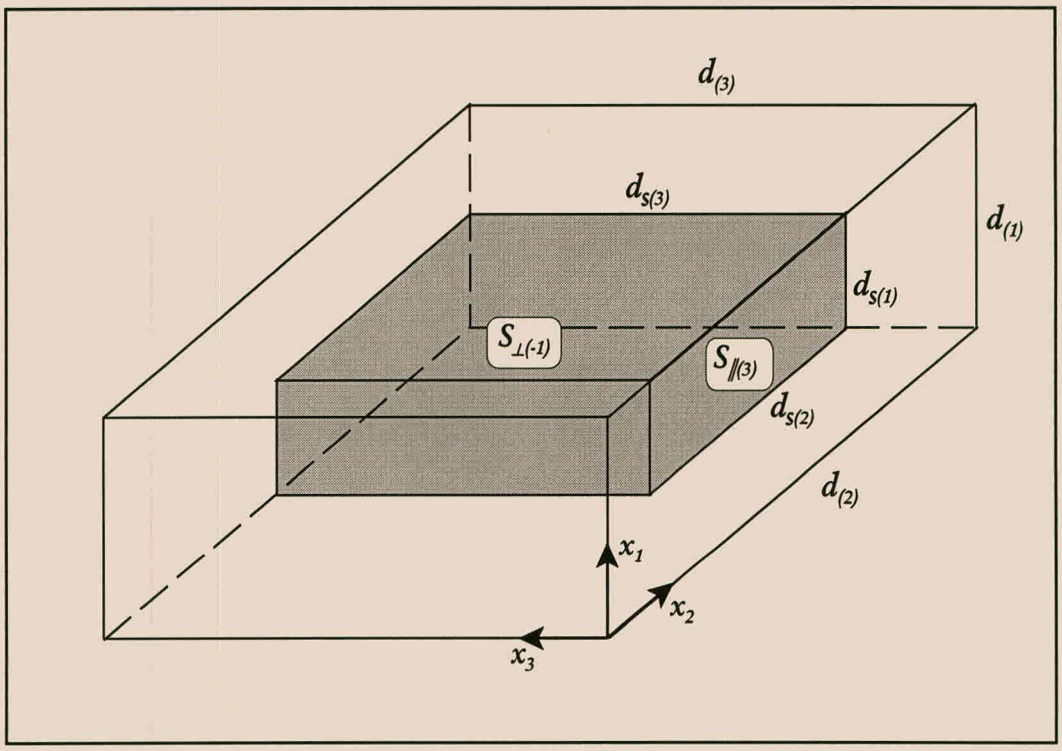

Figure 3.14. A right-handed parallellepipedal RUC for anisotropic granular porous media which contains a block of solid material centrally within the fluid volume of the RUC.

It is once again viewed that

- the channel sections in the RUC within which flow occurs are equivalent to sections of parallel plates which are formed by the solid cube in the RUC under consideration and those of neighbouring RUC's.

To envisage the channel sections it is necessary to conceptually take into account the positioning of neighbouring RUC's. For simplicity the respective parallel plate sections are referred to by the direction of the outwardly directed normal vector on each plate and their orientation with respect to the streamwise direction. For example, the surface section with a positive normal vector of ν_3 and which forms part of a channel section which conducts flow parallel to the macroscopic flow direction (or streamwise direction) is denoted by $S_{\|(3)}$. The normal vectors on fluid-solid surfaces have been defined to be positive when pointing out of the fluid-phase into the solid. Two surface sections, namely $S_{\|(3)}$ and $S_{\perp(-1)}$ are illustrated in Figure 3.14.

According to this approach, the RUC in Figure 3.14 exhibits 'four' channel sections for

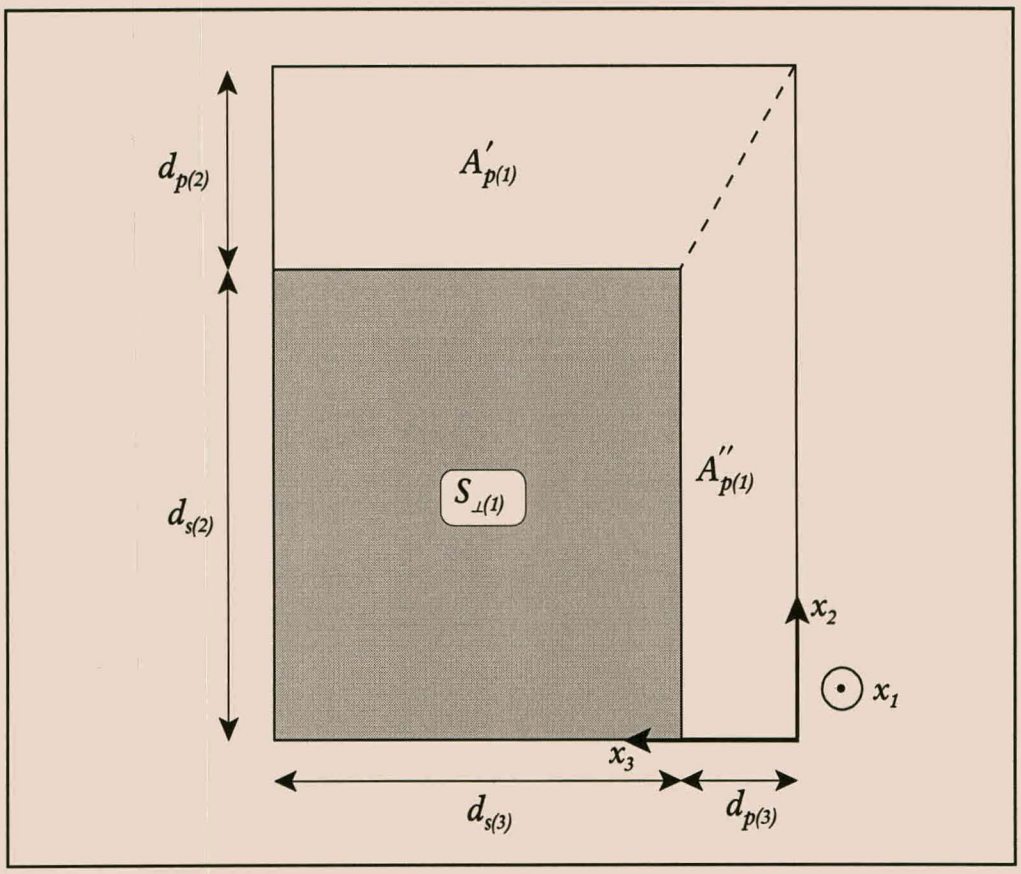

Figure 3.15. A top view of an RUC where the solid material has been moved to one corner to show the two streamwise channel areas more clearly.

streamwise flow in the x_1-direction. These are actually half channels since the corresponding parallel plates completing the channel sections are situated in neighbouring RUC's. Since the boundaries of an RUC intersect the channel sections it is allowed, for ease of reference, to move the solid material in the RUC in the x_2x_3-plane into a corner as shown in Figure 3.15. This then yields two different sets of parallel plates which conduct streamwise flow in the x_1-direction. This conceptual rearrangement of the solid constituent does not alter any of the geometric characteristics formerly derived for the RUC. The different streamwise channel sections, formed by the different sets of parallel plates, have different dimensions, since the solid surface areas differ and, more importantly, the spacing between the plates are different. For a uniform streamwise pressure gradient across the RUC, the flow speeds in these two streamwise channels are different. If it is assumed that

- the intersection between the two channels is divided equally between the channels

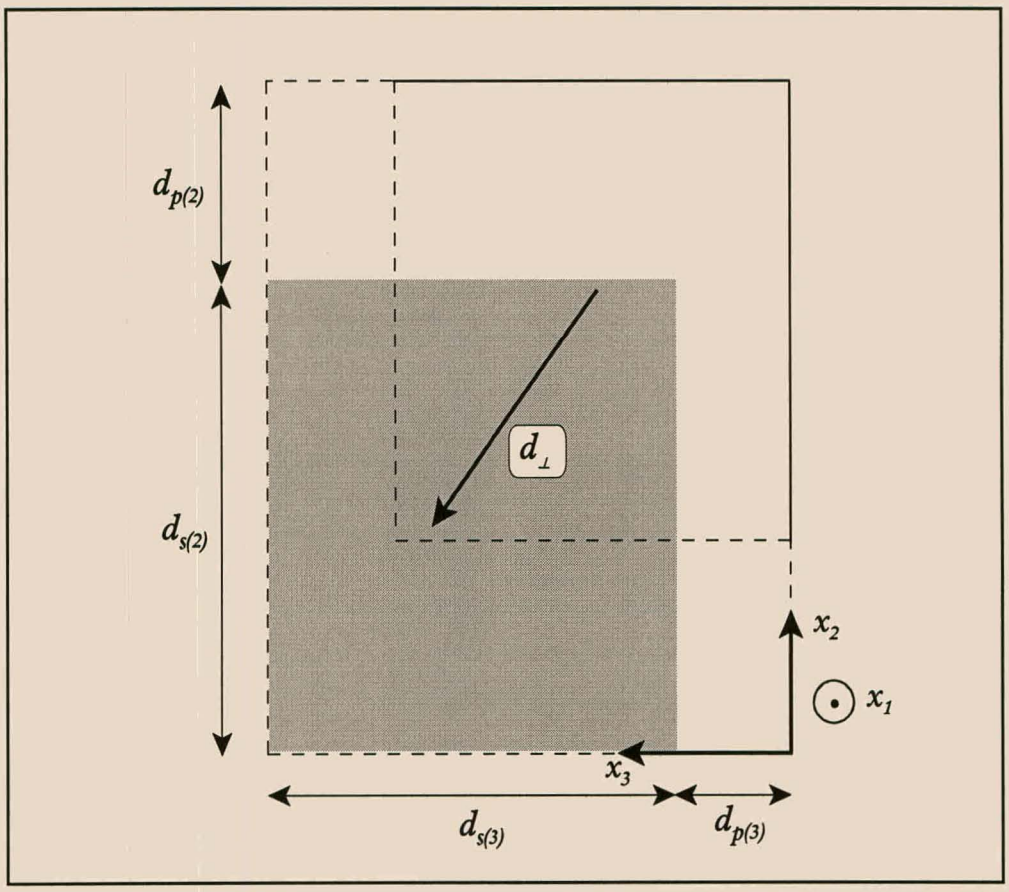

Figure 3.16. A top view of an RUC where the solid material has been moved to one corner to show the entrance pore area (white space) end exit pore area (surrounded by dashed lines).

then the cross-sectional areas of these two channel sections are given by

$$A'_{p(1)} = d_{p(2)}d_{s(3)} + \frac{1}{2}d_{p(3)}d_{p(2)} \tag{3.120}$$

and

$$A''_{p(1)} = d_{p(3)}d_{s(2)} + \frac{1}{2}d_{p(3)}d_{p(2)} \tag{3.121}$$

respectively. As shown in Figure 3.15, this yields a total effective cross-sectional area, $A_{p(1)}$, of

$$A_{p(1)} = d_{(2)}d_{(3)} - d_{s(2)}d_{s(3)}. \tag{3.122}$$

The length of the streamwise extent of the flow is equal to $d_{(1)}$. The effective streamwise

volume available for fluid transport in the streamwise direction is given, with the x_1-coordinate as the streamwise direction, by

$$U_{f\mathcal{L}(1)} = A_{p(1)}d_{(1)}. \tag{3.123}$$

In the RUC's for foamlike materials two transverse channels which are perpendicular to each other and perpendicular to the streamwise direction are clearly visible. However, this is not the case for the granular RUC and a single transverse channel section with an arbitrary direction in the x_2x_3-plane is considered to be formed between the surface perpendicular to the streamwise direction ($S_{\perp(-1)}$) within the RUC under consideration and the corresponding surface in a neighbouring RUC. Therefore, for the RUC in Figure 3.14, the fluid which moves through the streamwise channels will flow between the $S_{\perp(-1)}$ and $S_{\perp(1)}$ surfaces to form a transverse channel. This viewpoint may be illustrated by considering the two-dimensional cross-section of an RUC in Figure 3.16 in which the fluid which flow through the RUC in the x_1-direction has reached the streamwise extent of the RUC in the streamwise channel sections to the right and below the solid material. The fluid then moves across the solid to exit in the streamwise direction through an opening illustrated by the dashed lines in Figure 3.16. According to this approach it is assumed that

- the average transverse channel length, $d_\perp$, is equal to the distance which the centroid of the fluid within the RUC moves transversally across $S_{\perp(-1)}$

and it is given by

$$d_\perp = \sqrt{\frac{d_{s(2)}^2 d_{s(3)}^2 \left((d_{(2)} - d_{s(2)})^2 + (d_{(3)} - d_{s(3)})^2\right)}{(d_{(2)}d_{(3)} - d_{s(2)}d_{s(3)})^2}}. \tag{3.124}$$

The different velocities in the streamwise channel sections will also influence the manner in which the fluid moves transversally across $S_{\perp(-1)}$ and the translation of the centroid may be weighted towards the larger of the two velocities. However, the extent to which these velocities influence the translation is neglected. Furthermore, the flow in the transverse channel is not necessarily parallel to any of the selected coordinate directions.

The transverse channel area, $A_\perp$ may be calculated from the following expression for the fluid volume, namely

$$A_{p(1)}d_{(1)} + A_\perp d_\perp = U_f. \tag{3.125}$$

By making use (3.124) and (3.125) it then follows that

$$A_{\perp} = \frac{(d_{(2)}d_{(3)} - d_{s(2)}d_{s(3)})(U_f - A_{p(1)}d_{(1)})}{d_{s(2)}d_{s(3)}\sqrt{(d_{(2)} - d_{s(2)})^2 + (d_{(3)} - d_{s(3)})^2}}$$

$$= \frac{A_{p(1)}(d_{(1)}d_{s(3)} - d_{s(1)}d_{s(3)})}{d_{s(3)}\sqrt{(d_{(2)} - d_{s(2)})^2 + (d_{(3)} - d_{s(3)})^2}}. \tag{3.126}$$

According to the definition of the tortuosity introduced in Section 2.6.9, the tortuosity component in the x_1-direction is given by

$$\chi_{11} = \frac{U_f}{U_{f\mathcal{L}(1)}} = \frac{U_f}{A_{p(1)}d_{(1)}} \tag{3.127}$$

and, unfortunately, (3.127) cannot be further factorised to obtain a unique relation between the tortuosity and porosity as in the case of isotropic granular media. The discussion of the geometric characteristics is concluded by the total fluid-solid surface area in the RUC which is given by

$$S_{fs} = 2d_{s(2)}d_{s(3)} + 4d_{s(1)}d_{s(2)}. \tag{3.128}$$

Similar geometric features and flow patterns may be determined should the macroscopic flow be along any of the other RUC-coordinate directions.

3.9.4 Velocity relationships

As previously mentioned, there are two sets of parallel plates with differing spacial distances between the plates in which the fluid flows in the streamwise direction through the RUC. According to the analysis of plane Poiseuille flow between two parallel plates, due to a constant pressure gradient of $-\Pi\,\widehat{\nu}_1(\Pi > 0)$ which includes the contribution from gravity (Whitaker, 1968), the average flow speed in each of these sets are

$$w_1' = \frac{d_{p(2)}^2}{12\mu}\Pi \tag{3.129}$$

and

$$w_1'' = \frac{d_{p(3)}^2}{12\mu}\Pi \tag{3.130}$$

respectively. Therefore, the average flow speed between each of the sets of parallel plates will differ, since equal pressure gradients apply to each set.

In addition to these two velocities, it is also necessary to take into account the streamwise channel average velocity defined for a general porous medium in (3.11). Since the definition of the effective streamwise volume, $U_{f\mathcal{L}(1)}$ does not distinguish between differing streamwise velocities, the single streamwise channel average velocity within the RUC is given by

$$\widehat{w}_1 = \frac{1}{U_{f\mathcal{L}(1)}} \iiint_{U_f} v_1 \, dU \tag{3.131}$$

which exists in each channel section. The importance of the channel average velocity lies in the relationship

$$q_1 = \epsilon u_1 = \frac{\epsilon \widehat{w}_1}{\chi_{11}} \tag{3.132}$$

where it is related to the superficial velocity and which is applicable to porous media in general.

It is, therefore, beneficial to relate the average velocity in each streamwise channel, $w_1^{'}$ and $w_1^{''}$ to the streamwise channel average velocity, $\widehat{w}_1$, in order to obtain a relation with the superficial velocity. This is achieved by considering the volumetric flow rate through these two channels which is given by

$$\begin{aligned} Q_1 &= A_{p(1)} \widehat{w}_1 \\ &= w_1^{'} A_{p(1)}^{'} + w_1^{''} A_{p(1)}^{''} \\ &= \frac{d_{p(2)}^2 A_{p(1)}^{'}}{12\mu} \Pi + \frac{d_{p(3)}^2 A_{p(1)}^{''}}{12\mu} \Pi \end{aligned} \tag{3.133}$$

where the areas $A_{p(1)}^{'}$ and $A_{p(1)}^{''}$ are the respective cross-sectional areas of the two channel sections as illustrated in Figure 3.15. From (3.133) it follows that the constant pressure gradient is

$$\Pi = \frac{12\mu A_{p(1)} \widehat{w}_1}{d_{p(2)}^2 A_{p(1)}^{'} + d_{p(3)}^2 A_{p(1)}^{''}}. \tag{3.134}$$

Using this expression with (3.129) and (3.130) it follows that

$$w_1' = \left(\frac{d_{p(2)}^2 A_{p(1)}}{d_{p(2)}^2 A_{p(1)}' + d_{p(3)}^2 A_{p(1)}''} \right) \widehat{w}_1 \tag{3.135}$$

and

$$w_1'' = \left(\frac{d_{p(3)}^2 A_{p(1)}}{d_{p(2)}^2 A_{p(1)}' + d_{p(3)}^2 A_{p(1)}''} \right) \widehat{w}_1, \tag{3.136}$$

respectively. From these expressions it is evident that should the size of any one of the channels becomes zero the velocity in the channel will also become zero and all the fluid will move through the remaining channel.

Besides the streamwise flow, it is also necessary to quantify the transverse flow perpendicular to the macroscopic flow direction. The average flow *speed* in the transverse channel, $v_\perp$, may be obtained from a mass balance over the RUC which yields

$$Q_1 = \widehat{w}_1 A_{p(1)} = v_\perp A_\perp \tag{3.137}$$

and according to (3.122) and (3.124) it follows that

$$v_\perp = \frac{A_{p(1)} \widehat{w}_1}{A_\perp} = \left(\frac{\sqrt{(d_{(2)} - d_{s(2)})^2 + (d_{(3)} - d_{s(3)})^2}}{(d_{(1)} - d_{s(1)})} \right) \widehat{w}_1. \tag{3.138}$$

This relationship between the magnitudes of the channel average velocity and transverse velocity may be rewritten as

$$v_\perp = \beta_{(1)} \widehat{w}_1 \tag{3.139}$$

where

$$\beta_{(1)} = \frac{A_{p(1)}}{A_\perp} = \frac{\sqrt{(d_{(2)} - d_{s(2)})^2 + (d_{(3)} - d_{s(3)})^2}}{(d_{(1)} - d_{s(1)})}. \tag{3.140}$$

These velocity relationships and geometric characteristics are subsequently used in the closure scheme for the fluid-solid surface integral in (3.117).

3.9.5 Modelling of the interstitial fluid-solid interaction

The macroscopic flow is considered in two different laminar flow regions, namely the Darcy regime at low Reynolds numbers and the Forchheimer regime at intermediate Reynolds numbers. The Reynolds number on which the distinction is based is the same as that defined in Section 3.7.2 and given in (3.50). In the Darcy regime the Reynolds number is fairly small and striving towards the lower limit of zero while in the Forchheimer regime the Reynolds number tends towards an upper limit of about 100. The flow is laminar at all times and do not enter the turbulent regime.

3.9.5.1 Low Reynolds number flow limit

In the low Reynolds number flow limit it is assumed that viscous drag predominates resulting in creeping flow without flow separation within the RUC. With the macroscopic flow in the x_1-direction, the shear stress terms $\iint_{S_{fs}} \mu v_{1,j}\nu_j dS$ only exist in the streamwise channels which have a total fluid-solid surface area of $2(S_{\|(2)} + S_{\|(3)})$. On the other hand, the pressure deviation term, $\iint_{S_{fs}} \overset{\circ}{p}\nu_1 dS$, yields a local pressure gradient along the transverse channel and, according to a balance of forces in this channel, this pressure force is equal to the viscous resistance within the transverse channel. The contribution of the pressure deviation to the surface integral may thus be incorporated by integrating the wall shear stress over the total fluid-solid interface S_{fs} instead of only over the streamwise part given by $2(S_{\|(2)} + S_{\|(3)})$. Accordingly, it therefore follows that

$$\begin{aligned}
\epsilon U_o P_{,1} &= \iint_{S_{fs}} (\mu v_{1,j}\nu_j - \overset{\circ}{p}\nu_1)\, dS \\
&= 2\iint_{S_{\|(2)}} \mu v_{1,2}\nu_2\, dS + 2\iint_{S_{\|(3)}} \mu v_{1,3}\nu_3\, dS - 2\iint_{S_{\perp(1)}} \overset{\circ}{p}\nu_1\, dS \\
&= 2\iint_{S_{\|(2)}} \mu v_{1,2}\nu_2\, dS + 2\iint_{S_{\|(3)}} \mu v_{1,3}\nu_3\, dS - 2\iint_{S_{\perp(1)}} \tau_\perp \nu_1 dS
\end{aligned} \tag{3.141}$$

where $\tau_\perp$ is the shear stress in the transverse channel. The normal velocity gradients on the fluid-solid surfaces in the different channels are also given by (3.55) and the shear stress in the transverse channel is equivalently given by

$$\tau_\perp = -\frac{6\mu v_\perp}{d_{p(1)}}. \tag{3.142}$$

By using (3.55), (3.142), the various velocity relations and (3.127), (3.141) may be written as

$$
\begin{aligned}
P_{,1} &= -\frac{12\mu}{\epsilon U_o}\left(\frac{w_1^{'}S_{\|(2)}}{d_{p(2)}} + \frac{w_1^{''}S_{\|(3)}}{d_{p(3)}} + \frac{v_\perp S_{\perp(1)}\nu_1}{d_{p(1)}}\right) \\
&= -\frac{12\mu}{\epsilon U_o}\left(\left(\frac{d_{p(2)}^2 A_{p(1)}}{d_{p(2)}^2 A_{p(1)}^{'} + d_{p(3)}^2 A_{p(1)}^{''}}\right)\frac{\widehat{w}_1 S_{\|(2)}}{d_{p(2)}}\right. \\
&\quad \left. + \left(\frac{d_{p(3)}^2 A_{p(1)}}{d_{p(2)}^2 A_{p(1)}^{'} + d_{p(3)}^2 A_{p(1)}^{''}}\right)\frac{\widehat{w}_1 S_{\|(3)}}{d_{p(3)}} + \frac{\beta_{(1)}\widehat{w}_1 S_{\perp(1)}}{d_{p(1)}}\right) \\
&= -\frac{12\mu\chi_{11}q_1}{\epsilon^2 U_o}\left(\left(\frac{d_{p(2)}A_{p(1)}d_{s(3)}d_{s(1)}}{d_{p(2)}^2 A_{p(1)}^{'} + d_{p(3)}^2 A_{p(1)}^{''}}\right) + \left(\frac{d_{p(3)}A_{p(1)}d_{s(2)}d_{s(1)}}{d_{p(2)}^2 A_{p(1)}^{'} + d_{p(3)}^2 A_{p(1)}^{''}}\right)\right. \\
&\quad \left. + \frac{\beta_{(1)}d_{s(2)}d_{s(3)}}{d_{p(1)}}\right), \qquad (3.143)
\end{aligned}
$$

where $\beta_{(1)}$ is given by (3.140), $A_{p(1)}$ is expressed by (3.122) while $A_{p(1)}^{'}$ and $A_{p(1)}^{''}$ are given by (3.119) and (3.121), respectively. Equation (3.143) is the final form for the surface integral term at low Reynolds numbers. However, when considering practical flow problems, further manipulation may be required depending on the available information.

3.9.5.2 Shear friction tensor

A shear friction tensor in the form of (3.69) may be defined for multi-directional flow through the RUC. Under such a flow condition, the streamwise direction is not aligned with any of the RUC-coordinates. Since the pressure loss is linearly related to the superficial velocity, the flow along each material direction may be analysed individually. Therefore,

$$
\begin{aligned}
F_{11} &= -\frac{12\mu\chi_{11}}{\epsilon^2 U_o}\left(\left(\frac{d_{p(2)}A_{p(1)}d_{s(3)}d_{s(1)}}{d_{p(2)}^2 A_{p(1)}^{'} + d_{p(3)}^2 A_{p(1)}^{''}}\right) + \left(\frac{d_{p(3)}A_{p(1)}d_{s(2)}d_{s(1)}}{d_{p(2)}^2 A_{p(1)}^{'} + d_{p(3)}^2 A_{p(1)}^{''}}\right)\right. \\
&\quad \left. + \frac{\beta_{(1)}d_{s(2)}d_{s(3)}}{d_{p(1)}}\right) \qquad (3.144)
\end{aligned}
$$

and by also conducting the previous analysis for the other two flow directions, it follows that

$$F_{22} = -\frac{12\mu\chi_{22}}{\epsilon^2 U_o}\left(\left(\frac{d_{p(3)}A_{p(2)}d_{s(1)}d_{s(2)}}{d^2_{p(3)}A'_{p(2)} + d^2_{p(1)}A''_{p(2)}}\right) + \left(\frac{d_{p(1)}A_{p(2)}d_{s(3)}d_{s(2)}}{d^2_{p(3)}A'_{p(2)} + d^2_{p(1)}A''_{p(2)}}\right) + \frac{\beta_{(2)}d_{s(3)}d_{s(1)}}{d_{p(2)}}\right) \tag{3.145}$$

where

$$A'_{p(2)} = d_{p(3)}d_{s(1)} + \frac{1}{2}d_{p(1)}d_{p(2)}$$
$$A''_{p(2)} = d_{p(1)}d_{s(3)} + \frac{1}{2}d_{p(1)}d_{p(3)}$$

and

$$\beta_{(2)} = \frac{\sqrt{(d_{(3)} - d_{s(3)})^2 + (d_{(1)} - d_{s(1)})^2}}{(d_{(2)} - d_{s(2)})}. \tag{3.146}$$

Similarly, the remaining diagonal component is given by

$$F_{33} = -\frac{12\mu\chi_{33}}{\epsilon^2 U_o}\left(\left(\frac{d_{p(1)}A_{p(3)}d_{s(3)}d_{s(3)}}{d^2_{p(1)}A'_{p(3)} + d^2_{p(2)}A''_{p(3)}}\right) + \left(\frac{d_{p(2)}A_{p(3)}d_{s(1)}d_{s(3)}}{d^2_{p(1)}A'_{p(3)} + d^2_{p(2)}A''_{p(3)}}\right) + \frac{\beta_{(3)}d_{s(1)}d_{s(2)}}{d_{p(3)}}\right) \tag{3.147}$$

with

$$A'_{p(3)} = d_{p(1)}d_{s(2)} + \frac{1}{2}d_{p(2)}d_{p(3)}$$
$$A''_{p(3)} = d_{p(2)}d_{s(1)} + \frac{1}{2}d_{p(2)}d_{p(1)}$$

and

$$\beta_{(3)} = \frac{\sqrt{(d_{(1)} - d_{s(1)})^2 + (d_{(2)} - d_{s(2)})^2}}{(d_{(3)} - d_{s(3)})}. \tag{3.148}$$

The fact that the shear friction tensor is diagonal follows from the assumption that the RUC is aligned with the principal axes of the permeability and the rectangular arrangement of the duct sections within the RUC.

3.9.5.3 Flow at intermediate Reynolds numbers

In many practical applications of flow through porous media the flow is not restricted to the Darcy regime but the flow rate may increase to intermediate Reynolds numbers and the flow then enters the so-called Forchheimer regime where the fluid velocity and pressure gradient are not linearly related (Bear, 1972). It is assumed, for flow at intermediate Reynolds numbers, that inertial resistance predominates over the effect of viscous forces (Ruth and Ma, 1992). This implies that the viscous contributions to the surface integral in (3.117) may be neglected.

Locally within an RUC the flow is considered to circulate symmetrically around the solid material and, due to inertial effects, eventually separates from the solid material at the downstream side as schematically illustrated in Figure 3.9. A recirculation zone may form on the downstream side of the solid material and the pressure in this area remains similar to that at the separation point (indicated by b in Figure 3.9) (Franzini and Finnemore, 1997). Since this pressure is always less than the pressure at the forward stagnation point, there results a net pressure difference tending to move the body with the flow, and this force is equal to the rate of momentum loss by the fluid. In the previous section where the flow through anisotropic foams was considered, this process was modelled equivalent to form drag across the solid constituent in the RUC. In this section, the pressure loss is analysed in more detail and alternative modelling approaches are discussed. Therefore, under the assumptions that

- viscous effects may be neglected,
- that the dominant inertial effects cause a recirculation zone downstream of the solid material
- and that the flow circulates symmetrically around the solid such that the pressure forces on opposing streamwise surfaces cancel out,

the fluid solid surface integral in (3.117) may be written as

$$\begin{aligned}
\epsilon U_o P_{,1} &= \iint_{S_{fs}} (\mu v_{1,j}\nu_j - \overset{o}{p}\nu_1)\, dS \\
&= -\iint_{S_{fs}} \overset{o}{p}\nu_1\, dS \\
&= -\iint_{S_{\perp(1)}} p\nu_1\, dS + \iint_{S_{\perp(1)}} \langle p\rangle^f \nu_1\, dS - \iint_{S_{\perp(-1)}} p\nu_1\, dS \\
&\quad + \iint_{S_{\perp(-1)}} \langle p\rangle^f \nu_1\, dS \\
&= -\iint_{S_{\perp(1)}} p\nu_1\, dS + \langle p\rangle^f S_{\perp(1)} - \iint_{S_{\perp(-1)}} p\nu_1\, dS - \langle p\rangle^f S_{\perp(-1)} \\
&= -\iint_{S_{\perp(1)}} p\nu_1\, dS - \iint_{S_{\perp(-1)}} p\nu_1\, dS. \qquad (3.149)
\end{aligned}$$

Here $\langle p\rangle^f$ is the interstitial phase average pressure related to the pressure deviation by (2.27). Since the interstitial phase average is a well-behaved function (as discussed in Section 2.3.1), the interstitial phase average pressures in the surface integrals are equal to the pressure at the centroid of an REV, and hence an RUC. The terms containing $\langle p\rangle^f$ therefore cancel out in the calculation above.

The next step is to obtain a quantification of the pressure difference on the opposing solid surfaces perpendicular to the streamwise direction. The dividing streamline which separates the recirculation zone from the bulk flow has a stagnation point on $S_{\perp(1)}$ as indicated by point a in Figure 3.9. This streamline also has an inflection point downstream of the solid at point c in Figure 3.9. If it is viewed that,

- on average, the pressure on the upstream side of the solid is uniform across the surface $(S_{\perp(1)})$ and equal to the value, p_a, at the stagnation point

then

$$\iint_{S_{\perp(1)}} p\nu_1\, dS = p_a S_{\perp(1)}\nu_1. \qquad (3.150)$$

Following Du Plessis (1994), the pressure on the downstream surface $(S_{\perp(-1)})$ may be obtained by applying the Bernoulli equation along the dividing streamline from the stagnation point on $S_{\perp(1)}$ to the inflection point of the streamline adjacent to the region of flow recirculation downstream of the solid. This yields

$$\frac{1}{2}\rho v_j^a v_j^a + \Omega^a + p_a = \frac{1}{2}\rho v_j^c v_j^c + \Omega^c + p_c \qquad (3.151)$$

where v_j^a and v_j^c are the respective fluid velocities on the streamline at points a and c as shown in Figure 3.9, p_a and p_c are the local pressures at points a and c, respectively and the Ω's are potential functions related to the body forces acting on the fluid (Whitaker, 1968). The assumptions which lead to this form of the Bernoulli equation are that the flow must be time-independent and non-viscous while the body forces which act on the fluid must be conservative and in the present case these are assumed to be solely due to the effect of gravity. These assumptions are the same as those governing the flow at intermediate Reynolds numbers. For a conservative external force, f_i^b acting on the fluid, the potential functions in (3.151) is equivalent to

$$f_i^b = -\Omega_{,i} \tag{3.152}$$

and for horizontal flow $\Omega^a = \Omega^c$ since the body forces are uniform at all points on the streamline. However, if the flow is not horizontal the two potential functions will differ from the horizontal case by values proportional to the distance from the horizontal datum level. However, similar changes will also be induced in the pressure terms which implies that the potential terms may be cancelled and the pressures in (3.151) then represent the local pressures at a and c which is due to the flow only. Furthermore, since the fluid is stationary at the stagnation point, $v_j^a = 0$ and (3.151) then yields

$$p_a = \frac{1}{2}\rho v_j^c v_j^c + p_c. \tag{3.153}$$

The reason for selecting the streamline through the inflection point is that at this point the pressure within the recirculation zone is equal to that on the opposite side of the streamline, and thus also equal to the pressure on the streamline. If it is furthermore assumed that

- the downstream pressure is uniformly distributed over the solid

then

$$\begin{aligned} \iint_{S_{\perp(-1)}} p\,\nu_1\,dS &= -p_c S_{\perp(-1)}\nu_1 \\ &= \left(\frac{1}{2}\rho v_j^c v_j^c - p_a\right) S_{\perp(-1)}\nu_1. \end{aligned} \tag{3.154}$$

A combination of (3.150) and (3.154) with (3.149) then yields

$$\epsilon U_o P_{,1} = -\frac{1}{2}\rho v_j^c v_j^c S_{\perp(-1)}\nu_1. \tag{3.155}$$

However, the velocity at the inflection point, v_j^c, is still unknown and a modelling choice has to be made here which involves an approximation of this velocity. Since the inflection point occurs downstream of the solid material and not directly in a streamwise channel, the magnitude of v_j^c may be nearly equal to $v_\perp$. In addition, the recirculation zone effectively diminishes the cross-sectional pore area and so increases the velocity such that it may be assumed that

- an appropriate asymptotic value for the magnitude of v_j^c is given by

$$v^c \approx v_\perp = \beta_{(1)}\widehat{w}_1. \tag{3.156}$$

A similar assumption was also introduced by Du Plessis (1994). Equation (3.155) thus becomes

$$\begin{aligned} \epsilon U_o P_{,1} &= -\left(\frac{\rho d_{s(2)} d_{s(3)}}{2}\right) v_\perp^2 \nu_1 \\ &= -\left(\frac{\rho d_{s(2)} d_{s(3)}}{2}\right) \beta^2 \widehat{w}\widehat{w}_1 \nu_1 \\ &= -\frac{\rho \beta_{(1)}^2 \chi_{11}^2 d_{s(2)} d_{s(3)} q q_1}{2\epsilon^2} \end{aligned} \tag{3.157}$$

which describes the pressure gradient at intermediate Reynolds numbers.

However, it may be worth exploring an alternative and possibly less complicated approximation for the pressure force. The recirculation and corresponding momentum loss is effectively a pressure drag process and (3.155) has the form of a pressure drag representation, namely a product between $\frac{\rho}{2}$, a square velocity and the area perpendicular to the mean flow. In general, the pressure drag is related to the square of a free stream velocity, v_∞, from which it then follows that

$$\begin{aligned} \epsilon U_o P_{,1} &= -\iint_{S_{fs}} \overset{o}{p} \nu_1 \, dS \\ &= -\frac{1}{2}\rho c_d v_\infty^2 S_{\perp(1)} \nu_1. \end{aligned} \tag{3.158}$$

Here $\frac{1}{2}\rho v_\infty^2$ is a kinetic energy term appearing in the definition of the drag force while c_d is the drag coefficient or friction factor. Different values for the friction factor may be selected, depending on the shape of the solid material within the RUC.

In the case of flow through porous media a free stream velocity is not clearly evident and there are two possible choices for the velocity appearing in (3.158).

1. In an RUC the streamwise channel average velocity may be selected as the free stream velocity, that is $v_\infty \approx \hat{w}$, since the flow approaches the solid material interstitially with this velocity. It then follows that (3.158) becomes

$$\begin{aligned} \epsilon U_o P_{,1} &= -\frac{1}{2}\rho c_d w_1^2 S_{\perp(1)} \nu_1 \\ &= -\frac{\rho \chi_{11}^2 c_d d_{s(2)} d_{s(3)} q q_1}{2\epsilon^2}. \end{aligned} \tag{3.159}$$

2. The free stream velocity may also be approximated by $v_\perp$ and in this case it follows that

$$\begin{aligned} \epsilon U_o P_{,1} &= -\frac{1}{2}\rho c_d v_\perp^2 S_{\perp(1)} \nu_1 \\ &= -\frac{\rho \beta_{(1)}^2 \chi_{11}^2 c_d d_{s(2)} d_{s(3)} q q_1}{2\epsilon^2}. \end{aligned} \tag{3.160}$$

There are effectively three different models for intermediate Reynolds number flow which are expressed by (3.157), (3.159) and (3.160), respectively. These models differ with regard to the appearance of c_d and $\beta_{(1)}$ in the final expressions. The advantage of (3.157) is that it only contains the $\beta_{(1)}$-factor, which may be determined from the geometry of the RUC according to (3.140). This elimitates the introduction of an additional parameter into the model. Equations (3.157) and (3.159) may be considered to be equivalent if c_d and $\beta_{(1)}^2$ play equivalent roles in these equations, namely to serve as approximation coefficients for the velocity around the solid structure. For the modelling of foams a form drag model equivalent to (3.159) seemed more appropriate, since it allowed the drag coefficient to be adapted to account for a solid constituent which deviated substantially from a square bar. Equation (3.160) is not suitable as it contains both c_d and $\beta_{(1)}$ and can only be similar to (3.157) if these coefficients are both equal to unity.

3.9.6 General momentum transport equation

3.9.6.1 Anisotropic granular porous media

When the two respective laminar limits are plotted logarithmically against the Reynolds number two asymptotes are obtained. As shown by Du Plessis (1994) and summarised by Du Plessis and Diedericks (1997), the asymptotic matching technique of Churchill and Usagi (1972) may be used with a shifting parameter of one to obtain a general momentum equation valid over both the Darcy and Forchheimer regimes by simply adding

the two different contributions. Therefore, a general momentum transport equation in the form of (3.6),

$$-\frac{1}{q}P_{,1} = Mq_1 + N \tag{3.161}$$

valid over both the Darcy and Forchheimer regimes may be obtained for anisotropic granular materials. Here N is given by (3.143) and, except for the ϵU_o factor, M is represented by either one of (3.157), (3.159) or (3.160). This implies that

$$N = \frac{12\mu\chi_{11}}{\epsilon^2 U_o}\left(\left(\frac{d_{p(2)}A_{p(1)}d_{s(3)}d_{s(1)}}{d^2_{p(2)}A'_{p(1)} + d^2_{p(3)}A''_{p(1)}}\right) + \left(\frac{d_{p(3)}A_{p(1)}d_{s(2)}d_{s(1)}}{d^2_{p(2)}A'_{p(1)} + d^2_{p(3)}A''_{p(1)}}\right) + \frac{\beta_{(1)}d_{s(2)}d_{s(3)}}{d_{p(1)}}\right) \tag{3.162}$$

$$M = \frac{\rho\chi^2_{11}d_{s(2)}d_{s(3)}f(c_d,\beta_{(1)})}{2\epsilon^3 U_o} \tag{3.163}$$

where $f(c_d,\beta_{(1)})$ may be equal to $\beta^2_{(1)}$ if the "Bernoulli model" is used or it may be equal to c_d or $\beta^2_{(1)}c_d$ depending on which one of the drag models is used. In (3.162) $A'_{p(1)}$ and $A''_{p(1)}$ are given by (3.120) and (3.121) while $\beta_{(1)}$ is expressed by (3.140). These equations are the final conclusions of this section and, unfortunately, a reliable data set in which the pressure gradient measurements are accompanied by detailed structural information of the anisotropic porous medium are not available to validate the granular model.

3.9.6.2 Isotropic granular porous media

The flow of Newtonian fluids through isotropic granular porous media has been analysed by Du Plessis and Masliyah (1991) as well as by Du Plessis (1994). For an isotropic material the RUC is cubic with a solid cube centrally within the RUC. Under the conditions of isotropy the physical as well as notational simplifications indicated in Table 3.6 may be introduced and the RUC then attains similar geometric characteristics in the different RUC directions.

Table 3.6. Characteristics of an RUC for isotropic granular porous media.

Geometric relation	Reference
$d_{(1)} = d_{(2)} = d_{(3)} = d$	
$d_{s(1)} = d_{s(2)} = d_{s(3)} = d_s$	
$A'_{p(1)} = A''_{p(1)}$	
$\chi_{11} = \chi = \dfrac{\epsilon}{1-(1-\epsilon)^{2/3}}$	(Du Plessis, 1994)
$d_s = (1-\epsilon)^{1/3} d$	(Du Plessis and Diedericks, 1997)
$d_p = d - d_s = d(1-(1-\epsilon)^{1/3}$	(Du Plessis and Diedericks, 1997)
$\beta_{(1)} = \beta_{(2)} = \beta_{(3)} = \beta = \sqrt{2}$	(Du Plessis, 1994)

By introducing these reductions and geometric relations for an isotropic RUC into (3.162) the low Reynolds number flow limit is given by

$$\begin{aligned} N &= \frac{12\mu\chi}{\epsilon^2 U_o}\left(\frac{2d_s^2+\beta d_s^2}{d_p}\right) \\ &= \frac{12\mu\chi d_s^2}{\epsilon^2 U_o d_p}\left(2+\sqrt{2}\right) \\ &= \frac{41\mu}{\epsilon d_s^2}\frac{(1-\epsilon)^{4/3}}{\left[1-(1-\epsilon)^{1/3}\right]\left[1-(1-\epsilon)^{2/3}\right]}. \end{aligned} \tag{3.164}$$

This expression is exactly the same as the result of Du Plessis (1994) where the different flow speeds in the transverse channels are also incorporated. Similarly, the reductions in Table 3.6 may be use in (3.163) to obtain

$$\begin{aligned} M &= \frac{\rho\chi^2 d_s f(c_d,\beta)}{2\epsilon^3 U_o} \\ &= \frac{\rho(1-\epsilon) f(c_d,\beta)}{2\epsilon d_s\left[1-(1-\epsilon)^{2/3}\right]^2}. \end{aligned} \tag{3.165}$$

If $f = 2$ then this expression is also the same as the equivalent expression obtained by Du Plessis (1994). A combination of these two expressions with (3.161) then yields the general momentum transport equation for the isotropic case.

Different modelling expressions for flow at intermediate Reynolds numbers through isotropic granular materials, which were derived in context of the RUC-model, have also appeared in literature. Du Plessis (1994) calculated the pressure difference by referring to the Bernoulli equation and used the correct value of $\beta = \sqrt{2}$ for isotropic granular materials. For two-dimensional flow over a cube $c_d = 1.1$ which indicates that (3.157) is not equivalent to (3.159) for isotropic granular porous media. Du Plessis and Diedericks (1997) assumed that $\beta = 1$ which implies that (3.159) is effectively equivalent to (3.160), but both are different from (3.157). Even in the isotropic case there is still some uncertainty as to which model is more appropriate for practical applications. For anisotropic media it is suggested that either one may also be used depending on the determinability of β or c_d.

3.9.7 Summary

During the course of this section a deterministic expression has been derived which relates the pressure gradient to the superficial velocity over the Darcy and Forchheimer regimes. The modelling was built on the RUC-model which was previously used for the anisotropic foamlike materials, except that an additional RUC which is unique to anisotropic granular porous media was introduced.

The flow at intermediate Reynolds numbers was analysed in detail and three different expressions for the flow in this regime were obtained. In the first approach the recirculation around the solid material was modelled through reference to the Bernoulli equation. In addition, two relations built on the concept of form drag were also introduced. There is no theoretical evidence which renders any of the expressions superior to the other and the advantage of one above the other will only become apparent through different applications.

3.10 Transverse flow across a prismatic bundle

In this section a deterministic expression giving the relation between the pressure gradient and superficial velocity for transverse flow across a prismatic bundle is presented. Typical examples of this kind of flow are fluid transport across a heat transfer tube bundle, wind blowing horizontally through an array of pine trees, the seepage along the side of a synthetic membrane and the flow of resin through fibres during resin transfer moulding. For this type of flow configuration the modelling is restricted to two dimensions. This is actually a special case of three-dimensional flow through an array of

prismatic objects where the length of the objects are infinitely long. On the other hand, it may also be considered as the two-dimensional analogue of flow through a granular porous structure.

The various steps to determine the pressure gradient equation are similar to the derivations in the previous two sections. For this case the general equation governing the flow is also given by (3.27) and, furthermore, neglecting the momentum dispersion as discussed in Section 3.6 is also appropriate for this flow condition. Therefore, the problem is once again to determine a closure scheme for the fluid-solid surface integral term in (3.43). This is achieved by introducing an appropriate RUC for the anisotropic prismatic bundle and then modelling the interstitial flow and pressure losses.

Pressure gradient expressions for Newtonian flow across isotropic prismatic bundles have been derived by Du Plessis (1991) and Van der Westhuizen and Du Plessis (1994). In these cases the porous medium was considered as being isotropic and the non-linear effects in the velocity-pressure gradient relationship at intermediate Reynolds numbers were modelled through consideration of flow development along the channel sections within the isotropic RUC. The present modelling exercise is extended to anisotropic porous media and the non-linear effects are attributed to local flow separation.

Firstly, an anisotropic RUC is introduced for the prismatic bundle and various geometric features and interstitial velocity relations are presented. The momentum transfer for creeping flow in the Darcy regime is considered whereafter the flow at intermediate Reynolds numbers in the Forchheimer regime is modelled. A general equation governing momentum transport over both these domains is then proposed by a simple addition of the two limiting conditions.

3.10.1 Modelling of the prismatic microstructure

The most prominent feature of this type of porous media is the fact that the solid matrix consists of unconsolidated parallel fibres where the length of the fibres is orders of magnitude larger than the cross-sectional dimensions of the fibres. The cross-sectional dimensions of the fibres may differ to yield the material anisotropic.

A Representative Unit Cell (RUC) for this type of anisotropic material may be obtained by generalising the RUC of Du Plessis (1991) and approximating the prismatic, quasi two-dimensional porous structure by a rectangular prismatic RUC of linear dimensions $d_{(1)}$ and $d_{(2)}$ on the sides and unit length parallel to the prism axes as illustrated in

Figure 3.17. The void part of the RUC, U_f, may be expressed as

$$U_f = \epsilon U_o = \epsilon d_{(1)} d_{(2)} z \tag{3.166}$$

where ϵ is the porosity of the medium, $d_{(1)}$ and $d_{(2)}$ are the respective side lengths of the RUC and z is the height of the RUC which is equal to the height of the fibres. To render the flow two-dimensional it is assumed that $z \gg d_{(1)}$ and $z \gg d_{(2)}$.

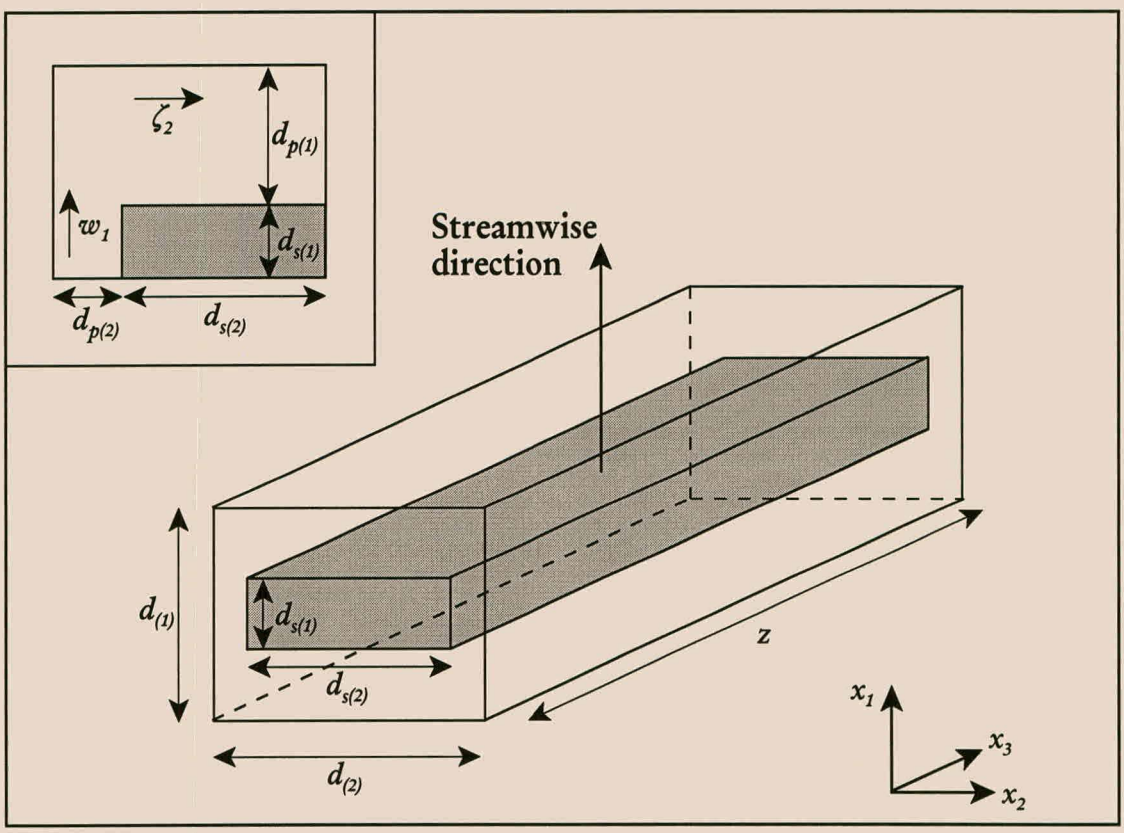

Figure 3.17. An RUC for an anisotropic fibre bed with the flow around the solid indicated in the insert.

The average geometric properties of the solid structure within the RUC may be resembled by a rectangular prism of solid material located centrally within the RUC and aligned parallel to the sides of the RUC as shown in Figure 3.17. This RUC captures the porosity, characteristic solid-to-solid length and typifying microstructural geometry of the porous medium. In addition to the assumptions governing an RUC presented in Section 3.5, it is also assumed, for crossflow transverse to the porous material, that

- the fluid traverses the porous medium and RUC perpendicular to the prism axes and there does not exist any velocity components parallel to the prism axes.

Initially it is also assumed that the RUC may be orientated with one side parallel to the specific discharge which allows the specification of a streamwise direction which is directed along one of the RUC-coordinates. It is further assumed that the flow is in the x_1-direction and the streamwise direction is indicated by the unit vector $\hat{\nu}_i$.

If the sides of the solid constituent are of length $d_{s(1)}$ and $d_{s(2)}$, respectively, then the volume of solid material within the RUC, U_s, is given by

$$U_s = d_{s(1)}d_{s(2)}z = (1 - \epsilon)d_{(1)}d_{(2)}z. \tag{3.167}$$

The effective streamwise channel area is given by

$$A_{p(1)} = d_{p(2)}z = (d_{(2)} - d_{s(2)})z \tag{3.168}$$

while the tortuosity for flow in the x_1-direction follows from (3.34) and is equal to

$$\chi_{11} = \frac{U_f}{U_{f\mathcal{L}(1)}} = \frac{\epsilon d_{(2)}}{d_{p(2)}} \tag{3.169}$$

where $d_{p(2)}$ is the channel width in the x_2-direction. Following along the same lines as Du Plessis (1991) it may also be deduced that

$$\frac{1}{\chi_{11}} = \left(1 - \frac{(1-\epsilon)d_{(1)}}{d_{s(1)}}\right) \tag{3.170}$$

which indicates that a unique relation expressing the tortuosity in terms of the porosity is not possible for the anisotropic RUC.

To estimate the interstitial flow velocities it is assumed that the flow is piecewise linear within each channel section as shown in Figure 3.2. In addition, the placement of surrounding solid prisms in neighbouring RUC's is governed by the assumption of maximum staggering. It therefore follows from (3.37) that

$$q_1 = \epsilon u_1 = \frac{\epsilon \widehat{w}_1}{\chi_{11}} \tag{3.171}$$

and for a comparison with the granular model it may be added that

$$\zeta_2 = \beta \widehat{w}_1 \tag{3.172}$$

where

$$\beta = \frac{d_{p(2)}}{d_{p(1)}}. \tag{3.173}$$

A mass balance over the RUC also implies that

$$\zeta_2 = \frac{d_{(2)}}{d_{p(1)}} q_1, \tag{3.174}$$

where ζ_i is the mean velocity in the transverse channel.

3.10.2 Modelling of the interstitial fluid-solid interaction

The momentum transport which occurs during transverse flow across anisotropic fibrous beds or prismatic bundles is also governed by (3.43) and in this section it is also expressed in the form of (3.6). This requires the flow to be analysed over the two laminar flow regimes.

3.10.2.1 Low Reynolds number flow limit

For creeping flow in the x_1-direction it is once again assumed that viscous effects dominate and that the flow in both the channels is fully developed. It thus follows that

$$\iint_{S_{fs}} v_{1,j} \nu_j dS = 2 v_{1,2} \nu_2 d_{s(1)} z \tag{3.175}$$

and the shear stresses which occur along the transverse channel in the x_2-direction do not contribute to the surface integral in (3.175). These stresses are represented by the local pressure gradients normal to the streamwise direction. Although the macroscopic pressure does not have a component in the x_2-direction, local pressure gradients are required to drive the flow through the channels normal to the streamwise direction. If the flow in these channels is also considered to be fully developed, then the local pressure gradient across a transverse channel is equal to the shear stress opposing the flow and it thus follows that

$$-\iint_{S_{fs}} \overset{o}{p} \nu_1 dS = 2 v_{2,1} \nu_1 d_{s(2)} z. \tag{3.176}$$

The shear stresses for fully developed flow between parallel plates are given by

$$\mu v_{i,j}\nu_j = -\frac{6\mu\overline{v}_i}{d_{p(\nu_k)}} \tag{3.177}$$

where the average speed in the channel, $\overline{v}$, is given by either $\widehat{w}_1$ or ζ_2 depending on the channel in the RUC under consideration. By combining this expression and (3.171) and (3.174) with (3.175) and (3.176) the pressure gradient becomes

$$\begin{aligned} P_{,1} &= -\frac{12\mu z}{\epsilon U_o}\left(\frac{\widehat{w}_1 d_{s(1)}}{d_{p(2)}} + \frac{\zeta_2 d_{s(2)}}{d_{p(1)}}\right) \\ &= -\frac{12\mu z}{\epsilon^2 U_o}\left(\frac{\chi_{11} d_{s(1)} q_1}{d_{p(2)}} + \frac{\chi_{11} d_{s(2)} d_{p(2)} q_1}{d^2_{p(1)}}\right) \\ &= -\frac{12\mu\chi_{11} q_1}{\epsilon^2 d_{(1)} d_{(2)}}\left(\frac{d_{s(1)}}{d_{p(2)}} + \frac{d_{p(2)} d_{s(2)}}{d^2_{p(1)}}\right). \end{aligned} \tag{3.178}$$

According to this expression the pressure gradient may be predicted from known values of the fibre dimensions and relative spacing between different fibres in addition to the porosity and fluid viscosity.

3.10.2.2 Shear friction tensor

For the case where the streamwise direction is in an arbitrary direction relative to the RUC-coordinates, the components of the pressure equation (3.43) may be obtained by analysing each individual flow component along the RUC-coordinates. This is possible since the channels in the RUC are at right angles to each other and the superficial velocity, channel velocities and shear stresses are linearly related to each other. The pressure gradient and superficial velocity are, therefore, related by

$$P_{,i} = -\mu F_{ij} q_j \qquad (i = 1,2; j = 1,2) \tag{3.179}$$

where F_{ij} is a diagonal shear friction tensor with components

$$F_{11} = \frac{12\chi_{11}}{\epsilon^2 d_{(1)} d_{(2)}}\left(\frac{d_{s(1)}}{d_{p(2)}} + \frac{d_{p(2)} d_{s(2)}}{d^2_{p(1)}}\right) \tag{3.180}$$

$$F_{22} = \frac{12\chi_{22}}{\epsilon^2 d_{(2)} d_{(1)}}\left(\frac{d_{s(2)}}{d_{p(1)}} + \frac{d_{p(1)} d_{s(1)}}{d^2_{p(2)}}\right). \tag{3.181}$$

The symmetry of the shear resistance tensor follows from the rectangular channel sections in the RUC.

3.10.2.3 Intermediate Reynolds number flow

The analysis of flow at intermediate Reynolds numbers presented for flow through granular materials is equally applicable to the prismatic bundle, except that the geometry of the RUC is less complicated. The are only two channels and the internal flow is collinear to the RUC-coordinates. Therefore, the flow recirculation around the solid constituent may also be schematized by Figure 3.9. Application of Bernoulli's equation to the dividing streamline, and following similar arguments regarding the flow and stagnation velocity presented in Section 3.9.5.3, lead to

$$\epsilon U_o P_{,1} = -\frac{1}{2}\rho v_j^c v_j^c d_{s(2)} z \nu_1 \tag{3.182}$$

which is equivalent to (3.155), as derived for the granular case. By assuming that the magnitude of the velocity at the inflection point is equal to the speed in the transverse channel, $v_i^c = \zeta_i$, the pressure gradient becomes

$$\begin{aligned} P_{,1} &= -\left(\frac{1}{\epsilon d_{(1)} d_{(2)} z}\frac{\rho \zeta_2^2 d_{s(2)} z \nu_1}{2}\right) \\ &= -\left(\frac{\rho \beta^2 \chi_{11}^2 q q_1 d_{s(2)}}{2\epsilon^3 d_{(1)} d_{(2)}}\right). \end{aligned} \tag{3.183}$$

In (3.183) the β-factor and the tortuosity may be eliminated through use of (3.173) and (3.169).

However, as noted in the previous section, the pressure loss may also be modelled as a form drag process. The pressure gradient across the solid in the RUC may be expressed as

$$\begin{aligned} \epsilon U_o P_{,1} &= -\iint_{S_{fs}} \overset{o}{p} \nu_1 \, dS \\ &= -\frac{1}{2}\rho c_d v_\infty^2 S_{\perp(1)} \nu_1 \end{aligned} \tag{3.184}$$

where v_∞ represents the free stream velocity as it appears in the definition of the drag force and c_d is a friction factor. If it is assumed that the free stream velocity is equal

to the streamwise channel average velocity, $v_\infty \approx \widehat{w}$, then (3.184) becomes

$$\begin{aligned} P_{,1} &= -\frac{\rho c_d \widehat{w}_1^2 d_{s(2)}}{2\epsilon d_{(1)} d_{(2)}} \\ &= -\frac{\rho c_d \chi_{11}^2 d_{s(2)} q q_1}{2\epsilon^3 d_{(1)} d_{(2)}}. \end{aligned} \tag{3.185}$$

The free stream velocity may also be approximated by $\zeta_2 = \beta \widehat{w}_1$ and in this case it follows that

$$\begin{aligned} P_{,1} &= -\frac{\rho c_d \beta^2 w_1^2 d_{s(2)}}{2\epsilon d_{(1)} d_{(2)}} \\ &= -\frac{\rho \beta^2 c_d \chi_{11}^2 d_{s(2)} q q_1}{2\epsilon^3 d_{(1)} d_{(2)}}. \end{aligned} \tag{3.186}$$

These modelling expressions are different and it is expected that the most appropriate method to represent the intermediate Reynolds number flow can only be assessed through validation of the model results against a sufficient number of measurements.

3.10.2.4 General equation for the anisotropic fibre bed

A rectangular RUC for anisotropic fibre beds has been introduced and various geometric relations have been presented. A closure model, similar to the model for the granular materials, has been developed for flow at low as well as intermediate Reynolds numbers. The general pressure gradient equation is given by

$$-\frac{1}{q_1} P_{,1} = M q_1 + N \tag{3.187}$$

where

$$N = \frac{12\mu\chi_{11}}{\epsilon^2 d_{(1)} d_{(2)}} \left(\frac{d_{s(1)}}{d_{p(2)}} + \frac{d_{p(2)} d_{s(2)}}{d_{p(1)}^2} \right) \tag{3.188}$$

and the inertial coefficient is given by

$$M = \frac{\rho f(\beta, c_d) \chi_{11}^2 d_{s(2)}}{2\epsilon^3 d_{(1)} d_{(2)}} \tag{3.189}$$

where the function $f(\beta, c_d)$ is given by β^2, c_d or $\beta^2 c_d$, depending on the appropriate model.

3.10.2.5 General equation for an isotropic fibre bed

For isotropic fibre beds, the dimensions of the RUC in the x_1- and x_2-directions are equal as well as the flow speeds in the two channel sections. This allows a notational simplification as presented in Table 3.7.

Table 3.7. Geometric simplifications for an RUC for isotropic fibre beds.

$d_1 = d_2 = d$
$d_{s(1)} = d_{s(2)} = d_s$
$d_{p(1)} = d_{p(2)} = d_p$
$A_{p(2)} = A_{p(3)} = A_p$
$\chi_{11} = \chi_{22} = \chi$

Accordingly, the geometry within the RUC is less complicated than for the anisotropic case and it is possible to deduce a number of additional geometric relations. According to the derivations of Du Plessis (1991), and summarised by Du Plessis and Diedericks (1997), it follows that the tortuosity in the isotropic case may be expressed in terms of the porosity by

$$\chi = \frac{\epsilon}{1-\sqrt{1-\epsilon}}. \tag{3.190}$$

Furthermore, the dimension of the solid constituent is given by

$$d_s = d\sqrt{1-\epsilon} \tag{3.191}$$

and the channel width may be expressed as

$$d_p = d - d_s = d\left(1-\sqrt{1-\epsilon}\right). \tag{3.192}$$

In the case of an isotropic porous medium (3.188) reduces to

$$N = \frac{24\mu\chi}{\epsilon^2 d^2}\left(\frac{d_2}{d_p}\right). \tag{3.193}$$

By introducing the geometric relations presented in (3.190) to (3.192) into this relation, then yields the friction coefficient

$$N = \frac{24\mu\sqrt{1-\epsilon}}{\epsilon d^2(1-\sqrt{1-\epsilon})^2} \tag{3.194}$$

which is also presented by Du Plessis and Diedericks (1997). By following similar steps the inertial coefficient for the isotropic model is given by

$$M = \frac{\rho f(c_d,\beta)\sqrt{1-\epsilon}}{2\epsilon d(1-\sqrt{1-\epsilon})^2}. \tag{3.195}$$

If the form drag approach is followed then $f(c_d,\beta) = c_d$ and (3.195) is then equal to the expression of Du Plessis and Diedericks (1997).

3.11 Summary and conclusions

In this chapter a general modelling methodology for the flow of Newtonian fluids through three different types of idealised porous media has been introduced. According to the modelling approach, it is firstly necessary to obtain the volume averaged flow equations governing the transport on the macroscopic level. Closure of the phase averaged momentum transport equation is aided by introduction of a pore-scale model. According to the pore-scale model the average geometry of the specific porous material is captured in an RUC. The concept of an RUC as introduced by Du Plessis and Masliyah (1988; 1991) and Du Plessis (1991) for isotropic media has been extended to include anisotropic materials.

The RUC's were then used for closure of the momentum transport equations. For creeping flow, it is assumed that the flow is fully developed in all channels and for intermediate Reynolds number flow inertial effects are assumed to dominate over the negligible frictional effects. Accurate quantification of the microscopic fluid-solid interaction resulted in a macroscopic balance equation valid over both the Darcy and Forchheimer regimes. The resulting pressure gradient equations are related to the geometric features of the porous medium and empiricism is minimised since the final expressions are in terms of macroscopic variables characteristic of the porous medium. The different steps which are required during the modelling approach are illustrated in Figure 3.18.

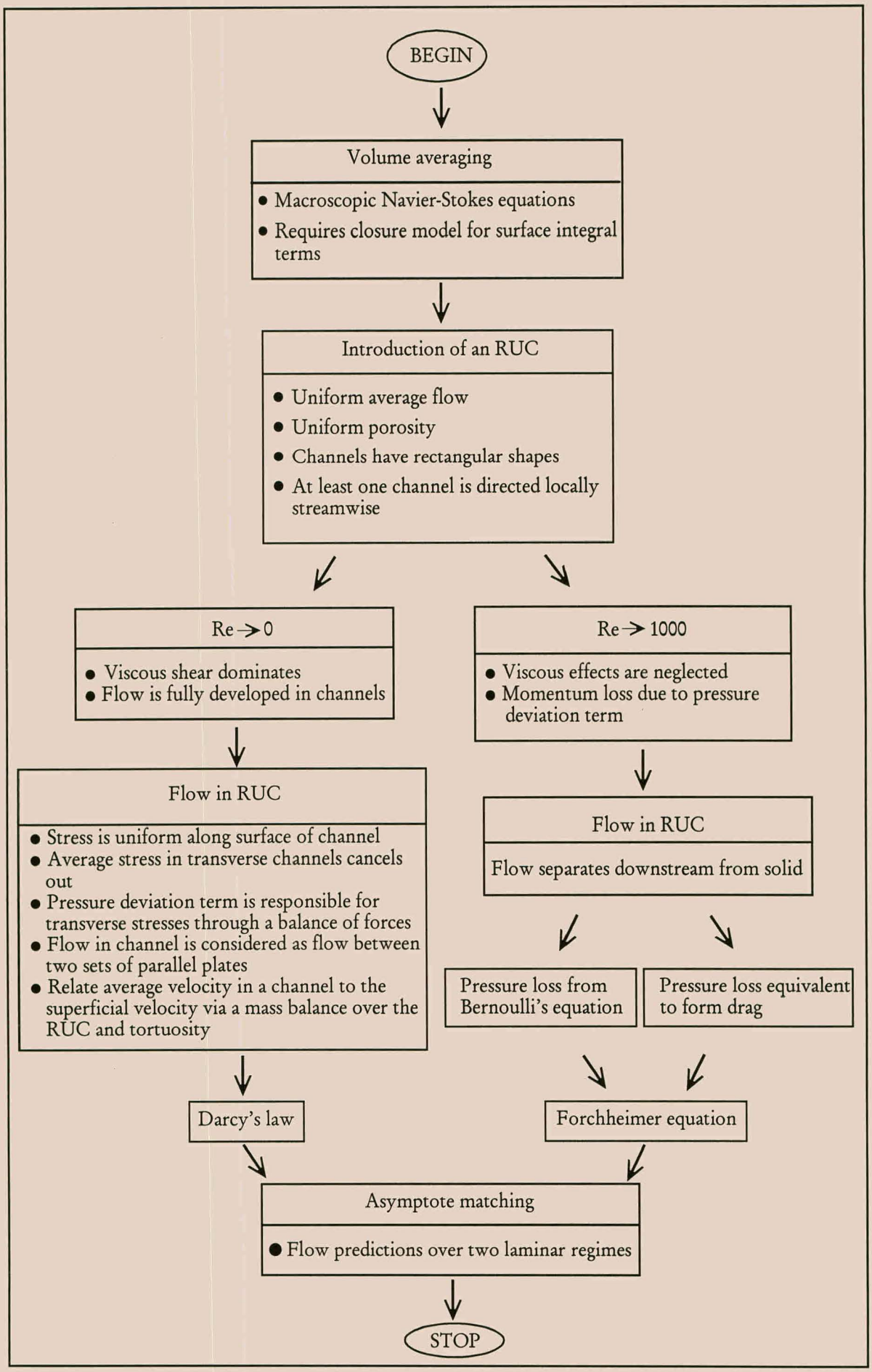

Figure 3.18. An overview of the modelling approach.

The approach outlined in the flow chart has been applied to three types of anisotropic porous materials, namely foamlike materials, granular materials and fibre beds. For the foams, the model has been validated against a particular test case. The experimental test case is particularly difficult to simulate since the material is a rolled-up knitted wire where the solid strands consist of a twisted double wire. It was determined that the model under predicted the measurements in the Darcy regime, but were accurate in the Forchheimer regime. The success of the model in the Forchheimer regime is attributed to the modelling of the form drag coefficient. The less accurate predictions in the Darcy regime is attributed to the under estimation of the fluid-solid surface area by approximately 20% when modelling the double wire as a single solid bar. The sensitivity of the model to certain geometric features has also been assessed. For verification of the model it is necessary to have detailed information regarding the local physical dimensions of the material and such experimental information could not be obtained for the granular and fibres models. Nevertheless, it is considered that the deterministic expressions for the relation between the pressure gradient and superficial velocity which have been presented are in a form which is useful for practical applications.

Chapter 4

ELECTRICAL CONDUCTION AND FORMATION FACTOR

4.1 Introduction and outline

Transport phenomena in porous media encompass a wide variety of branches, which include, amongst others, Newtonian and non-Newtonian fluid transport, heat transport, chemical diffusion and dispersion, electrical conduction and acoustic wave propagation. In the absence of a unifying theory accounting for all types of transport processes through porous media, different models describing a limited number of features are continuously being developed. Generally, each model contributes to an understanding of a particular transport process through porous media in its own right. However, the extension of any model to incorporate a greater number of transport phenomena may give an indication of which assumptions are fundamental to porous media transport and may serve as a basis for an eventual general theory. In this chapter the pore-scale RUC-model is used to aid the closure modelling required to obtain a macroscopic description of electrical conduction and charge transport in homogeneous porous media. An additional requirement of the closure modelling is that a suitable representation of the microscopic charge transport within the Representative Unit Cell (RUC) should be available. In this chapter the relation between the microscopic and macroscopic transport is provided by the general theory developed in Chapter 2 which relates microscopic fluxes to macroscopic fluxes via the lineality tensor and which has been applied to fluid transport in Chapter 3.

According to the discussion in Section 2.7.2.2, which follows the exposition of Clennell (1997), the electrical conduction behaves similarly to chemical diffusion, sound propagation and certain limits of pressure oscillations in porous media. For example,

Charlaix *et al.* (1988b) indicated through the study of pressure oscillations in porous media that inertial flow and other potential transport phenomena such as electrical conductivity in the fluid phase or steady diffusion are similar processes. By focussing on the modelling of electrical conduction in porous media a platform may be laid to extend the RUC-model to other transport domains although only in an indirect manner. Although the electrical conduction in porous media is a reasonably well-studied phenomenon, the study of known transport processes may lead to the production and characterisation of new materials such as composites and sintered glass (Lemaitre *et al.*, 1988). Besides this indirect interest in electrical conduction in porous media, it also plays an important role in chemical and petroleum engineering practice as well as in chemical reactors. For example, the soil electrical conductivity is also considered an important property in agricultural practice, as it usually serves as an indicator of soil salinity in the field. In experimental studies of soil leaching and chemical transport, changes in solution concentration within the soil profile are usually estimated in real time by interpretation of the measured electrical conductivity (Mualem and Friedman, 1991). The electrical conduction is expressed through Ohm's law and, therefore, the main objective of this chapter is to obtain a macroscopic form of Ohm's law in which the effective conductivity is expressed in terms of quantifiable porous medium parameters.

In addition, electrical well logs have been used for the quantitative determination of different reservoir parameters such as connate water saturation, formation permeability and connate water salinity. It was first suggested by Archie (1942) that electrical resistivity parameters may be employed to characterise the porous sedimentary rocks encountered in oil-well drilling. According to Wyllie and Spangler (1952), Archie's suggestion was pragmatical inasmuch as electrical resistivity measurements of rock formations are made during well drilling as a means of differentiating the formations penetrated by the drilling bit and of permitting an estimation to be made of the nature of the fluids contained within the pores of permeable rocks. As shown in Section 2.6.5, Archie (1942) introduced a dimensionless parameter, which he called the formation resistivity parameter or formation factor, which could be determined by measuring the resistivity of a rock saturated with a conducting electrolyte and dividing this resistivity by the resistivity of the electrolyte. The determination of the formation factor became an essential preliminary to the employment of the electric log for either the qualitative or quantitative interpretation of reservoir rocks for oil saturation (Wyllie and Rose, 1950). Therefore, another objective of this chapter is to provide deterministic expressions from which the formation factor may be determined solely from physical and measurable quantities of the porous rock. The expressions for the formation factor are also derived by making use of the RUC-model and the types of porous materials which are considered are restricted to isotropic and anisotropic fibrous beds, granular media

and foamlike materials. Since the formation factor is measurable without recourse to a specific model the results obtained may also serve as a quantitative test of the present model for further application to other flow phenomena.

The formation factor may be related to a tortuosity factor and since this tortuosity is thus derived from electrical measurements it would be appropriate to refer to it as the electrical tortuosity while the tortuosity appearing in certain expressions for the permeability is denoted as the hydraulic tortuosity (Dullien, 1979; Scheidegger, 1974; Bear, 1972). It would appear as if Wyllie and Rose (1950) where the first to suggest that the measurement of formation factor may lead directly to an evaluation of this tortuosity. Wyllie and Rose (1950) made the assumption that the tortuosity pertaining to the flow of electrical current through conducting fluids in porous media is closely related to the tortuosity which appears in equations describing the mass transfer of fluids in the same media. Through the assumption that the hydraulic tortuosity is equal to the electrical tortuosity the formation factor also became an important parameter for the calculation of permeability (Walsh and Brace, 1984). Therefore, the modelling of electrical conduction in porous media may be considered to be a natural extension to modelling the flow of Newtonian fluids in porous media. As clearly indicated by Clennell (1997) and Knackstedt and Zhang (1994), the electrical tortuosity is not equivalent to the hydraulic tortuosity. However, in the RUC-model the electrical flow lines and hydraulic flow lines are as a first estimate considered to be the same and a distinction between hydraulic and electric tortuosity is not made. Therefore, the relation between these two tortuosities is not pursued in this chapter, but consideration is given to deterministic expressions for the formation factor.

The first step in the modelling approach is to apply the volume averaging theory to the microscopic charge transport. This provides a sound mathematical platform from which to assess the macroscopic current and ease interpretation of the various contributing factors. Closure of the macroscopic current transport equation is provided by considering the rectangular representative unit cell approach as introduced by Du Plessis and Masliyah (1988) and applied to Newtonian fluid flow in the previous chapter. Therefore, the main aim of this chapter is to provide a deterministic prediction of electrical conduction, expressed through Ohm's law and the formation factor, in various porous media structures. This has the advantage that the results obtained are of practical value and minimises resistivity measurements.

In the first part of this chapter an overview of the macroscopic form of Ohm's law is presented. This discussion includes the electrical conductivity, the formation factor, different forms of Archie's law as well as additional relationships between the formation factor and tortuosity. An account is then given of the electrical conduction on the

microscopic level and the volume averaging theory is used to transform the microscopic balance equations to the macroscopic level. The Representative Unit Cell (RUC), introduced in Section 3.5, is again used as a pore-scale model in the closure modelling. The closure modelling consists of a derivation of the channel average current density and analyses of the fluid-solid surface integral term in the macroscopic charge balance equation by referring to the RUC's for three types of anisotropic materials. Through this process deterministic expressions for the macroscopic form of Ohm's law and the formation factor are derived for isotropic and anisotropic foamlike materials, fibre beds and granular porous media. The final part of this chapter consists of a validation process where the theoretical predictions are compared to measurements.

4.2 Ohm's law

The macroscopic form of Ohm's law which governs current flow through an electrolytically saturated porous medium with a non-conducting solid phase may be expressed as

$$\langle j_i \rangle = -\frac{1}{\rho_o} \langle V \rangle^f_{,i} = \sigma_o \langle V \rangle^f_{,i} \tag{4.1}$$

where ρ_o is the electrical resistivity of the porous medium saturated with an electrolyte, σ_o is the electrical conductivity of the saturated porous medium and it is per definition equal to the inverse of the resistivity (Kip, 1969), $\langle V \rangle^f$ is the externally applied electrical potential and $\langle j_i \rangle$ is the phase average current density expressed in amperes per unit area of the medium (Bear, 1972). This equation has been postulated in analogy with the local or microscopic form of Ohm's law except that the local resistivity or conductivity has been replaced by the macroscopic resistivity or conductivity. Since the influence of the porous medium on the current transport is contained within the electrical resistivity or conductivity, it may be used as a macroscopic characteristic geometric property of the porous medium. It is also readily measurable without recourse to any specific porous medium model.

The microscopic conductivity may depend on the properties of the electrolyte such as density and homogeneity as well as temperature (Popović, 1973). However, for a homogeneous electrolyte with constant physical properties at a uniform temperature the conductivity is uniform and may thus be represented by a scalar quantity. However, on the macroscopic level the conductivity appearing in the macroscopic Ohm's law is a parameter which also depends on physical properties of the porous medium. It may thus

differ according to the direction of charge transport if the porous medium is anisotropic. Therefore, Ohm's law should be written as

$$\langle j_i \rangle = \sigma_{oij} \langle V \rangle_{,j}^{f} \tag{4.2}$$

where σ_{oij} is the electrical conductivity tensor. During electrical conductivity measurements the externally applied electric potential field is in the same direction as the measured current which eliminates the necessity to consider the tensorial nature of the macroscopic electrical conductivity. However, by applying (4.1) to calculate the conductivity in a specific direction through an anisotropic material it is implicitly assumed that the macroscopic electrical conductivity tensor is symmetric. Bear (1972, p113) related the conductivity tensor to the symmetric 'tortuosity tensor', presented in (2.118), which he introduced when considering mass transport. Thereby it is implied that the conductivity tensor is also symmetric and for different experimental orientations of an anisotropic sample, different values of the macroscopic conductivity may be obtained. In this study the tensorial nature of the macroscopic electrical conductivity is not further investigated and it is assumed that when (4.1) is applied to a practical situation, the experimental arrangement is such that σ_o is the only conductivity value which is determined from measurements. As previously mentioned, the main objective of this chapter is to derive (4.1) by using the volumetric averaging theory and to express σ_o in terms of measurable characteristics of the porous medium.

4.3 Electrical conductivity

The microscopic electrical conductivity is a characteristic of the electrolyte which is present in the interstitial pore-space. The macroscopic electrical conductivity is a macroscopic porous medium characteristic which depends on properties of both the porous medium and the microscopic electrolyte. In this study the term electrical conductivity refers to the macroscopic conductivity and when the microscopic conductivity is implied specific reference is made to it. When an oscillating electric field is applied to a porous sample, it has experimentally been determined that at very low frequencies of approximately 1 Hz at 25°C conductivities measured on rock samples tend to approach a constant value which depends on temperature but is independent of further reduction in frequency (Keller, 1982). This is known as the direct current limit of the conductivity and is the main concern of this study. Consideration is not given to the frequency dependent alternating current limit of the conductivity.

Different models have been introduced to relate the geometric structure of the porous

material to the electrical conductivity. Mualem and Friedman (1991) introduced a capillary model and showed that for a saturated porous medium,

$$\sigma_o = \sigma_w \theta^{n+1} \tag{4.3}$$

where σ_w is the electrical conductivity of the soil solution or electrolyte and θ is an effective area which is smaller than the actual area available for flow due to an immobile zone near the surface. The effective area is given by $\theta = \Theta - \Theta_o$ where Θ is the areal cross-section of the soil solution in a unit area of a bulk soil. However, the ion mobility very close to the solid surface may be considerably diminished compared to the mobility at the central parts of the pores. To account for this they introduced, as an approximation, an immobilize zone in the immediate vicinity to the solid surface which is expressed in terms of a water content area, Θ_o. According to Mualem and Friedman (1991), n may be calibrated from soil water retention and hydraulic conductivity functions, but in the absence of these an empirical value of $n = 0.5$ is suggested.

Johnson *et al.* (1986) considered electrical conduction in an insulating porous medium saturated with a fluid of uniform conductivity σ_w. By considering certain types of perturbations in the potential they determined that the effective conductivity is given by

$$\sigma_o = \frac{1}{F}\left(\sigma_w + \frac{2\sum_s}{\Lambda}\right) + \boldsymbol{O}\left(\sum_s^2\right) \tag{4.4}$$

where F is the formation factor as defined in (2.43), Λ is an intrinsic measure of the interconnected pore-space which is directly related to the transport and $\sum_s$ is the interfacial conductivity. The quantity Λ is defined, in the present notation, by

$$\frac{2}{\Lambda} = \frac{\iint_{S_{fs}} |V_{,i} V_{,i}| dS}{\iint_{U_f} |V_{,i} V_{,i}| dU} \tag{4.5}$$

where V is the microscopic potential. According to Johnson *et al.* (1986), one accounts for the leading effect of surface conduction by means of a perturbation theory in which the relevant parameter, $2/\Lambda$, is an effective surface-to-pore volume ratio wherein each area or volume element is weighted according to the local value of the electric field which would exist in the absence of the surface mechanism. The main contribution of their work is the parameter Λ which is characteristic of the geometry of the porous medium

and according to Johnson *et al.* (1986), it is a universal parameter for a particular porous medium and a determination of it from one experiment is transferable to another. However, Bernabé and Revil (1995) have noted that Λ is not easy to determine from electrical conductivity measurements and to alleviate this problem Revil and Cathles (1999) have expressed Λ as

$$\Lambda \approx \frac{d_c}{2mF} \tag{4.6}$$

where d_c is the diameter of a tube in the capillary model, F is the formation factor and m is the cementing factor as it appears in Archie's law (as discussed in the next section).

Walsh and Brace (1984) assumed that the flow of Newtonian fluids through porous media is similar to the flow of electric current and attempted to find a relation between the permeability and conductivity. They deduced from measurements that the permeability is proportional to $\sigma_o^{1.5}$ for Westerley granite. Although similar expressions were found from other rock samples the exponent was generally not equal to 1.5.

4.4 Formation factor

4.4.1 Definition

During the measurements of electrical resistivities in determining reservoir characteristics, Archie (1942) found empirically that $\rho_o = F\rho_w$ where ρ_w is the resistivity of the electrolyte, ρ_o is the resistivity of the porous sample and F was termed the formation resistivity factor. This led to the formation factor being defined as

$$F \equiv \frac{\rho_o}{\rho_w}. \tag{4.7}$$

As indicated in Section 2.6.5 the formation factor may also be expressed in terms of the conductivity or resistance of the porous medium and electrolyte,

$$F = \frac{\sigma_w}{\sigma_o} = \frac{R_o}{R_w}. \tag{4.8}$$

The formation factor introduced by Archie (1942) was used to characterise the porous sedimentary rocks encountered in oil-well drillings. He determined that the formation

factor is a function of the type and character of the porous formation, and varies, among other properties, with the porosity and permeability of the reservoir rock. Nevertheless, he obtained an empirical relation between the formation factor and the porosity which became known as Archie's law.

4.4.2 Archie's law

One of the most successful empirical relations between the formation factor and porosity is known as Archie's law (Archie, 1942), which may be stated as

$$F = b\epsilon^{-m} \tag{4.9}$$

where b is a percolation coefficient and m is known as the cementing factor. By suitably adjusting the parameters b and m, remarkably good comparisons are obtained with measurements. In the original work, Archie (1942) took $b = 1$ and determined empirically that m varies between 1.8 and 2.0 for consolidated sandstones and $m \approx 1.3$ for clean unconsolidated sands. According to Keller (1982) the value of the parameter b varies from slightly less that one in classic detrital rocks to values as large as 3.5 in vesicular to tuffaceous rock. The parameter m varies from values as small as 1.3 in packed sand to values as large as 2.3 in tightly cemented classic rocks. Some additional values for these parameters according to Keller (1982) are presented in Table 4.1. In many instances b is simply taken as one leaving m as the only adjustable parameter. However, the cementing factor may still attain a large number of values depending on the nature of the material as may be illustrated by the data of Jackson *et al.* (1978).

Many models have been developed with the objective of explaining the success of Archie's law. For instance, Roberts and Schwartz (1985) confirmed that electrical conductivity and porosity may be approximated by a power law over a wide range of porosities. However, they used free scaling parameters to fit curves. Sen *et al.* (1981) briefly summarise certain aspects of capillary models, percolation theories and geologic features of the pore-space which are important in finding an expressions for Archie's law. They then propose a self-similar model where each rock unit consists of a spherical grain surrounded by other grains. Sen *et al.* (1981) obtained for Archie's law

$$F = \epsilon^{-1.5} \tag{4.10}$$

for essentially spherical particles. However, they also indicate that the exponent may be

different from 1.5 for different grain shapes. Their prediction compares very well with some experimental formation factors which they obtained for porous media comprised of fused glass beads with a porosity in the range of $0.026 \leq \epsilon \leq 0.4$. Lemaitre *et al.* (1988) obtained $m = 1.46$ for the formation factor in a binary mixture of spheres which does not differ much from the 1.5 in (4.10).

Table 4.1 Different forms of Archie's law ($F = b\epsilon^{-m}$) according to the rock lithology.

Description of rock	b	m
Weakly-cemented detrital rocks, such as sand, sandstone and some limestones, with a porosity range from 25 to 45%, usually Tertiary in age.	0.88	1.37
Moderately well cemented sedimentary rocks, including sandstones and limestones, with a porosity range from 18 to 35%, usually Mesozoic in age.	0.62	1.72
Well-cemented sedimentary rocks with a porosity range from 5 to 25%, usually Paleozoic in age.	0.62	1.95
Highly porous volcanic rocks with porosity in the range of 20 to 80%.	3.5	1.44
Rocks with less than 4% porosity, including dense igneous rocks and metamorphosed sedimentary rocks.	1.4	1.58

Wong *et al.* (1984) introduced a model consisting of a random resistor network on a simple cubic lattice from which they concluded that the scaling behaviour of both the conductivity and permeability of rocks are determined by the skewness of the pore-size distribution. They also performed measurements of electrical conduction in fused glass

beads and determined that (4.10) only yields adequate results for the porosity range $0.2 \leq \epsilon \leq 0.4$. For lower porosities they suggest that

$$F = \epsilon^{-2}. \tag{4.11}$$

It would appear as if $m = 2$ is the upper limit for the cementing factor when $b = 1$.

Besides Archie's law other types of relations have also been proposed to relate the formation factor to the porosity. Keller (1982) presents twenty different relations which were obtained by making use of geometrically deterministic pore structure models. According to Keller (1982) models with a non-deterministic or statistical description of pore geometries are more successful in predicting the formation factor.

4.4.3 Relation between formation factor and tortuosity

Many expressions for the hydrodynamic permeability contain the tortuosity as an explicit factor in addition to other geometric parameters of the porous structure, which include the porosity, an average pore diameter and the specific surface area (Scheidegger, 1974; Bear, 1972; Dullien, 1979). This lead to a large effort to determine the tortuosity from electrical methods in order to eliminate the tortuosity factor from permeability expressions or at least yield it a measurable parameter (Bear, 1972). However, in most of these analyses it is assumed that the flow paths taken by fluid particles are equivalent to those of the current flowing through the porous medium. As discussed in Section 2.7.2.2, recent calculations, for example Knackstedt and Zhang (1994), show the non-equivalence of fluid and electric transport. This supports the distinction which is made between the hydraulic tortuosity, χ or χ_h appearing in expressions for the permeability, and the electrical tortuosity χ_e.

Wyllie and Rose (1950) produced a relation between the formation factor, the porosity and the tortuosity, and in doing so they discarded the cementing factor in Archie's law as being only of qualitative value. According to Wyllie and Spangler (1952), this analysis seemed more realistic, since the formation factor is a parameter reflecting the influence of the pore geometry on electrolytic conduction through the pore system. Therefore, a relation between the formation factor and electrical tortuosity might give more physical insight into the transport of electric current than an empirically based relation such as Archie's law.

The influence of the porous medium on the flow of current has been ascribed to a number

of factors of which the most important are considered to be the reduced area available for transport and the increased path length available for charge transport (Wyllie and Spangler, 1952; Dullien, 1979). These influences have been modelled in a number of ways to relate the measurable formation factor to the porosity and tortuosity of the porous medium. One typical derivation of the relation between the formation factor and tortuosity by using the bundle of capillaries model of Comiti and Renaud (1989) is presented in Appendix A. Another approach is to consider the the resistance R_o of a homogeneous porous medium of length L and total cross-sectional area A_o saturated with a conducting fluid. For such a sample the resistance is be given by

$$R_o = \rho_o \frac{L}{A_o} \tag{4.12}$$

with ρ_o the resistivity of the saturated porous medium. In most models which relate the formation factor to the tortuosity it is argued that the resistance of the homogeneous porous medium saturated with conducting fluid may also be considered to be equal to the resistance of a volume of fluid of length L_e and area A_e, where $L_e > L$ and L_e is the average path length which an ion must travel through the porous medium (Wyllie and Rose, 1950; Wyllie and Spangler, 1952; Bear, 1972). According to this model the porous medium is actually viewed as a capillary of which each cross-section is equal to A_e and the total length of the tube is L_e. Thus the resistance of the saturated porous medium to the flow of current is

$$R_o = \rho_w \frac{L_e}{A_e} \tag{4.13}$$

where ρ_w is the resistivity of the electrolyte. According to (4.12) and (4.13)

$$\rho_w \frac{L_e}{A_e} = \rho_o \frac{L}{A_o} \tag{4.14}$$

from which it then follows (Bear, 1972) that

$$F = \frac{\rho_o}{\rho_w} = \frac{L_e}{L}\frac{A_o}{A_e}. \tag{4.15}$$

Different expressions for F have been obtained depending on the expression for A_e. For example, Wyllie and Rose (1950) and Wyllie and Spangler (1952) set $A_e \equiv A_f = \epsilon A_o$, which yields

$$F = \frac{L_e}{\epsilon L} = \frac{\chi}{\epsilon}. \tag{4.16}$$

Cornell and Katz (1953) proposed $A_e = \epsilon A_o \frac{L}{L_e}$, resulting in a formation factor of

$$F = \frac{1}{\epsilon}\left(\frac{L_e}{L}\right)^2 = \frac{\chi^2}{\epsilon}. \tag{4.17}$$

In this case provision is made for an additional path length and a reduced effective area. In all these cases it is also assumed that the flow paths for electric and fluid transport is equivalent and, therefore, it follows that $\chi = \chi_e$ in all these expressions. A number of additional relationships between the formation factor and tortuosity are given in, amongst others, Bear (1972) and Dullien (1979) where it is also indicated, similar to Walsh and Brace, that (4.17) seems to be the correct relation between formation factor and tortuosity.

As illustrated by Wyllie and Rose (1950) and Dullien (1979) the electrical flow is more sensitive to the cross-sectional area than fluid transport, and therefore, great care should be taken in assessing which effective area to incorporate into analyses of electric charge transport. This difference arises from the fact that the volumetric flow rate Q for fluid discharge along the x_1-coordinate in a capillary tube with uniform cross-section, A, is given by

$$Q = -\left(\frac{A^2}{12\pi}\right) p_{,1}$$

under a uniform pressure gradient of $p_{,1}$. On the other hand, should the tube be filled with an electric conductive fluid, the current may be expressed as

$$i = -\left(\frac{A}{\rho_w \pi}\right) V_{,1}$$

for a uniform electric potential gradient. Therefore, the viscous resistivity depends on the pore radius to the fourth power and the electrical resistivity to the radius squared (Wyllie and Rose, 1950; Wong *et al.*, 1984). Therefore, according to Dullien (1979), in a medium comprising both large and small pores, such as sandstones, the small pores contribute only negligibly to the permeability.

The sensitivity of current transport to the available area is closely related to an additional factor considered to influence the formation factor, namely the effect of constrictions in the channels. According to Dullien (1979) this effect greatly exceeds that of increased path length. He proposed that

$$\chi_e = \chi_h \delta \tag{4.18}$$

with δ a constriction factor which takes into account the special effects due to the convergent-divergent nature of the capillaries. This leads to a formation factor of

$$F = \frac{\chi_h \delta}{\epsilon}. \tag{4.19}$$

A constriction factor to account for the effect of constrictions in channels was also suggested by Petersen (1958; 1965) when considering diffusional transport in a capillary with periodic constrictions.

The effect of constrictions in pores on the electrical conductivity is illustrated by the formation factor of Avellaneda and Torquato (1991),

$$\frac{1}{F} = \frac{1}{U_o} \iiint_{U_f} \frac{V_{,i}}{E} \frac{V_{,i}}{E} dU \tag{4.20}$$

where $V_{,i}$ is the microscopic potential gradient, E is the magnitude of the electric field vector which implies that $V_{,i}/E$ is the normalised electric field in the pore-space. According to Revil and Cathles (1999), the distribution of the integrand in this equation acts as a weighted porosity and it gives less weight to pores which transmit little current. The electrical potential gradients are concentrated in the throats of the interconnected pore-space and, therefore, the throats contribute the most to $1/F$ as expressed in (4.20). This prompted Revil and Cathles (1999) to replace the porosity in the permeability as derived from a capillary model by $1/F$ which they consider to be a weighted porosity. As a matter of interest, Revil and Cathles (1999) consider Λ as a weighted length scale analogous to the length $2U_f/S_{fs}$ and replace this length with Λ to derive an expression for the permeability.

The formation factor of a homogeneous porous medium saturated with an electrolyte has also been analysed by Suman and Ruth (1993) and related to a number of geometric characteristics of the porous medium. A detailed discussion of their model is presented in Appendix C where it is indicated that the formation factor may be expressed in the present notation as

$$F = \frac{1}{\xi i_{(1)} L_{(1)}} \iiint_{U_f} j_1 dV + \frac{1}{\xi i_{(1)} L_{(1)} \rho_w} \iint_{S_{fs}} V \nu_1 dS. \tag{4.21}$$

In the derivation of (4.21) it is assumed that the macroscopic charge transport is in the x_1-direction, $i_{(1)}$ is the current in this direction, $L_{(1)}$ is the streamwise length of the

porous sample and the brackets in the subscripts indicate that the specific quantities are not vectors while ξ is the areosity,

$$\xi = \frac{A_e}{A_{o(1)}} \tag{4.22}$$

as defined in (2.49). In (4.22) $A_{o(1)}$ is the total area normal to the x_1-direction. According to Suman and Ruth (1993) and Hulin (1993), (4.21) clearly illustrates the various contributions to the formations factor. The first term on the right hand side corresponds to the decreased area in the direction of charge transport while the latter term corresponds to the voltage drop and charge flow normal to the macroscopic transport direction. According to Suman and Ruth (1993) this term is, therefore, closely related to the tortuosity of the system. An important feature of (4.21) is the areosity ξ appearing in the denominator of the factor by which each integral is multiplied.

On completion of the derivation of (4.21) Suman and Ruth (1993) introduce a number of RUC's which they consider to be building blocks of homogeneous porous medium. By repeating their RUC's the complete porous medium can be reconstructed. For homogenous porous media they obtain a formation factor of

$$F = \frac{\chi_e}{\xi} \tag{4.23}$$

where χ_e is an electrical tortuosity factor. According to Suman and Ruth (1993) the hydraulic and electrical tortuosities are not equivalent and, depending on the existence of multiple flow paths χ_e is not a simple relation between lengths, but it also depends on the area of the flow channels and the current in each channel.

4.5 Microscopic charge transport

In this section the balance equations for charge transport at the microscopic level are presented and briefly discussed. More emphasis is being put on the various assumptions for validity of Ohm's law at the microscopic level than on the derivation of the resulting equations. This study is restricted to solutions sufficiently dilute so that the solute species and their gradients do not interact. The solution might be an unionized solvent containing ionized electrolytes. Furthermore, any effect of an induced magnetic field on the charged particles is also considered negligible.

The various charged particles present in the electrolyte may be in motion which will lead to a flux of charged species through the system. The flux $N_{\alpha i}$ of species α is

$$N_{\alpha i} = c_\alpha v_{\alpha i} \tag{4.24}$$

where c_α is the molar concentration of species α and $v_{\alpha i}$ is its velocity. It is an average velocity for the species and not the velocity of individual molecules (Newman, 1973). For dilute solutions the molar flux contributions to each dissolved species from migration, diffusion and convection may be linearly superposed and is described by the Nernst-Planck equation

$$N_{\alpha i} = -z_\alpha u_\alpha \mathcal{F} c_\alpha V_{,i} - D_\alpha c_{\alpha,i} + c_\alpha v_i \tag{4.25}$$

(Probstein, 1989). Here z_α is the charge number of the charge species α which indicates the number of proton charges carried by an ion, $\mathcal{F}$ is Faraday's constant equal to the charge of one mole of singly ionized molecules, v_i is the mass averaged velocity of the solution and V is an externally applied electrostatic potential. The flux $N_{\alpha i}$ of species α, expressed in mol m^{-2} s^{-1}, is a vector quantity indicating the direction in which the species is moving and the number of moles going per unit time across a plane of unit area, oriented perpendicular to the flow of the species. An equivalent equation may be stated for the corresponding mass flux (Probstein, 1989).

The first term on the right hand side of (4.25) is referred to as the migration term and it is a characteristic of electrochemical systems or systems containing charged species (Newman, 1973). The quantity u_α appearing in (4.25) is called the mobility of an ion. When an electric field is applied to an electrolytic system cations in the solution are accelerated towards the negative pole of the field and anions to the positive pole. This acceleration is opposed by viscous drag which limits the maximum velocity to which the ions can be accelerated. This terminal velocity obtained with a unit electric field (1 V/m) is defined as the mobility of an ion. The mobility and diffusivity, D_α, of the charged species are related through the Nernst-Einstein equation. The quantity $z_\alpha \mathcal{F}$ is the charge per mole on a species. Multiplying it by the electric field gives the force per mole. Further multiplication by the mobility gives the migration velocity and finally multiplication by the concentration yields the contribution to the net flux due to migration in an electric field.

The second and third terms on the right hand side of (4.25) are the usual terms required to describe nonelectrolytic systems and captures the diffusion of the species from regions

of high concentration to regions of lower concentration. The three terms on the right hand side of (4.25) thus represent three mechanisms of mass transfer, namely migration of a charged species in an electric field, molecular diffusion due to a concentration gradient and convection due to the bulk motion of the fluid.

Due to the motion of the charged species, there will be a current i, which is defined as the unit charge that moves through a unit area per unit time (Kip, 1969). The current is a scalar quantity which is related to the current density j_i, measured in ampere per square metre, by the equation

$$i = \iint_A j_i \nu_i dA \tag{4.26}$$

where dA is an element of the cross-sectional area A and ν_i is a normal vector on the area element. The integral is taken over the cross-section through which the current is calculated. When the current density is uniform (4.26) may be integrated to give

$$i = j_i \nu_i A \tag{4.27}$$

and when the area is taken perpendicular to the current density, this becomes

$$i = jA \tag{4.28}$$

where A is the cross-sectional area of the conductor. Expressed as a current density j_i, the flow of charge (Newman, 1973) is

$$j_i = \mathcal{F} \sum_\alpha z_\alpha N_{\alpha i} \tag{4.29}$$

$$= -\mathcal{F}^2 \sum_\alpha z_\alpha^2 u_\alpha c_\alpha V_{,i} - \mathcal{F} \sum_\alpha z_\alpha D_\alpha c_{\alpha,i} + \mathcal{F} v_i \sum_\alpha z_\alpha c_\alpha. \tag{4.30}$$

Here the current density, expressed in amperes per unit area, is made up of contributions from the applied electric field, the concentration gradients and the convection of charge. It is also important to note that this expression is strictly valid only in dilute solutions. The current density may also be obtained on considering the equivalent mass fluxes (Newman, 1973; Probstein, 1989; Masliyah, 1994).

In solutions which are electrically neutral,

$$\sum_\alpha z_\alpha c_\alpha = 0 \tag{4.31}$$

and the convective contribution to the current density in (4.30) vanishes. This is equivalent to stating that the bulk motion of a fluid with no charge density can contribute nothing to the current density. This is usually true for aqueous electrochemical solutions except in thin regions near charged boundaries. These regions are termed electric double layers or Debye sheaths and have thickness on the order of 1 to 10 nanometres. Should the existence of electric double layers be incorporated, the electric field is coupled with the fluid mechanics through the Lorentz body force

$$f_{Ei} = \rho_E E_i$$

where the charge density is given by $\rho_E = \mathcal{F}\sum_\alpha z_\alpha c_\alpha$, which must be added to the momentum transport equation (Probstein, 1989). The double layer is important when very small charged particle interactions and charged surface phenomena are considered, but is generally unimportant with respect to bulk flow characteristics and will be considered negligible for the remainder of this study. Furthermore, if concentration gradients are also considered absent then the second term on the right hand side of (4.30) also disappears. In conductivity measurements an alternating current is used so that concentration differences will not build up and also to reduce polarization at the electrodes (Newman, 1973). With these assumptions the current density may then be expressed as

$$j_i = \mathcal{F} v_i \sum_\alpha z_\alpha c_\alpha. \tag{4.32}$$

Since the negative gradient of the electrostatic potential is equal to the electric field E_i, that is

$$E_i = -V_{,i}. \tag{4.33}$$

The velocity of migration of an ion which is proportional to the charge on the ion and the electric field may be expressed as

$$v_{\alpha i} = -z_\alpha u_\alpha \mathcal{F} V_{,i}. \tag{4.34}$$

This equation illustrates that when a gradient in electrostatic potential is applied to the solution an electric force, $-z_\alpha \mathcal{F} V_{,i}$ is exerted on each ion species. The force per mole exerted on a charged particle is equal to the magnitude of the particle charge

multiplied by the sign of the charge and the electric field. The application of the electric field therefore results in unequal electrical forces on the different species as a result of differences in the species charge, which is negative on one species and positive on another. The motion of these charged species then gives rise to a current density, j_i which is the sum of the currents carried by the two kinds of ions. It is obtained by multiplying the ionic velocities by the concentrations and the charges and adding to yield

$$j_i = \mathcal{F} \sum_{\alpha} z_\alpha c_\alpha v_{\alpha i}. \tag{4.35}$$

In view of the assumption of electro neutrality expressed in (4.31) and for systems where the magnitudes of the charge numbers are equal, (4.32) and (4.35) may be combined to express the current density as

$$j_i = -\sigma_w V_{,i} = -\frac{1}{\rho_w} V_{,i} \tag{4.36}$$

where

$$\sigma_w = \mathcal{F}^2 \sum_{\alpha} z_\alpha^2 u_\alpha c_\alpha. \tag{4.37}$$

Equation (4.36) is generally referred to as Ohm's law in point form (Probstein, 1989; Newman, 1973; Popović, 1973), but in the context of porous media transport it is the microscopic form of Ohm's law. The coefficient σ_w in this relationship between the current density and the gradient of the potential is a transport property of the solution known as the conductivity with units of ohm^{-1} m^{-1}. It is per definition equal to the inverse of the resistivity ρ_w (Kip, 1969).

Ohm's law may be illustrated by considering an aqueous solution of cupric sulfate placed between two copper electrodes. The process consists of the dissolution of copper at the positive electrode, the anode,

$$Cu \rightarrow Cu^{++} + 2e^-$$

the passage of cupric ions through the solution and the deposition of copper at the negative electrode, the cathode (Newman, 1973). In the solution, cupric sulfate will dissociate into charged cupric ions Cu^{++} and sulfate ions $SO_4^{=}$, which are driven through the solution by the electric field. The cupric ions are driven toward the negative electrode

and the sulfate ions toward the positive electrode. In this case $z_+ = 2$, $z_- = -2$ and the concentrations c_+ and c_- can be identified with the stoichiometric concentration of cupric sulfate. Furthermore, since the solution is electrically neutral, that is, the charges in the cations are balanced by the charges on the anions, the ionic concentrations follow from (4.31) and are related by

$$z_+c_+ + z_-c_- = 0. \tag{4.38}$$

In this case (4.35) may be written as

$$j_i = z_+c_+\mathcal{F}\, v_{+i} + z_-c_-\mathcal{F}\, v_{-i} \tag{4.39}$$

where the positive ions are denoted by the subscript (+) and the negative ions by the subscript (–).

Equations (4.34), (4.39) and (4.38) may be combined to yield

$$j_i \;=\; z_+c_+\mathcal{F}(v_{+i} - v_{-i}) \;=\; -z_+c_+\mathcal{F}^2(z_+u_+ - z_-u_-)V_{,i}. \tag{4.40}$$

The conductivity may thus be expressed as

$$\sigma_w \;=\; \mathcal{F}^2\sum_\alpha z_\alpha^2 u_\alpha c_\alpha \;=\; z_+c_+\mathcal{F}^2(z_+u_+ - z_-u_-) \tag{4.41}$$

where the latter step follows from the fact that $z_+ = z_-$ (Popović, 1973). Consequently (4.40) may be viewed as an illustration of Ohm's law. Since the concentration of the solution is considered uniform, both cupric ions and sulfate ions contribute to the conduction mechanism in the solution. However, only the cupric ions enter into the electrode reaction and pass through the electrode-solution interface. Thus, if the sulfate ions are carrying part of the current in the solution but are not being passed through the electrode boundary, they must accumulate near the anode and become depleted near the cathode. This brings up the consideration of concentration variations and diffusion. However, in conductivity measurements this can be avoided by applying an alternating current to the solution (Newman, 1973).

An alternative expression for Ohm's law may be obtained by considering any conductor of length L and cross-sectional area A perpendicular to the applied electrostatic potential. For such a conductor it follows that

$$V_{,i}\hat{\nu}_i \;=\; \frac{V_{hl}}{L} \tag{4.42}$$

with $V_{hl} = V_h - V_l$ being the potential difference between any two points of the conductor a distance L apart. From (4.36) and (4.28) it also follows that

$$i = \frac{V_{hl} A}{\rho_w L} \tag{4.43}$$

which implies that

$$V_{hl} = \frac{i\rho_w L}{A} = j\rho_w L = iR_w \tag{4.44}$$

where $i = jA$ is the current in the conductor and R_w is the resistance of the conductor. Equations (4.36) and (4.44) are the main contributions of this section, since they illustrate different forms of Ohm's law which is assumed to govern the charge transport at the microscopic level.

4.6 Macroscopic charge transport

Transport phenomena within porous media are only amendable to measurement at the macroscopic level and requires that the microscopic balance laws be transformed to the macroscopic level. In the present analysis this is achieved by invoking the volumetric averaging approach as presented in Appendix B and outlined in detail in, amongst others, Hassanizadeh and Gray (1979), Bachmat and Bear (1986) and Bear and Bachmat (1991). Accordingly, the microscopic form of Ohm's law may be averaged volumetrically over a Representative Elementary Volume (REV) of the porous medium to derive a macroscopic balance law for charge transport. As discussed in Section 2.4 the specific representative elementary volume over which the average is taken is defined as an elementary control volume comprising both fluid and solid material which are present in the correct locally averaged proportions. This will ensure that the averaged quantities are single-valued functions of the location and of time, independent of the size of the REV.

The averaged quantities are related to the microscopic quantities through averaging operators. In addition to defining the operators, a number of averaging rules have also been established in Appendix B for transforming microscopic balance equations to the macroscopic level. These rules are presented in Section 2.4.2 and according to averaging Rule 4 in Table 2.2 the phase average of a spatial derivative is related to the average

of the gradient through the spatial averaging theorem which may be written as

$$\langle \phi_{jkl...,i} \rangle = \epsilon \langle \phi_{jkl...} \rangle^f_{,i} + \frac{1}{U_o} \iint_{S_{fs}} \phi_{jkl...} \nu_i \, dS + \langle \phi_{jkl...} \rangle^f \epsilon_{,i} \tag{4.45}$$

where S_{fs} is the fluid-solid interface within the REV and ν_i is an outwardly directed unit normal vector on the differential area dS (Bear and Bachmat, 1991, p121). If the porous medium is homogeneous with respect to the porosity, as is assumed in this study, the porosity gradient vanishes from this expression.

The macroscopic charge transport equation is obtained by volume averaging (4.36) over an REV to obtain

$$\langle j_i \rangle = -\left\langle \frac{1}{\rho_w} V_{,i} \right\rangle \tag{4.46}$$

where $\langle j_i \rangle$ is the macroscopic phase average current density. For a constant resistivity and porosity, application of (4.45) to (4.46) yields

$$\langle j_i \rangle + \frac{\epsilon}{\rho_w} \langle V \rangle^f_{,i} + \frac{1}{\rho_w U_o} \iint_{S_{fs}} V \nu_i \, dS = 0. \tag{4.47}$$

During the volume averaging process certain information concerning the microscopic configuration of interphase boundaries and the actual variations of quantities within each phase is lost. The macroscopic effects of these factors are still retained in the form of new variables which arise through the course of the averaging, such as the surface integral in (4.47). This term accounts for the decrease in current transport due to the geometry and the type and degree of connectivity of the porous system and it is related to the tortuosity of the porous domain (Suman and Ruth, 1993). One of the prime concerns of this study is to write this surface integral in terms of measurable parameters. This equation is the final conclusion of this section and for further analysis of the surface integral some of the information lost during the averaging process must firstly be recaptured and forms the subject of the next section.

4.7 Geometric pore-scale modelling

The secondary modelling necessary for closure of the macroscopic equation (4.47) is provided here by consideration of a Representative Unit Cell (RUC) as introduced

by Du Plessis and Masliyah (1988) and discussed in Section 3.5. Accordingly, the information regarding the porous microstructure lost during the averaging process is recaptured and the transport phenomenon occurring within the porous material may then be approximated within the RUC.

In this chapter, consideration is given to electric charge transport which takes place through three types of homogeneous materials, namely prismatic fibre bundles where the macroscopic direction for current flow is perpendicular to the longitudinal axes of the prismatic arrangement, through foamlike materials and through granular porous media. In each case the transport is considered for both the isotropic and anisotropic cases. A number of rectangular anisotropic RUC's have already been developed and introduced in Sections 3.7.1, 3.9.3 and 3.10.1 for the these three types of porous environments. It was also indicated that in the limit of isotropy the anisotropic RUC's reduce to those introduced by Du Plessis and Masliyah (1988) and Du Plessis *et al.* (1994) for an isotropic foamlike material, while an RUC for a two-dimensional prismatic bundle is presented in Du Plessis (1991). The average geometry of a granular porous medium which is rigid, stationary and locally isotropic with respect to average geometric properties was modelled by Du Plessis and Masliyah (1991) and Du Plessis (1994). A summary of these three types of isotropic RUC's is also presented by Du Plessis and Diedericks (1997).

In addition to the general geometric features of an RUC discussed in Section 3.5, a number of features specifically related to transport through the RUC may be recapped. Firstly, the duct sections, or equivalently the solid material, are arranged in such a manner that there is no lateral exchange of charge or fluid with neighbouring RUC's, but the fluid or charge carriers which are forced through an RUC is maximally displaced laterally within the cell before it exits. This implies that internally the relative positioning of material is subjected to both maximal staggering and maximum interconnection of duct sections. Although the connectivity of the void space of the materials represented by the various RUC's may differ, it is implicitly assumed in the present model that the existence of dead-end pores is prohibited and transport processes are not limited by a percolation threshold. For coherence of the model it is also required that the hypothetical arrangement of duct sections in neighbouring RUC's be incorporated for adequate analysis of any particular transport phenomenon. It is also important to note that the fluid-fluid connections or pore openings on all the sides of an RUC are the effective cross-sectional fluid areas for transport in a particular direction and these are defined in (3.28). In all the RUC's any cross-sectional area perpendicular to a channel yields the same effective cross-sectional area for transport in that particular direction. In all cases it is also assumed that one channel section may always be orientated along the

direction of macroscopic fluid or charge transport. This macroscopic transport direction is denoted by the unit vector $\widehat{\nu}_i$ and is referred to as the *streamwise* direction.

With regard to the transport of charge carriers through an RUC, the following may be noted. Due to the assumption of maximum staggering and since each channel section is rectangular without constrictions, the total void volume is available for charge transport. This implies that the hydraulic flow lines for fluid transport are equivalent to the electrical flow lines. It is therefore not possible to distinguish between hydraulic and electrical tortuosity in the RUC-model. Nevertheless, although the two types of tortuosities are considered to be equal, deterministic expressions for the resistivity appearing in Ohm's law and the formation factor are derived. These predictions are compared to measurements to assess the success of the modelling approach.

4.8 Channel average current density

In Section 2.7.5 a relation was derived between different macroscopic transport fluxes, namely the intrinsic phase average flux, the phase average flux and the streamwise channel average flux. In an RUC the actual flux of an extensive quantity in the channels are approximated by referring to the channel average flux which in turn is related to the macroscopic transport fluxes via the lineality tensor. The derivation in Section 2.7.5 is applicable to the transport of a general extensive quantity which is indicated by Γ. Should Γ be equal to the molar quantity of a specific chemical species α in an electrolyte, then γ represents the molar concentration c_α of the species and from (4.24) and (2.65) it follows that

$$\widetilde{n}_{\gamma i} = c_\alpha v_{\alpha i} = N_{\alpha i}. \tag{4.48}$$

The microscopic velocity $v_{\alpha i}$ corresponds to the microscopic velocity of the charged α-particles. It then follows from (2.81) that

$$\langle N_{\alpha i} \rangle = \epsilon \langle N_{\alpha i} \rangle^f = \epsilon \langle N_{\alpha m} \rangle \mathcal{L}_{mi} \tag{4.49}$$

which is a relationship between the various fluxes of a specific charged species. In this case the electric lineality tensor for a specific species is given by

$$\mathcal{L}_{ij} = \frac{1}{U_f} \iiint_{U_f} \widetilde{\nu}_i \widehat{\nu}_j \, dV \tag{4.50}$$

where $\tilde{\nu}_i$ is a unit tangent vector to the flux line at each point and $\hat{\nu}_i$ is a unit vector indicating the macroscopic flux direction. It has to be noted that (4.49) is applicable to any molecular diffusion process.

Since the current density is the quantity which is generally deduced from measurements, it is important to obtain a relation similar to (4.49) for the different current densities in stead of the flux of each charged species. For instance, from (4.49) and the fact that z_α is constant for each species, it follows that

$$\begin{aligned}\langle j_1 \rangle &= \frac{1}{U_o}\iiint_{U_f} j_i \, dU \\ &= \frac{1}{U_o}\iiint_{U_f} \mathcal{F}\sum_\alpha z_\alpha N_{\alpha i} \, dU \\ &= \mathcal{F}\sum_\alpha \frac{z_\alpha}{U_o}\iiint_{U_f} N_{\alpha i} \, dU \\ &= \mathcal{F}\sum_\alpha \left(z_\alpha \langle N_{\alpha i}\rangle\right). \end{aligned} \tag{4.51}$$

By replacing $\langle j_i \rangle$ with $\langle j_i \rangle^f$ and U_o with U_f in the above derivation it may be shown that

$$\langle j_i \rangle^f = \mathcal{F}\sum_\alpha \left(z_\alpha \langle N_{\alpha i}\rangle^f\right). \tag{4.52}$$

Therefore, if (4.49) is multiplied by $\mathcal{F} z_\alpha$ and summed over all species then

$$\langle j_i \rangle = \epsilon \langle j_i \rangle^f. \tag{4.53}$$

To extend (4.53) to include the channel average current density, it is necessary to introduce one other assumption which states that

- the flow lines for the different species are equivalent and these lines are also equivalent to the flow lines of the current density.

This assumption seems reasonable considering that the current density is a response to the transport of all the different species and all the species should make equal use of the available pore-space. The consequences of this assumption are that the effective transport volume and lineality tensor for each species and for the current density are equal, that is

$$\hat{U}_{\alpha\mathcal{L}} = \hat{U}_{f\mathcal{L}} \qquad \text{and} \qquad \mathcal{L}_{\alpha ij} = \mathcal{L}_{ij}. \tag{4.54}$$

The channel average current density is related to the channel average flux of α-species through the relation

$$\begin{aligned}
\overline{j}_i \equiv \langle j_i \rangle^c &= \frac{1}{\widehat{U}_{f\mathcal{L}}} \iiint_{U_f} j_i \, dU \\
&= \frac{1}{\widehat{U}_{f\mathcal{L}}} \iiint_{U_f} \mathcal{F} \sum_\alpha (z_\alpha N_{\alpha i} \, dU) \\
&= \mathcal{F} \sum_\alpha \left(\frac{z_\alpha}{\widehat{U}_{f\mathcal{L}}} \right) \iiint_{U_f} N_{\alpha i} \, dU \\
&= \mathcal{F} \sum_\alpha \left(\frac{z_\alpha}{\widehat{U}_{\alpha\mathcal{L}}} \right) \iiint_{U_f} N_{\alpha i} \, dU \\
&= \mathcal{F} \sum_\alpha (z_\alpha \langle N_{\alpha i} \rangle^c) \, .
\end{aligned} \tag{4.55}$$

Therefore, if (4.49) is multiplied by $\mathcal{F} z_\alpha$ and summed over all species then it also follows that

$$\mathcal{F} \sum_\alpha z_\alpha \langle N_{\alpha i} \rangle = \epsilon \mathcal{F} \sum_\alpha (z_\alpha \langle N_{\alpha m} \rangle^c \mathcal{L}_{\alpha m i}) \tag{4.56}$$

which yields

$$\langle j_i \rangle = \epsilon \mathcal{F} \sum_\alpha (z_\alpha \langle N_{\alpha m} \rangle^c \mathcal{L}_{m i}) \tag{4.57}$$

where use was made of (4.51). By using (4.55), this equation becomes

$$\langle j_i \rangle = \epsilon \mathcal{F} \overline{j}_m \mathcal{L}_{m i} \tag{4.58}$$

and by combining (4.53) and (4.58), it follows that

$$\langle j_i \rangle = \epsilon \langle j_i \rangle^f = \epsilon \overline{j}_m \mathcal{L}_{m i} \tag{4.59}$$

where a notational simplification was introduced, namely $\langle j_i \rangle^c \equiv \overline{j}_i$. During charge transport through an electrolytically saturated porous medium the microscopic flow of the charged particles may be comparable to interstitial plug flow. Therefore, the channel average current density may then be considered to be a fairly accurate estimate of the actual microscopic current density.

4.9 Charge transport and formation factor

In this section the RUC's introduced in Chapter 3 for anisotropic prismatic bundles, foamlike porous media and granular materials are used to solve the fluid-solid surface integral term in (4.47). By using the results of the closure modelling the macroscopic form of Ohm's law and the formation factor are obtained for each idealised type of material. On completion of the modelling concerning anisotropic materials certain simplifications are introduced to obtain the isotropic limit of the results.

The basic idea behind the closure modelling is that the surface integral in (4.47) is performed over the fluid-solid surface sections of the transverse channels which have normal vectors in the x_1-direction. It is assumed that the potential is uniform on each surface section which implies that on completion of the integration, (4.47) is proportional to the voltage difference across the transverse channels multiplied by the area of a transverse surface section. To write the potential difference as a potential gradient similar to (4.42) it is necessary to make an assumption regarding the distance between the high and low voltages across the channel. Since it is assumed that the potential is uniform on each surface section it seems appropriate to take as this distance the distance by which the transverse surface sections are staggered with regard to each other. This distance, $L_\perp$ is equal to the distance separating the centroid of the two parallel plates over which the integration in (4.47) is performed.

4.9.1 Anisotropic two-dimensional prismatic bundle

4.9.1.1 Geometric relations and the channel average current density

Two-dimensional crossflow through an anisotropic tube bundle, which resembles a structure of fibres was formerly considered in Section 3.10. An RUC for the anisotropic prismatic bundle is illustrated in Figure 3.17 and a number of geometric relations have also been introduced in Section 3.10.1. Of particular relevance is the component of the lineality tensor for flow in the x_1-direction,

$$\begin{aligned} \mathcal{L}_{11} &= \frac{1}{U_f}\iiint_{U_f} \tilde{\nu}_1\hat{\nu}_1\, dU \\ &= \frac{A_{p(1)}d_{(1)}}{U_f} \\ &= \frac{d_{p(2)}d_{(1)}}{\epsilon d_{(1)}d_{(2)}} \end{aligned} \tag{4.60}$$

and the effective streamwise volume

$$\begin{aligned}\widehat{U}_{f\mathcal{L}} &= \iiint_{U_f} \widetilde{\nu}_m \widehat{\nu}_m \, dU \\ &= A_{p(1)} d_{(1)} \\ &= d_{p(2)} z d_{(1)}. \end{aligned} \tag{4.61}$$

For this particular arrangement of solid material within the RUC illustrated in Figure 3.17, the distance by which the transverse parallel plates are staggered is

$$L_\perp = d_{p(2)}. \tag{4.62}$$

If the macroscopic flow of charge is in the x_1-direction then it follows from (4.59) and (4.60) that

$$\begin{aligned}\overline{j}_1 &= \frac{\langle j_1 \rangle}{\epsilon \mathcal{L}_{11}} \\ &= \left(\frac{d_2}{d_{p(2)}} \right) \langle j_1 \rangle . \end{aligned} \tag{4.63}$$

Since the solid is non-conductive the current in the streamwise channel, i, is equal to that in the transverse direction and may be used to approximate the average current density in the transverse channel, $j_\perp$. It then follows with application of (4.28) to each channel that

$$j_\perp = \frac{d_{p(2)}}{d_{p(1)}} \overline{j} \tag{4.64}$$

since the area of the transverse channel differs from that of the channel in the macroscopic transport direction. Here $j_\perp$ is the magnitude of the current density in the transverse channel and $\overline{j}$ is the magnitude of the channel average current density.

4.9.1.2 Interstitial transport modelling

Ohm's law and the formation factor for this type of porous medium are obtained by solving the surface integral in (4.47). In analysing this surface integral it is apparent that the relevant fluid-solid surface normal to the macroscopic transport direction which

contributes to the potential integral is given by $A_{fs} = d_{s(2)}z$. Therefore, by utilising (4.36) and the geometric relations of the RUC, it follows that

$$\begin{aligned}\frac{1}{\rho_w U_o}\iint_{S_{fs}} V\nu_1\, dS &= \frac{(V_h - V_l)A_{fs}\,\widehat{\nu}_1}{\rho_w U_o} \\ &= \frac{j_\perp A_{fs} L_\perp\,\widehat{\nu}_1}{U_o} \\ &= \frac{d_{p(2)}d_{(2)}\,\langle j_1\rangle}{d_{p(1)}d_{p(2)}}\frac{d_{s(2)}z d_{p(2)}}{d_{(1)}d_{(2)}z}.\end{aligned} \tag{4.65}$$

From (4.47) and (4.65) it can be shown that the macroscopic form of Ohm's law for the prismatic bundle is given by

$$\langle j_1\rangle = -\frac{\epsilon}{\rho_w}\left(1 + \frac{d_{p(2)}d_{s(2)}}{d_{p(1)}d_{(1)}}\right)^{-1}\langle V\rangle^f_{,1}. \tag{4.66}$$

From a comparison of (4.66) with (4.1) it follows that

$$\rho_o = \frac{\rho_w}{\epsilon}\left(1 + \frac{d_{p(2)}d_{s(2)}}{d_{p(1)}d_{(1)}}\right). \tag{4.67}$$

The formation factor for the prismatic bundle follows from (4.7) and (4.67), and it is given by

$$F = \frac{1}{\epsilon}\left(1 + \frac{d_{p(2)}d_{s(2)}}{d_{p(1)}d_{(1)}}\right). \tag{4.68}$$

According to (4.68) the formation factor is expressed in terms of the physical characteristics of the porous medium. The formation factor may also be expressed as

$$\begin{aligned}F &= \frac{1}{\epsilon}\left(\frac{d^2_{p(1)}d_{p(2)}d_{(1)}z + d^2_{p(2)}d_{s(2)}d_{p(1)}z}{d^2_{p(1)}d_{p(2)}d_{(1)}z}\right) \\ &= \frac{1}{\epsilon}\left(\frac{d^2_{p(1)}\widehat{U}_{f\mathcal{L}} + d^2_{p(2)}d_{s(2)}d_{p(1)}z}{d^2_{p(1)}\widehat{U}_{f\mathcal{L}}}\right)\end{aligned} \tag{4.69}$$

where $\widehat{U}_{f\mathcal{L}}$ is the effective streamwise volume expressed in (4.61) and the transverse fluid volume is $U_f - \widehat{U}_{f\mathcal{L}} = d_{s(2)}d_{p(1)}z$. It is interesting to note from this expression

that only in the limiting case where the two channel sections are of equal width, that is when $d_{p(1)} = d_{p(2)}$, is the formation factor given by

$$F = \frac{\chi_{11}}{\epsilon}. \tag{4.70}$$

Furthermore, according to this model the formation factor is only related to the tortuosity and not to the square of the tortuosity.

4.9.2 Isotropic two-dimensional prismatic bundle

For an isotropic fibre bed the RUC still contains a prism of length z, but it has a square cross-sectional area. The RUC for the isotropic case may be deduced from the anisotropic RUC provided that the simplifications presented in Table 3.7 are introduced. According to the RUC for the isotropic two-dimensional prismatic bundle illustrated in Figure 4.1, the porosity and void volume are related by

$$U_f = \epsilon U_o = \epsilon z d^2. \tag{4.71}$$

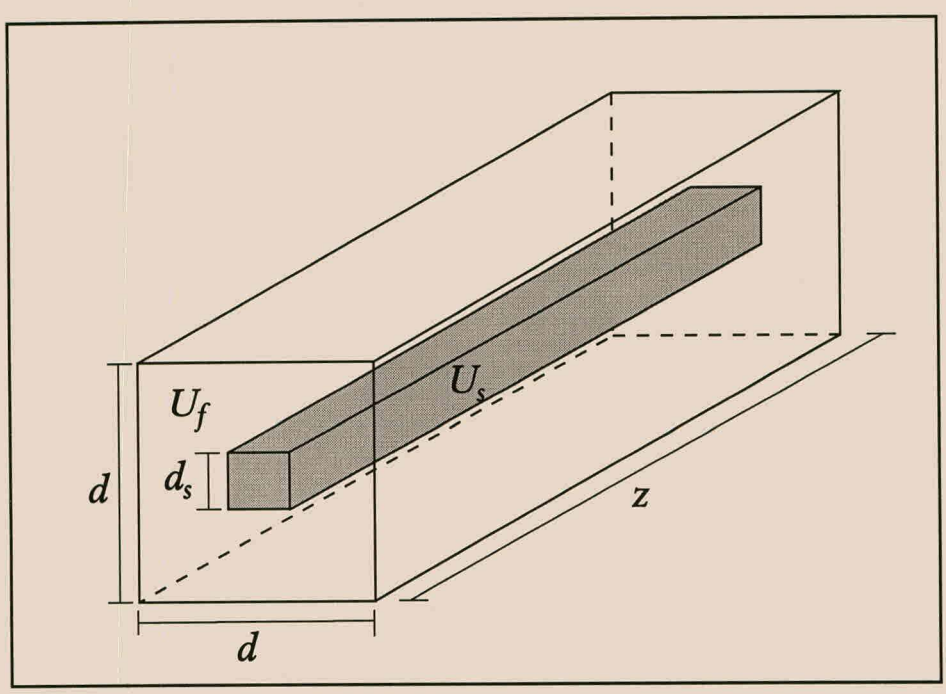

Figure 4.1. Rectangular prismatic RUC for an isotropic unidirectional fibre bed.

Since the square sides of the prism within the RUC are of length d_s, the volume of solid material is given by

$$U_s = d_s^2 z = (1-\epsilon) z d^2 \tag{4.72}$$

for a prism of length z. The effective channel areas may be expressed (Du Plessis, 1991) as

$$A_p = d_p z = \frac{\epsilon z d}{\chi}. \tag{4.73}$$

The equivalent hydraulic and electric tortuosities,

$$\chi = \frac{U_f}{A_p d} = \frac{d_\chi}{d}$$

may in this case also be considered to be the quotient of the linear displacement d and the total tortuous path length d_χ, which is available within the RUC for flow under the constant cross-section, A_p. According to Du Plessis (1991) it may be expressed as

$$\chi = \frac{\epsilon}{1-\sqrt{1-\epsilon}} = 1+\sqrt{1-\epsilon}. \tag{4.74}$$

This function is graphically presented in Figure 4.2.

According to these simplifications the surface integral in (4.65) may be written for the isotropic case as

$$\frac{1}{\rho_w U_o} \iint_{S_{fs}} V \nu_1 \, dS = \sqrt{1-\epsilon} \langle j_1 \rangle \tag{4.75}$$

where use was made of (4.72). From (4.66) and (4.72), it then follows that Ohm's law is given by

$$\langle j_1 \rangle = -\frac{\epsilon}{\rho_w} \left(\frac{1}{1+\sqrt{1-\epsilon}} \right) \langle V \rangle_{,1}^f. \tag{4.76}$$

The formation factor for the isotropic bundle is thus given by

$$F = \frac{\chi}{\epsilon} \tag{4.77}$$

which is graphically illustrated in Figure 4.3.

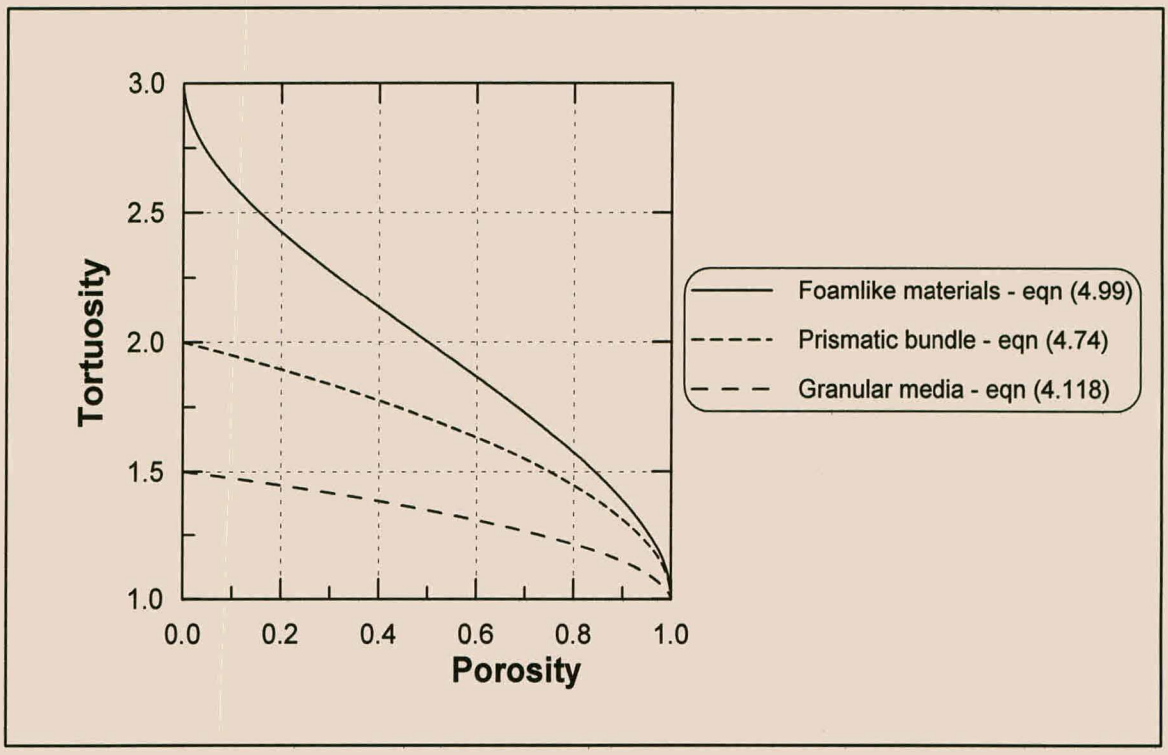

Figure 4.2. Tortuosity as a function of porosity for different types of isotropic porous media.

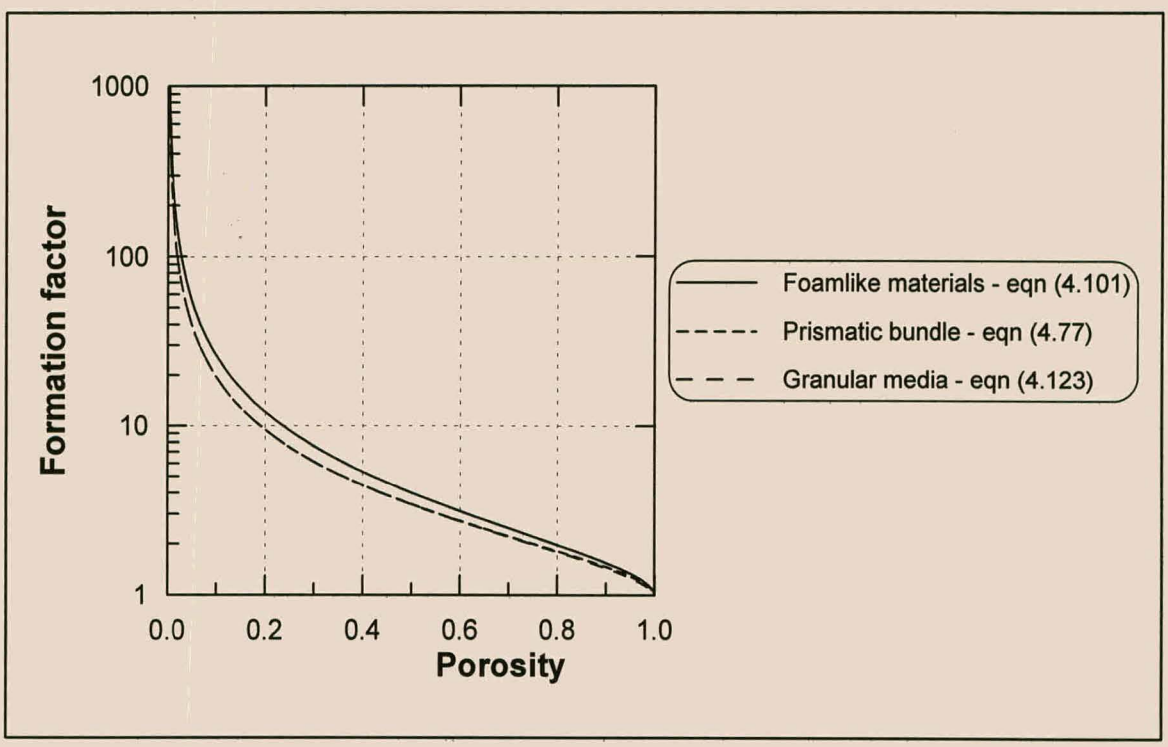

Figure 4.3. Formation factor as a function of porosity for different types of isotropic porous media.

4.9.3 Electrical conduction in anisotropic foamlike materials

4.9.3.1 General

In Section 3.7.1, two types of anisotropic foams have been introduced, namely foams of Type A and foams of Type B. In Type A foams the different channels may vary in size, but the solid material consists of uniform strands and in foams of Type B the pores are of equal area but their length as well as the dimensions of the solid material may differ. An RUC for a Type A foam is presented in Figure 3.4 while an RUC for a Type B foam is given in Figure 3.5. In this section, the electrical conduction is assessed in both of these two types of foamlike materials. In contrast to the modelling of the fluid transport presented in Section 3.7.2 where it was necessary to consider the flow through a number of RUC's, for the analysis of charge transport the use of one RUC for each type of foam is sufficient. The modelling procedure is illustrated by referring to the RUC's presented in Figures 3.6 and 3.7 for foams of Type A and foams of Type B, respectively.

Attention can now be focussed on the surface integral in (4.47) which represents the voltage drop over the transverse channels normal to the discharge direction. Since this voltage drop is responsible for transverse charge flow, the surface integral term is responsible for local current flow normal to the macroscopic streamwise direction as also illustrated by Suman and Ruth (1993). According to the microscopic form of Ohm's law as presented in (4.36), the voltage drop $V_{,i}$ is applied uniformly across the area A for the total length of the conductor. However, although the fluid-solid surfaces which contribute to the surface integral in (4.47) are parallel to the channel sections, which in the RUC are viewed as a local conductors, it is considered that the differences in potential transversely along a channel cause a current to flow in the particular transverse channel. The transverse distance over which this voltage drop is applied is modelled as being equal to the distance by which the two parallel plates over which the integral is performed are staggered. For the channel in the x_2-direction this distance is indicated by $L_{\perp(2)}$ while $L_{\perp(3)}$ indicates the staggered distance in the channel in the x_3-direction over which the microscopic potential difference is assumed to be applied. This modelling approach and notation are applicable to both types of foams.

Therefore, with reference to Figures 3.6 and 3.7 as well as to (4.44) it follows for both types of foams that

$$\begin{aligned} \frac{1}{\rho_w U_o}\iint_{S_{fs}} V\nu_1\, dS &= \frac{1}{\rho_w U_o}\left(V_{h(3)}G - V_{l(3)}D + V_{h(2)}I - V_{l(2)}E\right) \\ &= \frac{1}{U_o}\left(j_{\perp(3)}GL_{\perp(3)} + j_{\perp(2)}IL_{\perp(2)}\right) \end{aligned} \tag{4.78}$$

where $V_{h(2)}$ and $V_{h(3)}$ indicate the high voltage end of the channels in the x_2- and x_3-directions, respectively while $V_{l(2)}$ and $V_{l(3)}$ represent the lower voltages in the two different channels. The fluid-solid surfaces over which the integration is performed are denoted by G, D, I and E and these surfaces are illustrated in Figure 3.6 for foams of Type A and they are given in Figure 3.7 for foams of Type B. The magnitudes of the current densities in each of the channel sections are denoted by $j_{\perp(2)}$ and $j_{\perp(3)}$, respectively. It may be noted that each of these current densities are associated with different vectors representing the current densities in each of the transverse channels. Equation (4.78) is applicable to foams of Type A as well as to foams of Type B. However, for further analysis it is necessary to consider each type of foam individually.

4.9.3.2 Foams of Type A

The average geometry of a foam of Type A has been modelled in Section 3.7.1 where two RUC's for this foam have been introduced. In addition to the geometric features previously presented in Section 3.7.1, the fluid or void volume U_f may also be expressed as

$$U_f = A_{p(1)}d_{(1)} + d_s d_{p(2)} d_{p(1)} + d_s d_{p(3)} d_{p(1)} \tag{4.79}$$

from which it follows that

$$d_s(d_{p(2)} + d_{p(3)}) = \frac{U_f - A_{p(1)}d_{(1)}}{d_{p(1)}}. \tag{4.80}$$

The two parallel plates in the channel in the x_2-direction which are perpendicular to the streamwise direction are not transversely aligned, but their centroids are a distance $d_{p(2)}$ apart. It is considered that this is the distance between the higher and lower local voltages in the channel in the x_2-direction. It thus follows that

$$L_{\perp(2)} = d_{p(2)} \tag{4.81}$$

and similarly for the channel in the x_3-direction

$$L_{\perp(3)} = d_{p(3)}. \tag{4.82}$$

According to the RUC for foams of Type A presented in Figure 3.6, the fluid-solid surface sections G and I are expressed as

$$G = d_{p(2)}d_s \qquad \text{and} \qquad I = d_{p(3)}d_s \tag{4.83}$$

respectively and it may be noted that in foams of Type A the solid material consists of strands of uniform cross-sectional area d_s^2.

To use the RUC in the closure modelling of the flow of electric charge, it is also required to introduce relations between the different current densities in the different channels. As mentioned in the introduction to this section, the electrical flow lines are assumed to be equivalent to the hydraulic flow lines in an RUC and, therefore, the electrical and hydraulic linealities are equal. It thus follows from (4.59) that

$$\begin{aligned} \langle j_1 \rangle^c \equiv \bar{j}_1 &= \frac{\chi_{11}}{\epsilon} \langle j_1 \rangle \\ &= \frac{d_{(2)}d_{(3)}d_{(1)}}{A_{p(1)}d_{(1)}} \langle j_1 \rangle . \end{aligned} \tag{4.84}$$

It is also important to obtain estimates of the average current densities in the transverse channel sections. The three channel sections form three resistors connected in series because the current has to flow through each of the channels consecutively. Since the current is the same in each channel, the magnitudes of the current densities are related by

$$j_{\perp(2)} = \frac{A_{p(1)}}{A_{p(2)}} \bar{j}_1 \tag{4.85}$$

$$j_{\perp(3)} = \frac{A_{p(1)}}{A_{p(3)}} \bar{j}_1 . \tag{4.86}$$

The differing lengths of the channel sections do not influence the relations between the current densities, but they are scaled according to the different areas of the channels similar to the velocity relations in Section 3.7.1.

With this information at hand it is possible to continue the analysis of (4.78). By making use of the relations presented above, the surface integral term is written as

$$\begin{aligned}\frac{1}{\rho_w U_o}\iint_{S_{fs}} V\nu_1\, dS &= \frac{1}{U_o}\left(\frac{A_{p(1)}}{A_{p(3)}}\frac{U_o}{A_{p(1)}d_{(1)}}\langle j_1\rangle\, d_{p(3)}d_s d_{p(2)}\right.\\ &\quad\left.+\ \frac{A_{p(1)}}{A_{p(2)}}\frac{U_o}{A_{p(1)}d_{(1)}}\langle j_1\rangle\, d_{p(2)}d_s d_{p(3)}\right)\\ &= \left(\frac{A_{p(1)}d_s}{A_{p(3)}d_{(1)}} + \frac{A_{p(1)}d_s}{A_{p(2)}d_{(1)}}\right)\langle j_1\rangle\\ &= \left(\frac{U_f - A_{p(1)}d_{(1)}}{d^2_{p(1)}d_{(1)}}\right)\langle j_1\rangle \end{aligned} \tag{4.87}$$

where use was made of (4.80). If this expression for the fluid-solid surface integral is inserted into (4.47), then the macroscopic charge transport equation in the x_1-direction becomes

$$\langle j_1\rangle + \frac{\epsilon}{\rho_w}\langle V\rangle^f_{,1} + \left(\frac{U_f - A_{p(1)}d_{(1)}}{d^2_{p(1)}d_{(1)}}\right)\langle j_1\rangle = 0 \tag{4.88}$$

which may be rewritten as

$$\left(1 + \frac{U_f - A_{p(1)}d_{(1)}}{d^2_{p(1)}d_{(1)}}\right)\langle j_1\rangle = -\frac{\epsilon}{\rho_w}\langle V\rangle^f_{,1}. \tag{4.89}$$

On comparison with Ohm's law presented in (4.1) and according to (4.7), the formation factor for foams of Type A is given by

$$F = \frac{1}{\epsilon}\left(1 + \frac{U_f - A_{p(1)}d_{(1)}}{d^2_{p(1)}d_{(1)}}\right). \tag{4.90}$$

This expression for the formation factor is not equivalent to the ratio between the tortuosity and porosity. However, should the channel sections have equal dimensions, that is if $d_{p(1)} = d_{p(2)} = d_{p(3)}$ then (4.90) reduces to the more familiar $F = \frac{\chi}{\epsilon}$.

4.9.3.3 Foams of Type B

An RUC for foams of Type B as well as some corresponding geometric features have been introduced in Section 3.7.1. As illustrated in Figure 3.7, the surface sections indicated by G and I may be expressed as

$$G = d_{s(3)}d_p \qquad \text{and} \qquad I = d_{s(2)}d_p. \tag{4.91}$$

In the RUC presented in Figure 3.7, there are four fluid-solid surface areas which are normal to the streamwise direction. Two of these surfaces form part of a channel in the x_2-direction while the other pair forms part of a channel in the x_3-direction. Each of these two sets of parallel plates is staggered a distance of d_p. It is considered that the distance over which the local transverse potential difference develops is equal to this staggered distance and, therefore,

$$L_{\perp(2)} = L_{\perp(3)} = d_p. \tag{4.92}$$

According to (4.59), the average charge density in the streamwise channel, which in this case is directed in the x_1-direction, is related to the phase average current density through the relation

$$\langle j_1 \rangle^c \equiv \bar{j}_1 = \frac{\chi}{\epsilon} \langle j_1 \rangle = \frac{U_o}{A_p d_{(1)}} \langle j_1 \rangle . \tag{4.93}$$

According to (4.44), the current densities in the different channel sections are equal since the channels are of equal cross-section, A_p. Therefore,

$$\bar{j}_1 = j_{\perp(2)} = j_{\perp(3)} \tag{4.94}$$

where $j_{\perp(2)}$ and $j_{\perp(2)}$ are the magnitudes of the mean current densities in the channels in the x_2- and x_3-directions, respectively.

By making use of these expressions the surface integral term in (4.78) may be further developed to yield

$$\begin{aligned} \frac{1}{\rho_w U_o} \iint_{S_{fs}} V \nu_1 \, dS &= \frac{1}{U_o} \left(\frac{U_o}{A_p d_{(1)}} \langle j_1 \rangle \, d_p^2 d_{s(3)} + \frac{U_o}{A_p d_{(1)}} \langle j_1 \rangle \, d_p^2 d_{s(2)} \right) \\ &= \left(\frac{d_{s(3)} + d_{s(2)}}{d_{(1)}} \right) \langle j_1 \rangle . \end{aligned} \tag{4.95}$$

By combining this expression with (4.47), the macroscopic form of Ohm's law may be written as

$$\langle j_1 \rangle + \frac{\epsilon}{\rho_w} \langle V \rangle^f_{,1} + \left(\frac{d_{s(3)} + d_{s(2)}}{d_{(1)}} \right) \langle j_1 \rangle = 0 \tag{4.96}$$

which yields

$$\begin{aligned}\langle j_1 \rangle &= -\frac{\epsilon}{\rho_w}\left(1 + \frac{d_{s(3)} + d_{s(2)}}{d_{(1)}}\right)^{-1} \langle V \rangle_{,1}^{f} \\ &= -\frac{\epsilon}{\rho_w}\left(1 + \frac{A_p d_{s(3)} + A_p d_{s(2)}}{A_p d_{(1)}}\right)^{-1} \langle V \rangle_{,1}^{f} \\ &= \frac{\epsilon}{\rho_w \chi_{11}} \langle V \rangle_{,1}^{f} \end{aligned} \tag{4.97}$$

since $A_p d_{s(3)} + A_p d_{s(2)} = U_f - A_p d_{(1)}$. The formation factor for foams of Type B then follows from (4.1) and (4.7) and it is given by

$$F = \frac{\chi_{11}}{\epsilon}. \tag{4.98}$$

As shown in Table 3.1, the tortuosity may be expressed in terms of measurable geometric parameters of the porous medium which implies that the formation factor may be obtained from the geometry of the porous material.

4.9.4 Isotropic foamlike materials

In the case of isotropic foamlike materials the porous medium does not possess any directional preferences and a number of geometric simplifications, which are summarised in Table 3.3, may be introduced to the RUC's for anisotropic foams. The RUC's for foams of Type A and foams of Type B are then both cubic and represent the high and low porosity RUC's of isotropic foamlike materials as presented by Du Plessis *et al.* (1994) and Du Plessis and Diedericks (1997) and illustrated in Figure 4.4. For the RUC of isotropic foamlike materials the tortuosity may be expressed in terms of the porosity and, according to (3.93), this relation is given by

$$\chi = 2 + 2\cos\left[\frac{4\pi}{3} + \frac{1}{3}\arccos(2\epsilon - 1)\right] \tag{4.99}$$

which is illustrated in Figure 4.2. It then follows from (4.89) and (4.97) that the macroscopic form of Ohm's law for isotropic foamlike materials is given by

$$\langle j_1 \rangle = \frac{\epsilon}{\rho_w \chi} \langle V \rangle_{,1}^{f} \tag{4.100}$$

with a formation factor of

$$F = \frac{\chi}{\epsilon}. \tag{4.101}$$

The change of the formation factor with a corresponding change in porosity is schematically illustrated in Figure 4.3.

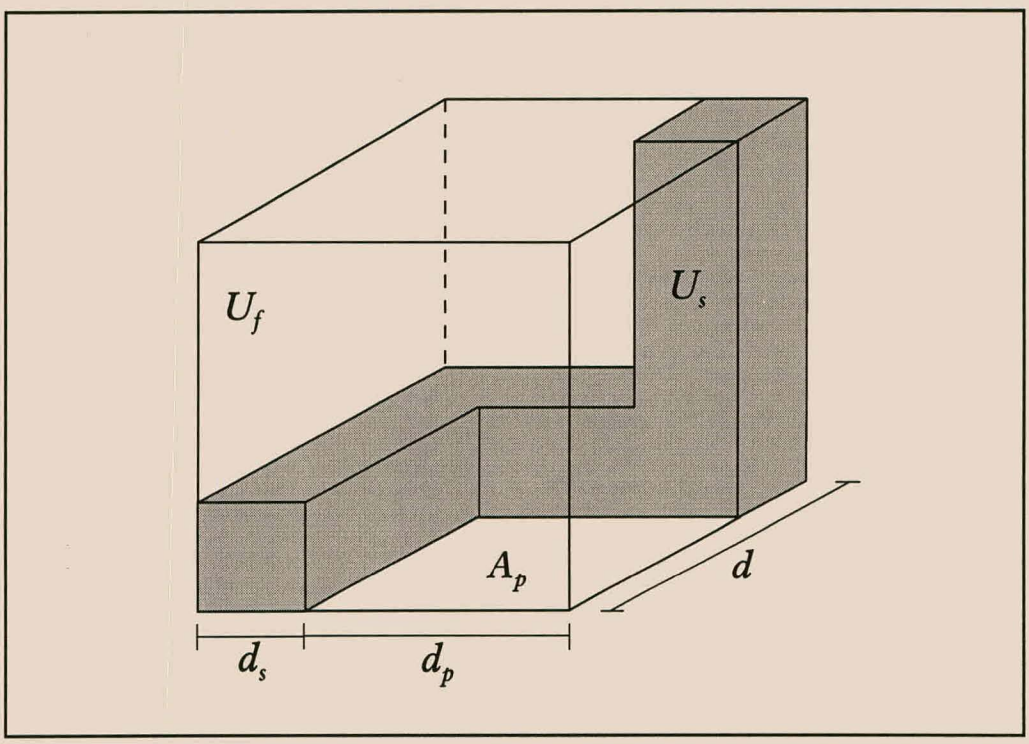

Figure 4.4. Cubic RUC for an isotropic foamlike porous medium.

This result was also obtained by Diedericks and Du Plessis (1996), although they used a different approach to model the fluid-solid surface area which contributes to the surface integral term as well as the transverse distance over which the potential is applied. According to Diedericks and Du Plessis (1996), the fluid-solid surface area which contributes to the surface integral in (4.47) was denoted by A_{fs} and for isotropic foams with a porosity below 0.5 its contribution is from the end zones of the transverse channels which implies that $A_{fs} = A_p$. Furthermore, for $0 \leq \epsilon \leq 0.5$ the distance between the high and low potentials was considered to be equal to the transverse distance through which charge is transported in a channel which yields $L_\perp = (d - d_p)$. For higher porosity foams $A_{fs} = d_p d_s$ and in this porosity range the charge is transported transversely in each channel through a distance $L_\perp = (d - d_s) = d_p$. However, it is apparent that

$$A_{fs} L_\perp = d_p^2 (d - d_p) \tag{4.102}$$

for the whole porosity range. The difference between this model and the present model is that Diedericks and Du Plessis (1996) assumed that the transverse distance $L_\perp$ is equal to the distance through which charge is transported transversally, whereas in the present model this distance is modelled as being equal to the distance over which the potential difference develops. The present model seems more appropriate, since a first order Taylor expansion is used for the transformation: $(V_h - V_l)/L_\perp \equiv -dV/dx_2$. In this case $L_\perp$ is related to the potential difference and not the length of transport.

Du Plessis and Diedericks (1997) employed a similar approach as used in the present study except that some typographic errors appear in their analysis of the electric charge transport. In equation (73) of Du Plessis and Diedericks (1997) the factor 2 in the denominator should be in the nominator, since there are two equivalent transverse channels in the cubic RUC for isotropic foams. It may be noted that according to the sentence preceding their equation (73), and since multiplication is distributive, the factor $S_\perp$ should be interpreted as being equal to $\frac{1}{8}S_{\perp total}$ where $S_{\perp total}$ is the total surface area which are not aligned streamwise. In their Table 2, the staggered distance $\Delta L_\perp$ should also be equal to the pore width, d_p, and not the solid width. With these changes the formation factor of Du Plessis and Diedericks (1997) for isotropic foamlike materials is equal to the formation factor presented in (4.101).

4.9.5 Conduction in anisotropic granular porous media

The closure modelling, which is required to obtain a macroscopic equation which governs charge transport in anisotropic granular porous media, is provided by considering the local transport conditions within an RUC. A rectangular parallelpipedal RUC which is representative of anisotropic granular porous media has been introduced in Section 3.9.3 and is illustrated in Figure 3.14. A number of geometric characteristics derived from the RUC are also presented in Section 3.9.3.

This model is geometrically more complicated than the previous two models, since the streamwise channel actually consists of two different channel sections and the transverse channel is not necessarily parallel to the streamwise sides of the RUC. Therefore, an important area to consider is the effective area of the transverse channel, $A_\perp$. Since it is assumed that the charge carriers and Newtonian fluid make equal use of the available void volume in the RUC, the transverse area determined in (3.126), is also applicable to the flow of transverse electric current. Therefore, the transverse channel area is also

given by

$$A_\perp = \frac{(d_{(2)}d_{(3)} - d_{s(2)}d_{s(3)})(U_f - A_{p(1)}d_{(1)})}{d_{s(2)}d_{s(3)}\sqrt{(d_{(2)} - d_{s(2)})^2 + (d_{(3)} - d_{s(3)})^2}}$$
$$= \frac{A_{p(1)}(d_{(1)}d_{s(3)} - d_{s(1)}d_{s(3)})}{d_{s(3)}\sqrt{(d_{(2)} - d_{s(2)})^2 + (d_{(3)} - d_{s(3)})^2}}. \tag{4.103}$$

From the geometry of the RUC and (4.28) it follows that

$$j_\perp = \frac{A_{p(1)}}{A_\perp}\bar{j}_1 \tag{4.104}$$

where $A_{p(1)}$ is the channel area perpendicular to the streamwise direction and $A_\perp$ is the area through which the charge must be transported transversely before leaving the RUC. This equation relates the magnitudes of the transverse current density ($j_\perp$) to the only component of the channel average current density ($\bar{j}_1$). Furthermore, according to (4.59) the channel average current density and phase average current density are related by

$$\bar{j} = \frac{\chi_{11}}{\epsilon}\langle j_1 \rangle = \frac{U_o}{A_{p(1)}d_{(1)}}\langle j_1 \rangle . \tag{4.105}$$

As discussed in Section 3.7.1 when considering fluid transport, the flow may take a short cut obliquely across the solid constituent during transverse flow which led to the introduction of the transverse channel length, $d_\perp$. This diagonal transverse displacement is equal to the eventual transverse displacement of the centroid of a discharge which is forced transversely due to the staggering of solid material and it is related to the transverse channel area through (3.125). However, according to the model of local charge transport the distance which separates the high voltage from the lower voltage along the transverse channel is equal to the distance between the centroids of the two staggered fluid-solid surface areas, $L_\perp$, and not $d_\perp$. For the RUC in Figure 3.15 this distance is given by

$$L_\perp = \sqrt{(d_{(2)} - d_{s(2)})^2 + (d_{(3)} - d_{s(3)})^2}. \tag{4.106}$$

The macroscopic form of Ohm's law for anisotropic granular porous media may be determined in much the same manner as was done for the previous two types of materials.

Therefore,

$$\begin{aligned}\frac{1}{\rho_w U_o}\iint_{S_{fs}} V\nu_1\, dS &= \frac{(V_h - V_l)d_{s(2)}d_{s(3)}\widehat{\nu}_1}{\rho_w U_o}\\ &= \frac{1}{U_o}\left(j_\perp L_\perp d_{s(2)}d_{s(3)}\right)\widehat{\nu}_1\\ &= \frac{1}{U_o}\left(\frac{A_{p(1)}}{A_\perp}\frac{U_o}{A_{p(1)}d_{(1)}}\langle j_1\rangle L_\perp d_{s(2)}d_{s(3)}\right)\\ &= \left(\frac{L_\perp d_{s(2)}d_{s(3)}}{A_\perp d_{(1)}}\right)\langle j_1\rangle .\end{aligned} \tag{4.107}$$

By inserting this equation into (4.47), the macroscopic charge transport through anisotropic granular porous media may be written as

$$\langle j_1\rangle + \frac{\epsilon}{\rho_w}\langle V\rangle^f_{,1} + \left(\frac{L_\perp d_{s(2)}d_{s(3)}}{A_\perp d_{(1)}}\right)\langle j_1\rangle = 0. \tag{4.108}$$

The macroscopic form of Ohm's law applicable to anisotropic granular porous media is thus given by

$$\langle j_1\rangle = -\frac{\epsilon}{\rho_w}\left(1 + \frac{L_\perp d_{s(2)}d_{s(3)}}{A_\perp d_{(1)}}\right)^{-1}\langle V\rangle^f_{,1} \tag{4.109}$$

where $L_\perp$ is given by (4.106) and $A_\perp$ is presented in (4.103). According to (4.7) and (4.109) the formation factor is given by

$$F = \frac{1}{\epsilon}\left(1 + \frac{L_\perp d_{s(2)}d_{s(3)}}{A_\perp d_{(1)}}\right). \tag{4.110}$$

This equation cannot be expressed in the familiar form of $F = \frac{\chi}{\epsilon}$ or $F = \frac{\chi^2}{\epsilon}$due to the complex geometric structure within the RUC.

4.9.6 Conduction in isotropic granular porous media

The average geometry of essentially isotropic granular porous media has been incorporated in a cubic RUC by Du Plessis and Masliyah (1991) who also derived a number of geometric characteristics from the RUC layout. The reductions which may be introduced to the RUC for anisotropic granular materials as well as some geometric relations

of isotropic granular porous media are presented in Table 3.6. The RUC for isotropic granular porous media then take on a cubic form and conforms to the RUC of Du Plessis and Masliyah (1991) as illustrated in Figure 4.5.

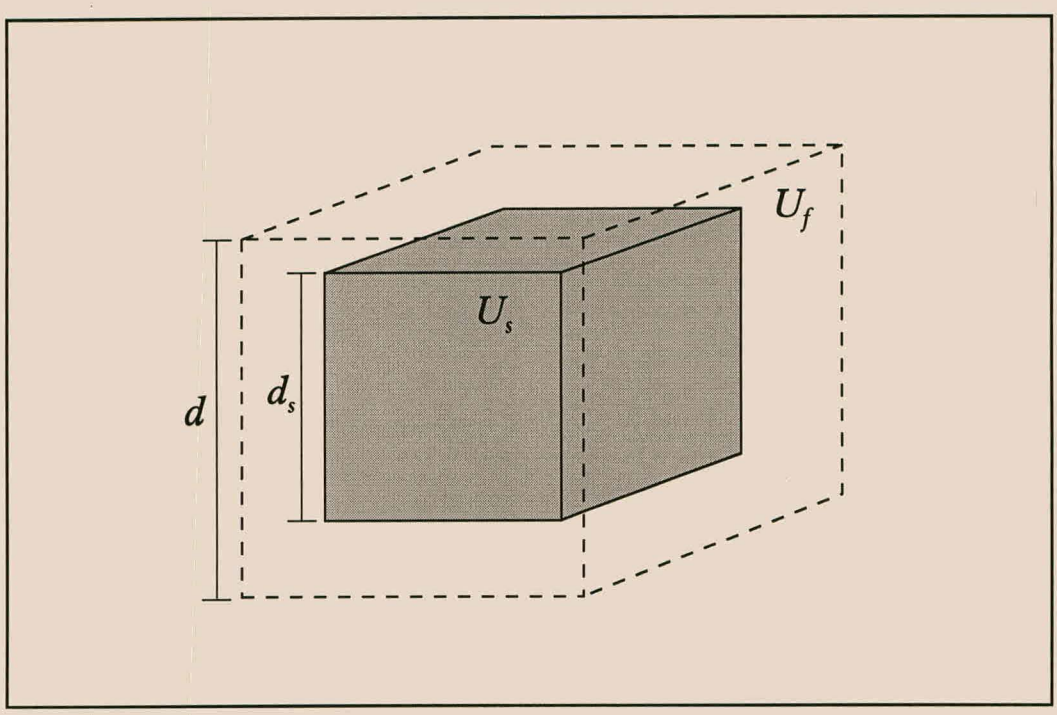

Figure 4.5. Cubic RUC for an isotropic granular porous medium.

For the isotropic RUC, the sides of the solid cube d_s and the volume of solid material U_s are related by

$$U_s = d_s^3 = (1-\epsilon)d^3 \tag{4.111}$$

while the fluid volume of the RUC is

$$U_f = \epsilon U_o = \epsilon d^3. \tag{4.112}$$

The area of the solid cube is given by

$$A_s = d_s^2 = (1-\epsilon)^{2/3} d^2 \tag{4.113}$$

while the effective channel area normal to the macroscopic charge direction is

$$A_p = d^2 - d_s^2. \tag{4.114}$$

In this case it follows from (4.103) that the transverse channel area is related to the streamwise flow area by

$$A_\perp = A_p/\sqrt{2} \tag{4.115}$$

which according to (4.104) implies that

$$j_\perp = \sqrt{2}\,\bar{j}_1. \tag{4.116}$$

Furthermore, the channel average current density and phase average current density are related by

$$\bar{j}_1 = \frac{d^2}{A_p}\langle j_1 \rangle . \tag{4.117}$$

An advantage of the isotropic RUC is that the tortuosity may be uniquely expressed in terms of the porosity. According to Du Plessis and Masliyah (1991), the equivalent hydraulic and electric geometric tortuosity, $\chi = U_f/A_p d$, may be expressed as

$$\chi = \frac{\epsilon}{1-(1-\epsilon)^{2/3}} \tag{4.118}$$

which is also schematically represented in Figure 4.2. The effective channel area may also be expressed in terms of the tortuosity as

$$A_p = \frac{\epsilon d^2}{\chi}. \tag{4.119}$$

For the RUC of the isotropic case the diagonal distance between the centroids of the two fluid-solid surface sections normal to the streamwise direction follows from (4.106) and is given by

$$L_\perp = \sqrt{2}(d - d_s). \tag{4.120}$$

By using the different geometric expressions introduced in this section, the fluid-solid

surface integral term in (4.47) may be written as

$$\begin{aligned}\frac{1}{\rho_w U_o}\iint_{S_{fs}} V\,\nu_1\,dS &= \frac{(V_h - V_l)d_s^2\nu_1}{\rho_w U_o}\\ &= \frac{2d_s^2(d-d_s)\langle j_1\rangle}{A_p d}\\ &= \frac{2(1-\epsilon)^{2/3}\left(1-(1-\epsilon)^{1/3}\right)\langle j_1\rangle}{(1-(1-\epsilon)^{2/3})}\\ &= \frac{2(1-\epsilon)^{2/3}\langle j_1\rangle}{(1+(1-\epsilon)^{1/3})}\end{aligned} \tag{4.121}$$

where use was made of, among others, (4.44), (4.116) and (4.119).

Should (4.121) be combined with (4.47) then it follows for all porosity values that Ohm's law for the isotropic granular model may be written as

$$\langle j_1\rangle = -\frac{\epsilon}{\rho_w}\left(1+\frac{2(1-\epsilon)^{2/3}}{(1+(1-\epsilon)^{1/3})}\right)^{-1}\langle V\rangle^f_{,1}\,. \tag{4.122}$$

The formation factor then follows from (4.7) and (4.122) and is given by

$$F = \frac{1}{\epsilon}\left(1+\frac{2(1-\epsilon)^{2/3}}{(1+(1-\epsilon)^{1/3})}\right). \tag{4.123}$$

The formation factor according to this expression is schematically illustrated in Figure 4.3.

In this section the formation factors of three types of anisotropic and isotropic porous media have been determined. For the anisotropic materials the expressions are in terms of geometric characteristics of the porous material while the expressions for the isotropic materials only requires the porosity as dependent parameter. A comparison of the formation factor predictions for the isotropic cases is illustrated in Figure 4.3. Although the geometric structure of the RUC's for the granular materials and fibre beds are different, the predicted formation factors are similar to such an extend that the differences are not visible on Figure 4.3. The predictions for the foamlike materials are generally higher than for the other two types of materials. However, the differences are not adequate to use the formation factor as a parameter to distinguish different types of materials from each other. In the remainder of this chapter these relationships are further used to validate the accuracy of the models in predicting the formation factors.

4.10 Comparison with experimental data

4.10.1 Isotropic foamlike materials

Measurements of electrical conduction have mostly been directed towards granular materials with the result that not many measured formation factors are available for comparison with the model for foams. However, some electrical conductivity measurements have been performed by Dr. A. Montillet at the Laboratoire de Génie de Procédés, IUT-Saint-Nazaire in France on two high porosity nonconductive foamlike materials saturated with an electrolyte. The foams are characterised by their grade (G), which stipulates the number of pores per inch. The electrolyte selected was $KClO_4$. Some characteristics of the foams together with the measured formation factors are listed in Table 4.2. Also included in the table are the predicted formation factors as calculated from (4.101).

Table 4.2. Comparison of predicted formation factors (eqn (4.101)) and measured formation factors for isotropic foams.

Grade	Porosity	F_{exp}	F_{an}	F_{an}/F_{exp}
G 10	0.971	1.19	1.24	1.04
G 20	0.973	1.14	1.23	1.08

In general, the predictive results compare fairly well with the measured formation factors. In the case of these high porosity foams there are only a 4% and 8% difference between the measured and predicted formation factors in the two foams, respectively.

During an analysis of acoustic wave propagation in porous media Cummings and Chang (1987) used the tortuosity as a geometric feature in their expressions. When comparing their results to measurements the tortuosity was obtained through measuring the electrical resistance which can also be used to infer the formation factor. In one series of tests Cummings and Chang (1987) used polyether foams with a porosity of $\epsilon = 0.958$. The electrical resistance of a particular volume of rectangular parallelepiped shape of saline solution was measured in a conductivity cell. Thereafter, a piece of foam, cut to be of the same shape and size of the volume of solution, was saturated with the solution and its resistance was determined. It then follows from their results that the measured formation factor is $F = 1.218$. A comparison of the prediction using (4.101) with this measurement is summarised in Table 4.3.

Table 4.3. Comparison between predicted formation factor (eqn (4.101)) and the measured formation factor from Cummings and Chang (1987).

Porosity	F_{exp}	F_{an}	F_{an}/F_{exp}
0.958	1.22	1.30	1.07

In this case the prediction is also fairly accurate with only a 7% difference between the calculated and predicted values.

4.10.2 Isotropic fibres

Sen and Kan (1987) investigated the electrical conduction in a periodic array of charged cylinders immersed in an electrolyte. The main aim of their work is to investigate the contribution from the double layers which is expressed through the surface ion number density. However, they present the following expression for the formation factor in the limit where the surface ion number density is zero and the transport is only due to bulk conduction in the void space:

$$\frac{1}{F} = 1 - \frac{2(1-\epsilon)}{1+(1-\epsilon)S_2/\pi - 3(1-\epsilon)S_4^2/\pi^4}. \tag{4.124}$$

For this equation Sen and Kan (1987) give the lattice-structure factors as $S_2 = \pi$ and $S_4 = 0.03235\pi^4$, respectively.

This expression for the formation factor is compared to the prediction obtained for isotropic prismatic bundles presented in (4.77) in Figure 4.6. However, (4.124) is not applicable to the whole porosity range since (4.124) yields negative formation factors at porosity values lower than approximately $\epsilon \leq 0.1555$. This may be due to the inclusion of a percolation limit, although Sen and Kan (1987) do not make any mention of such a feature in their model. As shown in Figure 4.6, the formation factors from (4.124) above their porosity limit are slightly lower than the present model up to about $\epsilon = 0.4$ where the predictions are similar. It may also be mentioned that equation (9) in Sen and Kan (1987) does not yield their equation (10) in the limit of uncharged particles.

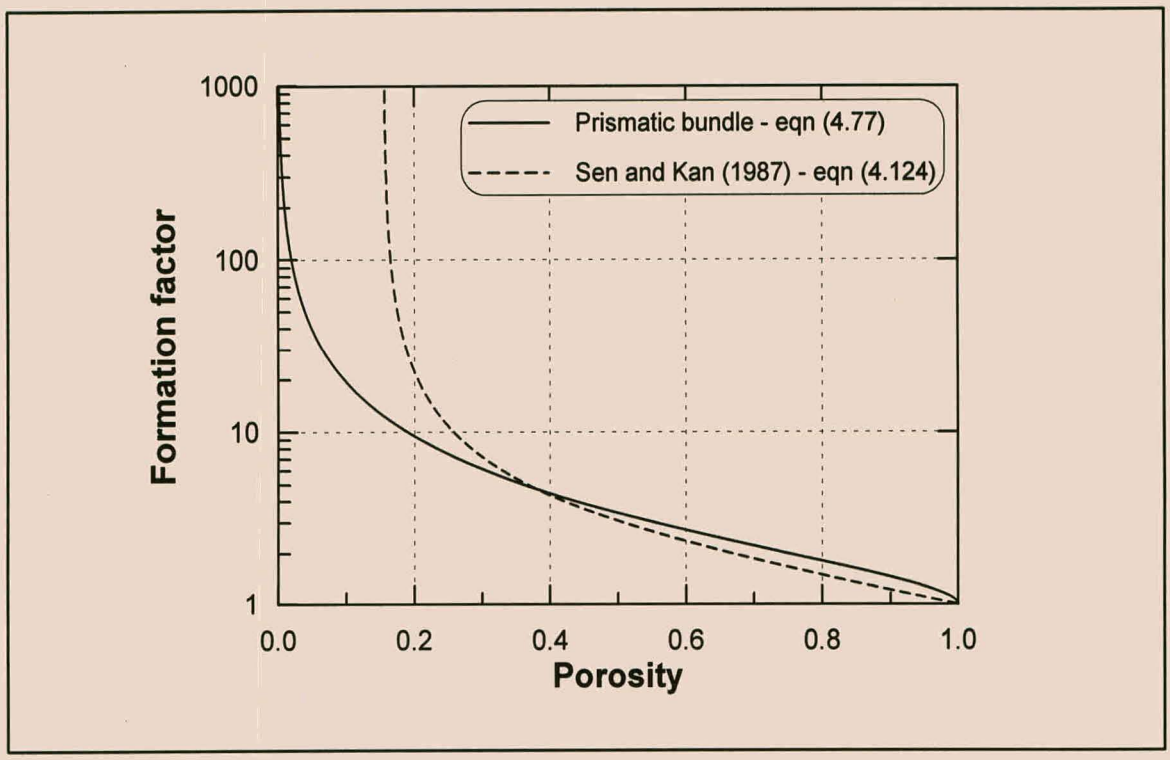

Figure 4.6. Formation factors for isotropic fibre beds according to two different models.

4.10.3 Isotropic granular materials

A number of experiments have been performed to investigate current flow in granular-type porous media. The predicted formation factors are, therefore, firstly compared to some experimentally measured formation factors in a number of sandstones. The first set of measured formation factors is obtained from Wyllie and Spangler (1952) and lies in the region of $\epsilon = 0.2$ as listed in Table 4.4 and illustrated in Figure 4.7.

Koplik *et al.* (1984) present a model to determine the electrical conductivity and the permeability of an isotropic material from the microscopic geometry of the pore-space. According to their model, serial sections of the pore-space are used to determine an equivalent random network of elliptical cylinders and the transport coefficients of this network are then related to the conductivity of an equivalent random set of resistors. The model was verified by using a sample of Massilon sandstone with most grains having a diameter on the order of 400 μm. A comparison of (4.123) with the model of Koplik *et al.* (1984) and the measurements is presented in Table 4.5.

The granular model performs better than the model of Koplik *et al.* (1984) although there is still a substantial difference of about 27% between the prediction of (4.123) and the measured formation factor.

Table 4.4. Comparison of predicted formation factors (eqn (4.123)) with measured formation factors from Wyllie and Spangler (1952).

Material	Porosity	F_{exp}	F_{an}	F_{an}/F_{exp}
Oligocene sandstone (ss)	0.218	13.1	8.6	0.66
F151 Pennsylvanian ss.	0.163	20.1	11.7	0.58
F154 Pennsylvanian ss.	0.181	14.0	10.5	0.75
F220 Pennsylvanian ss.	0.195	13.9	9.7	0.70
F250 Pennsylvanian ss.	0.205	13.0	9.2	0.71
F252 Pennsylvanian ss.	0.185	16.9	10.3	0.61
F228 Pennsylvanian ss.	0.201	17.5	9.4	0.54

Table 4.5. Comparison of predicted formation factors (eqn (4.123)) with measured formation factors from Koplik *et al.* (1984).

Porosity	F_{exp}	F_{Koplik}	F_{an}	F_{an}/F_{exp}
0.22	11.8	5.7	8.6	0.73

Formation factors of materials with reasonably low porosities are given in Table 4.6 for a number of different types of sandstones and dolomite as obtained from Cornell and Katz (1953). Each of the sandstones had a well-defined quartz grain structure while the fractured faces of the brown dolomite samples revealed an irregular crystalline structure. In addition, Cornell and Katz (1953) also mention that considerable variations in the properties of different samples taken from the same bulk sample were found and the results should be interpreted with due regard to the variable nature of the materials being considered. These measurements are also illustrated in Figure 4.7 and in general higher formation factors are measured than presently predicted by (4.123).

Table 4.6. Comparison of predicted formation factors (eqn (4.123)) with measured formation factors from Cornell and Katz (1953).

Material	Porosity	F_{exp}	F_{an}	F_{an}/F_{exp}
Wilcox sandstone	0.175	15.5	10.9	0.70
	0.158	17.4	12.1	0.70
	0.160	16.6	12.0	0.72
Bromide sandstone	0.110	36.2	17.7	0.49
	0.030	62.5	66.2	1.06
	0.022	86.8	90.4	1.04
	0.123	30.0	15.7	0.52
Burbank sandstone	0.150	39.1	12.8	0.33
	0.163	34.8	11.7	0.34
Brown dolomite	0.143	49.8	13.5	0.27
	0.125	49.8	15.5	0.31
	0.095	64.7	20.5	0.32

Measured formation factors in materials which exhibit a more distinct granular structure are provided by Carman (1956) and compared to the predicted values in Table 4.7. These measurements are also illustrated in Figure 4.7. The materials selected include glass spheres, some with variable diameters, and some clean sands. The majority of the porosity values of these materials are in the region of $\epsilon = 0.4$ with the lowest value near $\epsilon = 0.1$. In this case the predictions of (4.123) are more accurate than in the case of the sandstones, indicating that the granular model is a fairly accurate representation of materials with distinct granular structures.

Table 4.7. Comparison of predicted formation factors (eqn (4.123)) with measured formation factors from Carman (1956).

Material	Porosity	F_{exp}	F_{an}	F_{an}/F_{exp}
Glass spheres (8 mm)	0.435	3.3	4.0	1.21
Glass spheres (3 mm)	0.368	4.0	4.9	1.23
Glass spheres (3 mm)	0.402	3.5	4.4	1.26
White sand ($125 - 210\mu$m)	0.403	4.0	4.4	1.10
Dune sand ($< 297\mu$m)	0.398	4.1	4.5	1.10
Glass powder ($120 - 180\mu$m)	0.470	3.6	3.7	1.03
Glass sand	0.379	4.5	4.7	1.04
Quartz sand	0.415	4.1	4.2	1.02
Sand	0.381	4.0	4.7	1.18
Spheres	0.350	4.3	5.2	1.21
Glass spheres	0.254	6.1	7.3	1.20
	0.187	8.8	10.2	1.16
	0.139	13.0	13.9	1.07
	0.262	6.0	7.1	1.18
Spheres and sand	0.102	19.2	19.1	0.99

Bacri *et al.* (1987) investigated experimentally the effect of pore-size distributions on hydrodynamic dispersion. To this end they measured, amongst others, the electrical conduction, permeability, porosity and molecular diffusion coefficients in three materials, namely a packed bed of 200 μm glass beads, a fireproof brick and a mill sandstone. As indicated in Table 4.8 the glass beads and the brick sample had similar permeabilities and tortuosities determined from electrical measurements, but according to Bacri *et al.* (1987) they looked very differently from direct microscopic observation. The beads were quasimonodisperse and the fireproof brick looked like a foam where pore bubbles

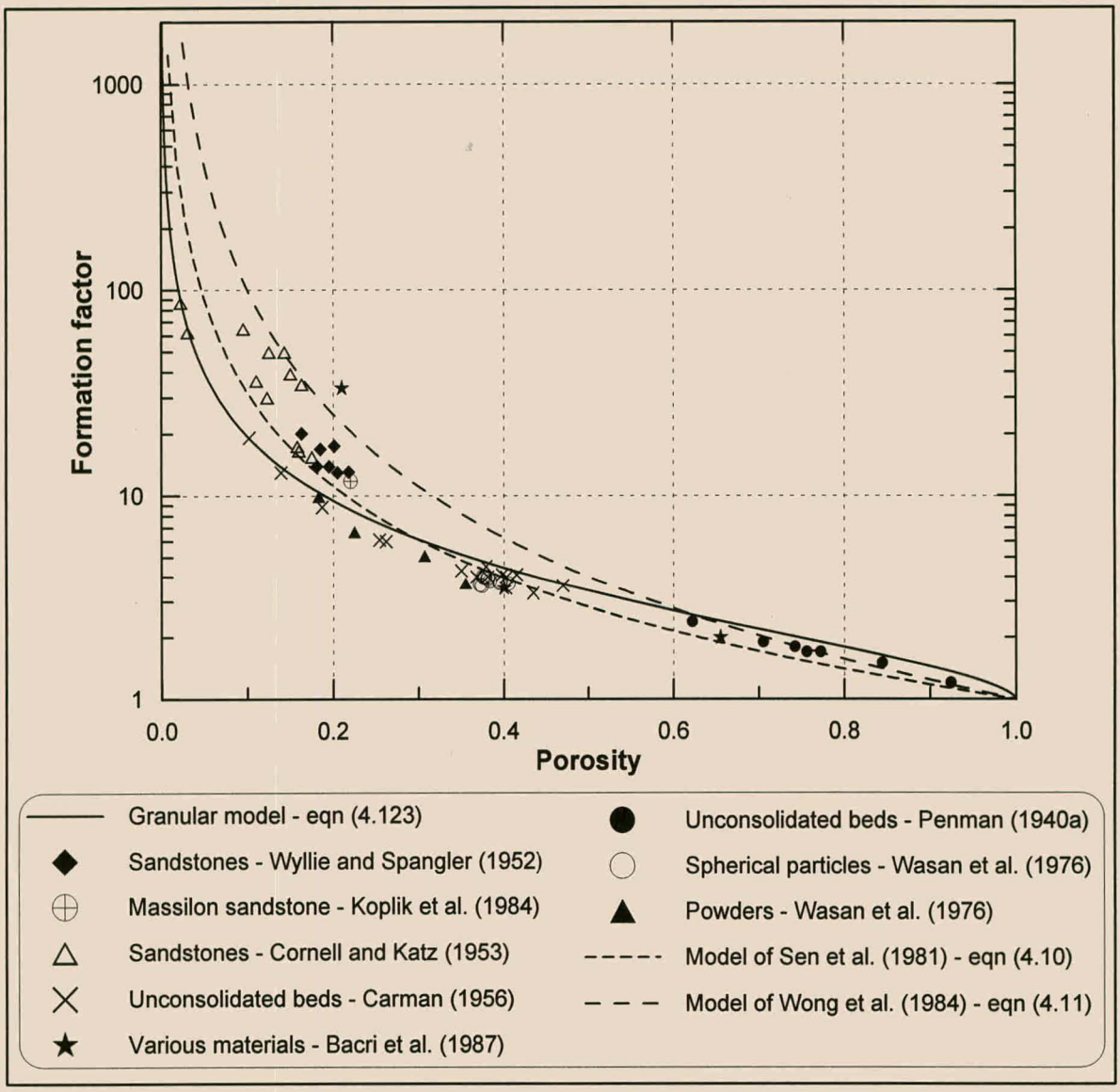

Figure 4.7. Analytical and experimental formation factors for different types of granular porous media.

Table 4.8. Measured porous medium characteristics as presented by Bacri *et al.* (1987) and formation factor predictions.

Porous medium	Porosity	χ_e	$F_{exp} = \chi_e/\epsilon$	F_{an}	F_{an}/F_{exp}
200-μm glass beads	0.400	1.4	3.5	4.43	1.26
Mill sandstone	0.21	7.0	33.3	8.99	0.27
Fireproof brick[1]	0.655	1.3	2.0	2.41	1.21
Fireproof brick[2]	0.655	1.3	2.0	2.73	1.37

[1]Modelled as a granular material using (4.123).
[2]Modelled as a foamlike material using (4.101).

were connected by small throats. The sandstone was much more tortuous, but its microscopic structure was close to that of the pack of glass beads. Although Bacri *et al.* (1987) presented tortuosity values, they used the expression $F = \chi_e/\epsilon$ to relate the tortuosity to the formation factor and this expression has been used to calculate the formation factors in Table 4.8. In this case the prediction for the glass beads is similar to the predictions for glass spheres of similar porosities presented in Table 4.7. Similar to previous results, the model does not predict the formation factor of the sandstone sample in the low porosity limit correctly. At least the model consistently under predicts the formation factors for low porosities. The predictions in the case of the fireproof brick is fairly accurate, although modelling the brick as a foam did not improve the results.

Obtaining formation factors in the high porosity range appears problematic, but is surpassed by realising that current transport and diffusion may be considered to be equivalent processes (Carman, 1956; Petersen, 1965; Probstein, 1989), as is partially illustrated in Section 2.7.2.2. Therefore, the ratio between the measured effective diffusion coefficient in the presence of a porous medium and the diffusion coefficient of the diffusing substance (D/D_e) is equivalent to the formation factor (Dullien, 1979, eqn (7.3.8)). In this manner formation factors are indirectly measured and a number of such measurements in the high porosity range, obtained from Penman (1940a) and also listed by Carman (1956), are given in Table 4.9 and are also illustrated in Figure 4.7. The materials selected for the comparison also exhibit an unconsolidated structure.

Wasan *et al.* (1976) also present diffusivity measurements which they compare to their predictions. Initially Wasan *et al.* (1976) used a capillary model similar to that of Comiti and Renaud (1989) where they concluded that the ratio between the effective diffusion coefficient and the microscopic diffusivity is given by

$$\frac{D_e}{D} = C\frac{\epsilon}{\chi^2} \tag{4.125}$$

where $\chi = L_e/L$ is the tortuosity defined as a ratio of lengths and C is a constriction factor which they added to the expression for D_e/D obtained from the capillary model. To evaluate the constriction factor and tortuosity Wasan *et al.* (1976) constructed geometric pore-scale models which took the form of unit cells which are repeated throughout the material. The first model which they present contains a system of annuli which consists of a number of hemispheres grouped around a central sphere. According to Wasan *et al.* (1976) this model is applicable to beds of spheres in the porosity range 0.35 to 0.45 and, according to Boshoff (1998), in this range their relation for the tortuosity corresponds closely to that Du Plessis and Masliyah (1991) presented in (4.118).

Table 4.9. Comparison of predicted formation factors (eqn (4.123)) with measured diffusional ratios from Penman (1940a).

Material	Porosity	$D/D_e \equiv F_{exp}$	F_{an}	F_{an}/F_{exp}
Natal soil	0.622	2.4	2.6	1.08
Talc	0.705	1.9	2.2	1.16
	0.742	1.8	2.0	1.11
	0.756	1.7	2.0	1.18
Koalin	0.772	1.7	1.9	1.12
Kieselguhr	0.844	1.5	1.6	1.07
	0.924	1.2	1.4	1.17

Table 4.10. Comparison of predicted formation factors (eqn (4.123)) with measured diffusional ratios from Currie (1960) as presented by Wasan *et al.* (1976) for porosities between 0.375 and 0.405.

Porosity	$D/D_e \equiv F_{exp}$	F_{Wasan}	F_{an}	F_{an}/F_{exp}
0.405	3.690	3.472	4.367	1.18
0.396	3.745	3.559	4.481	1.20
0.381	3.906	3.953	4.683	1.20
0.395	3.717	3.571	4.494	1.21
0.383	3.802	3.906	4.655	1.22
0.375	4.016	4.082	4.768	1.19
0.376	3.968	4.065	4.754	1.20

To verify their model, Wasan *et al.* (1976) used two sets of data. The first set is from Currie (1960) and the porous material constitutes glass spheres while the second set was obtained from measurements of Penman (1940b) and consists of sand where the grains had a rounded shape. The measurements as well as the predictions according to (4.123) and the predictions of Wasan *et al.* (1976) are presented in Table 4.10 and Table 4.11.

For these cases the predictions of the granular model presented in (4.123) consistently over predicts the measured formation factors. Furthermore, the present model is also not as accurate as the model of Wasan *et al.* (1976). These measurements are also included in Figure 4.7.

Table 4.11. Comparison of predicted formation factors (eqn (4.123)) with measured diffusional ratios from Penman (1940b) as presented by Wasan *et al.* (1976).

Porosity	$D/D_e \equiv F_{exp}$	F_{Wasan}	F_{an}	F_{an}/F_{exp}
0.377	4.016	3.610	4.740	1.18
0.372	3.636	3.676	4.812	1.32
0.374	3.597	3.610	4.783	1.33
0.378	3.968	3.597	4.725	1.19
0.381	3.968	3.953	4.683	1.18

To account for beds of spheres at high porosities and possibly non-spherical particles Wasan *et al.* (1976) introduced a unit cell model where each cell contains a particle located centrally within it. They considered, amongst others, that the particle may be a sphere or a cube. In the latter case the unit cell physically shows a close resemblance to the RUC for granular materials presented in Figure 4.5. To validate their model Wasan *et al.* (1976) used published data of the effective diffusion coefficient for gas diffusion through various types of powders and powder mixtures. One such data set obtained from Currie (1960) where the porous medium resembles a mixture of spheres and applicable to porosities between 0.183 and 0.355, is presented in Table 4.12.

Table 4.12. Comparison of predicted formation factors (eqn (4.123)) and measured diffusional ratios from Currie (1960) as presented by Wasan *et al.* (1976) for porosities between 0.183 and 0.355.

Porosity	$D/D_e \equiv F_{exp}$	F_{Wasan}	F_{an}	F_{an}/F_{exp}
0.225	6.667	5.618	8.354	1.25
0.355	3.704	4.405	5.073	1.37
0.183	9.901	9.804	10.401	1.05
0.307	5.076	5.376	5.964	1.17

It is instructive towards further validation of the model to also compare the present results with some other empirical and theoretical formation factor predictions. Since Archie's law describes the relation between formation factor and porosity fairly well, two limiting forms of this equation are also included in Figure 4.7. The two limits of Archie's law are those proposed by Sen *et al.* (1981), presented in (4.10), and Wong *et al.* (1984) given in (4.11). On comparison with the theoretical predictions it is apparent that the present prediction for granular materials correspond reasonably with the analysis of Sen *et al.* (1981) presented in (4.10), especially in the porosity range $0.2 \leq \epsilon \leq 0.4$ where Wong *et al.* (1984) also obtained (4.10). According to the analysis of Wong *et al.* (1984) it is more appropriate to use a higher cementing factor for materials with a lower porosity and this is also reflected in the graph of (4.11) which is also included in Figure 4.7. The present predictions differ from the analysis of Wong *et al.* (1984) in the low porosity limit and this is indicative of the fact that the present analysis does not address the low porosity limit adequately. This is also reflected in the comparison with the sandstone data.

4.10.4 Discussion and conclusions

Use of the volumetric averaging process in obtaining macroscopic transport equations requires that the constitutive terms which arise through the course of the averaging be adequately addressed. Many of these terms incorporate microscopic fluxes and to be of practical value these terms must be modelled in terms of macroscopic measurable parameters. The general estimation presented in Chapter 2 provides a mathematical basis from which an estimate of such fluxes and their gradients, can be obtained. However,

the general theory is still dependent on a specific porous medium model for closure of the macroscopic equations. Three different porous medium models representative of three idealised types of anisotropic porous media have been introduced as well as the RUC's which represent the isotropic limit of these materials.

The model used to approximate the average geometric structures of the materials may appear unrealistic, but it does take into account the correct dimensionality and scale lengths of the real porous medium and is therefore considered to be conceptually applicable. It has the advantage that it differentiates between different types of materials, although the predictions presented in Figure 4.3 indicate that the formation factor is not sensitive to the distinctive features of the three models as the formation factor predictions for the isotropic prismatic bundle and granular model are equal, while the predictions for isotropic foamlike materials are in a close proximity of the other two models. Besides modelling the geometry, the physics of the transport phenomenon must also be adequately addressed to obtain reliable results. The consequence of the present model is that the formation factor may be expressed only as a function of the geometry of the porous medium without any adjustable parameters. Besides being able to predict formation factors for various industrial applications, comparison with known values may also serve as validation of the model.

The present predictions of the formation factor for anisotropic materials as well as the isotropic granular medium indicate that the relations, $F = \chi/\epsilon$ or $F = \chi^2/\epsilon$, between the formation factor and hydraulic tortuosity, (Wyllie and Spangler, 1952; Johnson *et al.*, 1987), are not applicable to all types of porous structures. The former relation is only obtained if the diameter of the flow channels or pores have a fixed cross-sectional area throughout the medium. From the predictions illustrated in Figure 4.3 it is evident that the resistance to charge transport rises sharply for porosities below $\epsilon < 0.05$, but relative little resistance is offered in the high porosity limit. The respective resistances to the flow of electric current through the isotropic prismatic bundle and granular materials are similar as they predict similar formation factors, although the functional relation between the formation factor and porosity differs for these two materials. The formation factor predictions through the isotropic foamlike materials are higher, but not sufficient to enable the use of the formation factor measurements to differentiate experimentally between various types of porous medium structures.

The close correspondence of the predictions for the isotropic foamlike materials with the measurements indicate that the model adequately addresses the average geometric structure of foamlike materials and hence the success of Du Plessis *et al.* (1994) in modelling momentum transport in such high porosity foams.

In the comparison with the data from sandstones the weaker correspondence between measured and predicted formation factors is ascribed to various characteristics of the sandstones not incorporated by the basic model. These might include constrictions of channels as well as possible dead volumes not contributing to the electric current, but which are still calculated to be part of the porosity. Incorporation of an effective porosity, which is less than the measured porosity, will yield higher predicted formation factors and was applied to permeability predictions with reasonable success by Du Plessis and Roos (1994). Shankland and Waff (1974) also indicated that it is the porosity which corresponds to the interconnected pore-space which controls the electrical conduction. Knackstedt and Duplessis (1996) further improved the predictions of Du Plessis and Roos (1994) in the low porosity limit below $\epsilon = 0.1$ by incorporation of percolation phenomena. This indicates that the predictions of the formation factor in the low porosity limit may also be improved by incorporation of percolation effects which are not included in the basic RUC-model. Furthermore, the basic model does not include a possible pore size distribution in the sandstones which may influence fluid and current transport differently (Dullien, 1979).

The predicted formation factors in materials with a distinct granular structure are fairly accurate and close correspondence between the predictions for granular materials and experimental values over the whole porosity range has been obtained. In the low porosity range the measurements are grouped around $\epsilon = 0.4$. The increase in formation factor with decrease in porosity is predicted correctly. In the high porosity range the decrease of the ratio between the effective and normal diffusion coefficients, which is assumed to be equivalent to the formation factor, is also predicted fairly well.

Although more data is required for further comparison and testing of the model, and besides the low porosity limit, the results obtained thus far are encouraging.

4.11 Summary

A number of models which are used to quantify the formation factor have been presented. The equations governing charge transport on the microscopic level are also presented and it is indicated under which conditions Ohm's law is valid. The macroscopic charge transport equation is obtained through the volumetric averaging process.

Complete closure of the constitutive terms which arise through the course of the averaging process necessitated a representative estimation of the interstitial current density by using the lineality tensor. Rectangular Representative Unit Cells (RUC's) which

address the geometry of three types of anisotropic porous materials and three types of isotropic porous media have been introduced to quantify charge transport on the microscopic level.

Deterministic expressions in terms of the porosity and other porous medium characteristics have been derived for the formation factor in the idealised types of porous media. The predictions compare favourably with measured formation factors in the cases of isotropic foamlike materials and unconsolidated materials with a distinct granular structure. For consolidated sandstones the predictions are less accurate.

A complete analysis of charge transport in three types of homogeneous porous media, which include Ohm's law and the formation factor, has been developed. Deterministic formation factors may thus be obtained yielding valuable enhancement to the analyses of experiments regarding various industrial applications.

Chapter 5

CONCLUSIONS AND RECOMMENDATIONS

5.1 Introduction

This study commences with a discussion of different types of modelling approaches to obtain quantification of transport in porous media, with special attention being given to the volume averaging technique. A novel analysis of a flux related tortuosity tensor is presented as an addition to a discussion on various parameters used in porous media modelling.

Consideration is then given to the flow of Newtonian fluids in anisotropic porous media. During the closure modelling use is made of Representative Unit Cells (RUC's) and two different RUC's for foamlike materials are designed as well as RUC's for anisotropic granular materials and fibre beds. A general modelling technique, summarised in Figure 3.18, is then applied to each type of idealised material to obtain deterministic expressions for the relation between the superficial velocity and pressure gradient. The model for the foamlike materials is validated against a data set consisting of measured pressure gradients and flow velocities through a highly complex knitted wire rolled up to form a porous plug.

The same pore-scale RUC's, as well as the RUC's pertaining to the corresponding isotropic materials, are then used in the closure modelling of electrical charge transport and deterministic expressions for Ohm's law and the formation factor in three different types of homogeneous porous media are derived. The expressions for the formation factor applicable to isotropic materials are then validated against a substantial number of data sets as well as against other theoretical and semi-empirical models.

It may, therefore, be concluded that the two encompassing goals of this study, namely to make general theoretical contributions as well as to derive expressions for engineering applications have been achieved. The relations for the friction factor or permeability, inertial term and formation factor are expressed in terms of fluid properties as well as measurable geometric characteristics of porous media, thus giving the model predictive capabilities.

5.2 Main findings and conclusions

5.2.1 Flux field lineality and tortuosity

While reviewing the literature on tortuosity it became apparent that there are differences of opinion as to what tortuosity is and how to qualify the concept of tortuosity. In many instances, the different definitions are unique with each one correct in its domain of application. The flux related lineality, of which the tortuosity is the inverse, presented in Section 2.7, was obtained when deriving an estimate of local fluxes which is more representative of the actual flux than the intrinsic phase average flux. The flux related tortuosity depends on the local transport lines and requires a pore-scale model as well as local flow conditions to obtain its functional form from which the tortuosity value may be calculated for a particular application. It may, therefore, be used in conjunction with different types of pore-scale models.

It was also indicated that when Newtonian fluid transport is modelled with a capillary model consisting of uniform tubes the flux related tortuosity reduces to a ratio of lengths and serves the same role as the tortuosity introduced by Carman (1937), namely as a correction for the increased pore velocity compared to the intrinsic phase average velocity. The analysis of the flux related tortuosity may thus be considered as a theoretical definition for the Carman-type tortuosity in the context of the volume averaging theory. Furthermore, a key concept in the flux field tortuosity is the incorporation of the effective volume, or area in the case of an REA, contributing to the transport in the macroscopic flow direction compared to the total fluid volume. The idea of an effective area, or direction-dependent area, has been introduced by Ruth and Suman (1992) through the areosity scaler. However, it was indicated that the lineality tensor is an extension of the areosity scaler to a second order tensorial quantity applicable to various types of transport and flow directions.

5.2.2 The RUC-model

In the initial part of Chapter 2 the concept of a Representative Unit Cell (RUC) as initially introduced by Du Plessis and Masliyah (1988) has been discussed and some indication was given as to the use of the RUC's in engineering applications. This section also serves to highlight certain salient features which might be misinterpreted as illustrated by Suman and Ruth (1993) who reduced the concept of an RUC to a one-dimensional system of tubes or a repetitive cell in a network model. An RUC is only conceptual and corresponds to the smallest REV containing the average geometry.

New RUC's applicable to anisotropic foamlike materials, granular porous media and prismatic bundles were developed and applied in the closure modelling of Newtonian fluid transport and electrical conduction. The different steps which were followed during the modelling processes have been clearly presented since in RUC's with variable channel sections certain simplifying assumptions applicable to the isotropic modelling are not applicable. It is concluded that the general modelling strategy is equally applicable to isotropic and anisotropic materials. During the validation of the anisotropic foamlike model, a sensitivity analysis on the input indicated that the dimensions of an RUC should be determined fairly accurately as it may have a significant influence on the predictions. Determination of the linear dimensions is most probably the weakest link in applying the resulting expressions.

The closure modelling for both the fluid transport and electrical conduction centred around terms containing the integral of a quantity, which depends on the microscopic flux, over the fluid-solid surface area in an REV or RUC. It may be concluded that the RUC's are effective in aiding modelling of these types of terms.

5.2.3 Fluid transport

Deterministic expressions were derived for the pressure gradient as a function of the superficial velocity and geometric characteristics of the porous medium for three different types of idealised porous media. The expressions are valid in two laminar flow regions, namely the Darcy and Forchheimer regimes. The model for foamlike materials were validated against a benchmark data set and it was deduced that the measurements were predicted within 6% in the Forchheimer regime and in the Darcy regime the pressure gradient was under predicted by approximately 32%. Therefore, the model results may be used successfully as a first order estimate in applications where permeability measurements are not feasible.

5.2.4 Formation factor

The closure modelling for the charge transport was aided by employing the same RUC's that were used for modelling the fluid transport. This indicated that the RUC-model may successfully be extended to different types of flow processes. The expressions for the formation factor are not equal to χ^2/ϵ as derived from capillary models. It also appears from the present analysis that the formation factor may be expressed in terms of the tortuosity and porosity only when the flow channels have equal areas.

Besides analysing the formation factor for anisotropic porous media, formation factor expressions were also derived for isotropic foams, granular porous media and prismatic bundles. These predictions of the formation factor for isotropic materials have been compared to a number of experimental measurements from different sources. In general, the predictions for high porosity foamlike materials compared very well to the measurements and the predictions of the isotropic granular model compared favourably to the measurements provided that the porous material consists of definite granules above a porosity of approximately 0.2. For low porosity sandstones the predictions are less accurate and this is attributed to percolation effects not included in the RUC's. It is concluded that, in general, the formation factor expressions may be put to practical use.

5.3 Proposals for future research

The pore-scale RUC's and accompanying modelling strategy have successfully been applied to charge transport which essentially depends on the diffusion of charge carriers on the microscopic level. A possible next step might be to apply the model to stationary chemical diffusion.

The low porosity predictions of the formation factor indicated that the RUC-model does not account for blocked pores, effective porosities and percolation effects. From a geometric point of view it is debatable whether the RUC's should be extended to incorporate these features as well as to account for a possible pore size distribution. The reason being that the RUC's contain only the average geometry and it is doubtful whether too much detail should be incorporated, in which case it would be more productive to reconstruct actual building blocks of the material. The low porosity effects may be modelled as a separate geometric feature and then added to the results obtained from the RUC's.

The model predictions need to be verified against more experimental data. Generally, there is an abundance of measured permeabilities and formation factors, but there is a shortage of values of porous medium characteristics, such as different grain dimensions or pore sizes in the case of anisotropic materials. Although the parameters which are necessary for the model predictions can easily be determined, they are usually not measured since the permeability and formation factor are considered as independent parameters which cannot directly be related to structural parameter of the porous medium. The validation and general engineering use of the predictions in this study, as well as other studies using the RUC's, may be aided by a computer package which requires structural information as input and providing at least a first order accurate prediction of different transport processes applicable to a wide variety of isotropic and anisotropic porous media.

Appendix A
Capillary models

A.1 Introduction

A large number of models exist which describe transport phenomena in porous media and these models may be classified according to a number of different categories, for example, geometric models, statistical models, empirical models or numerical models, to name but a few. There is very often not a clear distinction between the models, but, following the classification system of Dullien (1979), a model may be described as geometrical if the main thrust of the model constitutes replacing the porous medium by a geometric equivalent. The main objective of this appendix is to present one type of geometric model, namely the capillary model, in more detail. Many variations of capillary models exists, but the main features of these models may be summed up in the Carman-Kozeny model for fluid flow at low Reynolds numbers. An additional reason for concentrating on the Carman-Kozeny model is to present the initial ideas of modellers to incorporate the tortuosity of the interstitial pore-space. Another capillary model, developed by Comiti and Renaud (1989), is also discussed since some of the experimental results used during this study have also been compared with this model.

A.2 The Carman-Kozeny model

In the Carman-Kozeny model the porous medium, which was initially considered to be a granular bed, is assumed to be equivalent to a group of parallel, similar channels, such that the total internal surface and the total internal volume are equal to the particle surface and to the pore-volume, respectively (Carman, 1937). According to the Poiseuille law for laminar flow in circular tubes of *diameter* d_c, the average fluid speed, w, across a cross-section of a tube of length L (Bird *et al.*, 1960) is

$$w = \frac{d_c^2}{32\mu}\frac{\Delta P}{L} \tag{A.1}$$

where μ is the viscosity of the fluid and ΔP is the pressure head difference over the column of overall length L. Initially the average velocity in a channel or pore, w, was replaced directly by the average fluid velocity, q, through the porous medium.

However, as it became apparent that the average speed in a pore is different from the overall seepage velocity, a more appropriate velocity was sought. In addition, a number of other adaptations must also be made to (A.1) to account for the fact that the flow is through an ensemble of tubes which represent the porous medium. These changes include the following:

- Firstly, Dupuit's assumption must be in invoked. According to Carman (1937), Dupuit was the first to realise that the seepage velocity q must be less than the actual velocity in the pores. If the pore-space in the bed be considered evenly distributed, then the porosity of a layer of infinitesimal thickness normal to the direction of flow will be equal to the porosity, ϵ of the bed as a whole. As, for such a layer, the fractional free volume will be equal to the fractional free area, the true velocity of flow must be approximated by

$$w = \frac{q}{\epsilon} \tag{A.2}$$

  which is the interstitial velocity. The division of the superficial velocity by the porosity in context of Darcy's law became known as Dupuit's assumption.

- A correction must be made for the fact that the channels in a porous medium are not necessarily circular. This is achieved by replacing the pore diameter d_c with four times the mean hydraulic radius, R_h. The mean hydraulic radius is defined as the ratio of the volume of fluid in a circular tube to the surface of the tube presented to the flow and for a circular pipe this leads to $d_c = 4R_h$. As shown in Section 2.6.3 (equation (2.40)), for a porous medium the mean hydraulic radius, R_h may be expressed as

$$R_h = \frac{\epsilon U_o}{S_{fs}}. \tag{A.3}$$

- A correction must be made for the fact that due to the tortuous character of the flow through the bed, the length of the equivalent channels should be L_e, where L_e is greater than the depth, L, of the bed.

If all these corrections are incorporated into (A.1) then the flow through the bed may be described by

$$q = \frac{\epsilon R_h^2}{k_o \mu} \frac{\Delta P}{L_e} \tag{A.4}$$

where k_o is a shape factor which depends on the cross-section of the channels. For a circular tube $k_o = 2$. Some other values for k_o are presented by Carman (1937). Equation (A.4) is referred to by Carman (1937) as the Kozeny equation.

However, Carman made an additional change to this equation. He pointed out that Dupuit's assumption is not sufficient but the velocity must be altered further. As noted by Carman: "If in any section of the bed normal to the direction of flow, the fractional free area is ϵ, then the average velocity parallel to the direction of flow must be $\frac{q}{\epsilon}$. As, however, the actual path pursued by an element of the fluid is sinuous, this represents only the component of velocity parallel to the direction of flow. Thus, the time taken for such an element of fluid to pass over a sinuous track of length, L_e, at a velocity $\frac{q}{\epsilon}\frac{L_e}{L}$, corresponds to that taken to pass over a distance L, at a velocity $\frac{q}{\epsilon}$. In short, the true value for w is $\frac{q}{\epsilon}\frac{L_e}{L}$ ". Therefore, he set

$$w = \frac{q}{\epsilon}\frac{L_e}{L}. \tag{A.5}$$

By inserting (A.5) into (A.2) instead of employing Dupuit's assumption, but still correcting for noncircular pores by setting $d_c = 4R_h$ and using L_e for the tube length, (A.2) may be written as

$$q = \frac{\epsilon R_h^2}{k_o \mu}\frac{\Delta P}{L}\left(\frac{L}{L_e}\right)^2. \tag{A.6}$$

Equation (A.6) became known as the Carman-Kozeny equation and the combined factor

$$k' = k_o\left(\frac{L_e}{L}\right)^2 \tag{A.7}$$

is the so-called Kozeny constant (Wyllie and Spangler, 1952). According to Dullien (1979, p171), this is the basic form of most geometric models, differing only in the method of calculating the mean hydraulic radius and in the value used for the Kozeny constant, which is a function of pore geometry.

The Carman-Kozeny equation is only valid for creeping flow within the low Reynolds number flow domain. For analyses of flow at higher Reynolds numbers a different approach is required as inertial effects are predominant over viscous forces. In this regard, Carman (1937) pointed out that the capillaries must then be considered to

be curved to account for inertial effects. Dullien (1979) also notes that the Carman-Kozeny model yields inadequate results if the particle shapes deviate strongly from a spherical shape and when there are a broad particle size distribution present and in consolidated media. According to Dullien (1979) the main reasons for the deviations of the predicted permeabilities of this model and measurements reside with the possibility that the Carman-Kozeny model does not predict the correct dependence of permeability on porosity and suggests that at high porosities the flow is more akin to flow around a submerged object than to flow in conduits. Other possible reasons for the deviation are the inability of the model to distinguish between various types of pore sizes and the fact that the model does not incorporate the bulging and narrowing of a particular flow channel. Some other criticisms against the Kozeny model are also given by Scheidegger (1954).

A.3 The model of Comiti and Renaud

Notwithstanding the shortcomings of the Carman-Kozeny model, capillary models are still developed and further refined. One such capillary-type model is the model of Comiti and Renaud (1989). This model appears to be quite successful, not only in the quantitative prediction of the intrapore viscous shear stresses of Darcy flow, but also in the troublesome inertial regime. The model was initially developed to obtain structural parameters for flow through anisotropic rectangular parallelepipedal particles, but it has also been applied to fluid flow through high porosity metallic foams. The model, therefore, does not distinguish between various types of porous media, but may be applied to granular as well as consolidated isotropic or anisotropic materials.

According to the model, the porous medium is considered to consist of m curved cylindrical channels, each of length L_e and diameter d_c within a container of height L and with a surface area S_c perpendicular to the flow. As illustrated in Figure A.1, adjacent channels do not intersect and there are no junctions or overlaps between channels. The tortuosity of the medium is defined as

$$\chi = \frac{L_e}{L} \tag{A.8}$$

where L is the height of the packed column. The diameter of the pores are also expressed

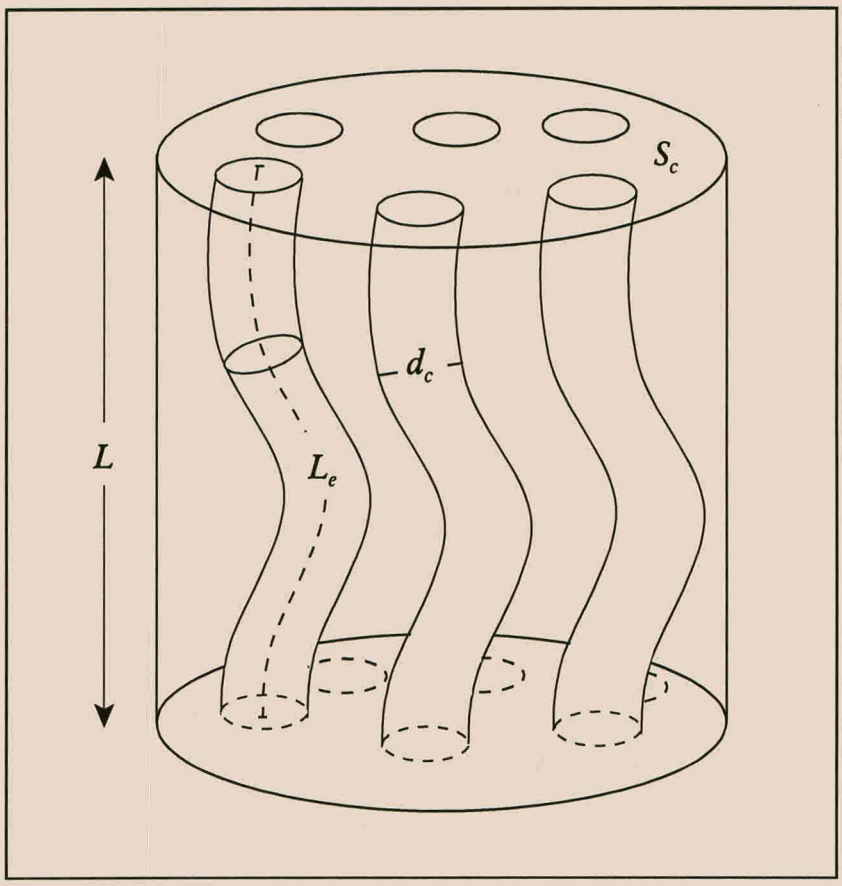

Figure A.1. A schematic representation of the capillary model of Comiti and Renaud (1989).

in terms of the hydraulic radius, therefore

$$\begin{aligned} d_c &= 4R_h \\ &= \frac{4\epsilon U_o}{S'_{fs}} \\ &= \frac{4\epsilon}{A_{vd}(1-\epsilon)}. \end{aligned} \tag{A.9}$$

This equation differs from the average pore diameter expressed in (2.41) due to the fact that Comiti and Renaud (1989) consider the fluid-solid surface to be the surface area of particles presented to the flow instead of the mean surface area of the particles. In general A_{vd} will be less than A_{vs} due to the possible overlapping of particles and thereby shielding it from the flow.

By using a similar argument as presented by Carman (1937) and Scheidegger (1974), they also equate the average time of flow through the bed to the time a fluid particle takes to move through the tortuous tubes to obtain the same conclusion as presented

in (A.5), namely

$$w = \frac{\chi q}{\epsilon} \tag{A.10}$$

where w is the averaged speed in a pore obtained from Poiseuille's law.

A.3.1 Interstitial flow modelling

According to this model the pressure drop over a range of Reynolds numbers, which include creeping- and inertial flow regimes, may be considered as the sum of two terms:

- The first, proportional to the flow velocity, is due to viscous resistance at the walls of the pore.
- The other, proportional to the square of the flow velocity, is due to inertial resistance and corresponds to kinetic energy losses caused by direction changes.

A.3.1.1 Interstitial viscous flow

In a similar manner as the Carman-Kozeny model, the starting point for modelling the flow is by applying the Poiseuille law for laminar flow in circular tubes of diameter d_c to obtain the average velocity across a cross-section of a pore as is given by (A.1). When the total distance which the fluid flows within the channels, L_e is inserted into this equation, the pressure difference is

$$\Delta P = \frac{32 k_s w \mu L_e}{d_c^2} = \frac{32 k_s q \chi \mu L_e A_{vd}^2 (1-\epsilon)^2}{16 \epsilon^3} \tag{A.11}$$

where k_s is a shape factor and μ is the dynamic viscosity. Therefore, the pressure gradient is given by

$$\frac{\Delta P}{L} = 2 k_s \chi^2 \mu A_{vd}^2 \frac{(1-\epsilon)^2}{\epsilon^3} q. \tag{A.12}$$

The shape factor k_s depends on the geometry of the pores and being consistent with k_o, for cylindrical tubes $k_s = 1$. However, as indicated by Comiti (1987), it may vary between 0.6 and 1.5 depending on the geometry of the pores.

A.3.1.2 Interstitial inertial effects

According to the Poiseuille law for turbulent flow in tubes which are not necessarily circular, the pressure drop over a tube of length L_e is given (Bird *et al.*, 1960) as

$$\Delta P = \frac{1}{2}\rho w^2 \frac{L_e}{R_h} f_r. \tag{A.13}$$

The hydraulic radius, R_h, accounts for the non-circular form of the actual pores and f_r is a roughness friction factor. By noting that $d_c = 4R_h$ and using equations (A.10) and (A.9), the pressure drop becomes

$$\frac{\Delta P}{L} = \frac{2\rho\chi^2 f_r q^2 L_e}{d_c \epsilon^2 L} = \frac{f_r \chi^3 A_{vd}(1-\epsilon)\rho q^2}{2\epsilon^3}. \tag{A.14}$$

To take into account the direction changes in the flow, it is assumed that the channels are very rough conduits of which the roughness, E, has the same range of magnitude as the diameter d_c. The friction factor is then calculated from the Nikuradse formula given by Duncan *et al.* (1960) as

$$\frac{1}{\sqrt{f_r/2}} = 2.46 \ln\left(\frac{d_c}{2E}\right) + 4.92. \tag{A.15}$$

With $E = d_c$, this equation yields $f_r/2 = 0.0986$.

The pressure drop corresponding to kinetic energy losses may be written as

$$\frac{\Delta P}{L} = 0.0968\chi^3 A_{vd} \frac{(1-\epsilon)}{\epsilon^3}\rho q^2 \tag{A.16}$$

which yields a squared dependence of pressure drop on velocity.

A.3.1.3 General equation

The pressure drop for fluid flow through a packed bed is obtained by combining (A.12) and (A.16), and may be written as

$$\frac{\Delta P}{Lq} = Mq + N \tag{A.17}$$

with

$$M = 0.0968\chi^3 A_{vd}\rho\frac{(1-\epsilon)}{\epsilon^3} \tag{A.18}$$

$$N = 2k_s\chi^2\mu A_{vd}^2\frac{(1-\epsilon)^2}{\epsilon^3}. \tag{A.19}$$

By means of pressure drop experiments M and N may be determined experimentally from which χ and A_{vd} can be determined. Comiti and Renaud (1989) further refined these expressions to account for the additional wall effects encountered during experiments in packed columns.

As noted by Montillet *et al.* (1992), structural parameters cannot be calculated from experimental data obtained with different fluid characteristics. It is, therefore, more appropriate to cast (A.17) in a form from which one can derive general calculations. This is achieved by defining a friction factor f, similar to (2.3), and a Reynolds number Re given by

$$f = \frac{\Delta P}{L}\frac{\epsilon^3 d_c}{(1-\epsilon)\rho q^2} \tag{A.20}$$

and

$$Re = \frac{\rho q d_c}{\mu} \tag{A.21}$$

respectively. By referring to these expressions (A.17) may be written as

$$\frac{f}{d_c} = A + \frac{B}{Re/d_c} \tag{A.22}$$

with

$$A = 0.0968\chi^3 A_{vd} \tag{A.23}$$

and

$$B = 2\chi^2 A_{vd}^2(1-\epsilon). \tag{A.24}$$

An additional advantage of the representation of f/d_c versus d_c/Re is that it is not necessary to explicitly know d_c.

A.3.2 Formation factor

As discussed in Section 2.6.5 the formation factor is a parameter which indicates the degree to which a porous medium filled with an electrolyte can conduct an electric current. It may be calculated from the resistivity of the electrolyte ρ_w and the resistivity of the saturated porous medium, ρ_o and is given (Archie, 1942; Wyllie and Spangler, 1952) by

$$F = \frac{\rho_o}{\rho_w} = \frac{R_o}{R_w} \tag{A.25}$$

where R_o is the resistance of the electrolytically saturated porous medium and R_w is the resistance of the volume of electrolyte of the same external dimensions as the saturated porous medium and measured using the same relative orientation of the electrodes. The resistance of the electrolyte to the flow of current without the presence of a porous medium in a container of the same dimensions as the porous medium is given by

$$\frac{1}{R_w} = \frac{S_c}{\rho_w L}. \tag{A.26}$$

where S_c is the surface area of the container perpendicular to the flow direction and L is its height. On the other hand, one may also argue that the resistance of the porous medium saturated with electrolyte is given by

$$\frac{1}{R_o} = \frac{S_c}{\rho_o L}. \tag{A.27}$$

However, the resistance of the saturated porous medium to the flow of current may also be determined alternatively. If the solid material of the porous medium is also conductive then the system may be viewed as consisting of two phases coupled in parallel (Jacquet, 1991). The one phase is the void space consisting of m tubes each with a resistance $R_{(i)}$ and the solid phase with a resistance R_s. The total resistance of the system is then given by

$$\frac{1}{R_o} = \sum_{i=1}^{m} \frac{1}{R_{(i)}} + \frac{1}{R_s}. \tag{A.28}$$

In the present case it is assumed that the solid matrix is nonconductive and, therefore, $1/R_s = 0$. If $s_{(i)}$ is the cross-section of tube i, then

$$\frac{1}{R_o} = \sum_{i=1}^{m} \frac{s_{(i)}}{\rho_w L_e} = \frac{m s_{(i)}}{\rho_w L_e} \tag{A.29}$$

since all the tubes have equal cross-sections and lengths, and the resistivity of the electrolyte is the same in each tube.

To calculate the electrical resistance of the saturated porous medium Wyllie and Spangler (1952) and Montillet (1994) set

$$m s_{(i)} = \epsilon S_c \tag{A.30}$$

to obtain

$$\frac{1}{R_o} = \frac{\epsilon S_c}{\rho_w L_e}. \tag{A.31}$$

According to (A.25), (A.26) and (A.31) it follows that

$$\begin{aligned} F &= \frac{R_o}{R_w} \\ &= \frac{\rho_w L_e}{\epsilon S_c} \frac{S_c}{\rho_w L} \\ &= \frac{\chi}{\epsilon}. \end{aligned} \tag{A.32}$$

A similar expression for the formation factor has also been obtained by various authors, for example, Wyllie and Rose (1950).

As noted in Section 2.6.5 the formation factor may be related to the porosity through an electrical retardation factor X_e. According to Clennell (1997), the coefficient X_e may be equal to either L_e/L or $(L_e/L)^2$ depending on how the formation factor-porosity relationship is derived. The derivation of (A.32) illustrates one path whereas Jacquet (1991), also using the capillary model, followed an alternative path and obtained a different expression for R_o and thus also for the formation factor. She refers to the definition of the porosity from which it follows that

$$\epsilon = \frac{U_f}{U_o} = \frac{m s_{(i)} L_e}{L S_c}. \tag{A.33}$$

This equation yields

$$ms_{(i)} = \frac{\epsilon S_c L}{L_e} \tag{A.34}$$

and (A.29) may then be written as

$$\frac{1}{R_o} = \frac{\epsilon L S_c}{\rho_w L_e^2} = \frac{\epsilon S_c}{\rho_w \chi^2 L}. \tag{A.35}$$

By equating the two expressions for the overall resistance, (A.27) and (A.35), it follows that

$$\frac{\rho_o L}{S_c} = \frac{\rho_w \chi^2 L}{\epsilon S_c} \tag{A.36}$$

which yields

$$F = \frac{\rho_o}{\rho_w} = \frac{\chi^2}{\epsilon}. \tag{A.37}$$

The discrepancy in the formation factors as given by (A.32) and (A.37) resides with the interpretation of $ms_{(i)}$. It would appear as if (A.37) is correct since it is calculated from the expression for the volumetric porosity and do not rely on any assumptions. The problem with using the areal porosity is that it ignores the fact that ϵS_c also contains the additional areas of capillaries being intersected obliquely at the ends which yields a flow area larger than the effective cross-sectional area of a channel. This may be remedied by realising that the area of each tube through which the current flows in the macroscopic flow direction is the effective flow area of the tube which may be denoted by $s^e_{(i)}$. It then follows that

$$ms^e_{(i)} = \xi S_c \tag{A.38}$$

where ξ is the areosity defined in (2.49). Equation (A.29) then becomes

$$\frac{1}{R_o} = \frac{\xi S_c}{\rho_w L_e} \tag{A.39}$$

and similar to the derivation of (A.32) it follows that

$$F = \frac{\chi}{\xi}. \tag{A.40}$$

It is indicated in Section 2.7.9 that the lineality is the inverse of the tortuosity and in combination with (2.94) and (A.40) it follows that

$$F = \frac{\chi}{\epsilon \mathcal{L}} = \frac{\chi^2}{\epsilon}. \tag{A.41}$$

Therefore, according to the capillary model the formation factor may be related to the square of the tortuosity.

Walsh and Brace (1984) revisited the capillary model of Wyllie and Rose (1950) and indicated that the effective flow area is a requirement to obtain (A.37) whereas an incorrect usage of the total fluid area leads to (A.32). Clennell (1997) assesses that consensus is firmly on the side of (A.37) being correct. The discrepancy is simply a reflection of the different models: one pore-space model conserves tube volume using stereological relationships between intercepted area and porosity while the other corrects for intercepted area of an inclined tube using an approximation that is exactly analogous to the modified Dupuit's relation used by Carman (1956). According to Clennell (1997), a truly rigorous derivation requires an assessment of the actual trajectories of electrical flow lines through the pore-space.

Appendix B
Averaging rules and identities

The objective of this appendix is to derive a number of averaging rules and identities as well as Slattery's averaging theorem from first principles by employing designated averaging operators. The phase average of a microscopic tensorial quantity, $\phi_{jkl...}$, is given by

$$\langle \phi_{jkl...} \rangle \equiv \frac{1}{U_o} \iiint_{U_f} \phi_{jkl...} \, dU \tag{B.1}$$

and the intrinsic phase average is defined as

$$\langle \phi_{jkl...} \rangle^f \equiv \frac{1}{U_f} \iiint_{U_f} \phi_{jkl...} \, dU. \tag{B.2}$$

The deviation of a microscopic quantity is given by

$$\overset{o}{\phi}_{jkl...} \equiv \phi_{jkl...} - \langle \phi_{jkl...} \rangle^f \tag{B.3}$$

and as indicated in Section 2.4.1

$$\langle \langle \phi_{jkl...} \rangle \rangle = \epsilon \langle \phi_{jkl...} \rangle \tag{B.4}$$

where ϵ is the porosity, defined as

$$\epsilon \equiv \frac{U_f}{U_o}. \tag{B.5}$$

Here U_f is the fluid volume and U_o the total volume of an REV for a two phase porous system.

B.1 Averaging identities

From the above definitions it is possible to establish a number of *identities* which will prove to be quite useful when transforming averaged balance equations. Balance equations usually contain a number of terms and, therefore, firstly consider the average of

a sum which may be written as the sum of the average. Therefore,

$$\begin{aligned}\langle \phi_{jkl\ldots} + \lambda_{pqr\ldots} \rangle &= \frac{1}{U_o} \iiint_{U_f} (\phi_{jkl\ldots} + \lambda_{pqr\ldots})\, dU \\ &= \frac{1}{U_o} \iiint_{U_f} \phi_{jkl\ldots}\, dU + \frac{1}{U_o} \iiint_{U_f} \lambda_{pqr\ldots}\, dU \\ &= \langle \phi_{jkl\ldots} \rangle + \langle \lambda_{pqr\ldots} \rangle . \end{aligned} \tag{B.6}$$

In the case of the average of a product between a constant and a dependent variable, the constant may be removed from the averaging operator. With β any constant it follows that

$$\begin{aligned}\langle \beta\, \phi_{jkl\ldots} \rangle &= \frac{1}{U_o} \iiint_{U_f} \beta\, \phi_{jkl\ldots}\, dU \\ &= \frac{\beta}{U_o} \iiint_{U_f} \phi_{jkl\ldots}\, dU \\ &= \beta\, \langle \phi_{jkl\ldots} \rangle . \end{aligned} \tag{B.7}$$

The relation between the phase average and intrinsic phase averages is given by

$$\begin{aligned}\langle \phi_{jkl\ldots} \rangle &= \frac{1}{U_o} \iiint_{U_f} \phi_{jkl\ldots}\, dU \\ &= \frac{U_f}{U_o} \frac{1}{U_f} \iiint_{U_f} \phi_{jkl\ldots}\, dU \\ &= \epsilon\, \langle \phi_{jkl\ldots} \rangle^f . \end{aligned} \tag{B.8}$$

Since an REV is selected such that the various averaged quantities are either uniform or vary linearly over the REV, it follows that

$$\begin{aligned}\left\langle \langle \phi_{jkl\ldots} \rangle^f \right\rangle^f &= \frac{1}{U_f} \iiint_{U_f} \langle \phi_{jkl\ldots} \rangle^f\, dU \\ &= \frac{\langle \phi_{jkl\ldots} \rangle^f}{U_f} \iiint_{U_f} dU \\ &= \langle \phi_{jkl\ldots} \rangle^f . \end{aligned} \tag{B.9}$$

It may be shown in a similar manner that

$$\langle \langle \phi_{jkl\ldots} \rangle \rangle^f = \langle \phi_{jkl\ldots} \rangle . \tag{B.10}$$

Since the phase average is taken over only the void or fluid volume of an REV, it follows that

$$\begin{aligned}\left\langle \langle \phi_{jkl\ldots} \rangle^f \right\rangle &= \frac{1}{U_o} \iiint_{U_f} \langle \phi_{jkl\ldots} \rangle^f \, dU \\ &= \langle \phi_{jkl\ldots} \rangle^f \frac{U_f}{U_o} \\ &= \epsilon \langle \phi_{jkl\ldots} \rangle^f . \end{aligned} \tag{B.11}$$

This identity is different from the one proposed by Gray (1975), since he calculates the phase average of a uniform quantity also over the solid phase.

It is also possible to obtain averages of other parameters which are uniform over an REV. If we set $\phi = 1$ in equation (B.1), it follows that

$$\begin{aligned}\langle 1 \rangle &= \frac{1}{U_o} \iiint_{U_f} 1 \, dU \\ &= \frac{U_f}{U_o} \\ &= \epsilon. \end{aligned} \tag{B.12}$$

The intrinsic phase average of $\phi = 1$ yields

$$\begin{aligned}\langle 1 \rangle^f &= \frac{1}{U_f} \iiint_{U_f} 1 \, dU \\ &= \frac{U_f}{U_f} \\ &= 1. \end{aligned} \tag{B.13}$$

An important feature of the deviation is that its average is zero,

$$\begin{aligned}\left\langle \overset{\circ}{\phi}_{jkl\ldots} \right\rangle &= \frac{1}{U_o} \iiint_{U_f} \overset{\circ}{\phi}_{jkl\ldots} \, dU \\ &= \frac{1}{U_o} \iiint_{U_f} \left(\phi_{jkl\ldots} - \langle \phi_{jkl\ldots} \rangle^f \right) dU \\ &= \frac{1}{U_o} \iiint_{U_f} \phi_{jkl\ldots} \, dU - \frac{1}{U_o} \iiint_{U_f} \langle \phi_{jkl\ldots} \rangle^f \, dU \\ &= \langle \phi_{jkl\ldots} \rangle - \left\langle \langle \phi_{jkl\ldots} \rangle^f \right\rangle \\ &= \langle \phi_{jkl\ldots} \rangle - \epsilon \langle \phi_{jkl\ldots} \rangle^f \\ &= \langle \phi_{jkl\ldots} \rangle - \langle \phi_{jkl\ldots} \rangle \\ &= 0. \end{aligned} \tag{B.14}$$

This identity is a direct result of (B.11). Although Gray (1975) does not concur with (B.11), he still enforces that the phase average of the deviation must be zero and accepts (B.14) as a necessary result. It also follows that the deviation of an average is

$$\begin{aligned}(\langle \overset{o}{\phi}_{jkl\ldots} \rangle) &= \langle \phi_{jkl\ldots} \rangle - \langle \langle \phi_{jkl\ldots} \rangle \rangle^f \\ &= \langle \phi_{jkl\ldots} \rangle - \langle \phi_{jkl\ldots} \rangle \\ &= 0. \end{aligned} \tag{B.15}$$

The deviation of a deviation is equal to the deviation,

$$\begin{aligned}\overset{o}{\overset{o}{\phi}}_{jkl\ldots} &= \overset{o}{\phi}_{jkl\ldots} - \left\langle \overset{o}{\phi}_{jkl\ldots} \right\rangle^f \\ &= \overset{o}{\phi}_{jkl\ldots} - \frac{1}{U_f} \iiint_{U_f} \left(\phi_{jkl\ldots} - \langle \phi_{jkl\ldots} \rangle^f \right) dU \\ &= \overset{o}{\phi}_{jkl\ldots} - \frac{1}{U_f} \iiint_{U_f} \phi_{jkl\ldots}\, dU + \frac{1}{U_f} \iiint_{U_f} \langle \phi_{jkl\ldots} \rangle^f \, dU \\ &= \overset{o}{\phi}_{jkl\ldots} - \langle \phi_{jkl\ldots} \rangle^f + \langle \phi_{jkl\ldots} \rangle^f \\ &= \overset{o}{\phi}_{jkl\ldots}. \end{aligned} \tag{B.16}$$

The average of a product between the deviation and an average may be analysed to yield

$$\begin{aligned}\left\langle \overset{o}{\phi}_{jkl\ldots} \langle \lambda_{pqr\ldots} \rangle \right\rangle &= \frac{1}{U_o} \iiint_{U_f} \overset{o}{\phi}_{jkl\ldots} \langle \lambda_{pqr\ldots} \rangle \, dU \\ &= \frac{1}{U_o} \iiint_{U_f} \left(\phi_{jkl\ldots} - \langle \phi_{jkl\ldots} \rangle^f \right) \langle \lambda_{pqr\ldots} \rangle \, dU \\ &= \frac{1}{U_o} \iiint_{U_f} \phi_{jkl\ldots} \langle \lambda_{pqr\ldots} \rangle \, dU \\ &\quad - \frac{1}{U_o} \iiint_{U_f} \langle \phi_{jkl\ldots} \rangle^f \langle \lambda_{pqr\ldots} \rangle \, dU \\ &= \langle \lambda_{pqr\ldots} \rangle \frac{1}{U_o} \iiint_{U_f} \phi_{jkl\ldots} \, dU \\ &\quad - \langle \lambda_{pqr\ldots} \rangle \langle \phi_{jkl\ldots} \rangle^f \frac{1}{U_o} \iiint_{U_f} dU \\ &= \langle \lambda_{pqr\ldots} \rangle \langle \phi_{jkl\ldots} \rangle - \langle \lambda_{pqr\ldots} \rangle \langle \phi_{jkl\ldots} \rangle^f \frac{U_f}{U_o} \\ &= \langle \lambda_{pqr\ldots} \rangle \langle \phi_{jkl\ldots} \rangle - \epsilon \langle \lambda_{pqr\ldots} \rangle \langle \phi_{jkl\ldots} \rangle^f \\ &= \langle \lambda_{pqr\ldots} \rangle \langle \phi_{jkl\ldots} \rangle - \langle \lambda_{pqr\ldots} \rangle \langle \phi_{jkl\ldots} \rangle \\ &= 0. \end{aligned} \tag{B.17}$$

It follows in a similar manner that

$$\left\langle \langle \phi_{jkl\ldots} \rangle \, \overset{o}{\lambda}_{pqr\ldots} \right\rangle = 0 \qquad \text{and} \qquad \left\langle \overset{o}{\phi}_{jkl\ldots} \, \langle \lambda_{pqr\ldots} \rangle^f \right\rangle = 0. \tag{B.18}$$

The phase average of the product of two deviations may be written as

$$\begin{aligned}
\left\langle \overset{o}{\phi}_{jkl\ldots} \overset{o}{\lambda}_{pqr\ldots} \right\rangle &= \frac{1}{U_o} \iiint_{U_f} \overset{o}{\phi}_{jkl\ldots} \overset{o}{\lambda}_{pqr\ldots} \, dU \\
&= \frac{1}{U_o} \iiint_{U_f} \overset{o}{\phi}_{jkl\ldots} \left(\lambda_{pqr\ldots} - \langle \lambda_{pqr\ldots} \rangle^f \right) dU \\
&= \frac{1}{U_o} \iiint_{U_f} \overset{o}{\phi}_{jkl\ldots} \, \lambda_{pqr\ldots} \, dU - \frac{1}{U_o} \iiint_{U_f} \overset{o}{\phi}_{jkl\ldots} \, \langle \lambda_{pqr\ldots} \rangle^f \, dU \\
&= \left\langle \overset{o}{\phi}_{jkl\ldots} \, \lambda_{pqr\ldots} \right\rangle - \left\langle \overset{o}{\phi}_{jkl\ldots} \, \langle \lambda_{pqr\ldots} \rangle^f \right\rangle \\
&= \left\langle \overset{o}{\phi}_{jkl\ldots} \, \lambda_{pqr\ldots} \right\rangle,
\end{aligned} \tag{B.19}$$

and in a similar manner it follows that

$$\left\langle \overset{o}{\phi}_{jkl\ldots} \overset{o}{\lambda}_{pqr\ldots} \right\rangle = \left\langle \overset{o}{\phi}_{jkl\ldots} \, \lambda_{pqr\ldots} \right\rangle. \tag{B.20}$$

A combination of these two results implies that

$$\left\langle \overset{o}{\phi}_{jkl\ldots} \overset{o}{\lambda}_{pqr\ldots} \right\rangle = \left\langle \overset{o}{\phi}_{jkl\ldots} \, \lambda_{pqr\ldots} \right\rangle = \left\langle \phi_{jkl\ldots} \, \overset{o}{\lambda}_{pqr\ldots} \right\rangle. \tag{B.21}$$

Furthermore, the deviation of a product may be written as

$$\begin{aligned}
(\phi_{jkl\ldots} \overset{o}{\lambda}_{pqr\ldots}) &= \phi_{jkl\ldots} \lambda_{pqr\ldots} - \langle \phi_{jkl\ldots} \lambda_{pqr\ldots} \rangle^f \\
&= \left(\overset{o}{\phi}_{jkl\ldots} + \langle \phi_{jkl\ldots} \rangle^f \right) \left(\overset{o}{\lambda}_{pqr\ldots} + \langle \lambda_{pqr\ldots} \rangle^f \right) \\
&\qquad - \left\langle \left(\overset{o}{\phi}_{jkl\ldots} + \langle \phi_{jkl\ldots} \rangle^f \right) \left(\overset{o}{\lambda}_{pqr\ldots} + \langle \lambda_{pqr\ldots} \rangle^f \right) \right\rangle^f \\
&= \overset{o}{\phi}_{jkl\ldots} \overset{o}{\lambda}_{pqr\ldots} + \overset{o}{\phi}_{jkl\ldots} \langle \lambda_{pqr\ldots} \rangle^f + \langle \phi_{jkl\ldots} \rangle^f \overset{o}{\lambda}_{pqr\ldots} \\
&\quad + \langle \phi_{jkl\ldots} \rangle^f \langle \lambda_{pqr\ldots} \rangle^f - \left\langle \overset{o}{\phi}_{jkl\ldots} \overset{o}{\lambda}_{pqr\ldots} \right\rangle^f - \left\langle \overset{o}{\phi}_{jkl\ldots} \langle \lambda_{pqr\ldots} \rangle^f \right\rangle^f \\
&\quad - \left\langle \langle \phi_{jkl\ldots} \rangle^f \overset{o}{\lambda}_{pqr\ldots} \right\rangle^f - \left\langle \langle \phi_{jkl\ldots} \rangle^f \langle \lambda_{pqr\ldots} \rangle^f \right\rangle^f \\
&= \overset{o}{\phi}_{jkl\ldots} \overset{o}{\lambda}_{pqr\ldots} + \overset{o}{\phi}_{jkl\ldots} \langle \lambda_{pqr\ldots} \rangle^f + \langle \phi_{jkl\ldots} \rangle^f \overset{o}{\lambda}_{pqr\ldots} \\
&\quad - \left\langle \overset{o}{\phi}_{jkl\ldots} \overset{o}{\lambda}_{pqr\ldots} \right\rangle^f
\end{aligned} \tag{B.22}$$

since

$$\left\langle \langle \phi_{jkl\ldots} \rangle^f \langle \lambda_{pqr\ldots} \rangle^f \right\rangle^f = \langle \phi_{jkl\ldots} \rangle^f \langle \lambda_{pqr\ldots} \rangle^f \tag{B.23}$$

and similar to (B.17)

$$\left\langle \overset{o}{\phi}_{jkl\ldots} \langle \lambda_{pqr\ldots} \rangle^f \right\rangle^f = 0. \tag{B.24}$$

Another important identity is the phase average of a product which may be written as

$$\begin{aligned}
\langle \phi_{jkl\ldots} \lambda_{pqr\ldots} \rangle &= \left\langle \left(\langle \phi_{jkl\ldots} \rangle^f + \overset{o}{\phi}_{jkl\ldots} \right) \left(\langle \lambda_{pqr\ldots} \rangle^f + \overset{o}{\lambda}_{pqr\ldots} \right) \right\rangle \\
&= \left\langle \langle \phi_{jkl\ldots} \rangle^f \langle \lambda_{pqr\ldots} \rangle^f + \langle \phi_{jkl\ldots} \rangle^f \overset{o}{\lambda}_{pqr\ldots} + \overset{o}{\phi}_{jkl\ldots} \langle \lambda_{pqr\ldots} \rangle^f \right. \\
&\quad \left. + \overset{o}{\phi}_{jkl\ldots} \overset{o}{\lambda}_{pqr\ldots} \right\rangle \\
&= \langle \phi_{jkl\ldots} \rangle^f \langle \lambda_{pqr\ldots} \rangle^f \langle 1 \rangle + \langle \phi_{jkl\ldots} \rangle^f \left\langle \overset{o}{\lambda}_{pqr\ldots} \right\rangle + \left\langle \overset{o}{\phi}_{jkl\ldots} \right\rangle \langle \lambda_{pqr\ldots} \rangle^f \\
&\quad + \left\langle \overset{o}{\phi}_{jkl\ldots} \overset{o}{\lambda}_{pqr\ldots} \right\rangle \\
&= \epsilon \langle \phi_{jkl\ldots} \rangle^f \langle \lambda_{pqr\ldots} \rangle^f + 0 + 0 + \left\langle \overset{o}{\phi}_{jkl\ldots} \overset{o}{\lambda}_{pqr\ldots} \right\rangle \\
&= \frac{1}{\epsilon} \langle \phi_{jkl\ldots} \rangle \langle \lambda_{pqr\ldots} \rangle + \epsilon \left\langle \overset{o}{\phi}_{jkl\ldots} \overset{o}{\lambda}_{pqr\ldots} \right\rangle^f .
\end{aligned} \tag{B.25}$$

The latter three equations are also provided by Gray (1975) and it is interesting to note from his analysis how it is possible to obtain these expressions without explicitly addressing the question of obtaining a phase average of an average. Therefore, differences of opinion regarding certain issues of the volume averaging theory are accommodated without seriously affecting the final identities and theorems. The identities proven in this section are summarised in Table 2.1.

B.2 Slattery's averaging theorem

Besides the averaging identities, it is also necessary to establish some *averaging rules* by which to transform microscopic balance equations to the macroscopic level. The first averaging rule which is considered addresses the transformation of an average of a spatial gradient to the gradient of the average. Various expressions exist for the average of the spatial gradient, but before deriving these it is first necessary to consider

Slattery's Averaging Theorem. Besides the theoretical importance of this theorem, it is also important from an historical point of view as its introduction provided the first step towards putting the volume averaging theory on a sound mathematical platform and providing a unified approach of obtaining a volumetric average of an equation governing the transport of a specific phase entity of a multiphase continuum. The first derivation of Slattery's averaging theorem was provided by Slattery (1967) while studying the flow of non-Newtonian fluids in porous media. It was also presented independently by Anderson and Jackson (1967) who derived the equation of motion for a fluidized bed and Whitaker (1967) when considering dispersive transport in porous media. Since its first appearances a number of alternative derivations have appeared, but in the present study, only two of the main lines of the derivation of the spatial averaging theorem are discussed.

B.2.1 Averaging theorem by analogy with the transport theorem

The derivation presented here closely follows the exposition of Whitaker (1969), since he provides a fairly detailed theoretical development of the spatial averaging theorem provided that the REV's under consideration are time and space independent.

The general transport theorem for any tensorial quantity $\phi_{jkl\ldots}$ may be written as

$$\frac{d}{dt}\iiint_{U_o(t)} \phi_{jkl\ldots}\, dU = \iiint_{U_o(t)} \frac{\partial \phi_{jkl\ldots}}{\partial t}\, dU + \iint_{S_o(t)} \phi_{jkl\ldots} v_m^b \nu_m\, dS \tag{B.26}$$

where $U_o(t)$ is a material volume bounded by the surface $S_o(t)$, which may move with velocity v_i^b, and ν_i is an outwardly directed normal vector on the differential element dS (Whitaker, 1968). The volume U_o may move through the domain with a velocity which may be different from the velocity of the fluid.

In applying the general transport theorem to transport in porous media, consider U_o to be an REV which may be translated through the porous domain such that its centroid is located on an arbitrary continuous curve. The position vector of points on this curve is described by $\overline{r}_i$ and if the arc length along this curve is denoted by s, then the REV may be considered to be a function of arc length rather than time. Therefore, it is allowed to associate with each point on the arbitrary curve followed by the centroid, an REV with volume $U_o(s)$ bounded by the surface $S_o(s)$. If the fluid volume of the averaging volume is denoted by $U_f(s)$ and its boundary by $S_f(s)$, then the general

transport theorem may be rewritten as

$$\frac{d}{ds}\iiint_{U_f(s)} \phi_{jkl\ldots}\, dU = \iiint_{U_f(s)} \frac{\partial \phi_{jkl\ldots}}{\partial s}\, dU + \iint_{S_f(s)} \phi_{jkl\ldots} \frac{dr_m}{ds}\, \nu_m\, dS \qquad \text{(B.27)}$$

where r_i is the position vector of an arbitrary point *on the fluid surface* of the averaging volume, which consists of S_{fs} and S_{ff} as illustrated in Figure B.1. Therefore, the arc length s fulfils the role of time and the averaging volume changes position as a function of s.

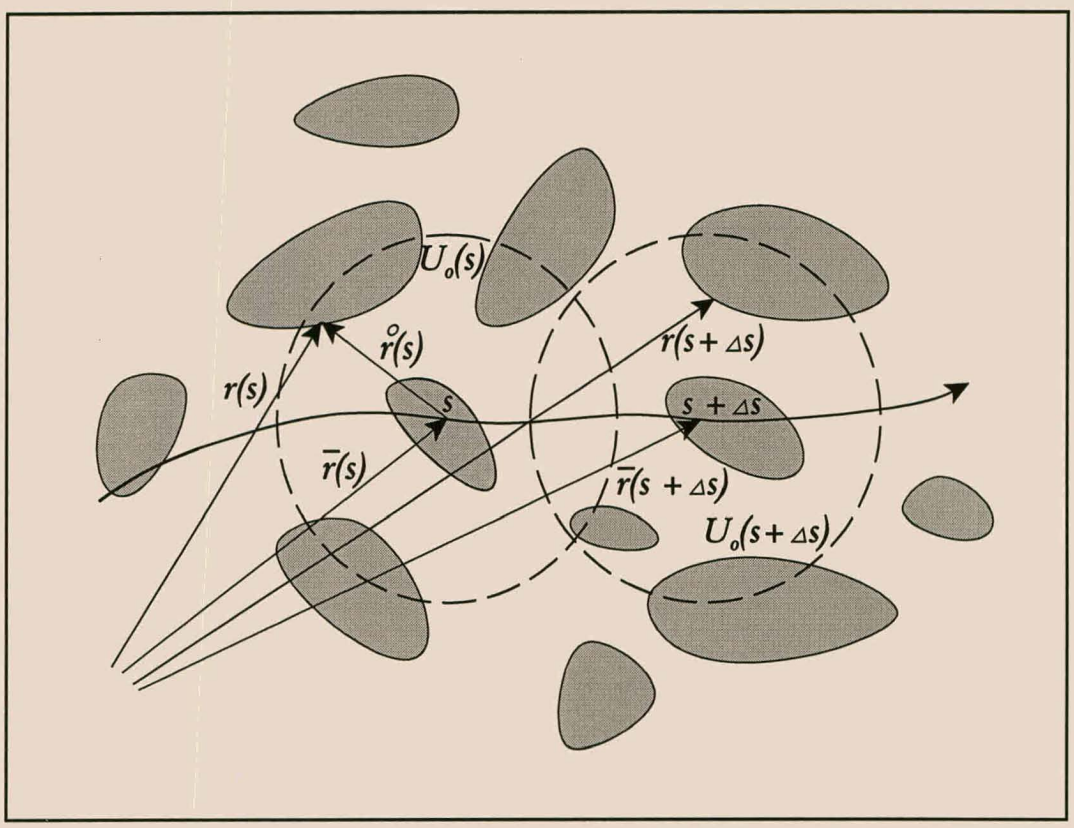

Figure B.1. Definition sketch for the derivative of a volume integral with respect to s.

As previously noted, the microscopic quantity under investigation may in general be a function of space and time, thereby implying that $\phi_{jkl\ldots} = \phi_{jkl\ldots}(x_i, t)$ where x_i indicates a spatial coordinate. These spatial coordinates may be expressed in terms of the arc length, such that $\phi_{jkl\ldots} = \phi_{jkl\ldots}(x_i(s), t)$. Therefore, the total derivative of $\phi_{jkl\ldots}$ with respect to s will in general be non-zero. However, the partial derivative

$$\frac{\partial \phi_{jkl\ldots}}{\partial s} = 0 \qquad \text{(B.28)}$$

since $\phi_{jkl...}$ does not explicitly depend on the arc length. As noted by Slattery (1967), this is equivalent to taking a derivative with respect to s while holding position and time fixed. Equation (B.27) may therefore be written as

$$\frac{d}{ds}\iiint_{U_f(s)} \phi_{jkl...}\, dU \;=\; \iint_{S_f(s)} \phi_{jkl...} \frac{dr_m}{ds}\, \nu_m\, dS. \tag{B.29}$$

As indicated in Figure 2.2, the boundary of the fluid volume within the REV may be subdivided into two area's, namely the fluid-solid surface $S_{fs}(s)$ and the fluid-fluid surface $S_{ff}(s)$, such that

$$S_f(s) \;=\; S_{fs}(s) \;+\; S_{ff}(s). \tag{B.30}$$

Therefore, (B.29) becomes

$$\begin{aligned}\frac{d}{ds}\iiint_{U_f(s)} \phi_{jkl...}\, dU \;=\; & \iint_{S_{fs}(s)} \phi_{jkl...} \frac{dr_m}{ds}\, \nu_m\, dS \\ & + \iint_{S_{ff}(s)} \phi_{jkl...} \frac{dr_m}{ds}\, \nu_m\, dS.\end{aligned} \tag{B.31}$$

The vector, $\dfrac{dr_i}{ds}$ is a tangent vector to the curve traced out by r_i (Swokowski, 1992). Since the fluid-solid surface is also the boundary of the averaging volume, it follows that on this interface the tangent vector is also always tangent to the interface and therefore

$$\left(\frac{dr_m}{ds}\right) \nu_m \Big|_{S_{fs}} \;=\; 0 \tag{B.32}$$

where the subscript S_{fs} indicates that (B.32) holds on the fluid-solid surface of the REV. When the REV is translated the curve traced out by r_i is not parallel to the existing fluid-fluid boundary, but it follows an arbitrary curve within U_f and, therefore, $\dfrac{dr_i}{ds}$ is not tangent to the fluid-fluid interface. Equation (B.32) thus becomes

$$\frac{d}{ds}\iiint_{U_f(s)} \phi_{jkl...}\, dU \;=\; \iint_{S_{ff}(s)} \phi_{jkl...} \frac{dr_m}{ds}\, \nu_m\, dS. \tag{B.33}$$

As illustrated in Figure B.1, $\overline{r}_i$ is the position vector which locates points on the arbitrary curve along which the centroid of the REV moves and $\overset{o}{r}_i\,(s)$ is the position vector of all points on $S_f(s)$ relative to this reference point, which imply that

$$r_i(s) \;=\; \overline{r}_i(s) + \overset{o}{r}_i\,(s). \tag{B.34}$$

As shown by Whitaker (1968), the directional derivative along a curve, which in the present case is the curve followed by the centroid of the averaging volume, may be written as

$$\frac{d}{ds} = \left(\frac{d\overline{r}_i}{ds}\right)\frac{\partial}{\partial x_i} \tag{B.35}$$

since the vector $\dfrac{d\overline{r}_i}{ds}$ is a unit tangent vector to the arbitrary curve followed by the centroid of the averaging volume. A combination of (B.34) and (B.35) with (B.33) then yields

$$\left(\frac{d\overline{r}_i}{ds}\right)\left(\iiint_{U_f(s)} \phi_{jkl\ldots}\, dU\right)_{,i} = \iint_{S_{ff}(s)} \phi_{jkl\ldots}\frac{d\overline{r}_m}{ds}\,\nu_m\, dS + \iint_{S_{ff}(s)} \phi_{jkl\ldots}\frac{d\overset{\circ}{r}_m}{ds}\,\nu_m\, dS. \tag{B.36}$$

When the averaging volume $U_o(s)$ is translated along the arbitrary curve, the unit vector $\dfrac{d\overset{\circ}{r}_i}{ds}$ is tangent to S_{ff} provided that $U_o(s)$ is translated without rotation and deformation. This restriction on the REV implies that the final result is only applicable if the REV's under consideration are independent of space and time. Under these conditions $\left(\dfrac{d\overset{\circ}{r}_m}{ds}\right)\nu_m = 0$ on S_{ff}. The unit vector $\dfrac{d\overline{r}_i}{ds}$ is uniform over the REV, and thus also over S_{ff}, provided that an equivalent REV be associated with each point in the porous domain through a translation without rotation and deformation from the original point of definition (Slattery, 1967). Therefore, (B.36) becomes

$$\frac{d\overline{r}_i}{ds}\left(\iiint_{U_f(s)} \phi_{jkl\ldots}\, dU\right)_{,i} = \frac{d\overline{r}_i}{ds}\iint_{S_{ff}(s)} \phi_{jkl\ldots}\nu_i\, dS. \tag{B.37}$$

Since the initial curve along which the averaging volume was translated was selected arbitrary, $\overline{r}_i$ is arbitrary, and thus implying that (B.37) may be written as

$$\left(\iiint_{U_f(\overline{r}_i)} \phi_{jkl\ldots}\, dU\right)_{,i} = \iint_{S_{ff}(\overline{r}_i)} \phi_{jkl\ldots}\nu_i\, dS \tag{B.38}$$

which gives us Slattery's Averaging Theorem. The specific dependence of U_f and S_{ff} on s has been changed to spatial coordinates, since characterising a specific averaging volume by the arc length is equivalent to characterising it with the position coordinates

of the centroid. This equation may be further developed by writing the left hand side as $(U_f \langle \phi_{jkl...} \rangle^f)_{,i}$ and by making use of (B.5) to yield

$$\langle \phi_{jkl...} \rangle^f_{,i} = \frac{1}{U_f} \iint_{S_{ff}} \phi_{jkl...} \nu_i \, dS - \frac{1}{\epsilon} \langle \phi_{jkl...} \rangle^f \epsilon_{,i}. \tag{B.39}$$

Therefore, the gradient of an intrinsic phase average is equal to the integral of the phase quantity over the external fluid-fluid surface of the averaging volume while the latter term takes into consideration the homogeneity of the porous material. The spatial averaging theorem as presented here, is derived in an alternate manner by Howes and Whitaker (1985) in which they derive the theorem more directly without referring to the general transport theorem and a more simplified proof is given by Whitaker (1985).

There also exist other methods of deriving Slattery's averaging theorem. Bear and Bachmat (1991, p120) also considers the translation of an REV while maintaining its shape. Furthermore, their proof is also applicable to a Cartesian tensorial quantity, but more concise than the one presented here.

B.2.2 Averaging theorem from distribution functions

A completely different type of proof is provided by Gray and Lee (1977), Cushman (1982) and Willis *et al.* (1991) in which they make use of a distribution function which characterises the distribution of phases within an REV. This type of derivation of the averaging theorem is more general than the one previously presented and it is applicable to time and space dependent averaging volumes.

In the initial stages of providing a proof for Slattery's averaging theorem by means of distribution functions, there was some uncertainty in obtaining the most appropriate and general form of the distribution function characterising a specific phase in an REV. For a two-phase system any three-dimensional region contains two boundary surfaces, one in contact with the fluid phase and the other in contact with the solid phase. Following Kinnmark and Gray (1984), an exceptable distribution function or indicator funtion, γ_d, may be defined as

$$\gamma_d(x_i, t) = \begin{cases} 1 \quad \text{if} \quad (x_i - x_i^{fs}) \nu_i^f < 0 & \Rightarrow \text{in fluid phase} \\ 0 \quad \text{if} \quad (x_i - x_i^{fs}) \nu_i^f > 0 & \Rightarrow \text{in solid phase} \end{cases} \tag{B.40}$$

where x_i is a general position vector, x_i^{fs} is the position vector of the phase interface and ν_i^f is a unit normal vector to the fluid-solid interface at x_i^{fs} directed out of the fluid phase and, furthermore, x_i and x_i^{fs} are collinear. From (B.40) it follows that γ_d is one within the fluid phase and zero in the rest of space. The fluid phase may consist of one or more non-overlapping finite volumes, each bounded by an orientable surface. The dependence of γ_d on time accounts for the expansion, contraction and deformation of the spatial domain. The distribution function may also be defined in terms of a limit of a sequence of functions and expressed in terms of the error function as illustrated by Kinnmark and Gray (1984) and Gray *et al.* (1993).

Another important feature to consider is the spatial gradient of the distribution function. As noted by Gray *et al.* (1993) and Gray and Lee (1977), the spatial gradient of γ_d is a vector pointing in the direction of greatest change in γ_d. Within, and exterior to, the region of interest, γ_d is uniform so that $\gamma_{d,i} = 0$. At a particular point on the boundary of the designated region, the direction of greatest change in γ_d is normal to the boundary and the magnitude of the change is characterised by the Dirac-delta function. Over the complete boundary the gradient of γ_d is

$$\gamma_{d,j} = -\left(\left(x_i - x_i^{fs}\right)\nu_i^f\right)_{,j}\boldsymbol{\delta}\left(g(x_i, x_i^{fs})\right) \tag{B.41}$$

where $g(x_i, x_i^{fs}) = 0$ defines the surface of the fluid-solid interface (Kinnmark and Gray, 1984). The distribution $\boldsymbol{\delta}$ is the multi-dimensional analogue of the Dirac distribution. As noted by Kinnmark and Gray (1984), this analogue is different from the commonly used multi-dimensional Dirac distribution which describes a spike at a point (Merzbacher, 1970). The Dirac analogue is zero everywhere except along the phase interface where $x_i = x_i^{fs}$. Additional technical detail regarding the gradient of the distribution function is provided by Cushman (1982).

More interesting than the gradient of the distribution function itself, is the integration of the product of a phase quantity with $\gamma_{d,i}$. Since the delta distribution function is zero everywhere except at the fluid-solid interphase, the value of an integral whose integrand is a delta function multiplied by some other quantity is just that quantity evaluated at the singular point of the delta function. Therefore, as shown by Kinnmark and Gray (1984), Kabala (1984) and Cushman (1982),

$$\iiint_{U_o} \phi_{jkl\ldots}(x_i)\gamma_{d,i}dU = -\iint_{S_{fs}} \phi_{jkl\ldots}(x_i^{fs})\nu_i\, dS \tag{B.42}$$

where S_{fs} is the fluid-solid interphase area within U_o.

As indicated in Figure 2.1, the position vector of any point within an REV may be expressed as

$$x_i = \overline{x}_i + \overset{\circ}{x}_i \tag{B.43}$$

where $\overline{x}_i$ is a position vector indicating the centroid of an REV and $\overset{\circ}{x}_i$ is the position vector of points within the REV relative to the centroid. As noted by Gray *et al.* (1993), a function $\phi_{jkl...}$ that depends on position in space may be expressed equivalently as $\phi_{jkl...}(x_i)$ or $\phi_{jkl...}(\overline{x}_i + \overset{\circ}{x}_i)$. The gradient of such a function may be obtained by differentiation using either x_i or $(\overline{x}_i + \overset{\circ}{x}_i)$ as the independent variable, such that

$$\phi_{jkl...,i} = \nabla_{x_i}\phi = \nabla_{\overline{x}_i + \overset{\circ}{x}_i}\phi \tag{B.44}$$

where the subscripts indicate relative to which reference frame the derivatives are taken. It also follows that

$$\begin{aligned} d\phi_{jkl...} &= \phi_{jkl...,i}\, dx_i \\ &= \phi_{jkl...,i}\, d(\overline{x}_i + \overset{\circ}{x}_i) \\ &= \phi_{jkl...,i}\, d\overline{x}_i + \phi_{jkl...,i} d\overset{\circ}{x}_i \end{aligned} \tag{B.45}$$

since $\overline{x}_i$ is not a function of $\overset{\circ}{x}_i$ and vice versa. From this equation the partial derivative of $\phi_{jkl...}$ with respect to the $\overline{x}_i$-coordinate system holding $\overset{\circ}{x}_i$ constant may be expressed as

$$\left.\frac{\partial \phi_{jkl...}}{\partial \overline{x}_i}\right|_{\overset{\circ}{x}_i} = \phi_{jkl...,i} \tag{B.46}$$

or in Gibbs notation

$$\nabla_{\overline{x}_i}\phi = \nabla_{\overline{x}_i + \overset{\circ}{x}_i}\phi. \tag{B.47}$$

Equivalently, the partial derivative of $\phi_{jkl...}$ with respect to the $\overset{\circ}{x}$-coordinate system holding the $\overline{x}_i$-coordinates constant may be written as

$$\left.\frac{\partial \phi_{jkl...}}{\partial \overset{\circ}{x}_i}\right|_{\overline{x}_i} = \phi_{jkl...,i} \tag{B.48}$$

or

$$\nabla_{\overset{\circ}{x}_i} \phi = \nabla_{\overline{x}_i + \overset{\circ}{x}_i} \phi. \tag{B.49}$$

It therefore follows that

$$\nabla_{x_i} \phi = \nabla_{\overline{x}_i + \overset{\circ}{x}_i} \phi = \nabla_{\overline{x}_i} \phi = \nabla_{\overset{\circ}{x}_i} \phi. \tag{B.50}$$

As indicated by (B.50), for a function whose spatial dependence may be expressed in terms of $\overline{x}_i + \overset{\circ}{x}_i$ rather than $\overline{x}_i$ or $\overset{\circ}{x}_i$ separately, the gradient with respect to either the $\overline{x}_i$ or the $\overset{\circ}{x}_i$-coordinates is identical (Gray *et al.*, 1993).

With this information at hand, it is possible to address the problem of obtaining the average of a spatial gradient. Therefore,

$$\begin{aligned} \langle \phi_{jkl...,i} \rangle &= \frac{1}{U_o} \iiint_{U_f} \phi_{jkl...,i} \, dU \\ &= \frac{1}{U_o} \iiint_{U_o} \gamma_d \phi_{jkl...,i} \, dU \\ &= \frac{1}{U_o} \iiint_{U_o} (\gamma_d \phi_{jkl...})_{,i} \, dU - \frac{1}{U_o} \iiint_{U_o} \gamma_{d,i} \phi_{jkl...} \, dU \end{aligned} \tag{B.51}$$

where the chain rule of differentiation was invoked to move from the second to third step. The latter integral in (B.51) involves the delta function which is zero everywhere except at the fluid-solid interface. By making use of (B.42), (B.51) becomes

$$\langle \phi_{jkl...,i} \rangle = \frac{1}{U_o} \iiint_{U_o} (\gamma_d \phi_{jkl...})_{,i} \, dU + \frac{1}{U_o} \iint_{S_{fs}} \phi_{jkl...} \nu_i \, dS. \tag{B.52}$$

If the spatial gradient in the first term is considered to be relative to the $\overline{x}_i$-coordinate system, then it may be removed from the integral, since the volume of integration is independent of $\overline{x}_i$. It thus follows that

$$\begin{aligned} \langle \phi_{jkl...,i} \rangle &= \left(\frac{1}{U_o} \iiint_{U_o} \gamma_d \phi_{jkl...} \, dU \right)_{,i} + \frac{1}{U_o} \iint_{S_{fs}} \phi_{jkl...} \nu_i \, dS \\ &= \langle \phi_{jkl...} \rangle_{,i} + \frac{1}{U_o} \iint_{S_{fs}} \phi_{jkl...} \nu_i \, dS \end{aligned} \tag{B.53}$$

which gives the average of a gradient in terms of the gradient of the average.

According to (B.47), it is also possible to interpret the spatial derivative on the right hand side of (B.52) to be relative to the $\overset{o}{x}_i$-coordinate axes. In this case, the divergence theorem as given by Bear and Bachmat (1991, eq2.1.42) may be applied to the first term on the right hand side of (B.52) to obtain

$$\langle \phi_{jkl...,i} \rangle = \frac{1}{U_o} \iint_{S_o} \nu_i \gamma_d \phi_{jkl...} \, dS + \frac{1}{U_o} \iint_{S_{fs}} \phi_{jkl...} \nu_i \, dS \tag{B.54}$$

where S_o is the complete surface of the averaging volume and ν_i is an outward unit normal vector on S_o. Since γ_d is zero where the surface of the averaging volume is in the solid phase and unity where the surface is in the fluid phase, the γ_d function implies only integration over S_{ff}, which is the portion of S_o in the fluid phase. Therefore, (B.54) becomes

$$\langle \phi_{jkl...,i} \rangle = \frac{1}{U_o} \iint_{S_{ff}} \nu_i \phi_{jkl...} \, dS + \frac{1}{U_o} \iint_{S_{fs}} \phi_{jkl...} \nu_i \, dS. \tag{B.55}$$

Equating the right hand sides of (B.53) and (B.55), yields

$$\langle \phi_{jkl...} \rangle_{,i} = \frac{1}{U_o} \iint_{S_{ff}} \nu_i \phi_{jkl...} dS \tag{B.56}$$

which is known as Slattery's averaging theorem (Slattery, 1967; Whitaker, 1969). It can be shown that (B.56) is equal to (B.39) by using the relation $\langle \phi_{jkl...} \rangle = \epsilon \langle \phi_{jkl...} \rangle^f$. The advantage of using generalised functions in deriving this theorem is that one does not need to keep account of all the boundaries of the various phases as integration takes place over the whole volume, but the distribution function ensures that the boundaries are correctly incorporated. As indicated by Gray and Lee (1977), Gray *et al.* (1993) and Cushman (1982), other averaging rules may also be derived by using generalised functions and more detail regarding the use of generalised functions is provided in these texts.

B.3 Volume average of a spatial gradient

Additional useful averaging rules regarding the average of a gradient may be derived from Slattery's averaging theorem. Gauss' divergence theorem for the fluid volume of

an REV yields

$$\begin{aligned}\iiint_{U_f} \phi_{jkl\ldots,i}\, dU &= \iint_{S_f} \phi_{jkl\ldots}\nu_i\, dS \\ &= \iint_{S_{fs}} \phi_{jkl\ldots}\nu_i\, dS + \iint_{S_{ff}} \phi_{jkl\ldots}\nu_i\, dS \end{aligned} \tag{B.57}$$

where S_f is the boundary of the fluid volume as given in (B.30). According to the divergence theorem the unit vector ν_i on the boundary of U_f is selected to point outwards from the volume (Swokowski, 1992) and, therefore, on all fluid-solid surfaces ν_i is directed out of the fluid phase into the solid. A substitution of the latter integral of (B.57) into (B.38) then gives

$$\iiint_{U_f} \phi_{jkl\ldots,i}\, dU = \left(\iiint_{U_f} \phi_{jkl\ldots}\, dU\right)_{,i} + \iint_{S_{fs}} \phi_{jkl\ldots}\nu_i\, dS. \tag{B.58}$$

Since the averaging volume U_o is uniform, it is possible to divide (B.58) by this volume to obtain

$$\frac{1}{U_o}\iiint_{U_f} \phi_{jkl\ldots,i}\, dU = \left(\frac{1}{U_o}\iiint_{U_f} \phi_{jkl\ldots}\, dU\right)_{,i} + \frac{1}{U_o}\iint_{S_{fs}} \phi_{jkl\ldots}\nu_i\, dS. \tag{B.59}$$

If we compare these integrals with the definition of a phase average in (B.1), this equation is equivalent to stating that

$$\langle \phi_{jkl\ldots,i}\rangle = \langle \phi_{jkl\ldots}\rangle_{,i} + \frac{1}{U_o}\iint_{S_{fs}} \phi_{jkl\ldots}\nu_i\, dS. \tag{B.60}$$

Equation (B.60) relates the average of a spatial derivative or a gradient to the spatial derivative of an average. In Gibbs' vector notation it may be written as

$$\langle \nabla\phi\rangle = \nabla\langle\phi\rangle + \frac{1}{U_o}\iint_{S_{fs}} \boldsymbol{\nu}\,\phi\, dS. \tag{B.61}$$

Veverka (1981) raised some questions regarding the validity of (B.61), but Howes and Whitaker (1985) have examined the derivation and confirmed its correctness.

If we apply a contraction to (B.60) by setting $j = i$, it follows that

$$\langle \phi_{ikl\ldots,i}\rangle = \langle \phi_{ikl\ldots}\rangle_{,i} + \frac{1}{U_o}\iint_{S_{fs}} \phi_{ijk\ldots}\nu_i\, dS \tag{B.62}$$

which may be written in Gibbs' notation as

$$\langle \boldsymbol{\nabla}\cdot\phi \rangle \;=\; \boldsymbol{\nabla}\cdot\langle\phi\rangle \;+\; \frac{1}{U_o}\iint_{S_{fs}} \boldsymbol{\nu}\cdot\phi\, dS. \tag{B.63}$$

Equations (B.62) and (B.63) are the more familiar forms in which these averaging rules appear in literature (Gray, 1975; Whitaker, 1969).

B.4 Gradient of porosity

Before writing the above expressions in terms of intrinsic phase averages, it is instructive to firstly consider some expressions regarding a spatial gradient in porosity. By employing the relation between the phase and intrinsic phase averages as presented in (B.6), it is possible to write (B.60) as

$$\langle \phi_{jkl\ldots,i} \rangle \;=\; \left(\epsilon\,\langle \phi_{jkl\ldots}\rangle^f\right)_{,i} \;+\; \frac{1}{U_o}\iint_{S_{fs}} \phi_{jkl\ldots}\nu_i\, dS. \tag{B.64}$$

As previously noted, $\phi_{jkl\ldots}$ represents any Cartesian tensorial quantity and if we select $\phi = 1$ then it follows from (B.64) that

$$\epsilon_{,i} \;=\; -\frac{1}{U_o}\iint_{S_{fs}} \nu_i\, dS \tag{B.65}$$

where use was made of (B.13). If we set $\phi = 1$ in (B.57) it follows that

$$\iint_{S_{fs}} \nu_i\, dS \;=\; -\iint_{S_{ff}} \nu_i\, dS. \tag{B.66}$$

In view of (B.65) the gradient in porosity is also given by

$$\epsilon_{,i} \;=\; \frac{1}{U_o}\iint_{S_{ff}} \nu_i\, dS. \tag{B.67}$$

B.5 Intrinsic phase average of a spatial gradient

By applying the relation $\langle \phi_{jkl\ldots} \rangle = \epsilon\,\langle \phi_{jkl\ldots}\rangle^f$ to (B.60) it follows that

$$\langle \phi_{jkl\ldots,i}\rangle^f \;=\; \langle \phi_{jkl\ldots}\rangle^f_{,i} \;+\; \frac{1}{U_f}\iint_{S_{fs}} \phi_{jkl\ldots}\nu_i\, dS \;+\; \frac{1}{\epsilon}\langle \phi_{jkl\ldots}\rangle^f \epsilon_{,i}. \tag{B.68}$$

Application of (B.65) to (B.64) yields

$$\begin{aligned}\langle \phi_{jkl...,i} \rangle &= \langle \phi_{jkl...} \rangle^f \epsilon_{,i} + \epsilon \langle \phi_{jkl...} \rangle^f_{,i} + \frac{1}{U_o} \iint_{S_{fs}} \phi_{jkl...} \nu_i \, dS \\ &= -\langle \phi_{jkl...} \rangle^f \frac{1}{U_o} \iint_{S_{fs}} \nu_i \, dS + \frac{1}{U_o} \iint_{S_{fs}} \phi_{jkl...} \nu_i \, dS + \epsilon \langle \phi_{jkl...} \rangle^f_{,i} \\ &= \frac{1}{U_o} \iint_{S_{fs}} \left(\phi_{jkl...} - \langle \phi_{jkl...} \rangle^f \right) \nu_i \, dS + \epsilon \langle \phi_{jkl...} \rangle^f_{,i} \end{aligned} \tag{B.69}$$

which implies that

$$\langle \phi_{jkl...,i} \rangle = \epsilon \langle \phi_{jkl...} \rangle^f_{,i} + \frac{1}{U_o} \iint_{S_{fs}} \overset{o}{\phi}_{jkl...} \nu_i \, dS. \tag{B.70}$$

In Gibbs' notation this equation may be written as

$$\langle \boldsymbol{\nabla} \phi \rangle = \epsilon \boldsymbol{\nabla} \langle \phi \rangle^f + \frac{1}{U_o} \iint_{S_{fs}} \boldsymbol{\nu} \overset{o}{\phi} \, dS. \tag{B.71}$$

Gray (1975) refers to this equation as the Modified Averaging Theorem. A contraction imposed on (B.70) yields in vector notation

$$\langle \boldsymbol{\nabla} \cdot \phi \rangle = \epsilon \boldsymbol{\nabla} \cdot \langle \phi \rangle^f + \frac{1}{U_o} \iint_{S_{fs}} \boldsymbol{\nu} \cdot \overset{o}{\phi} \, dS. \tag{B.72}$$

Equation (B.72) is also derived by Bear and Bachmat (1991) for a general tensorial quantity.

B.6 Average of a time derivative

For completeness it is also necessary to consider the average of a time derivative. This is achieved by once again considering the general transport theorem (Whitaker, 1968) for the transport of a phase quantity within the void volume U_f,

$$\frac{d}{dt} \iiint_{U_f} \phi_{jkl...} \, dU = \iiint_{U_f} \frac{\partial \phi_{jkl...}}{\partial t} \, dU + \iint_{S_f} \phi_{jkl...} v^b_m \nu_m \, dS \tag{B.73}$$

where v_i^b is the velocity of points on S_f which is the boundary of U_f. If the averaging volume is considered stationary, then the total time derivative may be changed to a partial derivative and we obtain

$$\frac{\partial}{\partial t}\iiint_{U_f} \phi_{jkl\ldots}\, dU = \iiint_{U_f} \frac{\partial \phi_{jkl\ldots}}{\partial t}\, dU + \iint_{S_f} \phi_{jkl\ldots} v_m^b \nu_m\, dS \tag{B.74}$$

which may be rewritten as

$$\begin{aligned}\frac{1}{U_o}\iiint_{U_f} \frac{\partial \phi_{jkl\ldots}}{\partial t}\, dU &= \frac{\partial}{\partial t}\left(\frac{1}{U_o}\iiint_{U_f} \phi_{jkl\ldots}\, dU\right) \\ &\quad - \frac{1}{U_o}\iint_{S_f} \phi_{jkl\ldots} v_m^b \nu_m\, dS\end{aligned} \tag{B.75}$$

where the division by U_o is possible since the REV is assumed to be stationary and uniform. By making use of the definition for a phase average and (B.30), this equation becomes

$$\begin{aligned}\left\langle \frac{\partial \phi_{jkl\ldots}}{\partial t} \right\rangle &= \frac{\partial \langle \phi_{jkl\ldots} \rangle}{\partial t} - \frac{1}{U_o}\iint_{S_{fs}} \phi_{jkl\ldots} v_m^b \nu_m\, dS \\ &\quad - \frac{1}{U_o}\iint_{S_{ff}} \phi_{jkl\ldots} v_m^b \nu_m\, dS.\end{aligned} \tag{B.76}$$

Although the averaging volume is stationary, the fluid-solid surface within the REV may not necessarily be stationary as the fluid volume may change within the averaging volume. On the other hand, the fluid-fluid interface forms part of the boundary of the averaging volume and it is therefore also stationary. This implies that the latter integral in (B.76) is zero. Therefore, the phase average of a time derivative reduces to

$$\left\langle \frac{\partial \phi_{jkl\ldots}}{\partial t} \right\rangle = \frac{\partial \langle \phi_{jkl\ldots} \rangle}{\partial t} - \frac{1}{U_o}\iint_{S_{fs}} \phi_{jkl\ldots} v_m^b \nu_m\, dS. \tag{B.77}$$

In Gibbs' notation this equation may be written as

$$\left\langle \frac{\partial \phi}{\partial t} \right\rangle = \frac{\partial \langle \phi \rangle}{\partial t} - \frac{1}{U_o}\iint_{S_{fs}} \phi\, \boldsymbol{v}^b \cdot \boldsymbol{\nu}\, dS. \tag{B.78}$$

A similar approach to obtain the latter two equations is proposed by Gray (1975), while a different derivation for these two equations are provided by Bear and Bachmat (1991, p117).

Appendix C

The formation factor according to Suman and Ruth (1993)

C.1 Modelling procedure

In this appendix a detailed account is given of the model of Suman and Ruth (1993) in which the formation factor of a homogeneous porous medium saturated with an electrolyte has been analysed and related to a number of geometric characteristics of the porous medium. According to Suman and Ruth (1993) the formation factor may be analysed by referring to a rectangular parallelepiped-shaped REV. The REV has linear dimensions $L_{(k)}$ and total face areas $A_{o(k)}$. The sides of the REV normal to the $k = 2, 3$ directions are insulated and electric potentials V_h and V_l are imposed on the upstream and downstream faces of the REV, respectively. The macroscopic flow of electric current is therefore in the $k = 1$ direction. An additional feature of the REV is that any cross-sectional cut normal to the x_1-direction yields an effective fluid-fluid area $A_{p(1)}$, which may mathematically be expressed as

$$A_{p(1)} = \iint_{A_{f(1)}} \tilde{\nu}_1 \hat{\nu}_1 \, dS \tag{C.1}$$

where $A_{f(1)}$ is the total fluid area normal to the x_1-direction, $\tilde{\nu}_1$ is the component in the x_1-direction of the unit vector $\tilde{\nu}_i$ representing the direction of the microscopic flow on the fluid-fluid area and $\hat{\nu}_1$ is the magnitude of a outwardly directed normal vector to the area element dS. The area $A_{p(1)}$ is the same as the effective streamwise area defined in a more general form for an REA presented in (2.87). They then define the areosity as

$$\xi = \frac{A_{p(1)}}{A_{o(1)}} \tag{C.2}$$

where $A_{o(1)}$ is the total area of the REV normal to the x_1-direction. As noted by Suman and Ruth (1993) and discussed in Section 2.6.6, the areosity is not equal to the areal porosity, since the areal porosity $\epsilon = A_{f(1)}/A_{o(1)}$ is associated with all open fluid area, whereas the areosity also incorporates the microscopic direction of flow. A

generalisation of the areosity to a situation where the flow is not necessarily confined to the x_1-direction is given in (2.93).

Their analysis of the formation factor commences by considering the macroscopic flow of electric current through the rectangular REV. According to (4.43) the electric current through the REV in the x_1-direction is

$$i_{(1)} = \frac{V_{hl} A_{o(1)}}{\rho_o L_{(1)}} \tag{C.3}$$

where $i_{(1)}$ is the macroscopic current in the x_1-direction and ρ_o is the resistivity of the REV saturated with an electrolyte. Since (C.3) is applied to an REV as a whole the resistivity appearing in this relation is that of the saturated porous medium. Solving for the resistivity from this equation and incorporation of the definition of the formation factor (4.7) then leads to

$$F = \frac{\rho_o}{\rho_w} = \frac{A_{o(1)} V_{hl}}{i_{(1)} \rho_w L_{(1)}}. \tag{C.4}$$

The microscopic form of Ohm's law according to (4.44) is

$$j_1 = \frac{1}{\rho_w} V_{,1}. \tag{C.5}$$

The factors which contribute to the formation factor may be highlighted by taking the intrinsic phase average of the microscopic form of Ohm's law. Therefore, the intrinsic phase average of Ohm's law,

$$\frac{1}{U_f} \iiint_{U_f} j_1 \, dU + \frac{1}{\rho_w} \langle V \rangle^f_{,1} + \frac{1}{\rho_w U_f} \iint_{S_{fs}} V \nu_1 \, dS = 0 \tag{C.6}$$

is obtained by applying (B.68) (or Identity number 2 in Table 2.2) to (C.5) and neglecting the porosity gradient since the material is considered to be homogeneous.

According to (B.39) which is derived in Appendix B using the volume averaging theory and as presented by (Bear and Bachmat, 1991, p123), the spatial gradient of a quantity may be expressed in terms of an integral over the fluid-fluid surface by

$$\langle \phi_{jkl\ldots} \rangle^f_{,i} = \frac{1}{U_f} \iint_{S_{ff}} \phi_{jkl\ldots} \nu_i \, dS - \frac{1}{\epsilon} \langle \phi_{jkl\ldots} \rangle_f \epsilon_{,i} \tag{C.7}$$

where $\phi_{jkl...}$ is a generic variable. If this identity is applied to the electric potential gradient over a particular porous medium domain, which is homogeneous with respect to porosity, then

$$\langle V \rangle^f_{,i} = \frac{1}{U_f} \iint_{S_{ff}} V \nu_i \, dS. \tag{C.8}$$

The macroscopic gradient of the applied electric potential is thus written in terms of an integral over the fluid-fluid interface on the boundary of any REV. The component of (C.8) in the x_1-direction may be expressed as

$$\langle V \rangle^f_{,1} = \frac{1}{U_f} \iint_{S_{ff}} V \nu_1 \, dS. \tag{C.9}$$

Inclusion of this expression into (C.6) then yields

$$\frac{1}{U_f} \iiint_{U_f} j_1 \, dU + \frac{1}{\rho_w U_f} \iint_{S_{ff}} V \nu_1 \, dS + \frac{1}{\rho_w U_f} \iint_{S_{fs}} V \nu_1 \, dS = 0. \tag{C.10}$$

The macroscopic gradient of the electrostatic potential has thus been written in terms of an integral over the fluid-fluid openings on the boundaries of the REV.

Suman and Ruth (1993) then analyse the second term in (C.10) by referring to the general parallelepiped-shaped REV. If V_h and V_l represent the high and low electrostatic potentials over the REV, then

$$\begin{aligned} \frac{1}{\rho_w U_f} \iint_{S_{ff}} V \nu_1 \, dS &= \frac{A_{p(1)}(V_l - V_h)}{\rho_w U_f} \\ &= -\frac{A_{o(1)} \xi V_{hl}}{\rho_w U_f} \\ &= -\frac{i_{(1)} L_{(1)} F \xi}{U_f} \end{aligned} \tag{C.11}$$

where the areosity of the RUC follows from (C.2) and the potential difference has been obtained from (C.4). If this result is inserted into (C.10) and the formation factor is solved from the resulting equation then

$$F = \frac{1}{\xi i_{(1)} L_{(1)}} \iiint_{U_f} j_1 dU + \frac{1}{\xi i_{(1)} L_{(1)} \rho_w} \iint_{S_{fs}} V \nu_1 dS \tag{C.12}$$

where the first term on the right hand side of (C.12) represents the integral of the component of the microscopic current density in the x_1-direction, j_1, over the total fluid volume U_f. The second term is the surface integral of the electric potential, V, on the fluid-solid interface, S_{fs} of the porous medium. According to Suman and Ruth (1993) and Hulin (1993) this equations clearly illustrates the various contributions to the formations factor. The first term on the right hand side corresponds to the decrease in voltage in the direction of charge transport, while the latter term corresponds to the voltage drop and charge flow normal to the macroscopic transport direction. This term is therefore closely related to the tortuosity of the system. It is also interesting to note that the reduced area available for charge transport is a consequence of the fluid-fluid integral in (C.10) as it gave rise to the areosity factor. This analysis seems sound since the first term which is related to the integral over S_{ff} accounts for the reduced area for charge transport and the other term which depends on S_{fs} gives a contribution due to the increased path length.

On completion of the derivation of (C.12), Suman and Ruth (1993) introduce a number of RUC's which they consider in the context of network theory to be building blocks of the porous medium under consideration. Therefore, by repeating their RUC's the complete porous medium can be reconstructed. For a homogenous porous medium this then leads to a formation factor of

$$F = \frac{\chi_e}{\xi} \tag{C.13}$$

where χ_e is the electric tortuosity and the areosity follows from (C.2).

According to Suman and Ruth (1993) two types of electric tortuosities emerge depending on the existence of multiple flow paths. In the case of flow channels which are not linked, such as in a capillary model, the tortuosity is a result of the sinuousness of the individual flow channels and it may be expressed as a ratio of lengths. However, if there are multiple flow paths which are connected at junctions then the tortuosity depends on the current in individual channels as well as on the length and diameters of the various conducting channels. The main contributions of Suman and Ruth (1993) are that the formation factor should be expressed in terms of the areosity and not the porosity (see C.2) and the electric tortuosity is not a ratio of lengths.

The criticism against the model of Suman and Ruth (1993) is that they do not interpret the concept of an RUC as introduced by Du Plessis and Masliyah (1988) correctly. An RUC is not a fundamental building block of the porous material, but only a representative unit that contains the average geometry of an REV. Furthermore, all the volume

averaged features in an REV should also be contained within an RUC. This correspondence between the general features of an REV and the specific detail in an RUC may be illustrated by considering the following contradiction in the model of Suman and Ruth (1993).

The origin of the areosity in the expression for the formation factor, (C.13) resides with the analysis of the surface integral of the electric potential gradient expressed in (C.12). However, according to the approach of Suman and Ruth (1993) (C.12) may also be analysed to yield

$$\begin{aligned} \iint_{S_{ff}} V\nu_1 \, dS &= \frac{(V_l - V_h)\xi A_{o(1)} L_{(1)}}{L_{(1)}} \\ &= \xi A_{o(1)} L_{(1)} \langle V \rangle^f_{,1} \end{aligned} \tag{C.14}$$

since the electric potential is assumed to be uniform over the upstream and downstream faces of the REV. In the parallelepiped-shaped REV, and some RUC's, discussed by Suman and Ruth (1993) the volume $\xi A_{o(1)} L_{(1)}$ is equal to the volume in which the microscopic current flows only in the x_1-direction, which constitutes only part of U_f and thus giving the inequality

$$\xi A_{(1)} L_{(1)} \neq U_f. \tag{C.15}$$

However, a comparison of (C.14) with (C.9) implies that

$$U_f = \xi A_{o(1)} L_{(1)} \tag{C.16}$$

which leads to a contradiction with (C.15), although both integrals are taken over the fluid-fluid interface of an REV. This contradiction casts some doubt on the manner by which Suman and Ruth (1993) introduce the areosity into an analysis of the macroscopic electric potential gradient.

This does not prove that the areosity is incorrect, since it is of great importance in determining estimates of interstitial velocities. Furthermore, should the porosity ϵ appear in (C.14) instead of ξ, then (C.9) will be regained, since $\epsilon A_{(1)} L_{(1)} = U_f$ and the areal and volumetric porosities are equal (Bear and Bachmat, 1991, p37). When analysing the volume averaged form of Ohm's law, presented in (C.6), it is suggested that the areosity be introduced through the latter surface integral and not the potential gradient term.

C.2 Application to the RUC-model

To apply the formation factor of Suman and Ruth (1993), which is presented in (C.13), to a specific porous material it is necessary to obtain the tortuosity and areosity. In this section these quantities are obtained by making use of the RUC-model of Du Plessis and Masliyah (1988). Three different RUC's representing isotropic foamlike materials, granular porous media and prismatic bundles have been summarised by Du Plessis and Diedericks (1997). The advantages of using these models are that the tortuosity is available as a function of the porosity and the geometric relationships within the RUC's are less complex than for the anisotropic RUC's. The only disadvantage is that it is not possible to distinguish between the electric and hydraulic tortuosities and they are assumed to be equal.

As indicated by Du Plessis and Diedericks (1997), it also follows from the specific geometry of the RUC's that

$$A_{p(1)} = A_p = \frac{\epsilon d^2}{\chi} \tag{C.17}$$

where d is the linear dimensions of the RUC's. It follows from this equation that the areosity for this specific structures is

$$\xi = \frac{A_p}{A(o)} = \frac{\epsilon}{\chi} \tag{C.18}$$

A number of other geometric characteristics may also be determined from the particular RUC configurations.

By applying (C.18) to (C.13) it follows that the formation factor is given by

$$F = \frac{\chi^2}{\epsilon} \tag{C.19}$$

where χ is the tortuosity of the porous material which is given by a different expression for each of the three types of isotropic materials. Therefore, application of the expression of the formation factor of Suman and Ruth (1993) to the isotropic RUC's presented by Du Plessis and Diedericks (1997) yields a square dependency of the formation factor on the tortuosity. As shown in Sections 4.9.2 and 4.9.4, by solving (4.47) directly from the RUC's leads to a formation factor which is linear in the tortuosity for the prismatic bundle and foamlike materials. The difference is attributed to the incorporation of the areosity in (C.13) by Suman and Ruth (1993).

References

Ahmed, N., and Sunada, D.K., 1969, Nonlinear flow in porous media, *Journal of the Hydraulics Division, Proceedings of the American Society of Civil Engineers*, **95**(HY6), 1847-1857.

Allen, M.B., Behie, G.A., and Trangenstein, J.A., 1988, Multiphase flow in porous media. Mechanics, mathematics, numerics, *Lecturing notes in Engineering*, editors C.A. Brebbia, S.A. Orzag, Springer-Verlag, N.Y., 1-49.

Anderson, T.B., and Jackson, R., 1967, A fluid mechanical description of fluidized beds, *Ind. Engng. Chem. Fundamental*, **6**, 527-538.

Aravin, V.I., and Numerov[1], S.N., 1965, *Theory of fluid flow in undeformable porous media*, Israel Program for Scientific Translations, Jerusalem.

Archie, G.E., 1942, The electrical resistivity log as an aid in determining some reservoir characteristics, *Transactions of the American Institute of Mining and Metallurgical Engineers*, **146**, 54-61.

Avellaneda, M., and Torquato, S., 1991, Rigorous link between fluid permeability, electrical conductivity, and relaxation times for transport in porous media, *Physics of Fluids A*, **3**, 2529-2540.

Bachmat, Y., 1972, Spatial macroscopization of processes in heterogeneous systems, *Israel Journal of Technology*, **10**(5), 391-403.

Bachmat, Y., and Bear, J., 1986, Macroscopic modelling of transport phenomena in porous media. 1: The continuum approach, *Transport in Porous Media*, **1**, 213-240.

Bacri, J.-C., Rakotomalala, N., and Salin, D., 1987, Experimental Evidence of Disorder Effects in Hydrodynamic Dispersion, *Physical Review Letters*, **58**(20), 2035-2038.

Barak, A.Z., and Bear, J., 1981, Flow at high Reynolds numbers through anisotropic porous media, *Advances in Water Resources*, **4**, 54-66.

Barak, A.Z., 1987, Comments on 'High Velocity Flow in Porous Media' by Hassanizadeh and Gray, *Transport in Porous Media*, **2**, 533-535.

Bear, J., 1972, *dynamics of fluids in porous media*, American Elsevier Publishing Company, Inc.

Bear, J., and Bachmat, Y., 1983, On the equivalance of areal and volumetric averages in transport phenomena in porous media, *Advances in Water Resources*, **6**, 59-62.

Bear, J., and Bachmat, Y., 1986, Macroscopic modelling of transport phenomena in

[1]Reference not read, referred to by Scheidegger (1974)

porous media. 2: Applications to mass, momentum and energy transport, *Transport in Porous Media*, **1**, 241-269.

Bear, J., and Bachmat, Y., 1991, *Introduction to modeling of transport phenomena in porous media*, Kluwer Academic Publishers, Dordrecht.

Beavers, G.S., and Sparrow, E.M., 1969, Non-Darcy flow through fibrous porous media, *J. Appl. Mech. Trans. ASME*, December, 711-714.

Bennethum, L.S., and Giorgi, T., 1997, Generalized Forchheimer Equation for Two-Phase Flow Based on Hybrid Mixture Theory, *Transport in Porous Media*, **26**, 261-275.

Bernabé, Y., and Revil, A., 1995, Pore-scale heterogeneity, energy dissipation and the transport properties of rocks, *Geophysical Research Lettres*, **22**, 1529-1532.

Bird, R.B., Stewart, W.E., and Lightfoot, E.N., 1960, *Transport Phenomena* John Wiley, New York.

Boshoff, L., 1998, *Tortuosity of isotropic porous media*, Unpublished M.Sc., Department of Applied Mathematics, University of Stellenbosch, Stellenbosch.

Brinkman, H.C., 1947a, A calculation of the viscous force exerted by a flowing fluid on a dense swarm of particles, *Applied Scientific Research*, **A1**, 27-34.

Brinkman, H.C., 1947b, On the permeability of media consisting of closely packed porous particles, *Applied Scientific Research*, **A1**, 81-86.

Carman, P.C., 1937, Fluid flow through granular beds, *Transactions of the Institution of Chemical Engineers*, **15**, 150-166.

Carman, P.C., 1956, *Flow of Gases through Porous Media*, Butterworths Scientific Publications.

Charlaix, E., Hulin, J.P., Leroy, C., and Zarcone, C., 1988a, Experimental study of tracer dispersion in flow through two-dimensional networks of etched capillaries, *Journal of Physics D, Applied Physics*, **21**, 1727-1732.

Charlaix, E., Kushnick, A.P., and Stokes, J.P., 1988b, Experimental Study of Dynamic Permeability in Porous Media, *Physical Review Letters*, **61**(14), 1595-1598.

Charlaix, E., and Gayvallet, H., 1991, Hydrodynamic Dispersion in Networks of Cappilaries of Random Permeability, *Europhysics Letters*, **16**(3), 259-264.

Churchill, S.W., and Usagi, R., 1972, A general expression for the correlation of rates of transfer and other phenomena, *American Institute of Chemical Engineering Journal* **18**(6), 1121-1128.

Clennell, M.B., 1997, Tortuosity: a guide through the maze, *Developments in Petrophysics*, Geological Society Special Publication, No. 122, 299-344.

Comiti, J., 1987, *Contribution à la modèlisation des lit fixes. Application aux lits de parallélépidèdiques: dégradation d'énergie, dispersion axiale, transfer de matièrie*, Unpublished Ph.D., Institut National Polytechnique, Grenoble.

Comiti, J., and Renaud, M., 1989, A new model for determining mean structure parameters of fixed beds from pressure drop measurements: Application to beds packed with parallelepipedal particles, *Chemical Engineering Science*, **44**(7), 1539-1545.

Corey, A.T., 1977, *Mechanics of Heterogeneous Fluids in Porous Media*, Water Resources Publications, Colorado.

Cornell, D., and Katz, D.L., 1953, Flow of Gases through Consolidated Porous Media, *Industrial and Engineering Chemistry*, **45**(10), 2145-2152.

Cummings, A., and Chang, I.-J., 1987, Acoustic propagation in porous media with internal mean flow, *Journal of Sound and Vibration*, **114**(3), 565-581.

Currie, J.A., 1960, Gaseous diffusion in porous media. Part 2: Dry granular material, *British Journal of Applied Physics*, **11**, 318-324.

Cushman, J.H., 1982, Proofs of the volume averaging theorems for multiphase flow, *Advances in Water Resources*, **5**, 248-253.

Cvetković, V.D., 1986, A Continuum Approach to High Velocity Flow in a Porous Medium, *Transport in Porous Media*, **1**, 63-97.

Dagan, G., 1989, *Flow and Transport in Porous Formations*, Springer-Verlag, Berlin.

Darcy[2], H.P.G., 1856, *Les fontanes publiques da la villa de Dijon*, Victor Dalmont, Paris.

Diedericks, G.P.J., and Du Plessis, J.P., 1995, On tortuosity and areosity tensors for porous media, *Transport in Porous Media*, **20**, 265-279.

Diedericks, G.P.J, and Du Plessis, J.P., 1996, Electrical conduction and formation factor in isotropic porous media, *Advances in Water Resources*, **19**(4), 225-239.

Diedericks, G.P.J., and Du Plessis, J.P., 1997, Modelling of flow through homogeneous foams, *Mathematical Engineering in Industry*, **6**(2), 133-154.

Diedericks, G.P.J., Du Plessis, J.P., Montillet, A., Comiti, J., and LeGrand, J., 1998, Flow through a highly porous multifilament knit, *Chemical Engineering Communications*, **167**, 21-49.

[2]Reference not read, referred to by Bear (1972)

Drew, D.A., 1983, Mathematical modelling of two-phase flow, *Annual Reviews of Fluid Mechanics*, **15**, 261-291

Dullien, F.A.L., and Azzam, M.I.S., 1973, Flow rate-pressure gradient measurements in periodically nonuniform capillary tubes, *AIChE Journal*, **19**(2), 222-229.

Dullien, F.A.L., 1975, New Network Permeability Model of Porous Media, *AIChE Journal*, **21**(2), 299-307.

Dullien, F.A.L., 1979, *Porous media fluid transport and pore structure*, Academic Press, London.

Dullien, F.A.L., 1991, Characterization of porous media - pore level, *Transport in Porous Media*, **6**, 581-606.

Dullien, F.A.L., and Dong, M., 1996, Experimental Determination of the Flow Trnsport Coefficients in the Coupled Equations of Two-Phase Flow in Porous Media, *Transport in Porous Media*, **25**, 97-120.

Duncan, W.J., Thom, A.S., and Young, A.D., 1960, *An Elementary Treatise on the Mechanisms of Fluids*, Edward Arnold Publishers Ltd.

Du Plessis, J.P., and Masliyah, J.H., 1988, Mathematical Modelling of Flow Through Consolidated Isotropic Porous Media, *Transport in Porous Media*, **3**, 145-161.

Du Plessis, J.P., and Masliyah, J.H., 1991, Flow Through Isotropic Granular Porous Media, *Transport in Porous Media*, **6**, 207-221.

Du Plessis, J.P., 1991, Saturated flow through a two-dimensional porous medium, *Advances in Water Resources*, **14**(3), 131-137.

Du Plessis, J.P., 1992a, Pore-scale modelling for flow through different types of porous environments, *Heat and Mass Transfer in Porous Media*, editors M. Quintard and M. Todorovic, Elsevier, Amsterdam, 249-262.

Du Plessis, 1992b, High Reynolds number flow through granular porous media, *Computational Methods in Water Resources IX*, **2**: Mathematical Modeling in Water Resources, editors T.F. Russel et al., Computational Mechanics Publications, Southampton, 179-186.

Du Plessis, J.P., Montillet, A., Comiti, J., and Legrand, J., 1994, Pressure drop prediction for flow through high porosity metallic foams, *Chemical Engineering Science*, **49**(21), 3545-3553.

Du Plessis, J.P., 1994, Analytical Quantification of Coefficients in the Ergun Equation for Fluid Friction in a Packed Bed, *Transport in Porous Media*, **16**, 189-207.

Du Plessis, J.P., and Roos, L.I., 1994, Predicting the Hydrodynamic Permeability of Sandstone with a Pore-scale Model, *Journal of Geophysical Research - Solid Earth*, **99/B10**, 19771-19776.

Du Plessis, J.P., and Roos, L.I., 1995, Numerical analysis of near-wall channeling in a packed bed, *Engineering computations*, **12**, 357-371.

Du Plessis, J.P., and Diedericks, G.P.J., 1997, *Pore-scale modelling of interstitial transport phenomena*, Chapter 2 of Fluid Transport in Porous Media, editor J.P. du Plessis, vol 13, *Advances in Fluid Mechanics*, Series editor M. Rahman, Computational Mechanics Publications, Southampton, 61-104.

Dupuit[3], J., 1863, *Etudes thèoriques et praticque sur le mouvement des eaux*, Dunod, Paris.

Epstein, N., 1989, On tortuosity and the tortuosity factor in flow and diffusion through porous media, *Chemical Engineering Science*, **44**(3), 777-779.

Ergun, S., and Orning, A.A., 1949, Fluid Flow through Randomly Packed Columns and Fluidized Beds, *Industrial and Engineering Chemistry*, **41**(6), 1179-1184.

Flügge, W., 1972, *Tensor Analysis and Continuum Mechanics*, Springer-Verlag New York Heidelberg Berlin.

Forchheimer, P., 1901, Wasserbewegung durch boden, *Zeitung Ver. Deutsch. Ing.*, **45**, 1782-1788.

Foscolo, P.U., Gibilaro, L.G., and Waldram, S.P., 1983, A unified model for particulate expansion of fluidised beds and flow in fixed porous media, *Chemical Engineering Science*, **38**(8), 1251-1260.

Franzini, J.B., and Finnemore, E.J., 1997, *Fluid Mechanics with Engineering Applications*, McGraw-Hill Companies, Inc.

Fried, J.J., and Combarnous, M.A., 1971, Dispersion in Porous Media, *Advances in Hydroscience*, vol. 7, editor Ven Te Chow, Academic Press, New York and London, 169-282.

Gibson, L.J., and Ashby, M.F., 1988, *Cellular Solids: Structure and Properties*, Pergamon Press.

Gray, W.G., 1975, A Derivation of the Equations for Multi-Phase Transport, *Chemical Engineering Science*, **30**(2), 229-233.

Gray, W.G., and O'Neill, K., 1976, On the General Equations for Flow in Porous Media and Their Reduction to Darcy's Law, *Water Resources Research*, **12**(2), 148-154.

[3]Reference not read, referred to by Bennethum and Giorgi (1997)

Gray, W.G., and Lee, P.C.Y., 1977, On the theorems for local volume averaging of multiphase systems, *International Journal of Multiphase Flow*, **3**, 333-340.

Gray, W.G., Leijnse, A., Kolar, R.L., and Blain, C.A., 1993, *Mathematical Tools for Changing Spatial Scales in the Analysis of Physical Systems*, CRC Press.

Greenkorn, R.A., and Kessler, D.P., 1970, Dispersion in Heterogeneous Nonuniform Anisotropic Porous Media, *Flow Through Porous Media*, American Chemical Society Publications, Washington DC., 160-178.

Guin, J.A., Kessler, D.P. and Greenkorn, R.A., 1971, The permeability tensor for anisotropic nonuniform porous media, *Chemical Engineering Science*, **26**, 1475-1478.

Gutfraind, R., and Hansen, A., 1994, Study of Fracture Permeability Using Lattice Gas Automata, *Transport in Porous Media*, **18**(2), 131-149.

Hannoura, A.A., and Barends, F.B.J., 1981, Non-Darct flow: State of the art, *Proc. Euromech 143, Delft*, 37-51.

Happel, J., and Brenner, H., 1965, *Low Reynolds Number Hydrodynamics with Special Applications to Particulate Media*, Prentice Hall Inc., Englewood Cliffs, N.J.

Haring, R.E., and Greenkorn, R.A., 1970, A Statistical Model of a Porous Medium with Nonuniform Pores, *AIChE Journal*, **16**(3), 477-483.

Hassanizadeh, M., and Gray, W.G., 1979, General conservation equations for multiphase systems: 1. Averaging procedure, *Advances in Water Resources*, **2**, 131-144.

Hassanizadeh, M., and Gray, W.G., 1980, General conservation equations for multiphase systems: 3. Constitutive theory for porous media flow, *Advances in Water Resources*, **3**, 25-40.

Hassanizadeh, S.M., and Gray, W.G., 1987, High velocity flow in porous media, *Transport in Porous Media*, **2**, 521-532.

Hassanizadeh, S.M., and Gray, W.G., 1988, Reply to Coments by Barak on 'High Velocity Flow in Porous Media', by Hassanizadeh and Gray, *Transport in Porous Media*, **3**, 319-321.

Hay, G.E., 1953, *Vector and Tensor Analysis*, Dover Publications Inc., New York.

Howes, F.A., and Whitaker, S., 1985, The spatial averaging theorem revisited, *Chemical Engineering Science*, **40**(8), 1387-1392.

Huber, A.T., and Gibson, L.J, 1988, Anisotropy of foams, *Journal of Materials Science*, **23**, 3031-3040.

Hulin, J.P., 1993, Comments on "Formation factor and tortuosity of homogeneous porous media" by R. Suman and D. Ruth, *Transport in Porous Media*, **12**, 291-292.

Irmay, S., 1961, Flow of fluid through porous media, *Encyclopaedic Dictionary of Physics*, J. Thewlis, Editor in Chief Pergamon Press, Oxford, London, **3**, 217-223.

Jacquet, C., 1991, *Characterisation geometrique et proprietes de transport de milieux poreux consolides*, Unpublished Ph.D., De l'institut National Polytechnique de Grenoble et de l'ecole Nationale Superieure des Mines de Saint-Etienne.

Jackson, P.D., Taylor-Smit, D., and Stanford, P.N., 1978, Resistivity-porosity-particle shape relationships for marine sand, *Geophysics*, **43**, 1250-1262.

Johnson, D.L., Plona, T.J., Scala, C., Pasierb, F., and Kojima, H., 1982, Tortuosity and acoustic slow waves, *Physical Review Letters*, **49**, 1840-1844.

Johnson, D.L., Koplik, J., and Schwartz, L.M., 1986, New Pore-Size Parameter Characterizing Transport in Porous Media, *Physical Review Letter*, **57**(20), 2564-2567.

Johnson, D.L., Koplik, J., and Dashen, R., 1987, Theory of dynamic permeability and tortuosity in fluid-saturated porous media, *Journal of Fluid Mechanics*, **176**, 379-402.

Kabala, Z.J., 1984, Comment on: An exposition of the distribution function used in proving the averaging theorems for multiphase flow, *Advances in Water Resources*, **7**, 144-145.

Kaczmarek, M., and Hueckel, T., 1998, Use of Porosity in Models of Consolidation, *Journal of Engineering Mechanics*, **124**(2), 237-239.

Kaviany, M., 1995, *Principles of heat transfer in porous media*, Springer-Verlag, Berlin.

Keller G.V., 1982, Electrical properties of rocks and minerals, Chapter 2 in *Handbook of Physical Properties of Rocks*, R.S. Carmichael ed., **1**, CRC Press, Inc., Florida.

Kemblowski, Z., and Michniewicz, M., 1979, A new look at the laminar flow of power law fluids through granular beds, *Rheologica Acta*, **18**, 730-739.

Kinnmark, I.P.E., and Gray, W.G., 1984, An exposition of the distribution function used in proving the averaging theorems for multiphase flow, *Advances in Water Resources*, **7**, 113-115.

Kip, A.F., 1969, *Fundamentals of Electricity and Magnetism*, McGraw-Hill International Book Company.

Knackstedt, M.A., and Zhang, X., 1994, Direct evaluation of length scales and structural parameters associated with flow in porous media, *Physical Review E*, **50**(3), 2134-2138.

Knackstedt, M.A., and Duplessis, J.P., 1996, Simple permeability model for natural granular media, *Geophysical Research Letters*, **23**(13), 1609-1612.

Koplik, J., Lin, C., and Vermette, M., 1984, Conductivity and permeability from microgeometry, *Journal of Applied Physics*, **56**(11), 3127-3131.

Koplik, J., Redner, S., and Wilkinson, D., 1988, Transport and dispersion in random networks with percolation disorder, *Physical Review*, **A37**, 2619-2636.

Lehner, F.K., 1979, On the validity of Fick's law for transient diffusion through a porous medium, *Chemical Engineering Science*, **34**, 821-825.

Lemaitre, J., Troadec, J.P., Bideau, D., Gervois, A., and Bougault, E., 1988, The formation factor of the pore space of binary mixtures of spheres, *Journal of Physics D: Applied Physics*, **21**, 1589-1592.

Liakopoulos, A.C., 1965, Variation of the Permeability Tensor Ellipsoid in Homogeneous Anisotropic Soils, *Water Resources Research*, **1**(1), 135-141.

Ma, H., and Ruth, D.W., 1993, The microscopic analysis of high Forchheimer number flow in porous media, *Transport in Porous Media*, **13**, 139-160.

MacDonald, I.F., El-Sayad, M.S., Mow, K., and Dullien, F.A.L., 1979, Flow through porous media - the Ergun equation revisited, *Ind. Eng. Chem. Fundam.* **18**(3), 199-208.

Maiti, S.K., Gibson, L.J., and Ashby, M.F., 1984a, Deformation and energy absorption diamgrams for cellular solids, *Acta. Metallurgica.*, **32**(11), 1963-1975.

Maiti, S.K., Ashby, M.F., and Gibson, L.J., 1984b, Fracture toughness of brittle cellular solids, *Scripta Metallurgica.*, **18**, 213-217.

Mallants, D., Jacques, D., Tseng, P-H., Van Genuchten, M.Th., and Feyen, J., 1997, Comparison of three hydraulic property measurement methods, *Journal of Hydrology*, **199**, 295-318.

Masliyah, J.H., 1994, *Electrokinetic Transport Phenomena*, Aostra Technical Publication Series 12.

Mast, R.F., and Potter, P.E., 1963, Sedimentary structures, sand shape fabrics, and permeability. II, *Journal of Geology*, **71**(4), 548-565.

Mei, C.C., and Auriault, J.-L., 1991, The effect of weak inertia on flow through a porous medium, *Journal of Fluid Mechanics* **222**, 647-663.

Merzbacher, E., 1970, *Quantum Mechanics*, John Wiley and Sons.

Montillet, A., Comiti, J. and, Legrand, J., 1992, Determination of structural parameters of metallic foams from permeametry measurements, *Journal of Materials Science*, **27**, 4460-4464.

Montillet, A., 1994, Personal communications.

Montillet, A., 1995, Fiabilité de la détermination de paramètres structuraux de mousses synthétiques à partir de mesures de chute de pression, *Récents Progès en Génie des Prosédés, Ed. Technique et Documentation, Lavoisier,* **9**(41), 125-130.

Mualem, Y., and Friedman, S.P., 1991, Theoretical Prediction of Electritical Conductivity in Saturated and Unsaturated Soil, *Water Resources Research*, **27**(10), 2771-2777.

Neuman, S.P., 1977, Theoretical derivation of Darcy's law *Acta Mechanica*, **25**, 153-170.

Newman, J.S., 1973, *Electrochemical Systems*, Prentice-Hall, Inc., Englewood Cliffs, New Jersey.

Nikolaevskii, V.N., 1959, Convective diffusion in porous media, *Prikl. Math. Mech.*, **23**(6), 1042-1050.

Nunge and Gill, 1970, Mechanisms Affecting Dispersion and Miscible Displacement, *Flow Through Porous Media*, American Chemical Society Publications, Washington DC., 180-196.

Penman, H.L., 1940a, Gas and Vapour Movements in the Soil I. The Diffusion of Vapours Through Porous Solids, *Journal of Agricultural Science*, **30**, 437-462.

Penman, H.L., 1940b, Gas and Vapour Movements in the Soil II. The Diffusion of Carbon Dioxide Through Porous Solids, *Journal of Agricultural Science*, **30**, 570-581.

Petersen, E.E., 1958, Diffusion in a Pore of Vaying Cross Section, *AIChE Journal*, **4**(3), 343-345.

Petersen, E.E., 1965, *Chemical Reaction Analysis*, Prentice-Hall, Englewood Cliffs, New Jersey.

Pettijohn, F.J., Potter, Siever, 1972, *Sand and Sandstone*, Springer-Verlag, Berlin, Heidelberg, New York.

Popović, B.D., 1973, *Introductory Engineering Electromagnetics*, Addison-Wesley Publishing Company.

Potter, P.E., and Mast, R.F., 1963, Sedimentary structures, sand shape fabrics, and permeability. I, *Journal of Geology*, **71**(4), 441-471.

Probstein, R.F., 1989, *Physicochemical Hydrodynamics, An Introduction*, Butterworths,

Boston, USA.

Punčochář, M., and Drahoš, J., 1991, The tortuosity concept in fixed and fluidized bed, *Chemical Engineering Science*, **48**(11), 2173-2175.

Qin, Y., and Kaloni, P.N., 1994, Convective Instabilities in Anisotropic Porous Media, *Studies in Applied Mathematics*, **91**, 189-204.

Quintard, M., and Whitaker, S., 1993, Transport in ordered and disordered porous media: volume-averaged equation, closure problems, and comparison with experiment, *Chemical Engineering Science*, **48**(14), 2537-2567.

Quintard, M., and Whitaker, S., 1994a, Transport in ordered and disordered porous media I: The cellular average and the use of weighting functions, *Transport in Porous Media*, **14**, 163-177.

Quintard, M., and Whitaker, S., 1994b, Transport in ordered and disordered porous media II: Generalized volume averaging, *Transport in Porous Media*, **14**, 179-206.

Quintard, M., and Whitaker, S., 1994c, Transport in ordered and disordered porous media III: Closure and comparison between theory and experiment, *Transport in Porous Media*, **15**, 31-49.

Quintard, M., and Whitaker, S., 1994d, Transport in ordered and disordered porous media IV: Computer generated porous media for three-dimensional systems, *Transport in Porous Media*, **15**, 51-70.

Quintard, M., and Whitaker, S., 1994e, Transport in ordered and disordered porous media V: Geometrical results for two-dimensional systems. *Transport in Porous Media*, **15**, 183-196.

Revil, A., and Cathles, L.M., 1999, Permeability of shaly sands, *Water Resources Research*, **35**(3), 651-662.

Rice, P.H., Fontugne, D.J., Latini, R.G., and Barduhn, A.J., 1970, Anisotropic Permeability in Porous Media, *Flow Through Porous Media* editor R. Nunge, American Chemical Society Publications, Washington DC., 47-56.

Roberts, J.N., and Schwartz, L.M., 1985, Grain consolidation and electrical conductivity in porous media, *Physical Review B*, **31**(9), 5990-5997.

Rothman, D.H., 1988, Cellular-automation fluids: A model for flow in porous media, *Geophysics*, **53**(4), 509-518.

Rumpf, H., and A.R., Gupte, 1971, Einflüsse der Porosität und Kornogrößenverteilung im Widerstandsgesetz der Porenströmung, *Chemic-Ing. Techn.*, **43**(6), 367-375.

Ruth, D., and Ma, H., 1992, On the Derivation of the Forchheimer Equation by Means of the Averaging Theorem, *Transport in Porous Media* **7**(3), 255-264.

Ruth, D., and Suman, R., 1992, The Rôle of Microscopic Cross Flow in Idealized Porous Media, *Transport in Porous Media*, **7**, 103-125.

Sabiri, N.E., Brahimi, M., and Comiti, J., 1996, Fluidization of various shaped particles by non-Newtonian purely viscous fluids, *Communications of the Fifth World Congress of Chemical Engineering*, 14-18 July 1996, San Diego (U.S.A.).

Sangani, A.S., and Acrivos, A., 1982, Slow flow past periodic arrays of cylinders with application to heat transfer, *International Journal of Multiphase flow*, **8**(3), 193-206.

Scheidegger, A.E., 1954, Statistical Hydrodynamics in Porous Media, *Journal of Applied Physics*, **25**(8), 994-1001.

Scheidegger, A.E., 1959, On the theory of flow if underground fluids in compressible strata, *Canadian Journal of Physics*, **37**, 276-284.

Scheidegger, A.E., 1961, General Theory of Dispersion in Porous Media, *Journal of Geophysical Research*, **66**(10), 3273-3278.

Scheidegger, A.E., 1974, *The Physics of Flow Through Porous Media*, 3rd ed., University of Toronto Press, Toronto.

Schopper, J.R., 1966, A theoretical investigation of the formation factor/permeability/ porosity relationship using a network model, *Geophysical Prospecting*, **14**, 301-314.

Sen, P.N., Scala, C., and Cohen, M.H., 1981, A self-similar model for sedimentary rocks with application to the dielectric constant of fused glass beads, *Geophysics*, **46**(5), 781-795.

Sen, P.N., and Kan, R., 1987, Electrolytic Conduction in Porous Media with Charges, *Physical Review Letters*, **58**(8), 778-780.

Shankland, T.J., and Waff, H.S., 1974, Conductivity in Fluid-Bearing Rocks, *Journal of Geophysical Research*, **79**(32), 4863-4868.

Slattery, J.C., 1967, Flow of Viscoelestic Fluids Through Porous Media, *AIChE Journal*, **13**(6), 1066-1071.

Slattery, J.C., 1972, *Momentum, Energy and Mass Transfer in Continua*, McGraw-Hill, New York.

Smit, G.J.F., Diedericks, G.P.J., and Du Plessis, J.P., 1998, Modelling Procedure for Prediction of Flow Through Porous Materials, *Advances in Fluid Mechanics II*, eds. M. Rahman, G. Comini and C.A. Brebbia, vol. 21, Computational Mechanics Publications,

Southampton, Boston, 233-240.

Smit, G.J.F., and Du Plessis, J.P., 1999, Modelling of non-Newtonian purely viscous flow through anisotropic high porosity synthetic foams, *Chemical Engineering Science*, **54**, 645-654.

Spearing, M., and Matthews, G.P., 1991, Modelling characteristic properties of sandstones, *Transport in Porous Media*, **6**, 71-90.

Sudicky, E.A., 1986, A Natural Gradient Experiment on Solute Transport in a Sand Aquifer: Spatial Variability of Hydraulic Conductivity and Its Role in the Dispersion Process, *Water Resources Research*, **22**(13), 2069-2082.

Suman, R., and Ruth, D., 1993, Formation factor and tortuosity of homogeneous porous media, *Transport in Porous Media*, **7**, 185-206.

Swokowski, E.W., 1992, *Calculus*, PWS-KENT Publishing Company.

Szabo, B.A., 1968, Permeability of Orthotropic Porous Mediums, *Water Resources Research*, **4**(4), 801-808.

Tek, M.R., 1957, Development of a generalized Darcy equation, *Petro. Trans. AIME*, **210**, 376-378.

Tokaty, G.A., 1971, *A History and Philosophy of Fluid Mechanics*, G.T. Foulis and Company Ltd., Henley-on-Thames, Oxfordshire.

Tompson, A.F.B., and Gray, W.G., 1986a, A Second-Order Approach for the Modeling of Dispersive Transport in Porous Media. 1: Theoretical Development, *Water Resources Research*, **22**(5), 591-599.

Tompson, A.F.B., and Gray, W.G., 1986b, A Second-Order Approach for the Modeling of Dispersive Transport in Porous Media. 2: Application to Solute Motion in Pipes and Capillary Tubes, *Water Resources Research*, **22**(5), 601-614.

Tompson, A.F.B., and Gray, W.G., 1986c, A Second-Order Approach for the Modeling of Dispersive Transport in Porous Media. 3: Application to Two Porous Media Problems, *Water Resources Research*, **22**(13), 1959-1971.

Tucker, C.L., and Dessenberger, R.B., 1994, Governing Equations for Flow and Heat Transfer in Stationary Fibre Beds, *Flow and Reology in Polymer Manufactering*, editor S.G. Advani, Elsevier Science B.V., 257-323.

Van der Westhuizen, J., and Du Plessis, J.P., 1994, Quantification of unidirectional fibre bed permeability, *Journal of Composite Materials*, **28**(7), 619-637.

Veverka, V., 1981, Theorem for the local volume average of a gradient revised, *Chemical*

Engineering Science, **36**, 833-838.

Walsh, J.B., and Brace, W.F., 1984, The Effect of Pressure on Porosity and the Transport Properties of Rock, *Journal of Geophysical Research*, **89**(B11), 9425-9431.

Ward, J.C., 1964, Turbulent flow in porous media, *J. Hydr. Div. ASCE*, **90**(HY5), 1-12.

Wasan, D.T., Wnek, W., Davies, R., Jacson, M., and Kaye, B.H., 1976, Analysis and Evaluation of Permeability Techniques for Characterizing Fine Particels Part I. Diffusion and Flow Through Porous Media, *Power Technology*, **14**, 209-228.

Wheatcraft, S.W., and Cushman, J.H., 1991, Hierarchical Approaches to Transport in Heterogeneous Porous Media, *Reviews of geophysics, supplement*, 263-269.

Whitaker, S., 1966, The equations of motion in porous media, *Chemical Engineering Science*, **21**, 291-300.

Whitaker, S., 1967, Diffusion and Dispersion in Porous Media, *AIChE Journal*, **13**(3), 420-427.

Whitaker, S., 1968, *Introduction to Fluid Mechanics*, Prentice-Hall, Inc., Englewood Cliffs, N.J.

Whitaker, S., 1969, Advances in the theory of fluid motion in porous media, *Industrial and Engineering Chemistry*, **61**, 14-28.

Whitaker, S., 1985, A simple geometrical derivation of the spatial averaging theorem, *Chemical Engineering Education*, **19**, 18-21 and 50-52.

Whitaker, S., 1986, Flow in porous media I: A theoretical derivation of Darcy's law, *Transport in Porous Media*, **1**, 3-25.

Whitaker, S., 1996, The Forchheimer Equation: A Theoretical Development, *Transport in Porous Media*, **25**, 27-61.

Whitaker, S., 1997, Volume averaged of transport equations, Chapter 1 of Fluid Transport in Porous Media, editor J.P. du Plessis, vol 13, *Advances in Fluid Mechanics, Series*, editor M. Rahman, Computational Mechanics Publications, Southampton, 1-60.

Willis, M.S., Tosun, I., Choo, W., Chase, G.G., and Desai, F., 1991, *A dispersed multiphase theory and its application to filtration*, Chapter 4 of Advances in Porous Media editors M.Y. Corapcioglu, vol. 1, Elsevier Science Publishers, Amsterdam, 179-293.

Wong, P., Koplik, J., and Tomanic, J.P., 1984, Conductivity and permeability of rocks, *Physical Review B*, **30**(11), 6606-6614.

Wyllie, M.R.J., and Rose, W.D., 1950, Some Theoretical Considerations Related to the Quantitative Evaluation of the Physical Characteristics of Reservoir Rock from Electrical Log Data, *Petroleum Transactions, AIME*, **189**, 105-117.

Wyllie, M.R.J., and Spangler, M.B., 1952, Application of electrical resistivity measurements to problem of fluid flow in porous media, *Bulletin of the American Association of Petroleum Geologists*, **36**(2), 359-403.

Zhang, X., and Knackstedt, M.A., 1995, Direct measurements of electrical and hydrodynamic tortuosity in porous solids, *Geophysical Research Letters*, **22**, 2333-2336.

Zick, A.A., and Homsy, G.M., 1982, Stokes flow through periodic arrays of spheres, *Journal of Fluid Mechanics*, **115**, 13-26.